2012-09-13

Sources and processes affecting atmospheric sulfur at the onset of Arctic winter

Seguin, Alison Michelle

UNIVERSITY OF CALGARY

Sources and Processes Affecting Atmospheric Sulfur at the Onset of Arctic Winter

by

Alison Michelle Seguin

A THESIS

SUBMITTED TO THE FACULTY OF GRADUATE STUDIES

IN PARTIAL FULFILMENT OF THE REQUIREMENTS FOR THE

DEGREE OF DOCTOR OF PHILOSOPHY

DEPARTMENT OF CHEMISTRY

CALGARY, ALBERTA

SEPTEMBER, 2012

Abstract

Arctic size segregated aerosols and SO_2 concentrations were measured at two sites at the onset of winter in 2007 and 2008. Concentrations of non sea salt sulfate are within the same range as previous studies in the Arctic. Apportionment with tracer ions and isotopes were used to distinguish between biogenic sulfur and sulfur from other sources including sea salt, anthropogenic and two local Arctic sources; the Smoking Hills and frost flowers.

A method to quantitatively differentiate between frost flower and sea salt sulfate using isotope analysis and constrained frost flower ratios is introduced. This is the first time contributions from frost flower in aerosols are reported quantitatively and reached a maximum of 2.3 nmol/m^3.

Fine aerosol anthropogenic sulfate concentrations were similar between the sites (Alert 0.8 ± 0.6 nmol/m^3; *Amundsen* 0.3 ± 0.4 nmol/m^3) and increased with the onset of winter. Ammonium, nitrate and non sea salt potassium correlated with anthropogenic sulfate at both locations. A strong relationship between anthropogenic sulfate and a deficit in aerosol chloride at Alert, Nunavut supports acidification of aerosols from long range transport in the Arctic fall.

The first simultaneous measurements of dimethylsulfide (DMS), biogenic SO_2, aerosol methanesulfonic acid (MSA) and biogenic sulfate in the Arctic were carried out. Median

biogenic SO_2 concentration was 0.07 nmol/m^3. MSA concentrations decreased with the onset of winter.

A median lifetime of 6.1 days for DMS during the sampling period was modeled. Measured MSA branching ratios (median values at Alert = 0.24; *Amundsen* = 0.28) were compared to ratios predicted by a DMS oxidation model and were found to be similar when modeled halogen and aqueous oxidation was low. DMS oxidation by $NO_3\cdot$ is expected to be the largest contribution to DMS oxidation in the Arctic fall. A DMS transport model predicts the region around the *Amundsen* during the campaign was a net source of DMS (median net transport out of the region =10 nmol m^{-3} day^{-1}) although the area at times acted as a sink. A net source of DMS from Arctic waters supports that sulfur chemistry in the Arctic is representative of regional and not local conditions.

Acknowledgments

I would like to thank my supervisor Dr. Ann-Lise Norman for the dedication, patience, and support that she has given me during my time at Calgary. The knowledge and values I have learned from her will be carried with me for many years.

I would like to thank my supervisory committee, Dr. Hans Osthoff and Dr. Kevin Thurbide, along with my candidacy and defence examiners Dr. Alexander, Dr. Mayer, Dr. Schriemer, and Dr. Wieser for their time and assistance.

Dr. Ofelia Rempillo has been my constant comrade through the SOLAS project. Her companionship from the Arctic to Calgary has been appreciated throughout the years. I would also acknowledge the friendships and contributions from present and past group members of the Science & Environmental Physics Research Group (Nasrin, Fwziah, and Jon). Thanks to Nenita Lozano, Jesusa Overend-Pontoy and Steve Taylor from the Isotope Science Laboratory for all their help in the lab. I would also like to thank Farzin Malekani and Vivian Wasiuta for their assistance with IC analysis.

I would like to thank Dr. Rachel Chang, Dr. Steve Sjostedt, and Dr. Jon Abbatt from the University of Toronto for their assistance on board the *Amundsen* and their knowledge and data from the campaign; Dr. Michael Scarratt and Dr. Sonia Michaud from Maurice Lamontagne Institute and the Arctic-SOLAS group from the University of Laval for the DMS water concentrations, and Andrew Platt and the people at Environment Canada -

Climate Chemistry Measurements and Research for their assistance with sample collection at Alert and the extra time they placed in my project. For making this project possible I would like to acknowledge Dr. Maurice Levasseur and Arctic-SOLAS, ArcticNet, and CFL for organizing field campaigns, Dr. Sangeeta Sharma from Environment Canada for sharing her expertise and instruments for DMS analysis and Captain Lise Marchand and the crew of *CCGS Amundsen* for their care and assistance during the field campaigns.

My work would not have been completed without the funding provided by SOLAS, NSERC, and IPY. I am extremely grateful for their assistance.

I would like to thank all the administrative staff from the Chemistry, Physics, and Environmental Science departments at the University of Calgary. My life would have been much more complicated without you.

I would like to thank Vivian, Diana, and Josh for keeping me happy and relatively stress free throughout my PhD. Your presence was always welcomed and your willingness to go up and beyond to help me (sometimes without me even asking) whenever I needed it was greatly appreciated. I would also like to thank all my friends who have helped me, supported me or have given me stress relief through out my graduate studies (especially, Paul, Adam, Jyotsna, Jennifer, Terry, Andrea, Andrew, and Mandy). Lastly I would like to express my gratitude towards Jeff and Gisell and to my parents for encouragement during my time as graduate student. Their patience has meant everything to me.

Table of Contents

List of Tables

List of Figures and Illustrations

List of Symbols, Abbreviations and Nomenclature

Symbol	Definition
Asl	Above sea level
BLH	Boundary layer height
CCGS	Canadian Coast Guard Ship
CCN	cloud condensation nuclei
CF-IRMS	Continuous Flow Isotope Ratio Mass Spectrometer
CLAW	Charlson, Lovelock, Andreae and Warren
$\delta^{34}S_{nss}$	Non sea salt sulfate (and non frost flower) sulfate $\delta^{34}S$ value
$\delta^{34}S_{nss\text{-}c}$	Calculated non sea salt sulfate $\delta^{34}S$ value (without considering Frost flowers)
DMS	Dimethylsulfide CH_3SCH_3)
DMSO	Dimethylsulfoxide (CH_3SOCH_3)
$DMSO_2$	Dimethylsulfone ($CH_3SO_2CH_3$)
DMSP	Dimethylsulfoniopropionate $(CH_3)_2SCH_2CH_2COO^-$)
F	Flux
FaBRECC	Facility for Biogeochemical Research on Environmental Change and the Cryosphere
FF	Frost flower
FF_{ratio}	The SO_4^{2-}/Na^+ molar ratio for frost flowers
GC-SCD	Gas Chromatograph – Sulfur Chemiluminescence Detector
HH	High Halogen
HYSPLIT	Hybrid Single-Particle Lagrangian Integrated Trajectory
H_x	Henry's law coefficient
IC	Ion chromatography
ICP-MS	Inductive Coupled Plasma Mass Spectrometer
IPCC	Intergovernmental Panel for Climate Change
IPY	International Polar Year
ISL	Isotope Science Laboratory
IUPAC	International Union of Pure and Applied Chemistry
k	Rate coefficient
LH	Low Halogen
LP-DOAS	Long path differential optical absorption spectroscopy
lw	Fractional liquid water content
ODE	Ozone Depletion Events
OMI	ozone monitoring instrument
Ox	removal of DMS by oxidation
MSA	Methanesulfonic acid
MSIA	Methylsulfinic acid (CH_3SO_2H)
MSA_{BR}	Branching ratio for MSA (i.e., $MSA/(SO_{4bio}+MSA)$
NASA	National Aeronautics and Space Administration
NOAA	National Oceanic and Atmospheric Administration
NSS	Non-sea salt

P	Pressure
RH	Relative humidity
SCD	Sulfur Chemiluminescence detector
SOLAS	Surface Ocean Lower Atmosphere Study
SS	Sea salt
SS_{ratio}	X/Na molar ratio for sea salt (X=any other sea salt ion)
T	Temperature
TUV	Tropospheric Ultraviolet and Visible Radiation Model
UVA	Ultraviolet A (400 nm–315 nm)
UVB	Ultraviolet B (315 nm–280 nm)
τ	Chemical life time
VOCs	Volatile Organic Compounds

Chapter One: Introduction

Sulfur has many sources and sinks in the atmosphere and as sulfate can impact properties of aerosols which in turn can have an impact on climate forcing. The Intergovernmental Panel of Climate Change (IPCC) has attributed the largest uncertainty of anthropogenic radiative forcing in global climate modeling to the uncertainties associated with aerosols (Solomon et al., 2007). Sulfate is the largest water soluble component of aerosols in the Arctic (Barrie and Bottenheim, 1991). Increases of near surface air temperatures can lead to large decreases in yearly sea ice extent, reduced snow cover, and melting of permafrost making the Arctic one of the most environmentally sensitive areas on the Earth (Turner and Marshall, 2011). The study of sources and processes affecting the sulfur budget at northern latitudes will contribute to the understanding of anthropogenic influences affecting the global atmosphere.

1.1 Aerosols

Aerosols can affect the climate both directly by scattering incident radiation and indirectly as cloud condensation nuclei (Haywood and Boucher, 2000). Aerosols are often described based on their physical characteristics such as size since the lifetime and light scattering properties are determined by size distribution. Aerosols can be classified into three different size ranges; Aitken nuclei, the accumulation range and the mechanically generated range (coarse aerosols). These are shown in Figure 1.1. Lifetimes, i.e., the abundance of aerosol divided by the production rate, for coarse

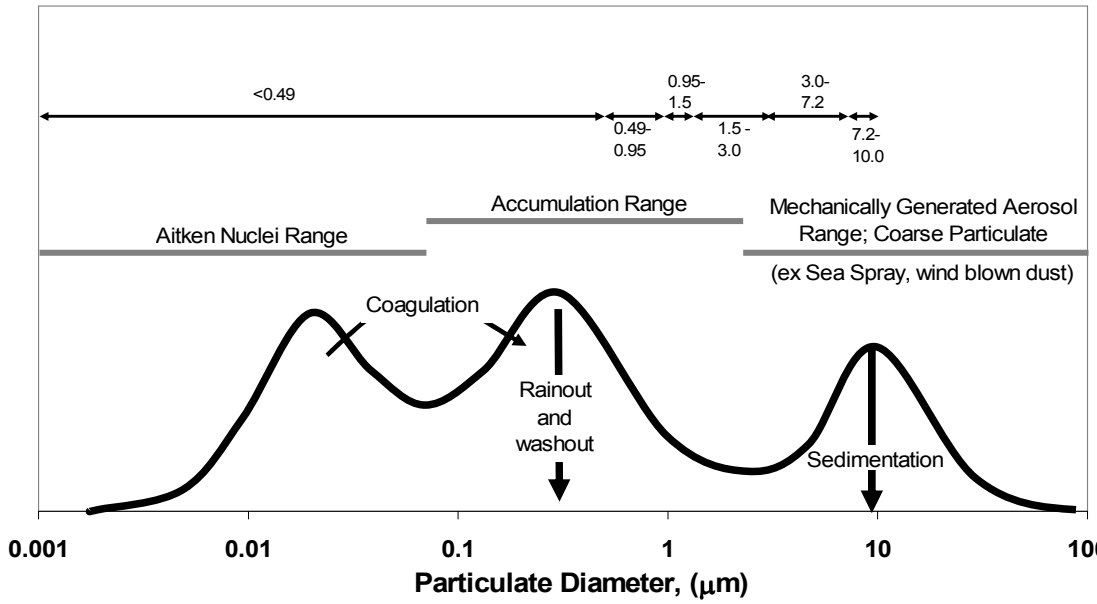

Figure 1.1 Schematic of atmospheric aerosol surface area distribution showing the size distribution of aerosols (Seguin, 2007 after Whitby, 1978).

aerosols are expected to be short (a few hours to one day) because of their removal by gravitational settling (Kaufman et al., 2002), while Aitken nuclei can condense quickly on existing aerosols. The lifetime of the accumulation mode is much longer (a few days to weeks) and long range transport of aerosols in this size range is possible (Kaufman et al., 2002). Many of the components found in aerosols in the Arctic are believed to be from long range transport and therefore in the accumulation mode (Cheng et al., 1993; Sirois and Barrie, 1999; Baltensperger and Furger, 2008).

Many studies to characterize aerosol components have been conducted in the Arctic (Li and Winchester, 1989*a*; Cheng et al., 1993; Sirois and Barrie, 1999; Ricard et al., 2002; Quinn et al., 2009). One of the largest sources of ions in aerosols, especially in the coarse

mode, is from mechanically generated aerosols at the sea surface (Baltensperger and Furger, 2008; Lewis and Schwartz, 2004). These aerosols have large amounts of ions associated with sea salt. Common constituents found in sea salt are found in similar ratios in aerosols when all ions are preserved. Some of these ratios are shown in Table 1.1. Since sea salt is a large contributor to aerosols, a calculation must be performed to determine the non sea salt contribution of ions. Assuming sea salt is the sole source of sodium in aerosols in the Arctic, a calculation can be made such that

$$X_{nss} = X_{measured} - Na_{measured} \cdot SS_{Ratio} \qquad 1.1$$

	mol/L (in sea water)	Cl^-	Na^+	Mg^{2+}	SO_4^{2-}	Ca^{2+}	K^+
Cl^-	547	1	1.16	10.3	19.5	53.4	54.6
Na^+	470	0.859	1	8.85	16.7	45.8	46.9
Mg^{2+}	53.1	0.0970	0.113	1	1.89	5.18	5.29
SO_4^{2-}	28.1	0.0514	0.0598	0.530	1	2.74	2.80
Ca^{2+}	10.3	0.0187	0.0218	0.193	0.365	1	1.02
K^+	10.0	0.0183	0.0213	0.189	0.357	0.978	1

Table 1.1 Molar ratios for common ions in sea water ([row]/[column]) (Seguin, 2007; concentrations from Maidment, 1993 and *CRC Handbook*, 2002)

where X_{nss} is the component X that is from non sea salt sources (where X = K^+, Ca^{2+}, Mg^{2+}, SO_4^{2-}, Cl^-, etc.), $X_{measured}$ is the measured concentration of that component, $Na_{measured}$ is the measured concentration of sodium and SS_{ratio} is the ratio between component X and Na^+ found in ocean water. This calculation can be made if and only if sea salt aerosols are the only source of Na^+ in the atmosphere which is most often the case.

If a negative value of X_{nss} is obtained, X_{nss} is considered depleted in the aerosol. Depletion of chloride and bromide in sea salt aerosols can occur because of the formation of gaseous inorganic chlorine or bromine components such HCl or HBr (Singh, 1995; Sander et al., 2003). $HCl_{(g)}$ is generally thought to form in acidic aerosols (Finlayson-Pitts and Pitts, 2000 and references within). Chloride in sea salt aerosols can react with acidic nitrogen and sulfur compounds by the following pathways (McInnes et al., 1994; Weis and Ewing, 1999; Sarin et al., 2010)

$$\mathbf{2NaCl_{(s)} + H_2SO_4 \rightarrow Na_2SO_{4(s)} + 2HCl_{(g)}} \qquad \mathbf{1.2}$$

$$\mathbf{NaCl_{(s)} + HNO_3 \rightarrow NaNO_{3(s)} + HCl_{(g)}} \qquad \mathbf{1.3}$$

Other mechanisms have been proposed for the release of chlorine and bromine from aerosols (Weis and Ewing, 1999; Laskin et al., 2003; von Glasow, 2008). Other gaseous products, including Cl_2, Br_2, ClNO and $ClNO_2$ among many others, may also be of importance for the deficit of chloride and bromide found in sea salt aerosols (Singh,

1995; Finlayson-Pitts and Pitts, 2000; von Glasow, 2008). Chloride depletion most often happens in areas of high pollution (Singh, 1995) but a chloride deficit has also been observed in the Arctic summer in Finland (Ricard et al., 2002). Chloride deficit in the Ricard et al. (2002) study coincided with air masses that had previously been in contact with both sea and continent (Scandinavia, Russia or central Europe) and therefore may have been influenced by both sea salt and pollution. A chloride deficit in aerosols has also been observed at Barrow during times when Arctic Haze is present (Quinn et al., 2009). Both nitrogen and sulfur components are significant components of Arctic Haze (Barrie and Bottenheim, 1991) and could influence the formation of $HCl_{(g)}$ when Arctic Haze is present.

1.2 Atmospheric Sulfur Sources

Sulfate in the atmosphere has many sources. Sea salt makes up one component (see Chapter 1.1) and natural sources of sulfate from volcanic and continental emissions (such as dust) can be of importance in many parts of the world (Bates et al., 1992*b*; Andrews et al., 2004). Biological sources of sulfur can contribute significantly to atmospheric sulfur loading especially in the remote marine atmosphere (Bates et al., 1992*b*; Faloona, 2009). Sulfur is an essential element in all biological organisms; organisms consist of approximately 0.25% dry weight of sulfur (Charlson et al., 1992). Sulfur in living organisms is usually in a reduced oxidation state and, when released into the atmosphere, will be eventually oxidized to form sulfate or other sulfur oxidation products (see Chapter 1.5.3). Anthropogenic sources such as the combustion of coal and oil can also release

sulfur into the atmosphere either as sulfate or SO_2 (Thode, 1991). Sulfur dioxide will oxidize further to sulfate in the atmosphere.

Two unique sources of sulfate in the Arctic also exist. An estimate of 2.7% of the Antarctic sea surface at any one time can be covered by frost flowers during the winter months (Rankin et al., 2002) and evidence of frost flowers in aerosols has been observed in the Arctic during fall months (e.g., Norman et al., 1999). The second source, located at 79º14`N 127º10`W is known as The Smoking Hills. Sulfur dioxide along with aerosols can be released in the atmosphere when exposed bituminous shale in sea cliffs are spontaneously ignited (Freedman et al., 1990).

1.3 Sulfur Isotopes

Sulfur isotopes can be used as a tool to aid in distinguishing between different sources of sulfur in the atmosphere (e.g., Nielsen, 1974; Newman et al., 1981, Roth et al., 2006). The two most abundant sulfur isotopes are ^{32}S and ^{34}S, which correspond to 95% and 4.33% of average crustal abundance (Charlson et al., 1992). A slight change in the average abundance of isotopes can occur as a result of mass selective reactions in nature. This fractionation of isotope abundance can be caused by both equilibrium and kinetic effects. More specific mass selective reactions include diffusion, evaporation, and biogenic sulfate-reduction processes (Thode, 1991; Johnson et al., 2002).

The deviations in sulfur isotope abundance, known as $\delta^{34}S$ values, can be expressed in parts per thousand (‰) as follows

$$\delta^{34}S = \left(\frac{(^{34}S/^{32}S)_{sample}}{(^{34}S/^{32}S)_{std}} - 1 \right) \times 1000 \qquad \textbf{1.4}$$

where ${}^{x}S$ is the amount of isotope x of sulfur and the subscripts denote values from the sample and from an international standard (Vienna-Canyon Diablo Troilite).

Sources can have various $\delta^{34}S$ values, and sources of sulfate considered in this thesis are displayed in Figure 1.2. The width of the bars displayed in Figure 1.2 represents minimum and maximum $\delta^{34}S$ values reported for each source, with the exception of dimethylsulfide (DMS) where the width represents analytical uncertainties (+17 ± 1.9‰; Calhoun, 1990). The $\delta^{34}S$ values of the fuel from the *Amundsen* were measured from the fuel that was used for the duration of study (Rempillo et al., 2011).

1.4 Arctic Atmosphere

The Arctic Ocean along with northern parts of North America, Greenland, Scandinavia, Russia and a number of islands are located in the Arctic. Geometrically, the Arctic is defined as the area north of 66º33’39”N and that have at least one day each year when the sun will not rise above the horizon (Turner and Marshall, 2011).

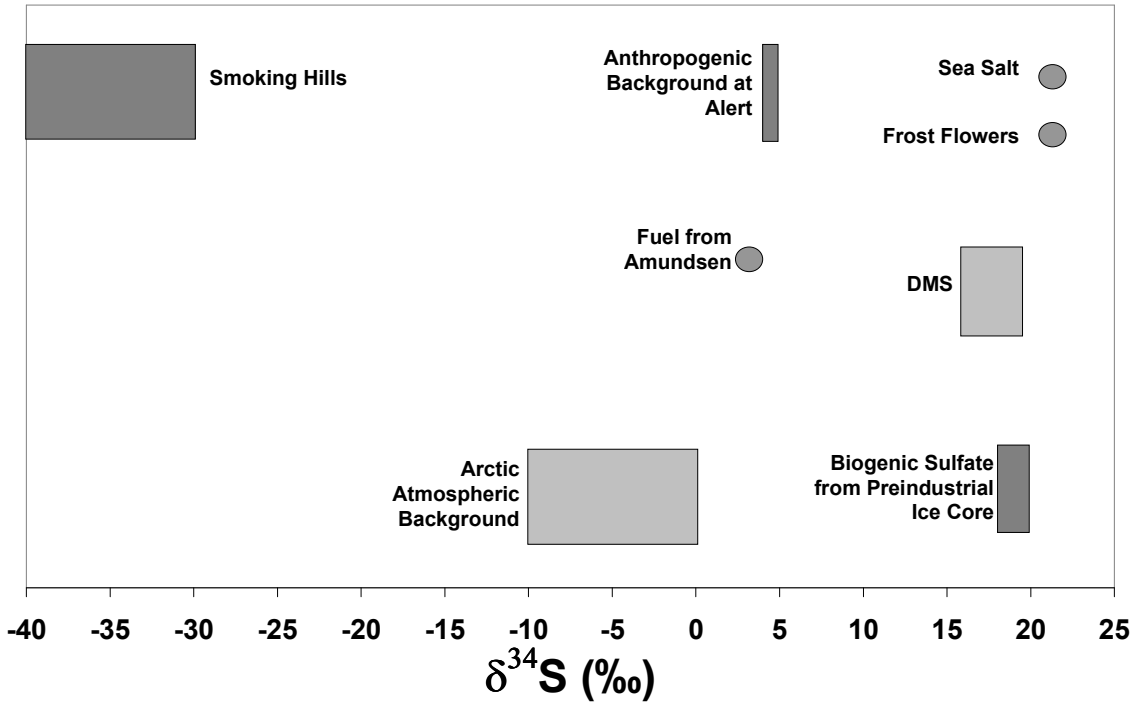

Figure 1.2 $\delta^{34}S$ values for some sulfur sources; width of bars indicate minimum and maximum $\delta^{34}S$ values expected in the Arctic for each of the sources, or, in the case of DMS, analytical uncertainties. (Sea salt from Rees et al. (1978), DMS from Calhoun (1990), Biogenic sulfate in ice core from Patris et al. (2000), Arctic atmospheric background, Fuel from *Amundsen* and Smoking Hills from Rempillo et al. (2011), Anthropogenic Background at Alert and Frost flowers from Norman et al., submitted)

Large changes in temperature are predicted in Polar Regions in response to global warming and the potential for positive feedback loops make the Arctic more susceptible to climate change than other areas of the world (Solomon et al., 2007). Summer sea ice extent in the Arctic reached a record minimum in 2007 and 2008 with multi-year ice

being reduced in extent and thickness (Fisheries and Ocean Canada, 2010). Minimum sea ice extents from the last 5 years are the lowest in satellite record (Perovich et al., 2011) with minimum sea ice extent in 2011 covering 3.33 million km^2, only 0.16 million km^2 greater than the 2007 record (Perovich et al., 2011). Sea ice conditions affect albedo which by definition affects the amount of solar radiation that is absorbed by the surface. The exchange of heat between the ocean and the atmosphere is affected by sea ice since sea ice can act as a barrier between ocean and atmosphere trace gas exchanges (Weeks, 2010).

1.4.1 Arctic Haze

The atmosphere of the Arctic is influenced by anthropogenic sources to a greater extent than the Antarctic atmosphere. Emissions from Eurasia and North America can contribute to pollutant and aerosol loading by long range transport especially during the winter when the north polar vortex extends southward (Baltensperger and Furger, 2008) leading to an increase of pollutants over the Arctic referred to as Arctic Haze. The term Arctic Haze was first used in the 1950s to describe the low visibility that was observed during flights in the Alaskan Arctic (Barrie, 1986 and references within). Aerosols found in Arctic Haze are similar to the chemical composition of smog in more polluted areas (Turner and Marshall, 2011).

Arctic Haze occurs in late winter and early spring when the polar vortex is at a maximum (Baltensperger and Furger, 2008). The aerosol light scattering coefficient between

January and April can be twenty to forty times higher than between June and September (Barrie et al., 1981). Removal mechanisms during the polar night for pollutants are slow because of the cold and stable atmosphere (i.e., little to no vertical mixing in the atmosphere), precipitation is minimal and no photochemistry occurs. Slow removal rates allow precursor gases and aerosols of Arctic Haze to build up in winter months (Quinn et al., 2007).

1.4.2 Ozone Depletion Events

Ozone depletion events (ODE) in the Arctic troposphere during the polar spring have also been the subject of many studies (Barrie et al., 1988; Simpson et al., 2007*b* and references within). Ozone concentrations at ground level during ODE rapidly decrease to concentrations close to zero (Finlayson-Pitts and Pitts, 2000). Elevated reactive halogen concentrations in the atmosphere, especially BrO· have been linked to these ODE. The bromine radical can react with ozone to produce BrO· and O_2. The BrO· can either photodissociate or react with itself or ClO· to produce more bromine radicals, which in can in turn can destroy more ozone (Finlayson-Pitts and Pitts, 2000; Bottenheim et al., 2002).

The mechanism by which bromine is activated from sea salt bromide to reactive atmospheric bromine is still uncertain (Morin et al., 2008) and it is unresolved why these events occur only during the polar spring. Suggestions regarding the importance of frost

flowers to the bromine chemistry have been discussed in a number of recent papers (e.g., Kaleschke et al., 2004; Morin et al., 2008; Simpson et al., 2007*a*).

1.4.3 Frost Flowers

Frost flowers are a significant source of sodium in the Antarctic winter (Wagenbach et al., 1998; Rankin et al., 2002) with as much as 60% of the yearly sodium in aerosols at coastal sites originating from brine or frost flowers (Rankin and Wolff, 2003). Evidence of frost flowers contributing to ion loading in Polar Regions have been observed in ice cores, precipitation and aerosols (Minikin et al., 1998; Rankin et al., 2002; Rankin and Wolff, 2003). Recent studies of frost flowers have focused on their role in atmospheric reactions such as mercury depletion events (Douglas et al., 2005, Sherman et al., 2012) and halogen chemistry (Morin et al., 2008; Piot and von Glasow, 2008; Douglas et al., 2012).

Frost flowers are formed on young sea ice surfaces. Small nodules (ice bumps) are formed on newly formed sea ice only a few cm thick. (Perovich and Richter-Menge, 1994). A large temperature gradient between seawater and the air above the water surface leads to water vapour saturation which can result in water vapour condensing onto the nodules. Within a few hours as the temperature decreases and the sea ice grows in thickness, brine on the sea ice surface can be drawn or wicked up onto the frost flowers. Concentrations of major ions are elevated immediately following formation (Douglas et al., 2012) because of the brine.

As the brine cools and loses water to the atmosphere by evaporation, salts remain on the frost flower and precipitate out. At -8º C, sodium and sulfate precipitate out as mirabilite ($Na_2SO_4 \cdot 10\ H_2O$) (Alvarez-Aviles et al., 2008). This can lead to a lower sulfate/sodium ratio in frost flowers relative to sea salt. A detailed discussion on the formation of frost flowers and the fate of mirabilite is conducted by Alvarez-Aviles et al. (2008). Frost flower contributions in aerosols are found in the large aerosol size fraction (Rankin and Wolff, 2003) since they are primary aerosols. Frost flowers can withstand gusts of winds (Obbard et al., 2009; Roscoe et al., 2011) but as frost flowers dry they are expected to become more fragile leading to possible contributions of frost flower in Arctic aerosols (Alvarex-Aviles et al., 2008).

1.5 Biogenic Sulfur in the Arctic

Dimethylsulfide (DMS) is the largest contributor to biogenic sulfate in the Arctic atmosphere (e.g., Leck and Persson, 1996*b*; Nilsson and Leck, 2002). During summer and early fall, high biological productivity in the Arctic Ocean can lead to gas phase transfers between the ocean and the atmosphere. DMS concentrations over the Arctic Ocean have been studied in the past (e.g., Sharma et al., 1999; Kerminen and Leck, 2001; Gabric et al., 2005) but simultaneous measurements of DMS, SO_2, aerosol MSA and biogenic sulfate along with other species important to DMS oxidation in the Arctic have not been performed previously.

1.5.1 The CLAW Hypothesis

The CLAW (Charlson, Lovelock, Andreae and Warren) hypothesis predicted a possible mechanism for cloud formation and climate feedback linked to the biota of the Earth (Charlson et al., 1987). It proposed that the 3-dimethylsulfoniopropionate (DMSP, $(CH_3)_2SCH_2CH_2COO^-$) released by phytoplankton in the ocean, could increase DMS concentrations in the air. DMS, once in the air, oxidizes to a number of products including gaseous H_2SO_4. $H_2SO_{4(g)}$ can scatter incident solar radiation and has the potential to nucleate and form new cloud condensation nuclei (CCN). These cloud condensation nuclei could influence cloud cover and increase cloud albedo which would decrease global temperature and in turn decrease the productivity of surface ocean biota (and hence hinder DMSP release); completing the negative feedback loop (Charlson et al., 1987). Since publication, the CLAW hypothesis has been referenced over 2000 times and has initiated many field campaigns in oceanic, atmospheric and climate sciences. Although it is now doubtful that the CLAW hypothesis alone accounts for such strong climate implications, it has introduced better appreciation of the complexity of biogeochemistry and climate physics involved (Quinn and Bates, 2011).

1.5.2 Dimethylsulfide Flux

Dimethylsulfide was first proposed to be an important component of the natural sulfur cycle in 1972 by Lovelock and colleagues (1972). DMS is derived from DMSP released from phytoplankton in the ocean (Charlson et al., 1987). Dimethylsulfide has a low

solubility in water with a Henry's law constant equal to 1.5 M/atm at 0 °C (Barnes et al., 2006) and therefore the ocean is often supersaturated with respect to DMS (Yang et al., 2011). DMS will therefore be released into the atmosphere from the ocean surface. The flux of a gas emitted from the ocean is given by

$$F = k \cdot \Delta C \qquad 1.5$$

where F is gas flux, ΔC is the concentration disequilibrium (units: moles/volume) and k is the overall transfer velocity (also called the gas transfer velocity or gas exchange coefficient) with units length/time. The concentration disequilibrium (ΔC) is dependent on the gas concentration in the water and to a lesser extent on the concentration in the overlying atmosphere and the Henry's law constant (Zemmelink, 2003; Seguin, 2007). The overall transfer velocity is dependent on wind speed and the Schmidt number of the gas in question (e.g., Yang et al., 2011; Ho et al., 2011). The Schmidt number for DMS is equal to

$$Sc_{DMS} = 2674.0 - 147.12T + 3.72T - 0.038T \qquad 1.6$$

where T is the temperature of the water in °C (Saltzman et al., 1993). The dependency of the overall transfer velocity on wind speed is based on past measurements (e.g., Liss and Merlivat, 1986; Nightingale et al., 2000; Ho et al., 2011). Measurements are usually normalized to carbon dioxide with the following equation

$$k_{gas1} = k_{CO_2}\left(\frac{Sc_{gas1}}{Sc_{CO_2}}\right)^{-n} \quad \textbf{1.7}$$

where k_x is the gas transfer velocity and Sc_x is the Schmidt number of each of the respective gasses and n is the Schmidt number exponent dependent on water surface characteristics (Liss and Merlivat, 1986). A number of relationships between wind speed and gas transfer velocity have been proposed. For example, Nightingale et al. (2000) carried out direct measurements of trace gases and found a best fit value of

$$\mathbf{k_{CO_2} = 0.222u^2 + 0.333u} \quad \textbf{1.8}$$

for the gas transfer velocity (k_{CO2}) in cm/h, where u is the wind speed (m/s) at a height of ten meters above the surface of the water. Other parameterizations that have been proposed for the relationship between gas transfer velocity and wind speed are reviewed in detail by Zemmelink (2003), Elliot (2009) and Yang et al. (2011).

1.5.3 Dimethylsulfide Oxidation

Once DMS is released into the atmosphere it is oxidized. Biogenic sulfate in the Arctic atmosphere comes from dimethylsulfide (DMS) oxidation. DMS oxidation, besides sulfate, can form a number of other oxidation products including two others that were

measured in this thesis; methanesulfonic acid (MSA) and SO_2. The study of DMS oxidation gives insight into biogenic loading in the atmosphere.

Atmospheric DMS can be oxidized by a range of oxygenated molecules including OH·, NO_3·, reactive halogens (e.g., Cl·, BrO·) or it can oxidize in or on aerosols (i.e., aqueous O_3 oxidation) (See Figure 1.3). The oxidation of DMS leads to a number of products and intermediates. These include methanesulfonic acid (MSA), dimethylsulfoxide (DMSO), dimethylsulfone ($DMSO_2$), methylsulfinic acid (MSIA), sulfate (SO_4^{2-}) and sulfur dioxide (SO_2) (Yin et al., 1990; Bandy et al., 1992; Berresheim et al., 1995; Barnes et al., 2006). DMS is oxidized in two ways; abstraction or addition. The abstraction pathway can occur when DMS reacts with Cl·, OH· or NO_3· to abstract hydrogen from DMS. The product of this reaction reacts with oxygen gas to produce CH_3SCH_2OO·. This radical, with further reactions, will eventually lead to the formation of CH_3SO_2· (see Figure 1.3). CH_3SO_2· can react to form either SO_2 via thermal decomposition or other side products by oxidation including MSA and H_2SO_4. SO_2 can be taken up into aerosols or produce H_2SO_4 in the gas phase. $H_2SO_{4(g)}$ may undergo binary nucleation and has the potential to form new cloud condensation nuclei but in most cases will be taken up on existing aerosols (Rempillo et al., 2011).

The addition pathway occurs when XO· (X = H, Cl, Br) radicals or O_3 react with DMS to form DMSO (CH_3SOCH_3) and is more prevalent at lower temperatures (Barnes et al., 2006). DMSO in the gas phase can be oxidized further to $DMSO_2$ (dimethylsulfone; $CH_3SO_2CH_3$) or MSIA (methylsulfinic acid, CH_3SO_2H). MSIA can form MSA or

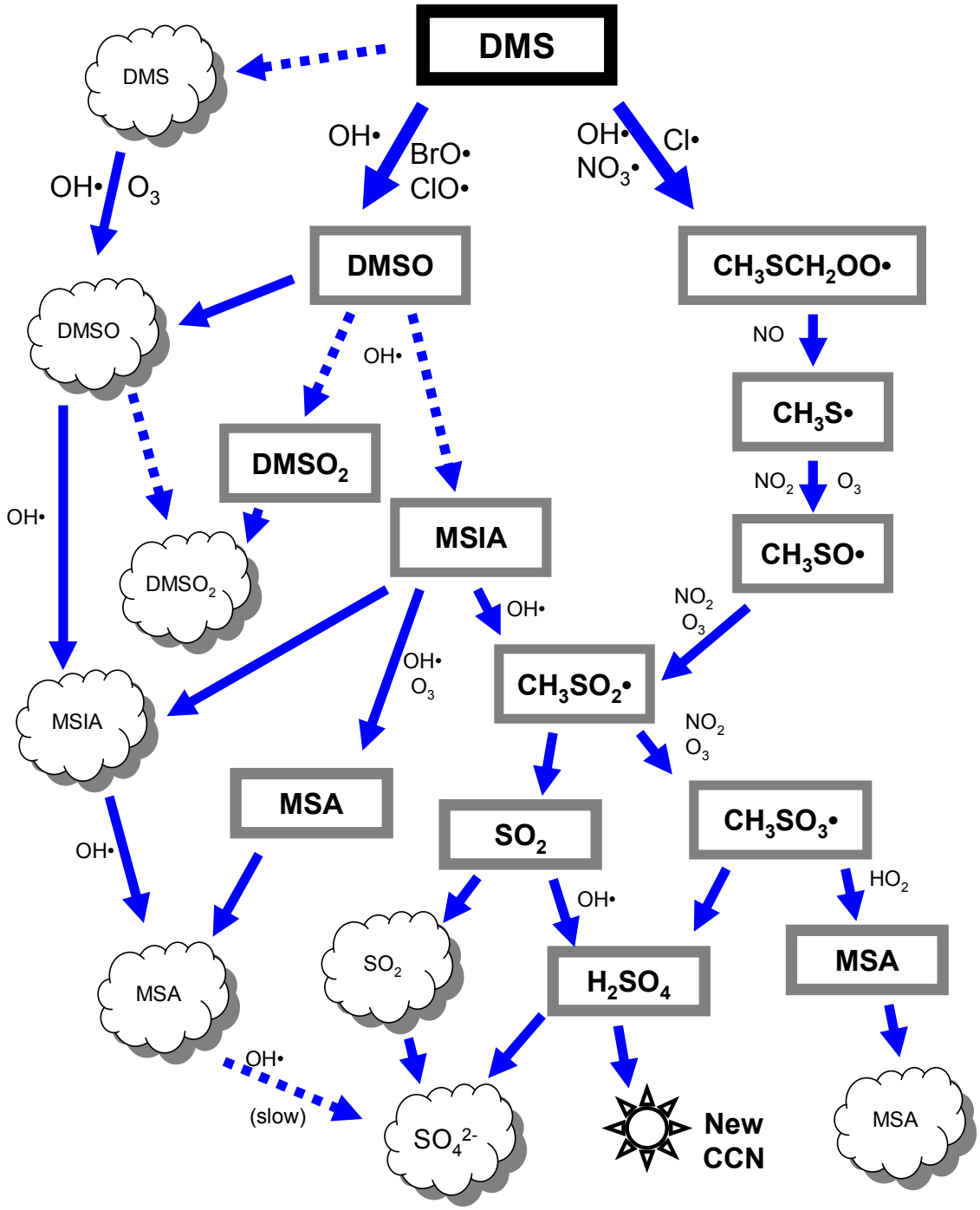

Figure 1.3 Simplified DMS oxidation pathways in the gas and aqueous phase (Modified from von Glasow and Crutzen, 2004).

$CH_3SO_2\cdot$. DMSO, $DMSO_2$ and MSIA are all highly soluble in water (Barnes et al., 2006) and their oxidation in the gas phase is expected to be minimal when aerosols and clouds are present (von Glasow and Crutzen, 2004).

DMS can also be oxidized in aerosols. Although DMS is not very water soluble, the high rate constants for oxidation in aqueous solutions can lead to significant oxidation of atmospheric DMS (Glasow and Crutzen, 2004; Barnes et al., 2006). DMS in aerosols can react with $OH\cdot$ and O_3. The aqueous oxidation of DMS by $OH\cdot$ is expected to be minor compared to gas phase $OH\cdot$ oxidation of DMS. In contrast, DMS oxidation by O_3 in clouds is expected to be higher than gaseous oxidation from O_3 (Gershenzon et al., 2001; Barnes et al., 2006). O_3 is present throughout the day (unlike $OH\cdot$ which reacts quickly and is depleted with lack of sunlight), and therefore the contribution of O_3 to the oxidation of DMS can occur throughout the day (Barnes et al., 2006). The oxidation from both of these radicals leads, in most cases, to the formation of DMSO.

Aqueous oxidation of DMSO will lead most likely to the MSIA intermediate before forming MSA. Some formation of $DMSO_2$ is possible but is expected to be small (Barnes et al., 2006). MSA can further react to produce sulfate (von Glasow and Crutzen, 2004) in aerosols but is expected to form at most approximately 10% of non sea salt sulfate in aerosols if in cloudy conditions and in cloud free conditions the reaction is expected to be unimportant (von Glasow and Crutzen, 2004).

1.6 Arctic SOLAS

The Canadian Surface Ocean – Lower Atmosphere Study (SOLAS) has conducted campaigns over the Pacific (2002) and Atlantic (2003) Oceans. Arctic SOLAS, in partnership with the International Polar Year (IPY), explored the interactions between sea ice, water circulation, marine microbiological activities and emissions of gases (CO_2 N_2O, VOCs, halocarbons and dimethylsulfide) from the Arctic Ocean. One of the key questions of this campaign is how gas transfer would be affected by a reduction in sea ice cover and increased areas of open ocean (Fisheries and Oceans Canada, 2010). Arctic SOLAS conducted research over two measurement periods aboard the Canadian Coast Guard Ship (*CCGS*) *Amundsen* between September and November 2007 and September and October 2008.

1.7 Objectives

The extent to which long range transport of aerosols affect the spatial distribution of sulfate loading in the Arctic is largely unknown. Barrie and Bottenheim (1991) compared a number of sites in the Arctic to determine sources of sulfate pollution. Long term measurements have also been conducted to examine trends associated with aerosol sulfur components in the Arctic (Cheng et al., 1993; Sirois and Barrie, 1999; Quinn et al., 2009). However, information on the spatial distribution of the aerosol sulfate contributions across the Arctic and how their size distribution change from one location to another is lacking. This study aims to address this issue.

Biogenic sulfur in the Arctic atmosphere is important because it has the potential to either warm or cool the atmosphere (e.g., Haywood and Boucher, 2000; von Glasow and Crutzen, 2004). Droplets in low clouds may incorporate local DMS oxidation products, enlarging the aerosols leading to darker clouds and reducing outgoing longwave radiation. In contrast, a cooling effect would result if DMS oxidation products are not incorporated into local cloud but instead either form new aerosols or are transported to higher altitudes where they scatter incident radiation back to space (Blanchet and Girad, 1995; von Glasow and Crutzen, 2004). In both of these latter two cases, the spatial distribution of biogenic sulfur would be more uniform than the case of local DMS oxidation.

Although DMS concentrations over the Arctic Ocean have been studied in the past (e.g., Sharma et al., 1999; Kerminen and Leck, 2001; Gabric et al., 2005) simultaneous measurements of DMS, SO_2, aerosol MSA and biogenic sulfate have not been conducted before in the Arctic. Sulfur isotopes can be used to aid in distinguishing between biogenic sulfur and other sources of sulfur (Nriagu et al., 1991; Li and Barrie, 1993; Norman et al., 1999; Rempillo et al., 2011; Norman et al., submitted). None of the previous aerosol sulfur isotope studies in the Arctic have looked at multiple locations over the same time period. Simultaneous measurements of atmospheric sulfur isotopes at different locations would aid in determining how uniform the spatial distribution of biogenic sulfur species is in the Arctic. A study of DMS and its major oxidation products will assist in investigating the importance of the influence of each DMS oxidation

pathway in the Arctic environment and aid in the understanding of biogenic sulfur loading and distribution in the Arctic.

Biogenic SO_2 has not been measured before in the Arctic because the contribution of biogenic SO_2 loading is usually masked by the long range transport of anthropogenic SO_2. SO_2 is an intermediate in the DMS oxidation pathway and if oxidized in the gas phase has the potential to form new CCN. With the use of sulfur isotopes, biogenic SO_2 concentrations and distribution in the Arctic atmosphere can be studied for the first time.

Other sources besides biogenic sulfate can contribute to aerosol loading in the Arctic. Transport and lifetime of these aerosols can affect the radiative forcing in the Arctic atmosphere (Shaw, 1991). Primary sea salt aerosols are often thought to occur in the larger size fraction (Chapter 1.1) and hence have a shorter life time than secondary aerosols. Sea salt aerosols, though, as they age can release gaseous halogen components into the atmosphere (Chapter 1.1). These halogens can have the potential to influence DMS oxidation. The presence of sea salt aerosol would also increase the potential for gaseous sulfur components, such as the products of DMS oxidation, to be taken into existing aerosols instead of forming new CCN. The presence of anthropogenic aerosols may lead to an increase in oxidation of gaseous sulfur compounds on or within existing aerosols. Anthropogenic contributions can lead to acidification of aerosols and can alter the chemical makeup of aerosols. A spatial comparison of sea salt and anthropogenic loading in the Arctic would aid in determining possible long range effects of these aerosols on the Arctic atmosphere.

The analysis of size segregated samples will aid in the understanding of how sulfur species are distributed in the atmosphere. Aerosols in the accumulation mode (Chapter 1.1) are expected to have a longer life time than those of larger aerosols (Kaufman et al., 2002) and therefore the study of size segregated samples may give insight between local and regional contributions. Comparison between size distributions at different locations can give insight into the extent that aerosol size has on chemical composition and long range transport. Consistency of size distribution in aerosols between locations is also of interest when looking at possible local conditions affecting aerosols.

Aerosol sampling was carried out in the Arctic during Fall 2007 and 2008. Aerosol ion concentrations and sulfur isotope values of aerosols collected at Alert and on board the *Amundsen* were determined. The findings presented in this thesis are a part of the Arctic SOLAS dataset to aid in the understanding of interactions between marine microbiological activity and the emissions of gases over the Arctic Ocean.

Aerosols and SO_2 samples were collected on board the *Amundsen* and at Alert, Nunavut to determine the influence of local versus regional effects of atmospheric sulfur chemistry in the Arctic. Spatial resolution of sulfur along with other compounds in aerosols will be used to look at local and regional effects in the Arctic environment.

A DMS oxidation model will be used to study the DMS oxidation pathways in the Arctic atmosphere with the onset of winter. MSA branching ratios modeled from the DMS oxidation rates will be compared to measured branching ratios found in aerosols to

determine the importance of the different oxidation pathways and oxidants in the Arctic atmosphere.

Chapter Two: Methods

2.1 Field Location

Measurements were conducted in the Canadian archipelago on board the *Canadian Coast Guard Ship (CCGS) Amundsen* and at Alert, Nunavut during the onset of winter in 2007 and 2008 which allowed for examination of regional and local effects of sulfur loading in the Arctic. Aerosol, SO_2 and DMS samples were collected aboard the *Amundsen* in the fall of 2007 and 2008 in partnership with Arctic SOLAS (Chapter 1.6). Aerosol and SO_2 samples were also collected at the Environment Canada station located at Alert, Nunavut (82º30 N, 62º30 W). Sampling locations are displayed in Figure 2.1.

2.2 Weather Parameters

Temperature, relative humidity, wind speed and air pressure were measured by the *Amundsen*'s meteorological station (Table 2.1) located on the ship's front mast. A summary of temperature, wind speed and relative humidity reported by Rempillo (2011) is displayed in Figure 2.2. Flux calculations by Rempillo (2011) (Chapter 6.6.2) used additional wind measurements conducted by Dr. Papakyriakou's group from the University of Manitoba (Table 2.1) from a meteorological tower on the foredeck of the *Amundsen* 14 meters above sea level (Else et al., 2011).

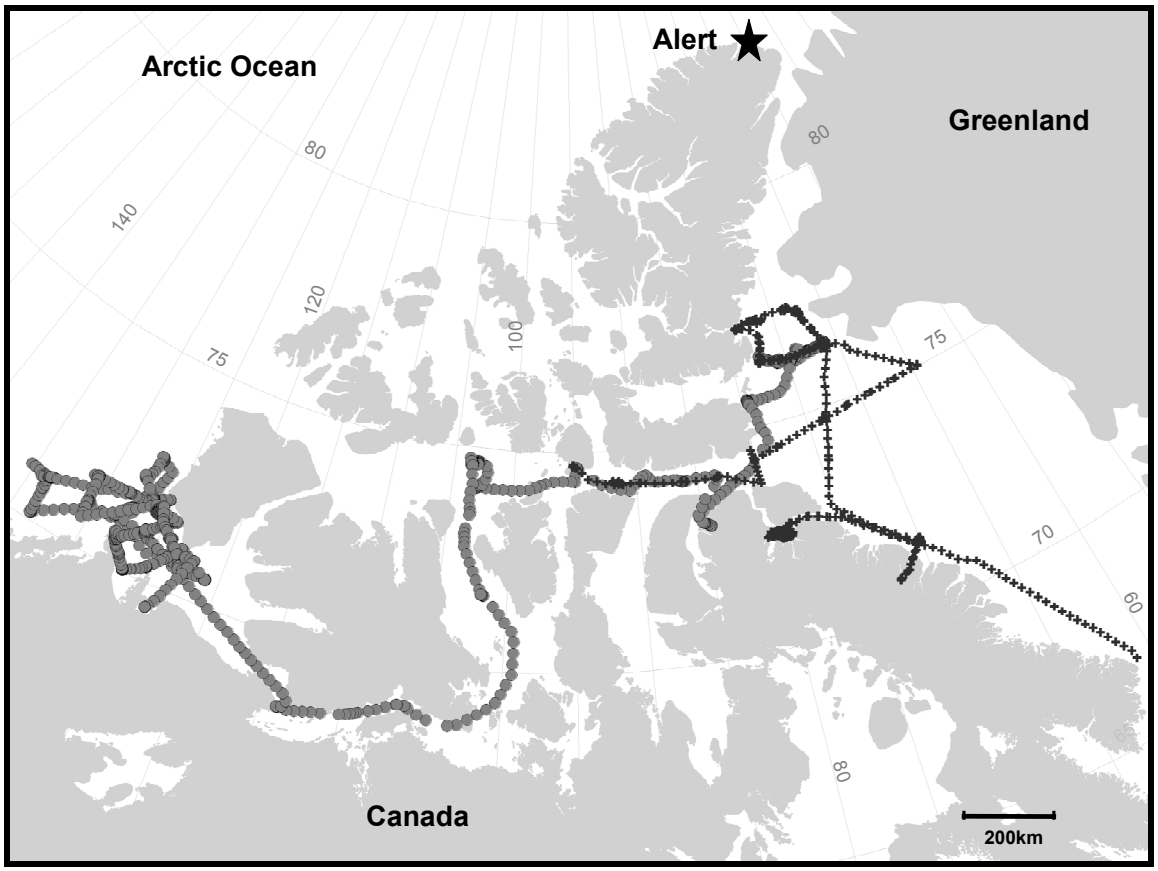

Figure 2.1 Sampling locations. Stationary location at Alert, Nunavut is displayed with a star. Route of the *Amundsen* is displayed with grey circles (2007) and black crosses (2008) with each point representing one hour intervals.

Weather parameters including temperature, relative humidity, pressure, wind speed and wind directions for Alert are archived hourly by Environment Canada (Environment Canada, 2011; Table 2.1). Average air temperature, wind speed and relative humidity for each sampling period (for size segregated samples) at Alert are shown in Figure 2.3

Measurements	Sample Set and Analysis	Personnel
Weather parameters	*Amundsen*	*Amundsen* crew, Papakyriakou group; University of Manitoba summarized by Rempillo (2011)
	Alert	Environment Canada (2011)
High Volume Samples	*Amundsen* • In field Collection	O. Rempillo A.M. Seguin
	• Laboratory processing	O. Rempillo
	• Isotope Analysis (PRISM)	O. Rempillo *
	• Ion Concentration (IC)	O. Rempillo †
	Alert • In Field Collection	Environmental Canada –Climate Chemistry Measurements and Research personnel
	• Laboratory processing	A.M. Seguin
	• Isotope Analysis (PRISM)	A.M. Seguin *
	• Ion Concentration (IC)	A.M. Seguin †
DMS Samples	*Amundsen* • In Field Collection	O. Rempillo A.M. Seguin A.-L. Norman ‡
	• Analysis (GC – SCD)	O. Rempillo A.M. Seguin A.-L. Norman ‡

* Prism was run by ISL laboratory personal
† Assistance with instrumental set up and trouble shooting was given by Farzin Malekani (Calgary), Vivian Wasiuta (FaBRECC) and the Arctic & Alpine Research Group under Dr. Martin Sharp (University of Alberta)
‡ 2007 only

Table 2.1 A list of key measurements conducted for the work presented in this thesis and the principle personnel responsible for each analysis

2.3 DMS Measurements

Atmospheric dimethylsulfide was measured on board the *Amundsen* (Table 2.1). Sampling was performed approximately every hour in 2007 and every 1.5 hours in 2008. Dimethylsulfide was analyzed using a Hewlett Packard 5890 Gas Chromatograph equipped with a Sievers sulfur chemiluminescence detector (GC- SCD). Collection and

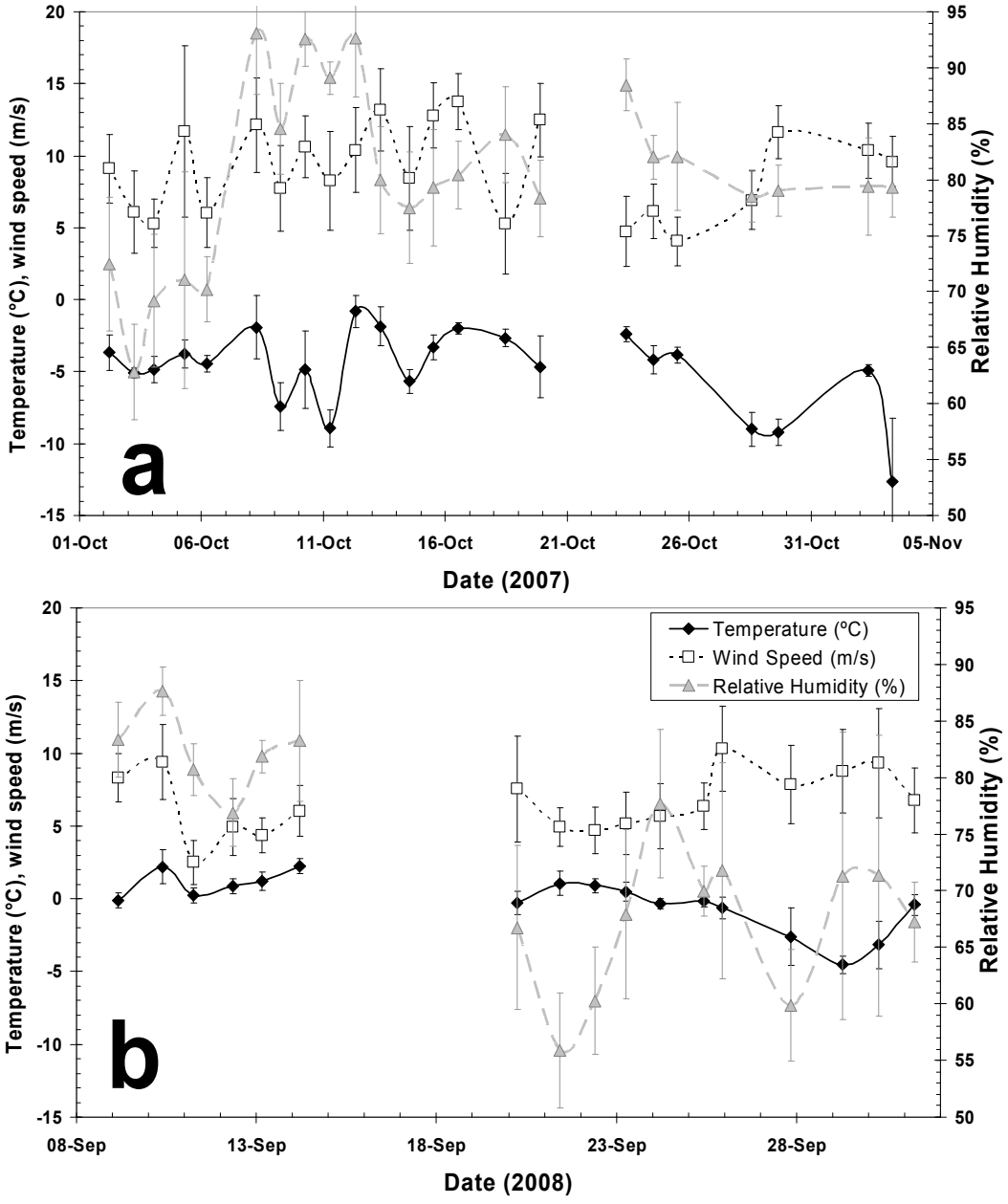

Figure 2.2 Temperature, wind speed and relative humidity averages coincident with sampling times of 2007 (a) and 2008 (b) on board the *Amundsen* (data reported by Rempillo, 2011).

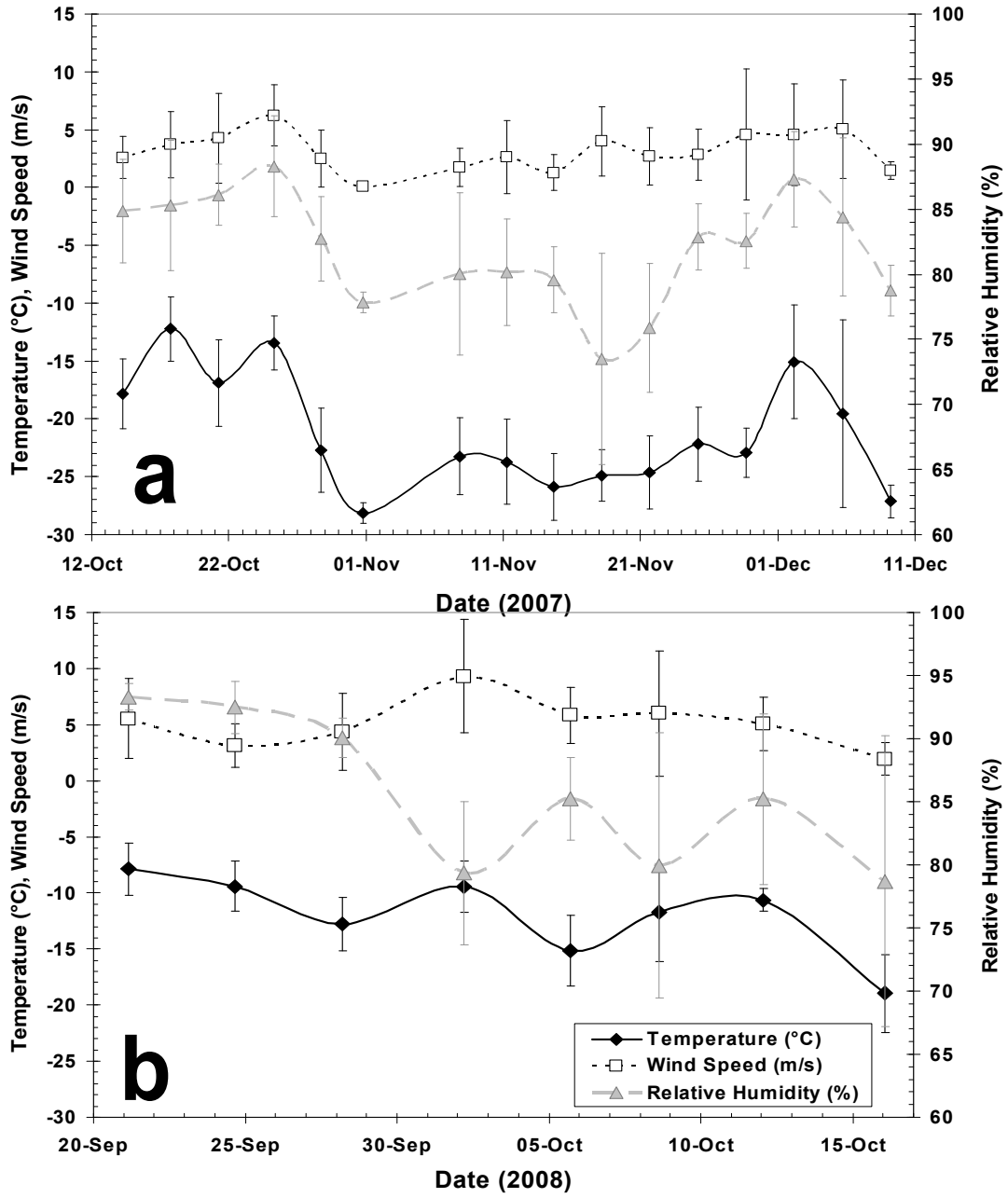

Figure 2.3 Temperature, wind speed and relative humidity averages coincident with sampling times of 2007 (a) and 2008 (b) at Alert. Hourly meteorological data from Alert (Environment Canada, 2011) was used to obtain averages.

analysis methods were similar to methods presented by Levasseur et al. (1997), Sharma et al. (1999) and Seguin (2007) and are explained in detail by Rempillo (2011). Error associated with DMS measurements is approximately 12% (Sharma et al., 1999; Rempillo, 2011)

2.4 High Volume Sampling

High volume samplers were deployed on board the *Amundsen* and at Alert (Table 2.1). Two high volume samplers were in operation for this study at each location. One collected total particulate matter and SO_2. The other was fitted with a cascade impactor to collect size segregated aerosol samples. Six different size bins were collected; < 0.49 μm, 0.49-0.95 μm, 0.95-1.5 μm, 1.5-3.0 μm, 3.0-7.2 μm, and > 7.2 μm aerodynamic diameter. The high volume sampler on board the *Amundsen* with the cascade impactor was fitted with a PM10 head and therefore the largest diameter size aerosols would have diameters between 7.2 μm and 10 μm. Particle size cut off with unity mass density at 25ºC and one atmosphere for spherical particles is at 50% collection efficiency (Tisch Environmental, 2004).

At Alert, a few hundred to more than a thousand kilometres north of the *Amundsen* traverse, the high volume sampler that collected size segregated samples was located at 82° 26.99' N, 62° 31.76' W (elevation 191m). The impact of blowing snow was mitigated by a specially designed housing to exclude snow as much as possible around the high volume sampler. The second high volume sampler for total aerosols and SO_2

was located approximately 200 meters away from the first (82° 27.05' N, 62° 30.49' W; elevation 180m) on the roof of a building (7 meters above ground). Total aerosol samples from this high volume sampler may have included blowing snow since this sampler was not contained within the protective housing. Because of mechanical failure, the total aerosol high volume sampler did not collect samples between October 18 and November 2 in 2007.

Determining the length of sampling time for High Volume Samplers is a balance between attempting to have the finest time resolution as possible, having enough sulfur on the sample size to be able to determine sulfur isotope ratios (e.g., Norman et al., 1999) and having the personnel to collect the samples. Total particulate matter and SO_2 samples were collected daily and size segregated periods were collected approximately every three days on board the *Amundsen*. Samples at Alert were collected two or three times a week by Environment Canada personnel (Table 2.1) for total particulate matter and SO_2 samples and twice a week for the size segregated samples.

2.4.1 High Volume Sampler Calibration

High volume samplers on board the *Amundsen* were operated at a flow rate of 1.10 ± 0.03 m^3/min and 1.00 ± 0.14 m^3/min for the size segregated and total particulate matter samplers respectively (Rempillo et al., 2011). Calibration of the instruments were carried out using a Kurz Instrument Inc. Model 341 High volume Sampler Calibrator for the total aerosol high volume sampler and a Tisch Environmental, Inc. TE-5028 Variable

Resistance Calibration Kit (Tisch Environmental, 2004) for the high volume sampler collecting size segregated samples. The two calibration methods were compared in the laboratory at the University of Calgary and found to be within 5%.

Flow rates were calibrated by Environment Canada at Alert. The high volume sampler collecting size segregated samples was operated at a flow rate of 1.21 ± 0.02 m^3/min in 2007 and 1.23 ± 0.02 m^3/min in 2008. The high volume sampler belongs to Environment Canada and is calibrated approximately every six months in accordance with Environment Canada protocols. It is worthwhile noting that the cut off for the size segregated samples is dependent on the flow rate of the high volume sampler (Tisch Environmental, 2004). Particle size cut off at 50% collection efficiency for spherical particles (mass density = 1) at standard temperature and pressure is <0.49um, <0.95um, <1.5um, <3.0, <7.2 and >7.2um at 1.13 m^3/min (Tisch Environmental, 2004). The slightly higher flow rate would result in a bias towards a higher cut off diameter for each size range.

Flow rate for the total particulate matter/SO_2 high volume sampler at Alert was measured to be 1.02 ± 0.03 m^3/min by Environment Canada personnel using the Kurz High Volume Sampler Calibrator. This is the maximum possible flow rate, as the flow rate controller was bypassed at the time of calibration. The flow rate controller is used to keep the flow rate constant when filter loading reduces pore spaces. When the flow controller system is bypassed the flow through the high volume sampler may decrease over time. The flow rate controller was bypassed for a majority of the sampling periods (i.e., after the high

volume sampler malfunction on November 2, 2007). This oversight was not discovered by Environment Canada personnel until the end of the sampling period in 2008. Pressure within the high volume sampler was recorded during some of the sampling periods (between 7.8 and 9.0 mm H_2O). Tests of the high volume sampler flow rate were conducted when that particular sampling unit was returned to Calgary. Pressure within the high volume sampler changed when the flow of the high volume sampler was purposely restricted. During sampling periods at Alert, pressure within the high volume sampler remained relatively constant (i.e., pressure at the start of the sampling period was usually the same as the end pressure with a maximum pressure difference of 0.8 mm H_2O). This pressure recorded at Alert corresponded to pressure that was found in Calgary when minimal restriction on flow occurred. Therefore the loading of the filters during sampling times in Alert had minimal impact on instrumental pressure and thus flow rate would also remain relatively consistent.

Another way to confirm that the flow rate was relatively constant on the high volume sampler collecting total aerosol samples is to compare the samples collected from it to the samples collected with those of the high volume sampler that collected size segregated samples. High volume samplers had overlapping sampling periods in both 2007 and 2008. If concentrations of the ions are compared between the two high volume samples and have low correlation it would support that the one high volume sampler did not have a constant flow. Correlation of the major ions (chloride, sulfate, sodium, potassium and magnesium) between the two instruments have R^2 values greater than 0.93, as illustrated in Figure 2.4. This supports the assertion that the flow rate remained constant throughout

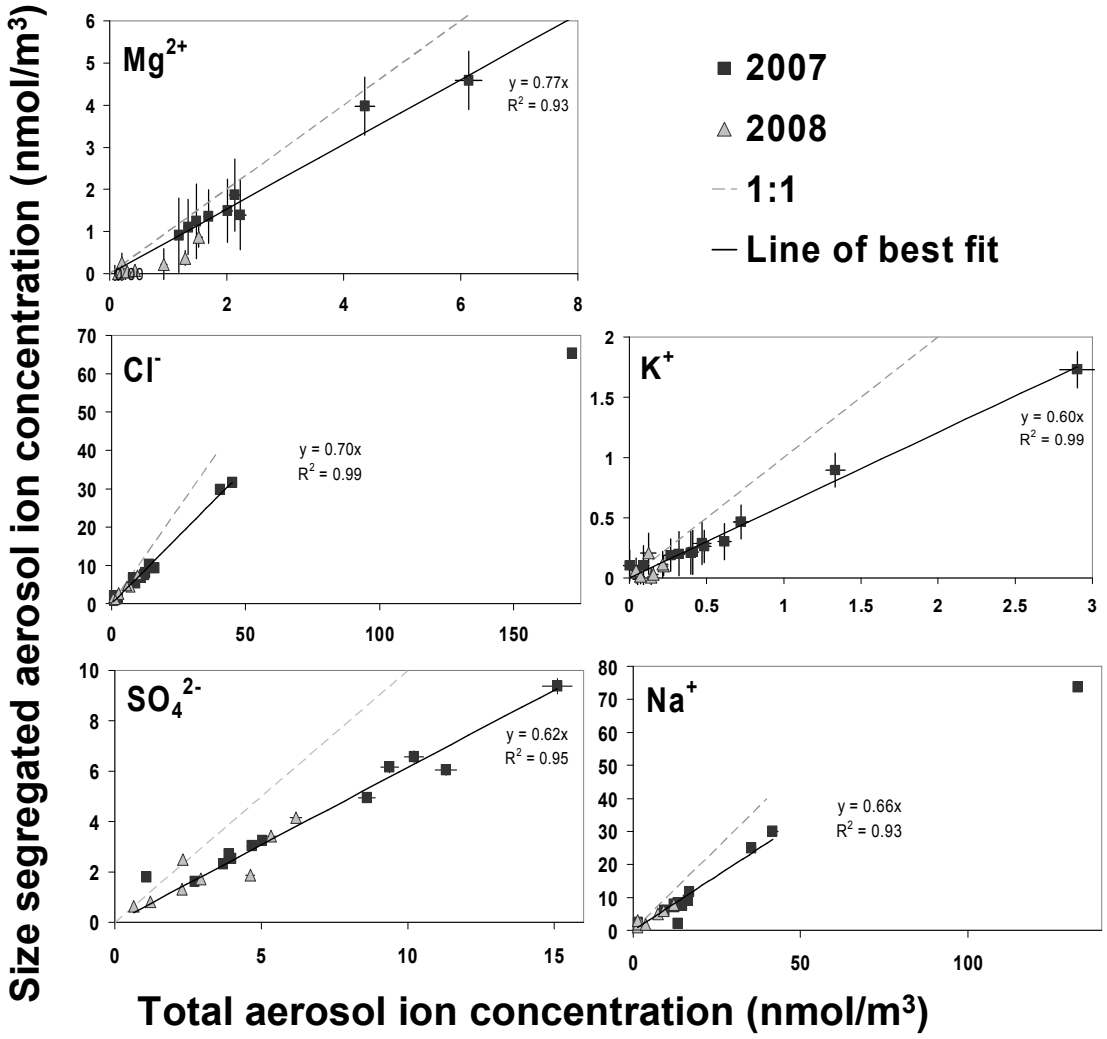

Figure 2.4 Comparison of ion concentration at Alert of the sum of the size segregated aerosol concentration for five different ions and the total aerosol ion concentration during the same sampling periods (n=19 for Mg^{2+}, Cl^- and Na^+, n = 20 for K^+ and SO_4^{2-}).

the sampling period. The other concern of the bypassed flow rate controller is the possibility that an overestimation of the flow rate would be a possible. An

overestimation of flow rate would result in an overestimation of volume and thus an underestimation in concentrations. It was found generally that the total aerosol sampler had higher concentrations than those for the summed size segregated samples (see Figure 2.4), thus supporting that the flow rate was not consistently lower than what was recorded.

It is of interest to note that the total aerosol samples' ion concentrations were approximately 35% higher than the sum of the size segregated samples (see Figure 2.4). This is opposite to what was expected if the total aerosol high volume sampler flow rate had been overestimated. The high volume samplers were not run in the exact same location and this may explain some variation between the two ion concentrations (see Chapter 2.1). The locations though were similar (i.e., a difference of 200 m) and a difference of 35% in the loading of atmospheric aerosols between the two locations does not seem likely.

The other possibility is an error associated with the flow rate of the high volume samplers that has not been taken into account. High volume samplers can be affected by chemical and physical artefacts although these are not usually systematic (Finlayson-Pitts and Pitts, 2000). Chemical artefacts could include reactions of collected particles with gaseous components leading to the volatilization from the collected aerosols or the absorption of the gaseous component (Finlayson-Pitts and Pitts, 2000). Particle bounce and resuspension of previously collected particles is a physical artefact that can lead to a decrease in collection efficiency of high volume samplers (Finlayson-Pitts and Pitts,

2000; Wedding et al., 1986). Air turbulence can also influence the efficiency of the high volume samplers (Finlayson-Pitts and Pitts, 2000). Since the location differed between the two high volume samplers, wind turbulence could be significantly different between them. The high volume sampler collecting size segregated samples had a housing to minimize impacts from blowing snow on the filter which would lead to smaller amounts collected compared to the high volume sampler collecting total aerosol. Both air turbulence and blowing snow may therefore have contributed to the 35% higher concentration in the total aerosol filters relative to the size segregated filters. Artefacts for high volume samplers and comparisons between different techniques have been explored by others (Wedding et al., 1980; Wedding et al., 1986; François et al., 1995).

The flow rate of 1.02 ± 0.03 m^3/min was used for error propagation for the high volume sampler that collected total particulate matter and SO_2 at Alert. It is noted that the sum of the size segregated samples are different than that of the total aerosol load and must be taken into consideration if concentrations between the two high volume samplers are being compared. The concentrations of the total aerosol samples throughout the thesis therefore will be higher than that of the sum of the slotted filters. The evidence presented above suggests ratios of ions should remain relatively consistent between the two high volume samplers.

2.4.2 Sample Preparation

Aerosols (both size segregated and total) were collected on quartz filters. SO_2 was collected under the total particulate matter filter on a separate cellulose acetate filter that was treated with a mixture of potassium carbonate and 10% glycerol solution prior to field deployment. This method has been carried out in many studies before (e.g., Saltzman et al., 1983; Norman et al., 2004; Seguin, 2007; Seguin et al., 2010).

Samples were stored in sealed plastic bags before being processed in the lab in Calgary. Both SO_2 and aerosol samples were placed in 18 MΩ deionized water to extract ions. 2mL of hydrogen peroxide was added to cellulose acetate filters to oxidize sulfur dioxide collected on the filter to sulfate. The samples were sonicated before being filtered. A portion of the filtrate was set aside for ion concentration measurements. The remaining filtrate was treated with barium chloride and acidified to a pH less than 3 with the addition of Environmental Grade HCl, to precipitate barium sulfate for isotope analysis.

Two or three field blanks each year were collected for each of the different types of filters (total aerosol, SO_2 and size segregated filters for both Alert and the *Amundsen*). Field blanks are filters that are loaded in the field on a high volume sampler with no air flow before being removed, stored and analyzed in the same manner as the samples and used in blank correction (Chapter 2.8).

2.5 Aerosol Dissolvable Ion Concentrations

Characteristics such as ion concentrations for atmospheric aerosol that are dissolvable in 18MOhm distilled water can be determined by finding the concentration of ions in the filtrate discussed in Chapter 2.4.2. Cation concentrations for aerosol samples from the *Amundsen* were measured on a Dionex DX500 ion chromatograph with a Dionex CD20 conductivity detector. A CG12A Guard Column and CS12A Analytical column was used on the instrument. 20mM of MSA was used as the eluent at a flow rate of 1.0 ml/min. Anion concentrations from the *Amundsen* aerosol samples were carried out using a Dionex IC-2500 ion chromatograph with an ED50 Electrochemical Detector. An AG15 Guard Column along with an AS15 Analytical Column was used. The eluent composition was KOH with a positive linear concentration gradient throughout the run. A flow rate of 1.2 ml/min was used. Both instruments are located at the Glacial Hydrochemistry Laboratory at the University of Alberta. Details of this analysis are given by Rempillo (2011).

Measurements of aerosol ion concentrations from Alert were conducted at the University of Calgary in the Environmental Science Laboratory. A Dionex integrated IC 1000 was used to measure both anions and cations. Chloride, sulfate, nitrite, nitrate and bromide anions were quantified. Cations that were quantified were sodium, potassium, magnesium and calcium. Anions were separated using a AS14, 4mm guard and AS14 analytical column (250 mm in length). A bicarbonate/carbonate solution (3.5mM Na_2CO_3/1.0 mM $NaCO_3$) was used as the eluent with a flow rate of 1.2mL/min. For cations, a CG12A

Guard column with a CS12A analytical column was used with 1.0 ml/min flow rate of 20mM MSA as the eluent. Concentrations in field blanks were measured and are used in blank correction (Chapter 2.8).

Because of relocation of the Glacial Hydrochemistry Laboratory at the University of Alberta and the unavailability of their instrument, methanesulfonate (MS^-) concentrations for Alert samples were measured at the Facility for Biogeochemical Research on Environmental Change and the Cryosphere (FaBRECC) at Queens University. Methanesulfonate is the cognate base of MSA and is the species present in aerosols. Naming conventions in previous papers (e.g., Sirois and Barrie, 1999, Quinn et al., 2009) have labelled this species as MSA. For consistency, this naming convention will also be used throughout this thesis. A Dionex ICS- 3000 liquid ion chromatograph was used and could determine both cations and anion simultaneously. AS18 analytical and guard columns were used with a KOH eluent (gradient elution 17 – 40 mM) and flow rate of 1.0 ml/min to separate anions, while cations were separated with CS12A analytical and guard columns, 16 mM MSA eluent and a flow rate of 0.5 ml/min.

Other ions were measured during this time. The analysis carried out by the FaBRECC Dionex ICS- 3000 was more precise at low concentrations than the University of Calgary Dionex integrated IC 1000 and therefore concentrations found at FaBRECC were used for many of the ions measured. Ions included chloride, nitrite, nitrate, sulfate, phosphate, MSA, fluoride, potassium, magnesium, calcium, sodium, lithium, ammonium and strontium. Unfortunately due to time and budget constraints only the total aerosol and

the finest size segregated samples (<0.49 μm) were measured at FaBRECC. Concentrations of lithium and fluoride were not significantly different from zero (i.e., propagated error was larger than calculated concentrations) for all samples measured. Phosphate had high variability in blanks. Therefore, Li^+, F^- and PO_4^{3-} are not looked at further in this thesis.

Cation and anion concentrations are determined from the ion chromatographs. Blank corrections are carried out at this point (see Chapter 2.8.1). Blank corrections can be carried out at this step since extraction volume ($V_{extraction}$) is the same between samples and blanks (if volume extraction is different, error calculations must be done after calculating the amount on the filter paper from blanks and samples; i.e., after equation 2.1). Amount of sample on each filter paper can be calculated by the following equation

$$X_{filterpaper(nmol)} = [X]_{extraction(ppm)} \cdot V_{extraction(mL)} \cdot (mw_{(g/mol)})^{-1} \quad \textbf{2.1}$$

where $[X]_{extraction(ppm)}$ is the blank corrected ion concentration measured in the portion of filtrate set aside for ion chromatography (see Section 2.4.2) measured in ppm, $V_{extration(mL)}$ is the total amount of water in mL used to extract the high volume sample and *mw* is the molecular weight of the ion in question.

Concentration of aerosol ions in the atmosphere can be calculated by

$$[X]_{air(nmol/m^3)} = \frac{X_{filterpaper(nmol)}}{FR_{(m^3/min)} \cdot t_{(min)}} \qquad 2.2$$

where [X] is the concentration of the ion X in the atmosphere in nmol/m^3, $X_{filterpaper}$ is the amount of the ion found on the filter paper in nmol (equation 2.1), *FR* is the flow rate of the high volume sampler in m^3/min and t is the duration of the sampling period in minutes.

2.6 SO_2 Concentrations

The Dionex integrated ion chromatograph system 1000 at the Environmental Science Laboratory at the University of Calgary was used for anion concentrations from the cellulose acetate filters used to collect SO_2 from the *Amundsen* as described by Rempillo (2011); Table 2.1. Instrumental conditions were the same as those for dissolvable aerosol anion samples described in Section 2.5. The same technique was used on the samples from Alert but an interfering peak was observed in the ion chromatogram in the field blanks that overlapped with the sulfate peak. The interfering peak appeared approximately 0.4 minutes (~24 seconds) before the sulfate peak (i.e. ~11.0 minutes vs. ~11.4 minutes) for the conditions that were being run on the ion chromatograph. See Figure 2.5 for an example. The area and height of the peak at 11.0 minutes was variable between filter blanks and interfered in determining the amount of sulfate in the sample especially in 2008 when SO_2 concentrations were usually lower and the interference peak more variable.

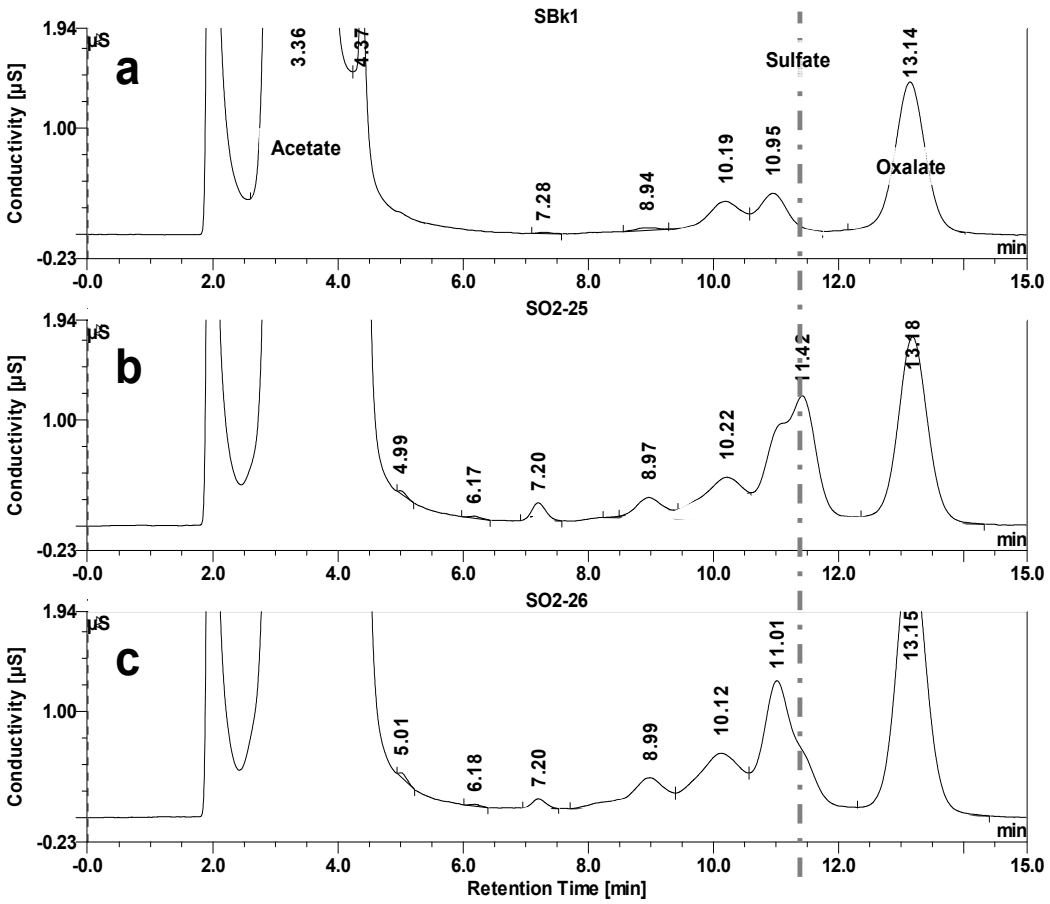

Figure 2.5 Chromatograms of SO_2 filter samples. The retention time of sulfate is shown with a dashed line. A blank (a) and two of samples (b & c) are shown. A peak with a retention time of 11.0 minutes is found in the blank and interferes with the reading of sulfate (retention time = 11.4 min).

Acetate and oxalate are suspected contaminants from the cellulose acetate filters. Acetate is expected to have an earlier retention time than sulfate (approximate retention time of 2.9 minutes; AS14 analytical column and flow rate 1.2mL/min; DIONEX, 2003). The AS14 analytical column manual does not include an oxalate peak retention time for the

bicarbonate/carbonate eluent (DIONEX, 2003) that was used in this study. Oxalate peaks, in a previous study, have been detected shortly after sulfate peaks in an application that used the AS14 analytical column but a different eluent (DIONEX, 1997). Other columns also predict similar retentions of sulfate and oxalate (Fritz and Gjerde, 2000). Tests to determine if oxalate was the interfering peak under the conditions for this study were carried out on the Dionex integrated IC 1000. It was found that oxalate had a retention time at 12.8 minutes in water and 13.1 minutes if a SO_2 matrix was spiked. The slightly different retention time is most likely due to pH or matrix effects (Haddad and Jackson, 1990). Acetate had a retention time of approximately 3.1 minutes. These peaks are seen in Figure 2.5 but do not interfere with the detection of sulfate (retention time 11.4 minutes).

The solutions containing the SO_2 samples are basic (pH > 10) because potassium carbonate is used to pre-treat the filters. Baseline disturbances and/or system peaks can be caused by large differences in pH of a sample and the eluent (Haddad and Jackson, 1990). A SO_2 sample was acidified with HCl to determine if peaks would be affected by pH within the matrix. Although retention time shifted slightly for many of the peaks (~0.3 minutes or less), the ghost peak was still a source of interference with the sulfate peak. The source of the peak with a retention time of 11.0 minutes is of interest for those who wish to carry out SO_2 analysis in the future, but due to time restraints on the instrument, and the fact that the determination of the source of the peak would still not assist in obtaining the amount of sulfur in the sample, gravimetric analysis to calculate SO_2 concentration was used.

Barium sulfate precipitate from the SO_2 sample was weighed for each sample prior to isotope analysis. Percent purity of the barium sulfate sample could be determined based on the area of the peak found in isotope analyses (see Chapter 2.7). Median percent purity was 72 ± 30% (1σ). Comparison between the ion chromatogram concentration and that found by gravimetric with percent purity was carried out for 2007 samples, when SO_2 concentrations were higher and the interfering peak in the ion chromatograph was not as variable. An R^2 value was found to be 0.97 with a slope of 0.98 (Figure 2.6). This is found to be similar to previous comparison between the two methods. SO_2 gravimetric and IC measurements methods were compared with data presented in Seguin (2007) and is shown in Figure 2.6 (R^2 = 0.97, slope = 0.96). Samples collected in 2007 and from Seguin (2007) show strong correlation between the two methods and both methods can be used to determine the amount of sulfur on the SO_2 filters. The gravimetric analysis is used for the 2008 sample set, where analysis from ion chromatography is not possible due to the interfering peak. For samples with low amounts of sulfur (<16 μmol), gravimetric error was set at ± 1.6 μmol (the offset between the two methods), at higher concentrations, 10% error is taken to compensate for possible loss of sulfur in the gravimetric method. The concentrations of SO_2 in the atmosphere can be calculated based on equation 2.2.

2.7 Sulfur Isotope Analysis

Isotope analysis was carried out at the Isotope Science Laboratory at the University of Calgary (Table 2.1). Sulfur isotope ratios from SO_2 and aerosol sulfate samples were

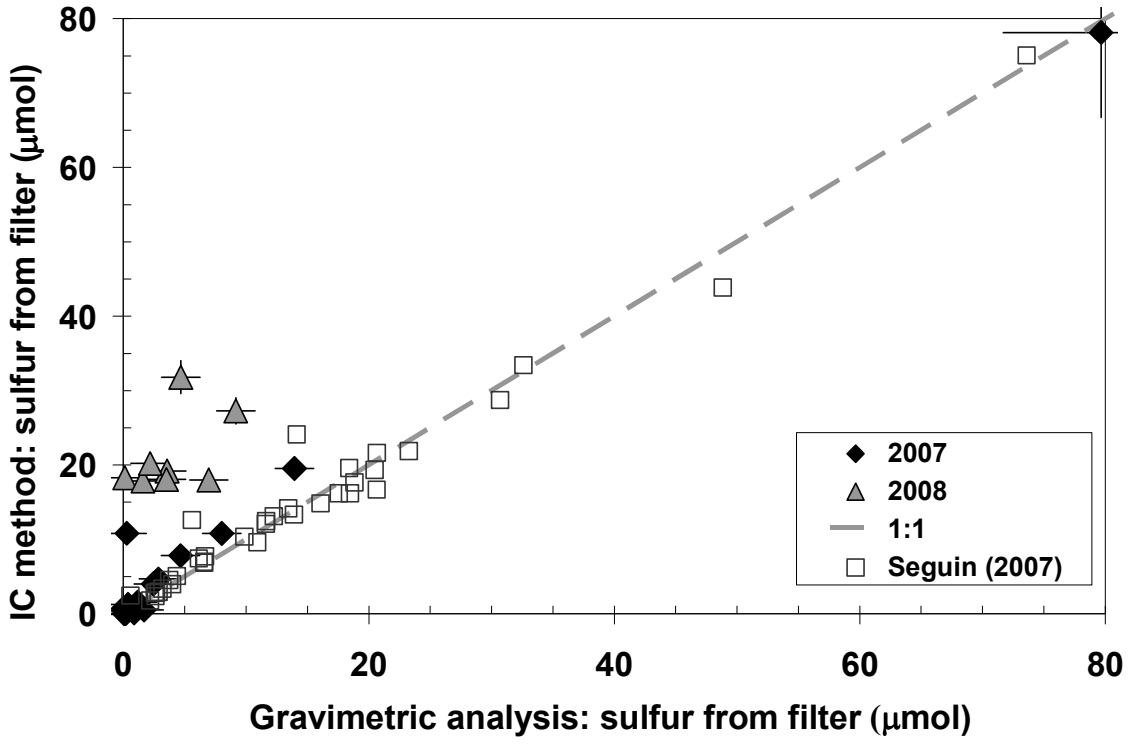

Figure 2.6 Sulfur on SO_2 filters determined by ion chromatography compared to gravimetric analysis. Previous measurements by Seguin (2007) are also displayed. Measurements from Seguin (2007) and data collected in 2007 in this study show strong correlation between the two measurements techniques. An interfering peak in the ion chromatography method over predicts amounts from the 2008 samples.

analysed using a Prism II continuous flow isotope ratio mass spectrometer (CF-IRMS) (Giesemann et al., 1994). Samples are passed through a Carlo Erba MA 1500 elemental analyzer to convert barium sulfate to SO_2. The SO_2 is carried into the mass spectrometer where it is ionized and separated into mass to charge ratios of 64, 65 and 66 amu. Current signals for individual collectors for each mass to charge ratio (64, 65 and 66

amu) are integrated over time to obtain a peak area for each ion. Ratios of these peak areas (65/64 and 66/64) are compared between a reference gas and that of the sample and can be used to determine the $\delta^{34}S$ value (Giesemann et al., 1994). Measurement uncertainty of $\delta^{34}S$ values based on replicates of a laboratory reference $BaSO_4$ from this method are ± 0.2 ‰.

Impurities in the $BaSO_4$ lead to sulfur amounts being smaller than expected. Sulfur samples that contained less than approximately 0.2 μmol of sulfur (i.e., raw data mass to charge ratio 64 amu peak areas are less than 4.5×10^{-9} Ampere seconds) were discarded from the rest of analysis. The signal response at low sulfur amounts is not linear and therefore $\delta^{34}S$ values are not considered reliable (Giesemann et al., 1994).

Raw data for the peak area of the mass to charge ratio of 64 amu signal over time (As) from the Prism can provide a way to determine purity of the sample (see Chapter 2.6) if standards are assumed to be pure. Each sample and laboratory standard is weighed individually before being introduced into the Prism. A calibration between the magnitude of the raw data 64 amu peak and the mass of the standards can be conducted. The area of the raw data 64 amu peak can be used to determine the amount of sulfur in each sample based on the calibration. The purity of the sample can be determined by

$$\%\,purity = \frac{m_{peakarea}}{m_{weighed}} \cdot 100\% \qquad \text{2.3}$$

where $m_{peakarea}$ is the mass calculated by using the peak area of the mass to ratio 64 amu raw signal and $m_{weighed}$ is the mass of the sample that was weighted prior to being introduced into the Prism.

2.8 Blank Corrections

2.8.1 Ion Blank Corrections

Field blanks were taken throughout the study and were used to carry out blank and error analysis for ion concentrations. Two or three field blanks were used for each type of filter each year. Since all filter samples were extracted in the same volume as their respective blanks, the concentration in the eluent from the sample can be calculated by

[sample] = [measured] - [blank] **2.4**

where [blank] is the concentration in the eluent from the blank (taken as the calculated mean of all the blank filters of that type), [measured] is the concentration measured from the IC and [sample] is the concentration in the eluent associated with the contribution from the sample. Standard deviation was determined for the ions of each type of blank and taken as the error of the blank. Therefore error associated with each eluent concentration would be

$$\Delta[sample] = \sqrt{(\Delta[measured])^2 + (\Delta[blank])^2} \qquad \textbf{2.5}$$

where Δ[X] is the error associated with the eluent concentrations of X (i.e., measured, blank and sample). The partial derivative rule for error propagation is used to calculate error of atmospheric concentrations. For a general function,

$$z = f(a,b,c,...) \qquad \textbf{2.6}$$

where a, b and c are independent variables with individual error associated with them, the equation for uncertainty for the partial derivative rule for error propagation is given by

$$(\Delta z)^2 = \left(\frac{df}{da}\Delta a\right)^2 + \left(\frac{df}{db}\Delta b\right)^2 + ... \qquad \textbf{2.7}$$

where Δx is the error associated with each individual variable.

2.8.2 Isotope Blank Corrections

Each type of filter field blank was measured for isotope analysis. Blanks of a specific type that did not have enough material for isotope analysis were combined to obtain a $\delta^{34}S$ value. Blanks for SO_2 filters from Alert did not have a significant amount of sulfur and amounts were not detected either gravimetrically or by ion chromatography.

Therefore SO_2 blank corrections were not needed. The $\delta^{34}S$ value for the sample can be determined by the following equation

$$\boldsymbol{\delta^{34}S_{sample} = \frac{\delta^{34}S_{measured}[measured] - \delta^{34}S_{blank}[blk]}{[sample]}} \qquad \textbf{2.8}$$

where $\delta^{34}S$ indicates isotopic values of the item in question and [X] indicates the eluent concentrations from the sample, the filter paper (blk) and amount measured (i.e., blank + filter paper). Uncertainty was calculated with the partial derivative rule for error propagation (Equation 2.7) or more specifically

$$\left(\Delta\delta^{34}S_s\right)^2 = \left(\frac{\partial\delta^{34}S_s}{\partial\delta^{34}S_m}\Delta\delta^{34}S_m\right)^2 + \left(\frac{\partial\delta^{34}S_s}{\partial[\text{measured}]}\Delta[\text{measured}]\right)^2 + \left(\frac{\partial\delta^{34}S_s}{\partial\delta^{34}S_{blk}}\Delta\delta^{34}S_{blk}\right)^2 + \left(\frac{\partial\delta^{34}S_s}{\partial[\text{blk}]}\Delta[\text{blk}]\right)^2 \qquad \textbf{2.9}$$

where subscript m indicates measured, s refers to the sample and blk refers to the blank.

Chapter Three: Sources of Sulfate

Aerosol sulfate is a major component of Arctic Haze, a springtime phenomenon as the Polar sun rises (Finlayson-Pitts and Pitts, 2000). A number of studies have looked at the composition of Arctic Haze (Barrie and Bottenheim, 1991; Pacyna, 1991; Quinn et al., 2007) at the time of the year when it is at a maximum (i.e., spring). Less is known about the Arctic atmosphere and the chemistry that affects aerosol formation in the fall. The SOLAS study took place in the fall of 2007 and 2008 and the contribution from biogenic sulfate to aerosol loading is expected to be large because the Arctic Ocean is relatively free of ice at that time, enhancing oceanic emissions of DMS (Chapter 1.6).

3.1 Atmospheric Aerosol Sulfate

3.1.1 Sulfate $\delta^{34}S$ Values

Sulfate concentrations and isotope values for size segregated and total aerosol samples were measured at Alert and in the Canadian archipelago on board the *Amundsen*. Total aerosol sulfate included sulfate from the ship's stack (samples from the *Amundsen*; Chapter 4.1), sea salt, frost flowers (samples from Alert; Chapter 3.3), background anthropogenic (Chapter 4) and biogenic sulfate (Chapter 5). $\delta^{34}S$ values ranged between +1.8 ‰ and +19.1 ‰ (median +14.0 ‰; Appendix B; Rempillo, 2011) for the *Amundsen* data set and between +4.7 ‰ and +11.7 ‰ at Alert (median +6.8 ‰; Appendix B). $\delta^{34}S$ values were also measured for size segregated aerosol samples collected at Alert and on

board the *Amundsen.* Aerosols with larger diameters collected on board the *Amundsen* tended to have larger $\delta^{34}S$ values (see Appendix Figure B.2) compared to the smaller size aerosols due to the larger sea salt presence in large aerosols as discussed in further detail in Chapter 3.4.1 and Appendix C. A similar distinction between large and small diameter aerosols was also observed at Alert in 2007 (Appendix Figure B.1). It is interesting to note that the variability in $\delta^{34}S$ values between different size bins in 2008 at Alert was lower than 2007 (Appendix Figure B.1). Variability in $\delta^{34}S$ values for size segregated samples may provide insight into the processes, aerosol lifetimes and sources influencing aerosols in each of the different size fractions. These concepts are explored in the following chapters.

3.1.2 Sulfate Concentration

Aerosol sulfate concentrations ranged from 0.63 nmol/m^3 to 24 nmol/m^3 for all samples collected during the SOLAS campaign in the Arctic. Multiple factors contributed to these sulfate concentrations including ship stack emissions on board the *Amundsen*. The contribution from ship emissions is covered in Section 4.1.

When examining the spatial variation in long range transport of anthropogenic sulfate it is essential to consider the smoke stack emissions from the *Amundsen*. CO_2 was monitored and can be used to identify smoke stack emission events (Section 4.1; Rempillo, 2011). Samples determined to have little to no influence by ship stack

emissions can be examined for regional sulfate sources and long range transport of anthropogenic sulfate to the Arctic.

Isotope analysis uncovered a significant regional source of sulfate in the vicinity of 71° N 125° W which is attributable to the Smoking Hills (Section 3.5.3; Rempillo, 2011). Samples affected by the Smoking Hills emissions were removed from the analysis of anthropogenic and biogenic components (Chapter 3.6).

Biogenic sulfate was examined (see Chapter 5) in all samples not affected by the Smoking Hills. This includes samples from the *Amundsen* that may be influenced by smoke stack emissions. This is possible because background anthropogenic sulfate from long range transport (-5 ± 5 ‰) has a similar $\delta^{34}S$ value compared to anthropogenic sulfur emissions from the *Amundsen* ($\delta^{34}S$ + 3‰; Rempillo et al., 2011). These two anthropogenic sulfate sources are grouped together during isotope analysis. This allows for the quantification of biogenic sulfate concentrations in the Arctic (Section 3.6) even when smoke stack emission are present.

Total aerosol sulfate concentrations ranged between 1.5 and 24 nmol/m^3 (median 5.3 nmol/m^3; Figure 3.1) on board the *Amundsen*. At Alert, the aerosol sulfate ranged between 0.63 and 15.4 nmol/m^3 (median 4.2 nmol/m^3; see Figure 3.1). Average concentrations are in a range that is typical in the Arctic for the season (Sirois and Barrie, 1999; Quinn et al., 2007). Concentrations found on board the *Amundsen* were usually larger when compared to Alert samples measured during the same time period and can be

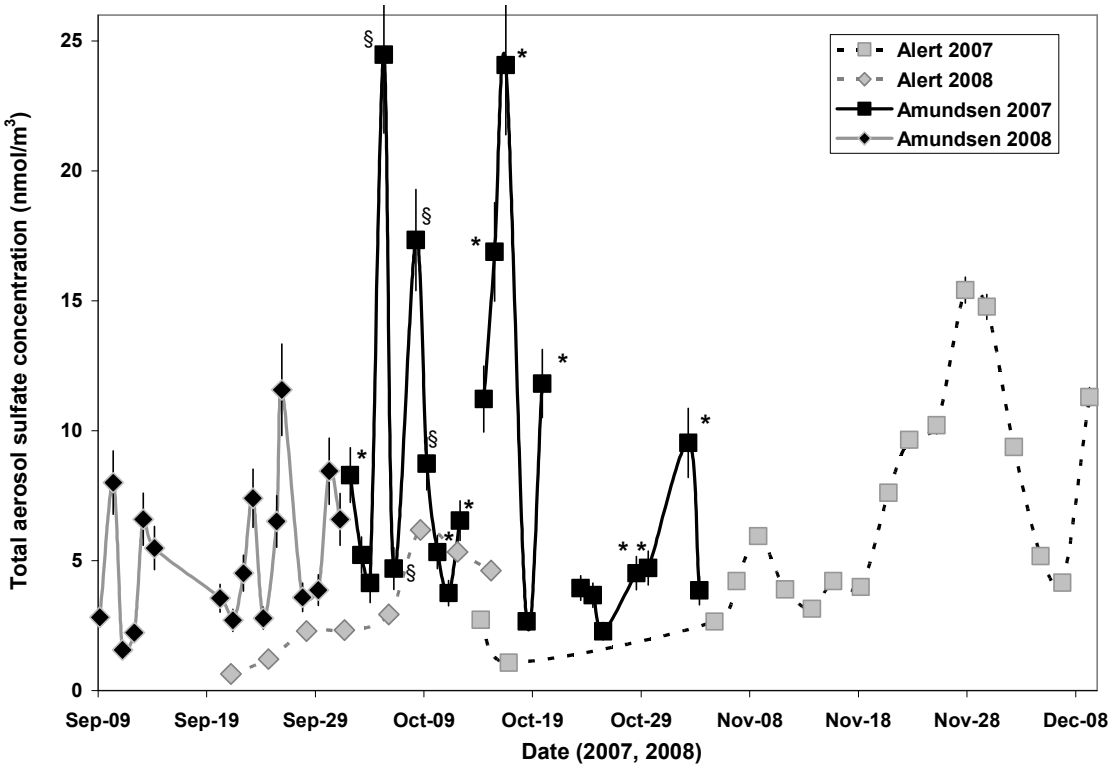

Figure 3.1 Concentration of sulfate in total aerosol at Alert and on board the *Amundsen* in 2007 and 2008. *Amundsen* data in 2007 marked with * identifies smoke stack emission events, § indicate samples in the 2007 *Amundsen* data set that did not have significant CO_2 data to identify smoke stack emission events.

attributed to the higher concentrations of sea salt sulfate in the Canadian archipelago than at Alert as discussed in Section 3.4.1 and/or anthropogenic smoke stack emissions (Chapter 4.1). Although the two different data sets are not co-located and sampling locations differed by hundreds of kilometres, it may be useful to compare non-ship stack anthropogenic as well as biogenic sulfate from long range transport once apportionment calculation have been performed (Chapter 3.6).

Sulfate can come from many different sources which may include lithospheric (dust/volcanic), sea salt, biogenic and anthropogenic sources (e.g., Andrews et al., 2004; Wadleigh, 2004; Seguin et al., 2010). In the Arctic, a local source of ^{32}S enriched sulfur emitted from the Smoking Hills in the North West Territories was detected in close proximity to the site in the *Amundsen* data set (Rempillo, 2011; see Chapter 3.5.3 and Appendix Figure B.2). A second source of sulfate, typically found only in the Polar Regions, is from frost flowers. Frost flower contributions in ice cores have received attention in the last decade (Rankin et al., 2002, Kunasek et al., 2010) and were determined to have an important influence on aerosol sulfate concentrations at Alert. Sea salt and frost flowers are sources of sodium and sulfate. Contributions to aerosols from these two sources are explored in this chapter (Section 3.3 and Section 3.4) followed by apportionment of other non sea salt sulfate sources.

3.2 Sea Salt Sulfate

Sea salt aerosols are formed from the action of the wind on the ocean and are often the dominant component in aerosols in the undisturbed marine environment (Lewis and Schwartz, 2004). Sea salt sulfate (SS SO_4^{2-}) concentrations in aerosols can be calculated by measuring sodium concentrations (although other sea salt ion concentrations such as magnesium and chloride, in some instances, can be used), and relating it to the known molar ratio of Na^+/SO_4^{2-} in sea water (e.g., Berresheim et al., 1995; Seguin et al., 2011), see Chapter 1.1. Concentrations of common ions in sea water along with their ratio to each other can be found in Table 1.1 in Chapter 1.1. Figure 3.2 and Figure 3.3 illustrate

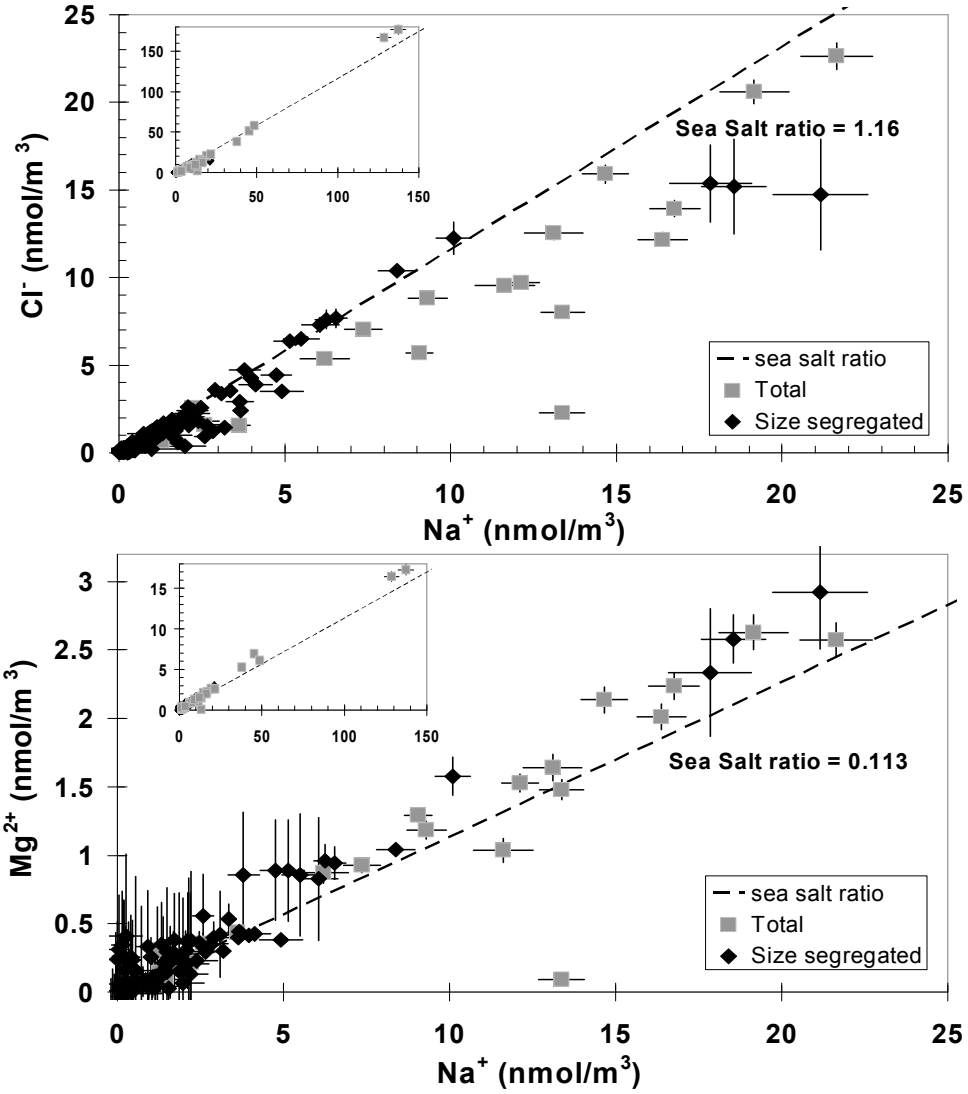

Figure 3.2 Ions in total aerosol (grey squares) and size segregated samples (black diamonds) found in aerosol samples at Alert compared to the sea salt ratio (dashed line). All data is shown in insert, where elevated concentrations are influenced by the presence of frost flowers (Section 3.3).

Cl^-/Na^+ and Mg^{2+}/Na^+ ratios in aerosols collected as part of this study at Alert and on board the *Amundsen*. Sea salt ratios for these same pairs of ions are also illustrated for

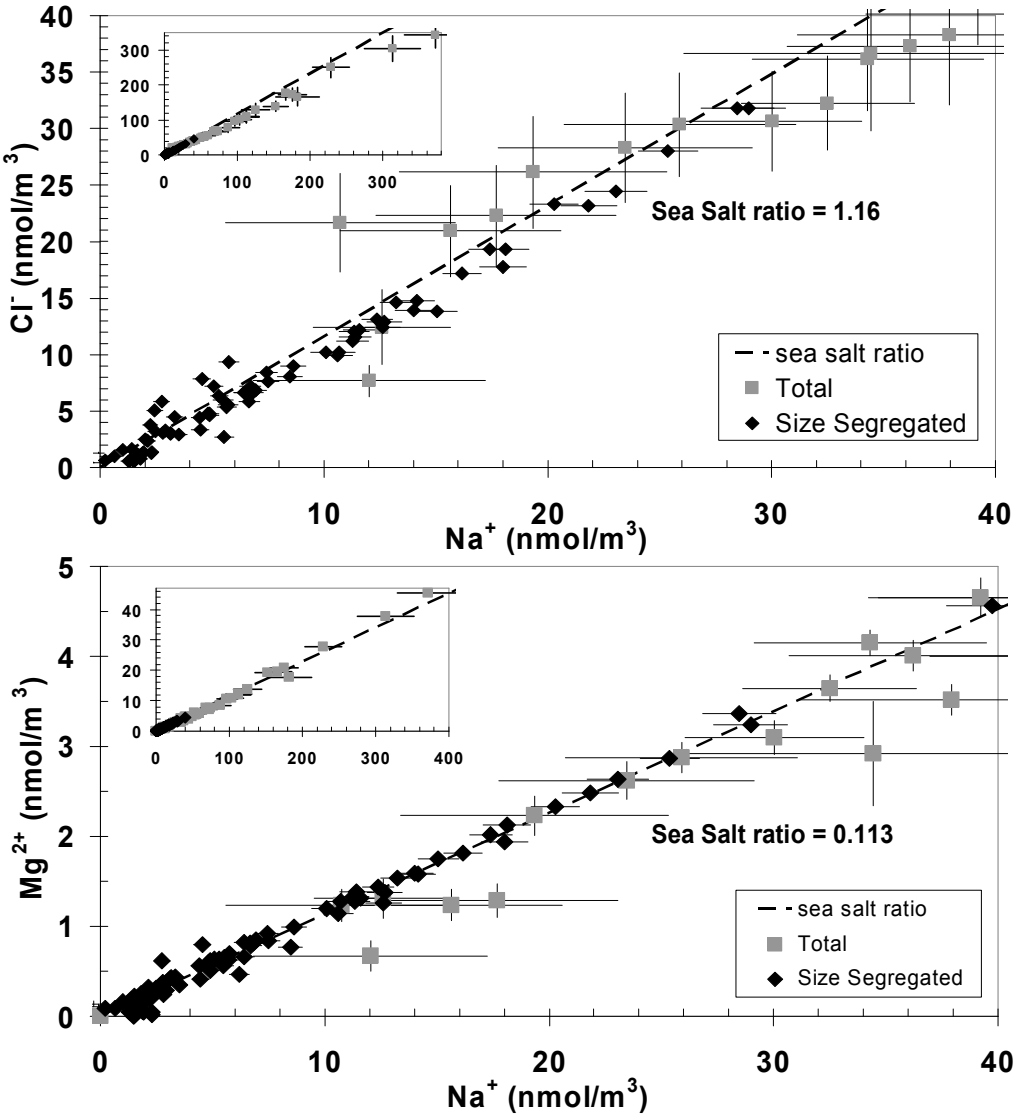

Figure 3.3 Ions in total aerosol (grey squares) and size segregated samples (black diamonds) found in aerosol samples collected on board the *Amundsen* compared to the sea salt ratio (dashed line). The entire data range is shown in the insert.

comparison. As shown, many of the samples fall within error of the sea salt ratio with the majority of Cl^-/Na^+ and Mg^{2+}/Na^+ ratios in aerosol samples collected on board the

Amundsen being within error of the sea salt ratio (Figure 3.3, Rempillo et al., 2011). Depletion of chloride relative to sodium for Alert samples (Figure 3.2) is discussed in more detail in Chapter 4.3.2. Concentrations for all sea salt aerosol concentrations are explored in more detail in Chapter 3.4.

3.3 Frost Flowers

3.3.1 Negative Non Sea Salt Sulfate

Non sea salt sulfate (NSS SO_4) is determined by finding the difference of the sulfate measured in the aerosol and that of the calculated sea salt sulfate (see Equation 1.1). A problem arose in the 1990's when calculated negative NSS SO_4^{2-} concentrations in precipitation at Antarctic coastal sites were discovered (Minikin et al., 1994, Rankin et al., 2002 and references within). This was due to the fractionation of sodium and sulfate that occurred on newly formed sea ice (i.e., frost flowers) which was determined to be a significant source of sodium in aerosols during the Antarctic winter (Rankin et al., 2002, Wagenbach et al., 1998). Although more work on frost flowers has been carried out in the Antarctic, there have been observations of frost flowers in the Arctic in previous studies (e.g., Norman et al., 1999; Beaudon and Moore, 2009). In the Antarctic a negative correlation was found between calculated NSS SO_4^{2-} and Na^+ concentrations in aerosols and ice cores; an indication that frost flower contribution strongly affected both sulfate and sodium concentrations (Wagenbach et al., 1998; Jonsell et al., 2005). This negative correlation is not found in this study (see Figure 3.4 for Alert data). Unlike the Antarctic,

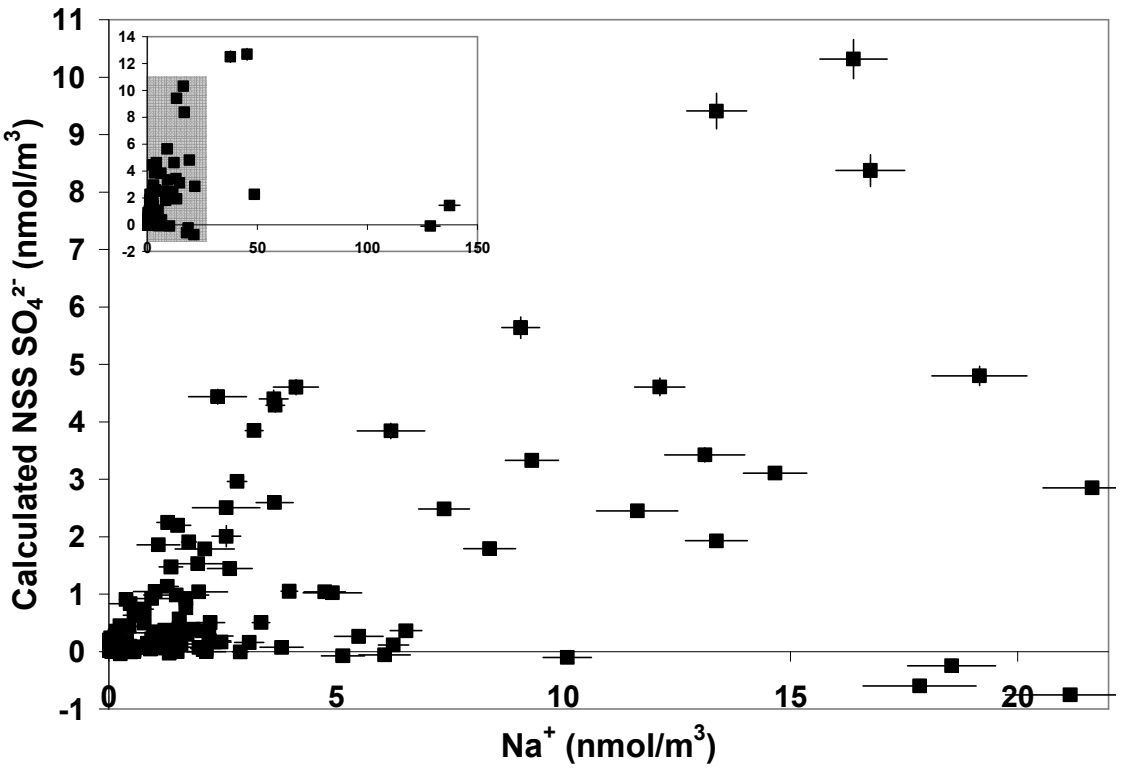

Figure 3.4 Calculated NSS SO_4^{2-} (equation 1.1) compared to Na^+ concentrations at Alert (in total and size segregated samples). The insert illustrates the entire range of values. The shaded region in the insert is magnified in the larger plot to demonstrate the spread in values. Calculated negative NSS SO_4^{2-} values are an indication of the presence of frost flowers.

anthropogenic sulfate is a significant source of aerosol sulfate in the Arctic (e.g., Barrie and Bottenheim, 1991; Sirois and Barrie, 1999) and may mask trends associated with the presence of frost flowers. However, even with anthropogenic influence, calculated negative NSS SO_4^{2-} concentrations (based on equation 1.1) were found for ten of the 137 size segregated samples measured at Alert. Out of these ten, six were significantly lower

than zero. Half of these occurred during the same sampling period, between November 19th and 23rd, 2007 and are a strong indication of the presence of frost flower sulfate during this period (Rankin et al., 2002).

No calculated negative NSS SO_4^{2-} was found with the *Amundsen* data set in the fall of 2007 or 2008 (Rempillo, 2011). However, for the *Amundsen* samples, a very strong sea salt signal (Rempillo et al., 2011) could mask frost flower signatures.

Six calculated negative NSS sulfate concentrations in samples from Alert seen in Figure 3.4 indicates at least some samples were influenced by frost flowers. The use of concentrations alone to determine frost flower contribution in aerosols does have weaknesses though. A negative NSS SO_4^{2-} concentration will reveal that frost flower influence is present but not how much. It could be that all the sodium was derived from frost flowers (molar ratio $SO_4^{2-}/Na^+ = FF_{ratio} = 0.012\text{-}0.024$, Rankin et al., 2002) or only a portion was from frost flowers with the rest coming from sea salt (molar ratio $SO_4^{2-}/Na^+ = SS_{ratio} = 0.0598$; Maidment, 1993). Samples without negative NSS SO_4^{2-} concentrations could also have frost flower influence to a lesser degree but this may be masked by the additional sulfur coming from biogenic or anthropogenic influences. This would be more significant in the Arctic than the Antarctic due to anthropogenic influences being more prevalent in the Northern hemisphere relative to the Southern hemisphere (Turner and Marshall, 2011). Frost flower research in the Arctic is not as prevalent as in the Antarctic for this reason. Unfortunately no clear way to determine the amount of sulfate coming from sea salt versus that from frost flowers has been

documented in the literature. Here, a method using stable isotopes is described that can be used to set limits on contributions of sulfate from sea salt and frost flowers.

Sulfur isotopes have been used to aid in determining the presence of frost flower contributions in aerosol and ice core studies (Norman et al., 1999; Jonsell et al., 2005; Kunasek et al., 2010). Previous work used patterns that were found with $\delta^{34}S$ values to determine frost flower presence. Kunasek et al. (2010) and Jonsell et al. (2005) looked at different *k* values where *k* represents the ratio of SO_4^{2-}/Na^+ in the aerosol or ice core. To stay consistent with literature ratios of SO_4^{2-}/Na^+ in aerosols this ratio will be expressed as *k* (i.e., SO_4^{2-}/Na^+) in this work. When needed, the inverse ratio (i.e., Na^+/SO_4^{2-}) will be represented by k^{-1}. Kunasek et al. (2010) and Jonsell et al. (2005) determined extremes for *k* due to frost flowers and sea salt and used this to calculate the range of non sea salt $\delta^{34}S$ ($\delta^{34}S_{nss}$) values.

$\delta^{34}S_{nss}$ values are usually calculated by

$$\delta^{34}S_T \cdot SO_4^{2-}{}_T = \delta^{34}S_{ss} \cdot SO_4^{2-}{}_{ss} + \delta^{34}S_{nss} \cdot (SO_4^{2-}{}_T - SO_4^{2-}{}_{ss}) \qquad 3.1$$

where $SO_4^{2-}{}_x$ is the concentration of either the total (T) or sea salt (ss) sulfate calculated by equation 1.1., $\delta^{34}S_T$ is the $\delta^{34}S$ value for the total sample, $\delta^{34}S_{ss}$ is the $\delta^{34}S$ value for sea salt (+21‰, Rees et al., 1978) and $\delta^{34}S_{nss}$ is the calculated $\delta^{34}S_{nss}$ value.

Norman et al. (1999) compared the fraction of calculated NSS SO_4^{2-} with that of calculated $\delta^{34}S_{nss}$ and found a linear relationship. The trend towards lower calculated $\delta^{34}S_{nss}$ values with an increasing fraction of sea salt was attributed to the presence of frost flowers in some of the samples (see Figure 3.5). A similar analysis can be carried out with samples from Alert in this study. $\delta^{34}S_{nss}$ values were calculated for each sampling period at Alert and are shown as a function of time in Appendix Figure B.3. A trend

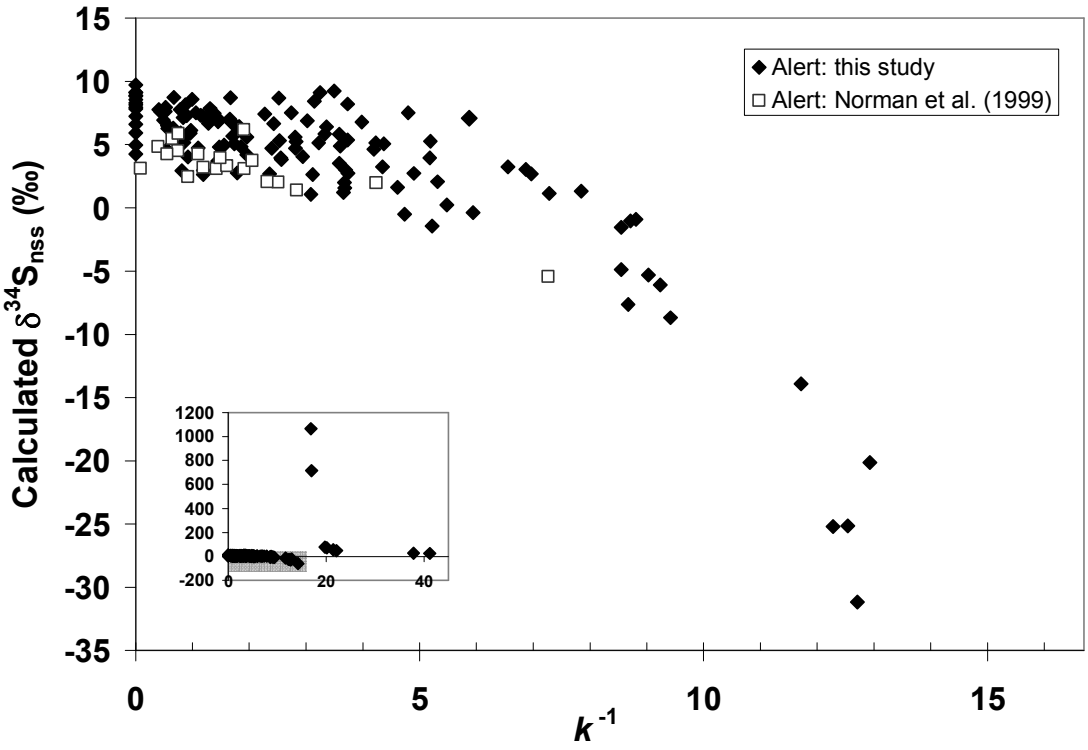

Figure 3.5 Calculated $\delta^{34}S_{nss}$ vs. k^{-1} (Na^+/SO_4^{2-} molar ratio). If all Na^+ was from sea salt no dependence on k should be observed and calculated $\delta^{34}S_{nss}$ values should range between +4.4‰ and +18‰ with a k^{-1} maximum ratio of 16.7 (the ratio of sea salt). Insert includes points that are larger than the k^{-1} of sea salt.

towards lower $\delta^{34}S_{nss}$ values was observed as k^{-1} approached that of sea salt (k^{-1} = 16.7, k = 0.0598; Figure 3.5) which is similar to what Norman et al. (1999) noted. However, the SOLAS Alert data set presented here contained samples with larger k^{-1} than Norman et al. (1999) and frost flowers contribute to a greater proportion of total sulfate in the aerosol compared to the Norman et al. (1999) study (Figure 3.5). Although Norman et al. (1999), Jonsell et al. (2005) and Kunasek et al. (2010) used isotopes to aid in the detection of the presence of frost flowers, quantification of frost flowers and distinguishing frost flower and sea salt amounts was not conducted. The work presented here quantifies frost flowers using theory. Minimum and maximum contributions of frost flowers can be constrained with the use of $\delta^{34}S$ values.

3.3.2 $\delta^{34}S$ Values and Limits of Frost Flower Contribution

$\delta^{34}S$ values for total sulfate are compared to k^{-1} (Na^+/SO_4^{2-} molar ratio) in Figure 3.6. If no frost flower correction was taken into account 100% sea salt would correspond to a k (SO_4^{2-}/ Na^+ molar ratio) being equivalent to 0.0598 (i.e., $k^{-1} = Na^+ /SO_4^{2-} = 16.7$). Mixing between sea salt and a non sea salt component would lead to a linear relationship with y-intercept of $\delta^{34}S_{nss}$ on Figure 3.6 If we consider the two non sea salt sulfate sources of biogenic ($\delta^{34}S$ +18 ± 1.5 ‰; Patris et al., 2000) and anthropogenic ($\delta^{34}S$ +4.4 ± 0.4 ‰; Norman et al., submitted; see Chapter 1.3 and Section 3.6 for information on $\delta^{34}S$ values from the sources), two mixing lines become the border of the mixing triangle (shaded mixing triangle in Figure 3.6) that represents the limits of the three sources in

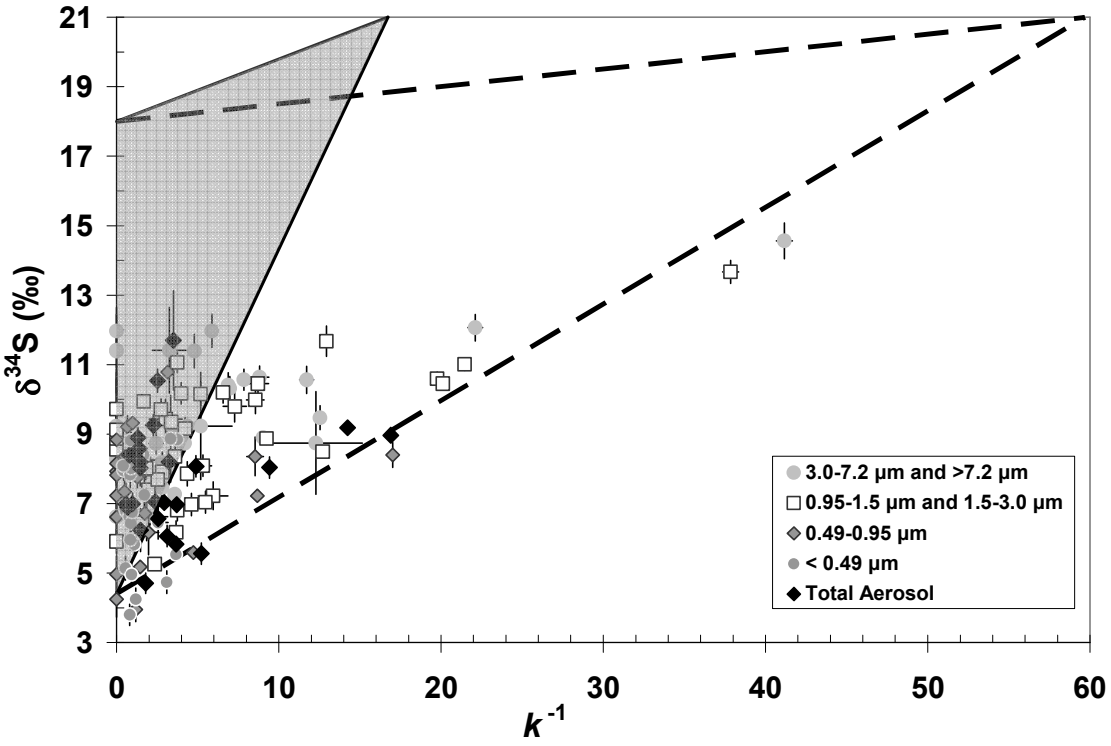

Figure 3.6 $\delta^{34}S$ values versus k^{-1} (Na^{+}/SO_4^{2-} molar ratio). Note that if no frost flowers are present data would fall within the shaded triangle.

question (sea salt, biogenic and anthropogenic). If no frost flowers were present and samples originated from these three sources, $\delta^{34}S$ values should fall within the shaded triangle illustrated in Figure 3.6.

Samples with k^{-1} above 16.7 (i.e., $k < 0.0598$) correspond with calculated negative NSS SO_4^{2-} concentrations (based on equation 1.1). Since frost flowers have an excess of sodium relative to sea water, samples with significant frost flower contribution would

yield smaller k (larger k^{-1}) than that for sea salt. There are additional data points that lie outside the shaded triangle in Figure 3.6 and can be explained as follows.

A $\delta^{34}S$ value of +21 ‰ for the frost flowers (defined as $\delta^{34}S_{ff}$) was determined by Norman et al. (submitted). There is no significant difference between $\delta^{34}S_{ff}$ values and that of sea salt ($\delta^{34}S_{ss}$) indicating little or no isotopic fractionation occurs in frost flower formation (i.e., during the precipitation of mirabilite from brine, see Chapter 1.4.3). If all sulfate in a sample originated from frost flowers a $\delta^{34}S$ value equal to the $\delta^{34}S_{ff}$ value would be expected for the sample, along with k similar to frost flowers ($k^{-1} = Na^{+}/SO_4^{2-} = (0.017)^{-1} = 58.8$; Kunasek et al., 2010). Using $\delta^{34}S_{ff}$ values and the k^{-1} value of frost flowers, a second triangle (dashed) is overlaid in Figure 3.6. Similar to the sea salt mixing triangle, two mixing lines between frost flower and either biogenic or anthropogenic sulfate can be determined. This second dashed triangle in Figure 3.6 represents the limits of $\delta^{34}S$ values expected when contributions of frost flowers, anthropogenic and biogenic sulfate are present. Note that a mid-point value for the frost flower ratio described in the literature was used and one must keep in mind a range for frost flower ratios has been reported (k = 0.012-0.024, Rankin et al., 2002). Samples that did not fall within the sea salt triangle (shaded triangle) fell within error of the second (dashed line) triangle. Since samples fall within error of the second triangle, this supports that all $\delta^{34}S$ values obtained at Alert can be explained by frost flowers. A further step can now be performed to determine the maximum and minimum amounts of sulfate (and thus sodium) that are contributed from frost flowers.

3.3.3 Calculations for Contribution of Sulfate from Frost Flowers

A number of simple relationships and equations can be used to calculate the contribution of frost flowers. This calculation here is based on aerosol data but could also potentially be used for ice core samples that are influenced by frost flower contributions.

3.3.3.1 Constraints Without the Use of Isotopes

The total amount of sodium (Na_T) in a sample from Alert is expected to come from either sea salt (Na_{ss}) or frost flowers (Na_{ff}) and therefore

$$Na_T = Na_{ff} + Na_{ss} \quad \textbf{3.2}$$

whereas sulfate (SO_{4T}) comes from multiple sources.

$$SO_{4T} = SO_{4\,ff} + SO_{4ss} + SO_{4nss} \quad \textbf{3.3}$$

where SO_{4nss} is the portion of sulfate that is neither sea salt nor frost flower derived. This would consist of biogenic and anthropogenic sources with limited lithospheric sources (see Chapter 3.5). At low concentrations (e.g., approximately below 0.5 nmol/m^3 Na^+ or 0.02 nmol/m^3 SO_4^{2-} in the size segregated samples), sulfate can be on the same order of magnitude as the measurement itself which would lead to high percent error associated

with these equations and each individual term. This is especially true for the size segregated samples that were measured with the less precise instrument at the University of Calgary (Section 2.5). Compared to the size segregated samples, ion concentrations had relatively lower percent error (median percent error for SO_4^{2-} = 5%, Na^+ = 10%) in the total and fine aerosol (<0.49 μm) because of the higher loading of the samples in SO_4^{2-}, the lower error associated with blank filters (Chapter 2.8.1) and the samples being measured on a more precise instrument (i.e., at FaBRECC, Section 2.5). Although high percent error may be associated with samples with low concentration, the contribution of these samples to the overall sulfate loading for the sampling period would be small. Also, aerosols influenced by frost flowers tend to have large ion concentration because of the high ion salinity associated with frost flowers (Wagenbach et al., 1998; Alvarez-Aviles et al., 2008) and samples containing low concentrations of sulfate and sodium would have low probability of being associated with frost flowers.

The molar ratio of SO_4^{2-}/Na^+ for sea salt (SS_{ratio}) is well known to be 0.0598 (i.e., Na^+/SO_4^{2-} = 16.7; Maidment, 1993). Frost flower ratios are predominantly reported as SO_4^{2-}/Na^+ ratios in the literature (e.g., Wagenbach et al., 1998; Rankin et al., 2002; Jonsell et al., 2005; Beaudon and Moore, 2009; Douglas et al., 2012). For frost flowers, the *k* value (FF_{ratio}) is more variable and has a ratio between 0.012-0.024 (Rankin et al., 2002). A midpoint value of 0.017 was used in the study by Kunasek et al. (2010) and will be used as a test scenario throughout this work too. The maximum (0.024) and the minimum (0.012) FF_{ratio} found by Rankin et al. (2002) will be used to perform a sensitivity test. Although some studies have determined a larger FF_{ratio} range (Alvarex-

Aviles et al., 2008; Douglas et al., 2012) values within the range stated by Rankin et al. (2002) have been found by numerous others (e.g., Wagenbach et al., 1998; Jonsell et al., 2005; Beaudon and Moore, 2009).

From here, we can determine the maximum and minimum contribution to sulfate in aerosols from frost flowers. The maximum contribution will be either the total amount of Na^+ multiplied by the frost flower ratio (all Na^+ is from frost flowers) or the total amount of sulfate present in the sample (all sulfate is from frost flowers). The minimum of the above two options is the maximum possible frost flower contribution to sulfate loading.

The minimum contribution of frost flower sulfate assumes all sulfate comes from sea salt and/or non-sea salt sulfate sources (i.e., anthropogenic and biogenic). This would make the contribution of frost flower sulfate zero. Although negative sea salt concentrations are calculated based on equation 1.1, negative concentrations cannot physically exist. In the case when *k* is less than that of sea salt, frost flowers must be considered. The minimum amount of frost flower contribution (SO_{4ffmin}) during these times would lead to no non sea salt sulfate (i.e., $SO_4^{2-}{}_{nss} = 0$; see Appendix E.1). Under these conditions,

$$SO_{4\,ff_{\min}} = \frac{SO_{4T} - SS_{Ratio} Na_T}{1 - \frac{SS_{ratio}}{FF_{ratio}}} \qquad \textbf{3.4}$$

where SS_{ratio} and FF_{ratio} is the sea salt and frost flower ratios of SO_4^{2-}/Na^+ (0.0598 and 0.017 respectively) and SO_{4T} and Na_T are the concentrations of the sulfate and sodium

measured in the sample (see Appendix E.1 for proof of equation). The maximum and minimum atmospheric concentration of sulfate in total aerosol from frost flowers at Alert are calculated and are displayed in Figure 3.7.

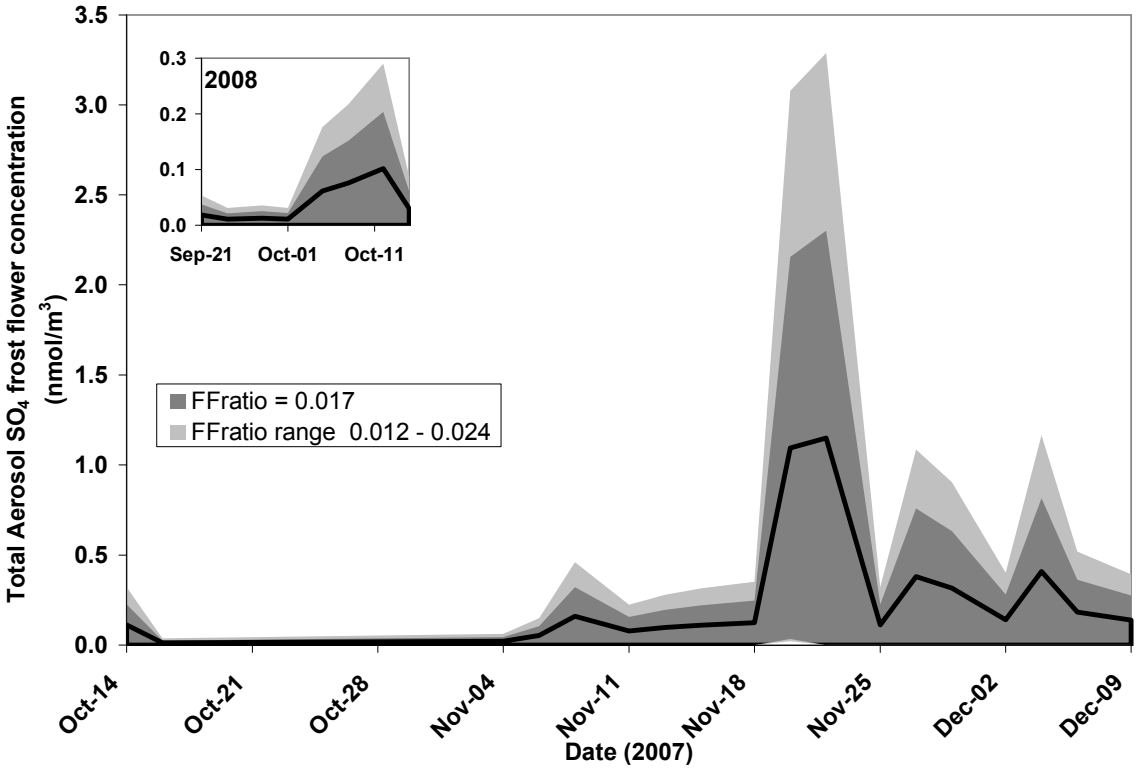

Figure 3.7 Atmospheric concentration of sulfate from frost flowers at Alert (without using isotope values). The light grey area represents the possible range of concentrations based on constraining the frost flower ratio between 0.024 and 0.012. The dark grey area represents the possible range of contribution of frost flowers to aerosol sulfate when the frost flower ratio is constrained to 0.017. The dark line is the average of the maximum and minimum of the last constraint.

Aside from one case in 2007, the minimum contribution from frost flowers in total aerosols does not differ from zero. This case occurred between November 19 to 21, 2007 which is at the same time when a number of size segregated samples had calculated negative non sea salt sulfate concentrations (Section 3.3.1). The possible contribution from frost flowers range up to 2.3 nmol/m^3 of sulfate. If a sensitivity test is carried out by differing the frost flower ratio between 0.012 and 0.024, the maximum possible contribution of sulfate from frost flowers increases to 3.3 nmol/m^3. Maximum possible frost flower contributions are lower in 2008 than 2007 which can be explained by the earlier sampling period in 2008 where temperature gradients were less conducive to frost flower formation as described in Section 3.3.4 . Although the restrictions outlined above can give a range of possible concentrations of sulfate from frost flowers, many of these do not differ from zero and a second constraint is needed to aid in the contribution of frost flowers to aerosol sulfate concentrations.

3.3.3.2 Isotope Constraints on Frost Flowers.

We know from isotope values that

$$\delta^{34}S_T \cdot SO_{4T} = \delta^{34}S_{ff} \cdot SO_{4\,ff} + \delta^{34}S_{ss} \cdot SO_{4\,ss} + \delta^{34}S_{nss} \cdot SO_{4\,nss} \qquad \textbf{3.5}$$

where subscripts indicate total (T), frost flower (ff), sea salt (ss) and non sea salt (nss) values and SO_{4x} is the concentration in eluent of each of the components (although, as

long as there is consistency between terms, this calculation can be carried out if SO_{4x} is the amount that is present on the filter paper or the sulfate concentration in air). One can use the above equation (equation 3.5) plus those from the previous section (equations 3.2 and 3.3) with sea salt and frost flower ratios to solve for the concentration (or amount, see above) of sulfate from frost flowers.

$$SO_{4\,ff} = \frac{Na_T \cdot SS_{Ratio}(\delta^{34}S_{nss} - \delta^{34}S_{ss}) + SO_{4_T}(\delta^{34}S_T - \delta^{34}S_{nss})}{\delta^{34}S_{ff} - \delta^{34}S_{nss} + \frac{SS_{ratio}}{FF_{ratio}}(\delta^{34}S_{nss} - \delta^{34}S_{ss})} \qquad \textbf{3.6}$$

Sea salt sulfate can be then be determined by

$$SO_{4\,ss} = SS_{Ratio}\left(Na_T - \frac{SO_{4\,ff}}{FF_{ratio}}\right) \qquad \textbf{3.7}$$

The $\delta^{34}S_{nss}$ value falls between +4.4 and +18.0‰ due to the endpoints of anthropogenic (+4.4‰) and biogenic (+18.0‰) sulfate (Chapter 3.6.1). Lithospheric sulfate at Alert is expected to be at a minimum as explained in Chapter 3.5.1.

The constraints found in Chapter 3.3.3.1 must also be observed. Overall all constraints for the maximum and minimum contributions of frost flowers can be determined by the extremes of $\delta^{34}S_{nss}$ (i.e., + 4.4 and +18.0‰) and the constraints introduced in 3.3.3.1. A value of 0.017 is used for the frost flower ratio (see Figure 3.8). Three total aerosol

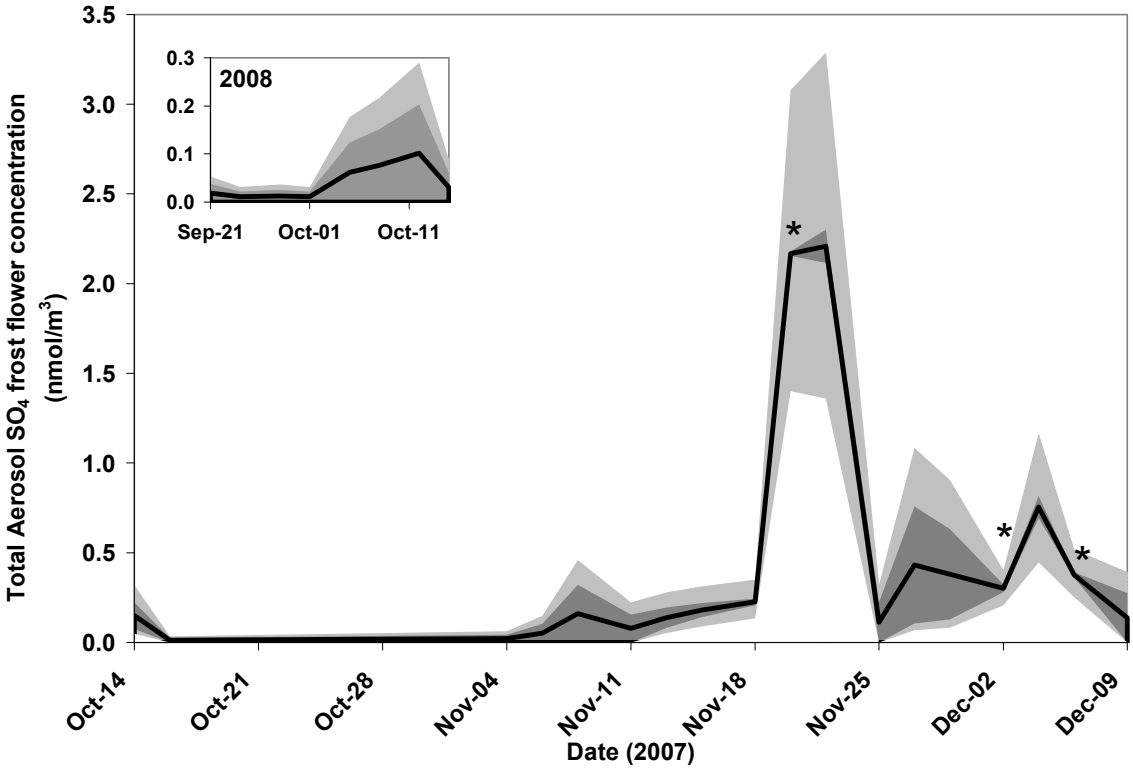

Figure 3.8 Atmospheric concentration of sulfate from frost flowers at Alert using isotope values and restraining the frost flower ratio. The light shade represents range when restricting $\delta^{34}S$ values, but not the frost flower ratio (i.e., frost flower ratio between 0.012 and 0.024). The dark grey is with the additional constraint of the frost flower (molar ratio 0.017). The dark line is the average of the maximum and minimum of the last constraint. The three times marked with * are samples where $\delta^{34}S$ values do not fall within the constraints in Chapter 3.3.2 but are within error.

samples fell outside both constraints and are marked with a * in Figure 3.8. If the range of possible frost flower ratios is considered (i.e., 0.012-0.024) these samples would fall

within the constraints. A sensitivity test constraining $\delta^{34}S$ values and testing frost flower ratios between 0.012- 0.024 is shown with light grey shading in Figure 3.8. As can be seen by the narrower dark grey band in Figure 3.8 compared to Figure 3.7, isotopes can greatly restrain the maximum and minimum frost flower contribution. Based on equation 3.6, 11 out of 26 total aerosol samples that were collected had a frost flower contribution that was significantly different than zero (assuming a frost flower ratio of 0.017). No samples in 2008 were significantly different than zero.

3.3.4 Frost Flower Contributions and Weather Parameters

As seen from Figure 3.8 there are large variations in sulfate concentrations from frost flowers. The highest concentrations occurred between November 19 and 23, 2007 (two sampling periods for total aerosol samples, one sampling period for size segregated samples).

Samples collected during the fall 2008 do not have frost flower concentrations that significantly differ from zero (see insert of Figure 3.8). Hourly temperatures recorded by Environment Canada (see Chapter 2.2) were averaged for sampling periods in 2008. The averages of the sampling periods in 2008 ranged between -8º and -19ºC with maximum temperatures ranging between -2º and -12ºC. Frost flowers have been found to grow when air temperatures are as warm as -12ºC (Perovich and Richter-Menge, 1994) and can form within twenty-four hours (Martin et al., 1995). Although some sampling periods in 2008 reached this temperature, in most cases maximum temperatures were above the

temperatures favouring frost flower growth. Also, sodium sulfate starts precipitating out of sea water at -8ºC and over half is expected to have precipitated out of the liquid phase by -10ºC (Richardson, 1976). The temperature for sodium sulfate precipitation is expected to be similar in frost flowers (Alvarez-Avilies et al., 2008). Sea water typically freezes at approximately -1.9ºC (Turner and Marshall, 2011) which leads to a temperature gradient in the atmosphere where frost flowers form. Temperatures at the height of frost flower formation can be warmer by as much as 6ºC relative to the ambient air temperature (Martin et al., 1996). This indicates that sulfate depletion may not be measureable in frost flowers that form at the upper range of frost flower formation temperatures. The much cooler temperatures in 2007 (averages range between -13º and -28ºC; maxima ranged between -4º and -26ºC; Chapter 2.2) leads to many sampling periods where frost flower formation was possible and is consistent with observable sulfate depletion.

Frost flowers not only are formed in cold weather but they also need calm wind conditions to form (Piot and von Glasow, 2008). With this being taken into consideration wind would also become an important factor to determine if aerosols have a potential frost flower signature. Frost flower aerosols, though, are primary aerosols and wind would be needed to carry the aerosols aloft (Piot and von Glasow, 2008). Wind speeds at Alert varied throughout each sampling period (see Figure 2.3 for standard deviation) with daily variations often greater than the variation between sampling periods. Therefore trends between wind speed and frost flower contribution to aerosol sulfate are not significant with the SOLAS Alert data set. Frost flowers have been found to be stable

and withstand gusts of winds in both laboratory settings (Roscoe et al., 2011) and in the field (Obbard et al., 2009). Alvarex-Aviles et al. (2008) suggest that once frost flowers dry they may become fragile and allow production of frost flower aerosols. The two highest concentrations of frost flower sulfate in total aerosols were observed at lower relative humidity (75% and 77%) compared to the average relative humidity for the 2007 season (81%). Aerosol samples taken between November 30 and December 7 that also had frost flower contributions did not follow the same pattern (see Figure 2.3) and frost flower contribution in aerosols occurred throughout the relative humidity range (daily average ranged between 73-93%).

3.3.5 Frost Flower Contributions and Air Mass Origin

Consideration of air mass origin may be more important than wind speed in determining if frost flower signature in aerosols will be present. Frost flowers aerosols would only occur in air masses travelling over areas where frost flowers are present. Therefore, it may be beneficial to look at back trajectories to determine if aerosols containing frost flower sulfate have a common origin. Back trajectories are shown in Appendix A. Aerosols that have significant frost flower contribution had back trajectories that, at some point, travelled along the northern shore of Ellesmere Island and at other times had air mass back trajectories from the north. For example, some sampling periods that are influenced by frost flowers occur between November 19-23, 2007 (containing the two samples that have the largest contribution of frost flower sulfate; Figure 3.8) and between November 30-December 7, 2007, have back trajectories that travel along the northern

shore of Ellesmere Island and are from the north (see Appendix A.1). Back trajectories during sampling periods that contain frost flower influences are relatively close to sea level (see Appendix A.1) and the direction of the wind seems to change throughout the sampling period with westerly and northerly winds predominant. This leads to a strong indication that either the northern coast of Ellesmere Island or the area north of Alert is an area of high frost flower formation. Other samples that do not have evidence of frost flowers have air mass back trajectories that also come from these directions and therefore one cannot assume that back trajectories from this area will always contain frost flower aerosols.

3.3.6 Frost Flower Contributions in Size Segregated Aerosols

Less than 8.4 nmol/m^3 of sodium (median 1.9 nmol/m^3) is found in the fine fraction of aerosols at Alert which is much lower than what is found in total aerosols (median 12.6 nmol/m^3). This indicates that little to no sea salt and/or frost flowers are present in aerosols with smaller diameters. Figure 3.9 shows the aerosol size distribution of frost flower sulfate. Frost flower sulfate is found predominantly in the coarser aerosols, as has been observed by others (Rankin and Wolff, 2003). Using the maximum frost flower contribution (i.e., the molar frost flower ratio is set to 0.024), the highest possible contribution of sulfate from frost flowers in the smallest size range (<0.49 μm diameter) is 10% and this occurs on the day when other size fractions show large amounts of frost flower contribution (see Figure 3.9; Appendix C). Minimum frost flower contribution to sulfate loading in this size range is 0% in most cases. This indicates that frost flower

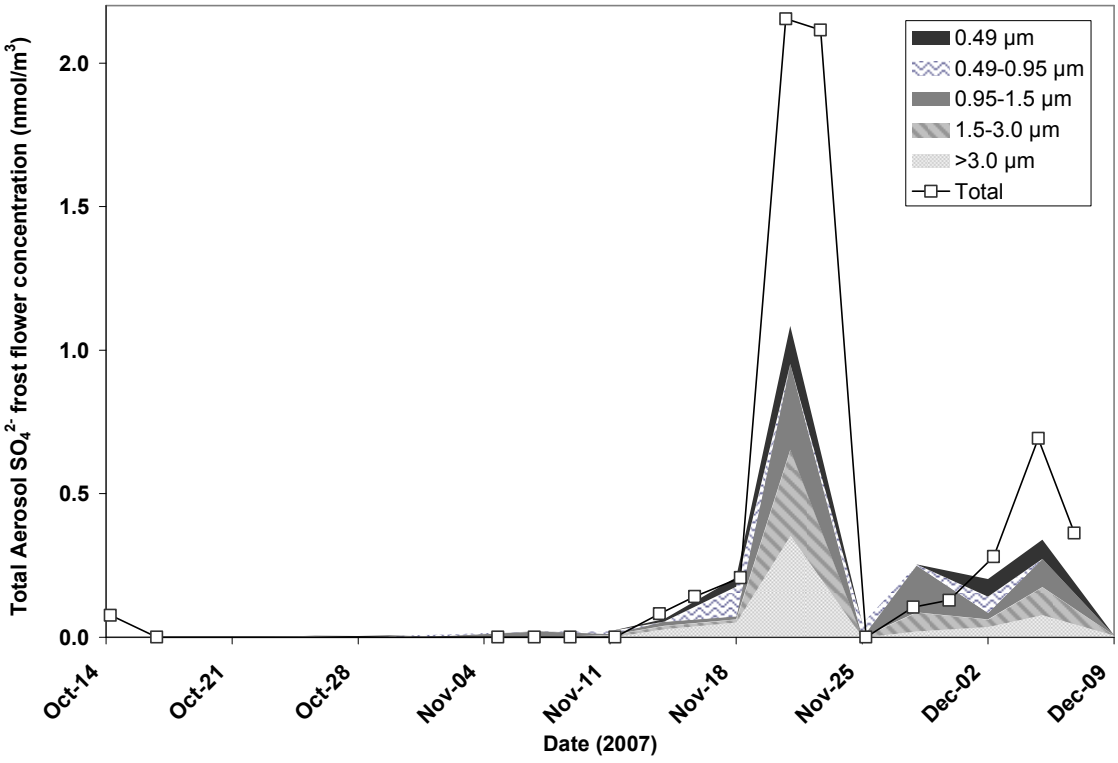

Figure 3.9 Minimum cumulative frost flower concentration in the different size segregated samples. Note that many of the 7.2 µm and 3.0-7.2 µm size segregated samples had no $\delta^{34}S$ data and therefore frost flower contributions from these size fractions are not displayed on the graph.

contribution is minimal in the fine aerosols (i.e., less than 10% of the sulfate concentration in the fine aerosols). Aerosol frost flower contributions must be near the source of frost flowers since larger aerosols have shorter lifetimes. This finding supports that frost flower contribution inland would be minimal and is consistent with properties of primary aerosols and studies that have found frost flowers close to the coast but not inland (Hara et al., 2004).

3.3.7 Frost Flower Salts

Frost flower presence is hard to determine because many of the frost flower ions (with the exception of sulfate) have ratios similar to those for sea salt. The ratios though, will change as different ions precipitate out in the form of a salt once saturation is reached in the brine. The most common salt to precipitate is mirabilite (i.e., Na_2SO_4) which leads to the calculated negative non sea salt sulfate discussed in Chapter 3.3.1. Sodium concentration would also decrease but since sodium concentrations are much higher than that of sulfate in sea water, the percent of sodium precipitated out is low. Only 13% of the sodium in the frost flowers would be removed if all sea salt sulfate was precipitated out (Rankin et al., 2002). Therefore, accurate measurements of sodium and other sea salt ions must be made in order to determine if sodium is depleted relative to other sea salt ions. Chloride is sometimes used when looking for signs of frost flowers (e.g., Alvarez-Aviles et al., 2008). Chloride and sodium were plotted against each other for samples of all size fractions in Figure 3.2. It is interesting to note that the two highest concentrations of sodium in aerosols are depleted compared to that of the sea salt ratio when comparing sodium relative to chloride (insert in Figure 3.2). This depletion is also seen when comparing magnesium and sodium. These two points are associated with the total aerosol on the days that high frost flower concentrations were detected. This is consistent with a depletion of sodium relative to chloride and magnesium when frost flowers are present. The next three highest concentrations of aerosol sodium fall within error of the sea salt ratio with chloride, but when compared to magnesium, these points show depleted sodium relative to the sea salt ratio.

Another abundant salt that precipitates out of brine is hydrohalite ($NaCl \cdot 2H_2O$). If precipitation of $NaCl \cdot 2H_2O$ occurred, it would deplete not only chloride (as mentioned above) but also sodium (i.e., the two most common sea salt ions). Comparison between these two ions and that of magnesium concentrations can be studied to determine if any significant depletion of sodium and chloride occurred. This salt only starts to begin to precipitate below -22.9 ^{o}C (Richardson, 1976), but because of the higher concentrations of Cl^- in sea water relative to SO_4^{2-}, $NaCl \cdot 2H_2O$ can precipitate four times the amount (by mass) than Na_2SO_4 (Light et al., 2003). Temperatures at the height of frost flowers (approximately 1-5 cm; Martin et al., 1996; Douglas et al., 2012) can be warmer than ambient temperature by as much as 6º C (Martin et al., 1996) and thus the ambient temperature will be cooler than that of the frost flowers. Keeping this in mind, temperatures below -22.9ºC were recorded at Alert many times (see Figure 2.3 in Chapter 2.2) in 2007. Figure 3.2 and Figure 3.10 display magnesium relative to sodium and chlorine concentrations at Alert. Two possible sampling periods where the formation of hydrohalite ($NaCl \cdot 2H_2O$) may be observed are November 26 to 28, 2007 and November 28 to 30, 2007. Temperatures for these two sampling periods averaged -22 ºC and -21 ºC and therefore $NaCl \cdot 2H_2O$ could possibly have formed for at least some of the sampling period. Magnesium is also found in crustal material at Alert (Sirois and Barrie, 1999) and therefore the elevated magnesium could potentially also be from crustal sources around Alert. This depletion of sodium and chloride relative to magnesium is not seen in the size segregated samples for the same time period. This may be attributed to the high uncertainty in magnesium for the larger diameter aerosol segregated samples (see Chapter 2.5). Therefore, although there is some possibility of precipitation of

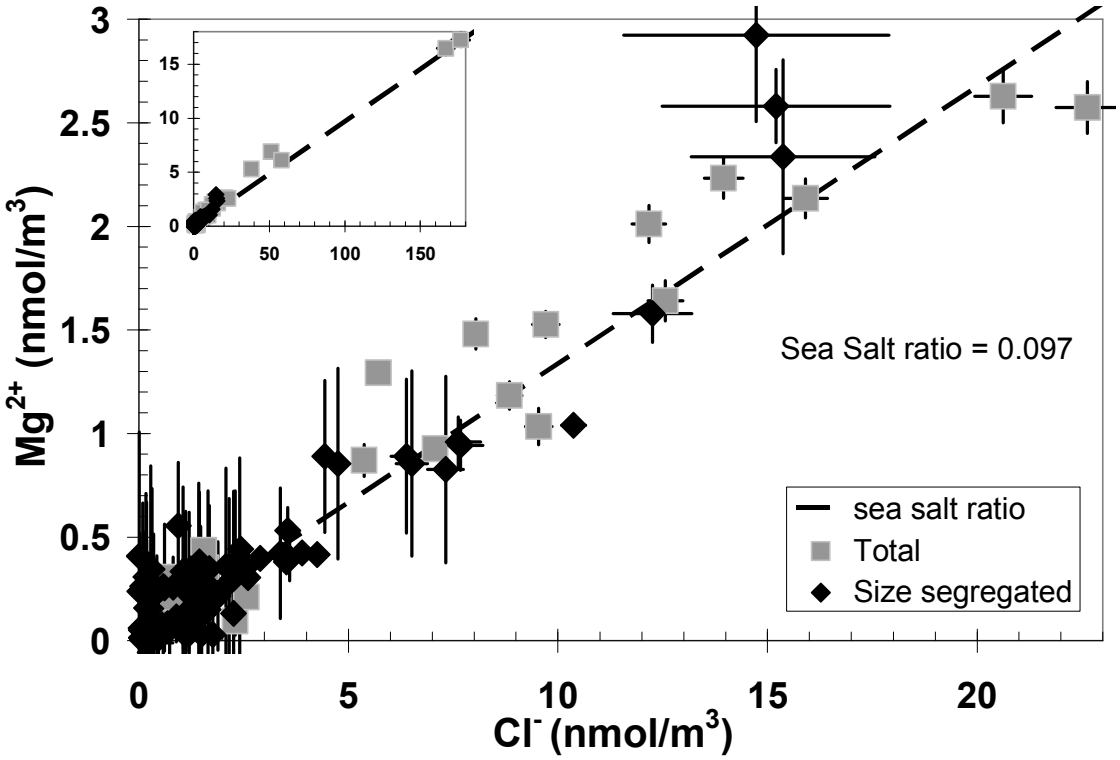

Figure 3.10 Magnesium and chloride concentrations at Alert found in total aerosol samples (grey squares) and size segregated samples (black diamonds) compared to the sea salt ratio (dashed line).

$NaCl \cdot 2H_2O$ in the frost flower aerosol it would require much more study with higher resolutions in ion concentrations than are presented here and an ability to distinguish between soil and frost flower components. Measurement of aluminum or iron concentrations would assist in identifying lithospheric contributions (Sirois and Barrie, 1999). See Chapter 3.5.1 for more description of crustal influences.

Another salt that precipitates out of frost flowers is ikaite ($CaCO_3 \cdot 6H_2O$); this salt starts precipitating out of solution at temperatures below -2^oC (Light et al., 2003). The temperature at Alert was always lower than the -2^oC needed and therefore calcium would be expected to be depleted relative to other sea salt ions if ikaite formation in frost flowers was significant. The fine and total aerosol calcium concentrations are compared with chloride concentrations in Figure 3.11 and were found to be elevated compared to sea salt, which is opposite of the argument above. Calcium is also expected to be derived from crustal material (Sirois and Barrie, 1999). Non sea salt Mg and NSS-Ca are most likely to be crustal in nature (see Chapter 3.5.1) and frost flower depletion of $CaCO_3 \cdot 6H_2O$ and $NaCl \cdot 2H_2O$ in this data set are not distinguishable.

3.3.8 Comments on Constraints for Future Studies

The $\delta^{34}S_{nss}$ values constrain contributions from frost flowers (see Section 3.3.3.2) but the method for determination of the constraints does have some limitations. The method introduced in Section 3.3.3 can be used not only in aerosols (as was demonstrated in this work) but also in ice cores where frost flower contributions could mask the contributions of the non sea salt sulfate in the sample. For future work, a number of assumptions and constraints must be taken into consideration when determining frost flower contributions to sulfate in the sample (either aerosol or ice core). The error introduced in cation and anion measurements, the restrictions on $\delta^{34}S_{nss}$ values and the ratio of FF_{ratio} used leads to uncertainty in the calculation of frost flower contribution to aerosol sulfate.

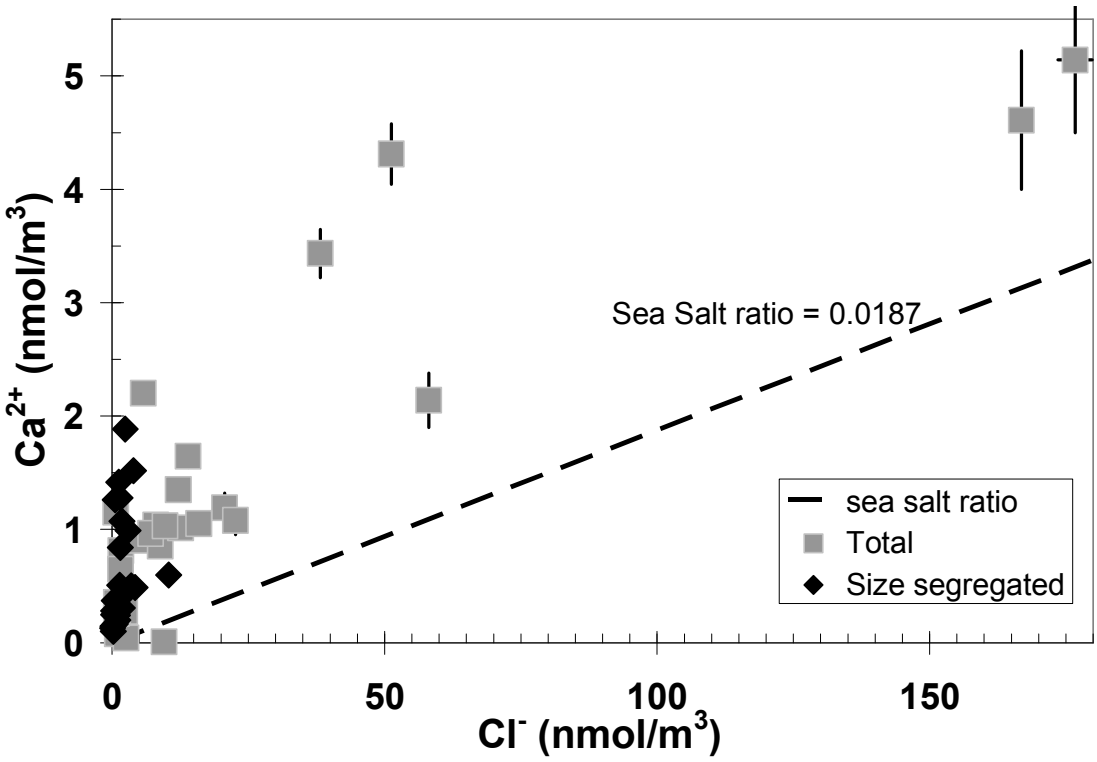

Figure 3.11 Calcium and chloride concentrations found in total aerosol samples (grey squares) and size segregated samples (black diamonds) at Alert compared to the sea salt ratio (dashed line)

3.3.8.1 Cation/Anion Measurements

Low concentrations of ions limit the ability to distinguish between sea salt and frost flowers (See Section 3.3.3.2) because of the high percent error associated with the measurements. Samples influenced by frost flowers tend to have larger ion concentrations (Wagenbach et al., 1998; Jonsell et al., 2005) and therefore for overall frost flower contribution, samples with low ion concentration have little contribution. In this study,

the fine (<0.49 μm) and total aerosol ion concentrations had a median error of 5% and 10% for SO_4^{2-} and Na^+ respectively. In future studies, error associated in the blank correction for ions should be at least this precise. Ice core samples, in theory, should have lower overall error for each measurement because no error is introduced by blank filters (Section 2.8.1). Therefore, frost flower contributions in ice cores may be more precise than in aerosol studies.

3.3.8.2 Restrictions on $\delta^{34}S_{nss}$ Values

Less error in the frost flower lower concentration would be introduced if there was a consistent background sulfur isotope signature in the sample. Since there is possibility of both anthropogenic (+4.4‰) and biogenic (+18‰) influences at Alert, both the $\delta^{34}S$ values must be considered when calculating frost flower contribution (see Section 3.3.3.2 and Figure 3.8). It is more likely that the anthropogenic sulfate becomes increasingly significant as the biogenic sulfur component is less prevalent as water freezes with the onset of winter. In Figure 3.8 the frost flower molar ratio SO_4^{2-}/Na^+ is kept constant at 0.017 and the maximum and minimum from the variability of $\delta^{34}S_{nss}$ values (anthropogenic and biogenic) is shown by the dark grey shading.

Constraining the $\delta^{34}S_{nss}$ value only assists in restricting frost flower contribution when the frost flower contribution is large relative to other sources of sulfate. At Alert, the restriction of $\delta^{34}S_{nss}$ values usually constrains the minimum concentration (compare

between Figure 3.7 and Figure 3.8). In future studies, if the $\delta^{34}S_{nss}$ value was known and constant, calculations could commence on not only the concentrations of each of the sulfate components but could also restrict the frost flower ratio. This could be the case in areas such as the Antarctic or in preindustrial ice cores where biogenic sulfate is expected to be the largest source of non sea salt sulfate and anthropogenic sulfate is expected to be minimal (Patris et al., 2002; Rankin and Wolf, 2003).

3.3.8.3 Frost Flower Ratio

Frost flower molar SO_4^{2-}/Na^+ ratios between 0.012 and 0.024 were used when investigating the maximum and minimum contribution of frost flowers (Figure 3.7, Figure 3.8). These frost flower ratios are those reported in aerosols by Rankin et al. (2002). Alvarez-Aviles et al. (2008) and Douglas et al. (2012) found larger ranges when measuring concentrations of ions in frost flowers directly. Frost flower SO_4^{2-}/Na^+ ratios are not consistent. Factors such as the temperature of frost flower formation and age of the frost flower (Alvarez-Aviles et al., 2008) can affect the molar ratio of ions in the frost flowers. Composition of the salts precipitating out explained in Chapter 3.3.7 will affect the frost flower molar ratios by possibly depleting Na^+, SO_4^{2-}, Cl^- and Ca^{2+}. As shown in Figure 3.7, the uncertainty in the frost flower ratio can lead to a large variation in the minimum and maximum amount contribution from frost flowers. In future studies, this variability of the frost flower SO_4^{2-}/Na^+ ratio, must be kept in mind when determining frost flower contributions.

3.4 Sea Salt Sulfate Revisited

Sea salt concentrations can now be determined using equation 3.7. Minimum frost flower contributions based on the constraints of $\delta^{34}S_{nss}$ values and a frost flower ratio of 0.017 are used for the calculation. Frost flowers are expected in aerosols only under specific atmospheric conditions (Alvarex-Aviles et al. 2008; Piot and von Glasow, 2008; Obbard et al., 2009; Roscoe et al., 2011) and thus the minimum value (based on equation 3.6, FF_{ratio}= 0.017; see Figure 3.8) is used for determining contribution from frost flowers to sulfate concentrations. This may lead to an underestimation during times of significant frost flower events but would be more accurate during the remainder of the sampling period when frost flower contributions are minimal. Concentrations of sea salt sulfate in total aerosol at Alert are displayed in Figure 3.12. The uncorrected sea salt sulfate calculated by using the sea salt ratio ($Na \cdot SS_{Ratio}$; see Section 1.1) is also shown in Figure 3.12 to illustrate the importance in including frost flowers in the corrections, especially after November when temperatures are colder and frost flowers become more prevalent. When frost flower concentrations are large (i.e., between November 19 – 23, 2007) sea salt sulfate concentrations can differ by over 7 nmol/m^3 between the two calculations (i.e., $Na \cdot SS_{ratio}$ vs. equation 3.7), which is more than two times the largest concentration of sea salt found during the study period. If frost contribution is minimal equation 3.7 approaches $Na \cdot SS_{ratio}$ and sea salt concentrations calculated from both calculations are the same (see Figure 3.12). This is observed, for example, for the duration of the 2008 sampling period.

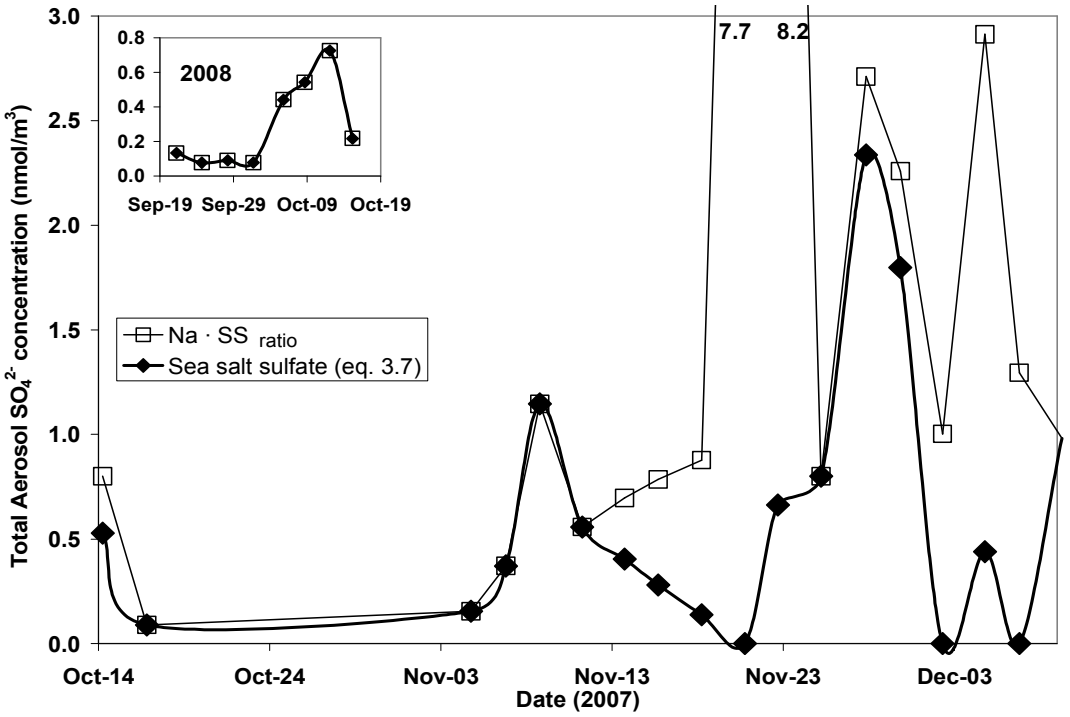

Figure 3.12 Sea salt sulfate concentrations in total aerosols collected at Alert based on equation 3.7 (black diamonds). Calculated sea salt concentrations that are not corrected for frost flower concentrations (i.e., $Na^+ \cdot SS_{ratio}$) are displayed with white squares. Insert displays sea salt concentrations at Alert for 2008.

3.4.1 Sea Salt Sulfate Concentration

Sea salt concentrations were greater on board the *Amundsen* than at Alert at all times. (see Figure 3.13) as might be expected given the location of the sampling units: high volume samplers would be expected to collect considerably more sea salt on board the *Amundsen* than at Alert (See Chapter 2.1 for location of samplers). Although Alert is considered a coastal location, the surrounding ocean typically remains frozen in the fall

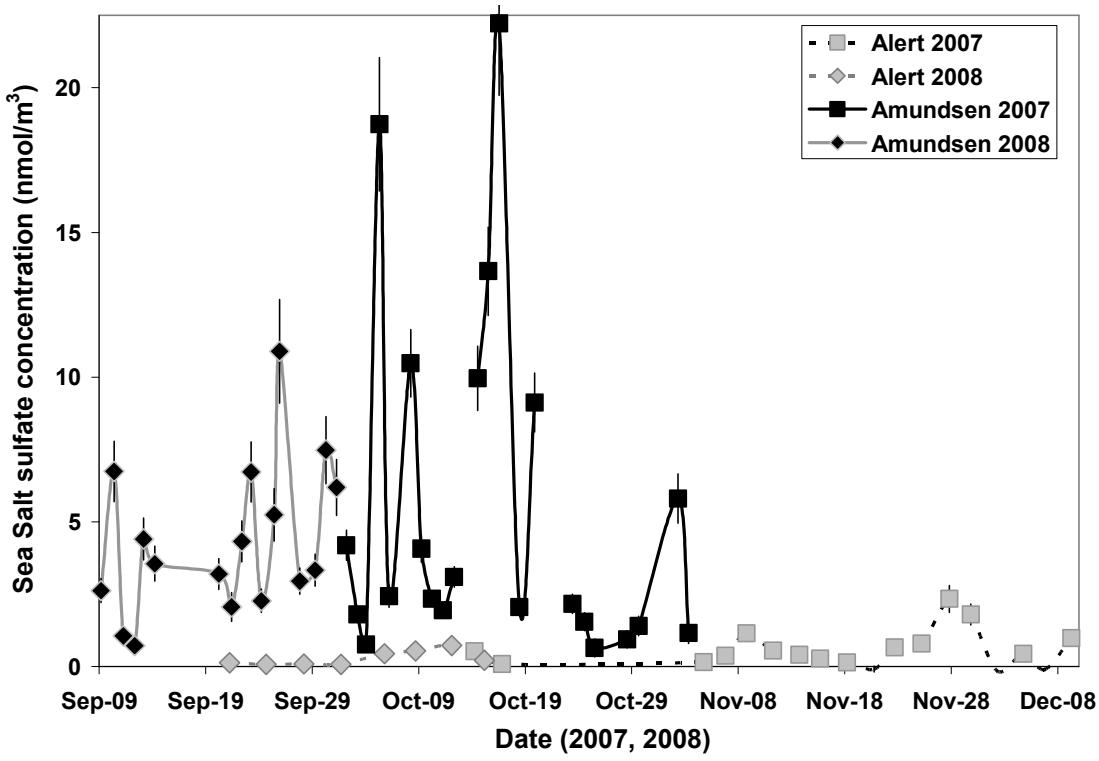

Figure 3.13 Comparison of sea salt sulfate concentrations in total aerosol at Alert and on board the *Amundsen* in 2007 and 2008

(Helmig et al., 2007). Sea salt is typically found in aerosols of the larger size fractions in the Arctic, although sea salt has occasionally been found in the fine aerosol (<0.49 μm) in previous works (Lewis and Schwartz, 2004; Seguin et al., 2011).

Total aerosol sea salt sulfate loading between the two sites (see Figure 3.13; Appendix C) is significantly different due to the difference in sea salt loading in the larger diameter aerosols. This is consistent with the idea of long range transport and that the size of the aerosol is strongly influenced by dry deposition velocity (Seinfeld and Pandis, 1998).

Dry deposition velocity increases between aerosol diameters 0.2 – 10 μm because of gravitational settling which increases with the square of the particle diameter (Seinfeld and Pandis, 1998). Therefore the large aerosols would tend to gravitationally settle out of the atmosphere faster and closer to the source, than those of smaller size.

Smaller size fractions are expected to have a longer lifetime and therefore it is expected that sea salt sulfate further away from the source (i.e., the ocean) may be carried by the fine fraction rather than coarse aerosols. Sea salt sulfate aerosols from the *Amundsen* were more likely found in the larger aerosol fractions: see Figure 3.14 for 2007 and Figure 3.15 for 2008 relative to Alert (Figure 3.16 and Figure 3.17). See Appendix C for details. Over 60% of sea salt is found in size fractions greater than 1.5 μm at all times in the *Amundsen* data set (no data for aerosols > 3.0 μm is available for sampling period October 13 – 17, 2007). The *Amundsen* high volume sampler that collected size segregated samples was fitted with a PM10 head and therefore sea salt aerosols greater than 10 μm would not be collected on the size segregated samples but would be present on the total aerosol filter. As seen from Figure 3.14 and Figure 3.15 this size fraction (i.e., >10 μm) may make up a significant amount of sea salt loading on the total aerosol samples.

Although sea salt sulfate is also found in the larger aerosol fractions at Alert, the results are more variable and a higher percentage of sea salt sulfate occurs in aerosols less than 0.49 μm in diameter (see inserts of Figure 3.16 and Figure 3.17, and Appendix C).

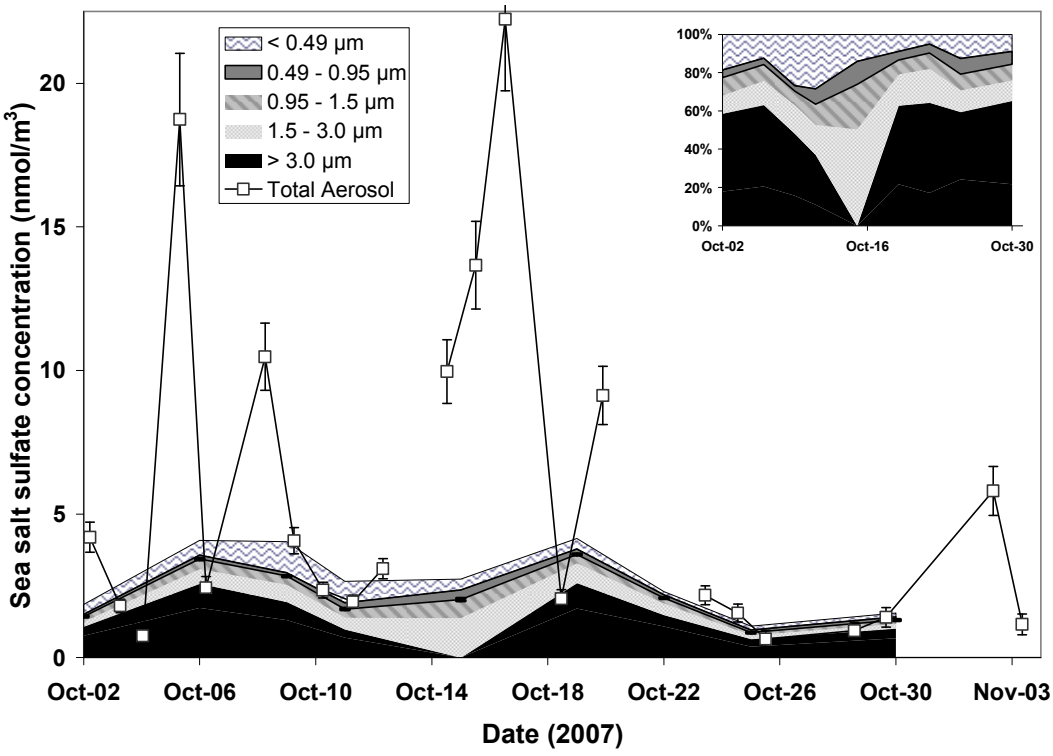

Figure 3.14 Sea salt sulfate in size segregated samples in 2007 from the *Amundsen*. Error is shown on the total and 0.95 -1.5 µm size range aerosols. Percent contribution is displayed in the insert. Size segregated concentrations are cumulative.

Concentrations of sea salt for fine aerosols (<0.49 µm) remained relatively constant between the two sites in 2008 (see Figure 3.18). More variation in the samples was observed in 2007 between the two sites (see Figure 3.18). Sea salt sulfate concentrations in the fine aerosols from the *Amundsen* in 2007 are elevated in some instances (i.e., between October 7– 13, 2007) relative to Alert and are higher compared to sea salt sulfate concentrations measured in 2008. Sea ice coverage between midnight on October 9th

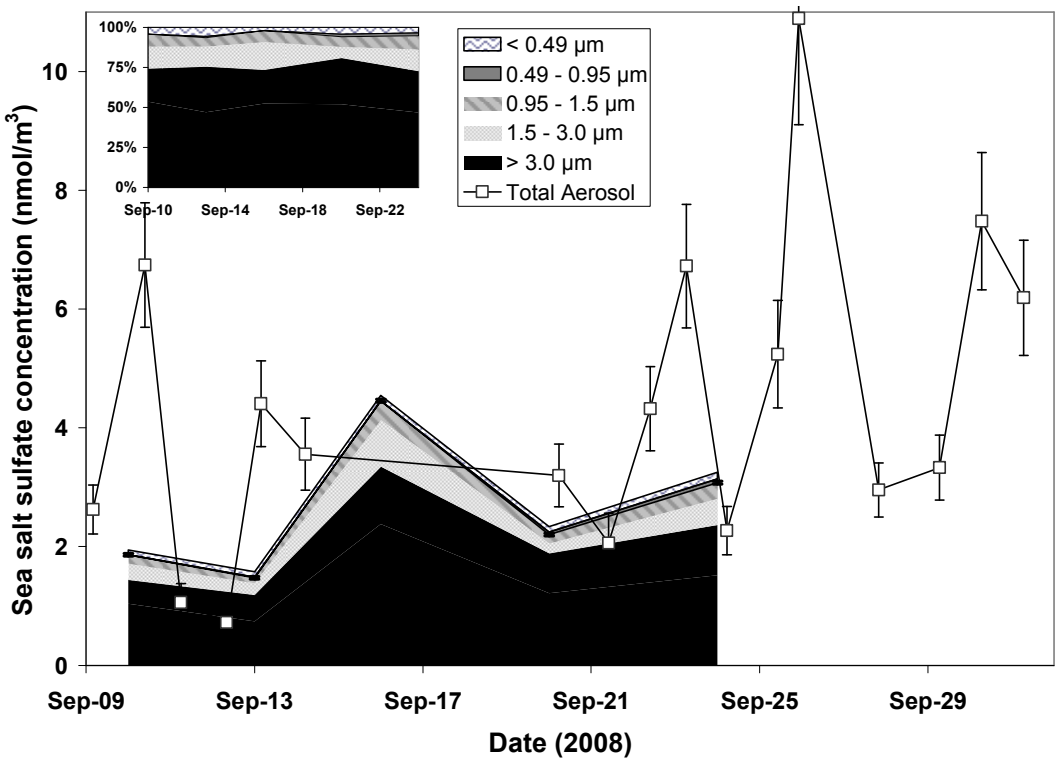

Figure 3.15 Sea salt sulfate in size segregated samples in 2008 from the *Amundsen*. Error is shown on the aerosol and 0.95 -1.5 µm size range aerosols. Percent contribution is displayed in the insert. Size segregated concentrations are cumulative.

and 11:30 on October 11 was significant (usually between 80 to 90% of the ocean surface) and may have influenced the fine aerosol sea salt sulfate contribution. In areas of high sea ice coverage blowing snow may contribute to the sodium loading of aerosols (Chapter 3.3). Blowing snow, though, would be comprised of primary and larger size aerosols (Chapter 3.3.6). Although the fine aerosol sea salt component was elevated

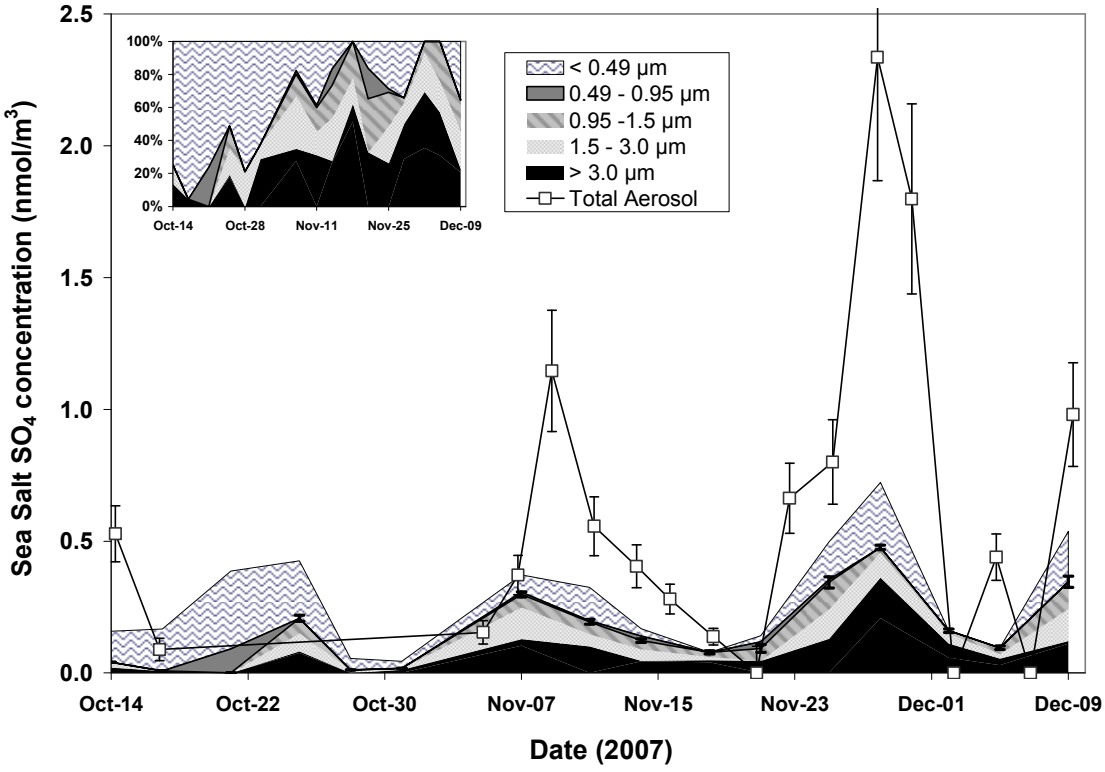

Figure 3.16 Sea Salt sulfate in size segregated samples in 2007 at Alert. Error is shown on the total and 0.95 -1.5 µm size range aerosols. Percent contribution is displayed in the insert. Size segregated concentrations are cumulative.

during these two times, the course aerosol components were not significantly affected (see Figure 3.14; Appendix C). Therefore blowing snow contributions are not consistent for an explanation of the elevated sea salt sulfate in the small size fraction during these times. Leck and Bigg (2005) suggest a process that could potentially introduce sea salt in the fine aerosol fraction particularly when productivity is high. Sea-ice algae and bacteria produce hydrophobic exopolymer secretions that are transferred from the micro

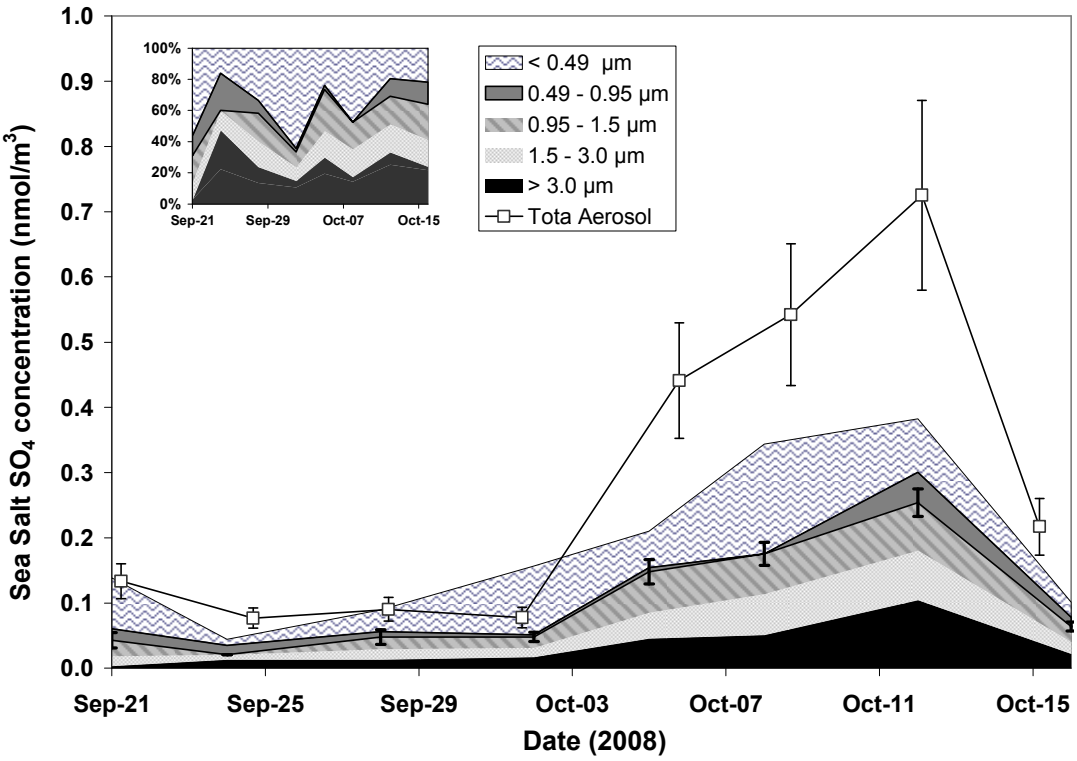

Figure 3.17 Sea salt sulfate in size segregated samples in 2008 at Alert. Error is shown on the total and 0.95 -1.5 µm size range aerosols Percent contribution is displayed in the insert. Size segregated concentrations are cumulative.

layer of the ocean to the atmosphere in spherical aerosols. Once in the air the lipid surface of these aerosols may dissolve in the presence of acidity, producing a burst of material that reflects the composition of the micro layer of the ocean. This may include sea salt components and could be an explanation for the elevated fine fraction of sea salt observed between October 7– 13, 2007. Rempillo (2011) reported high productivity during this sampling period which would support that the process proposed by Leck and Bigg (2005) may be of importance during this time period.

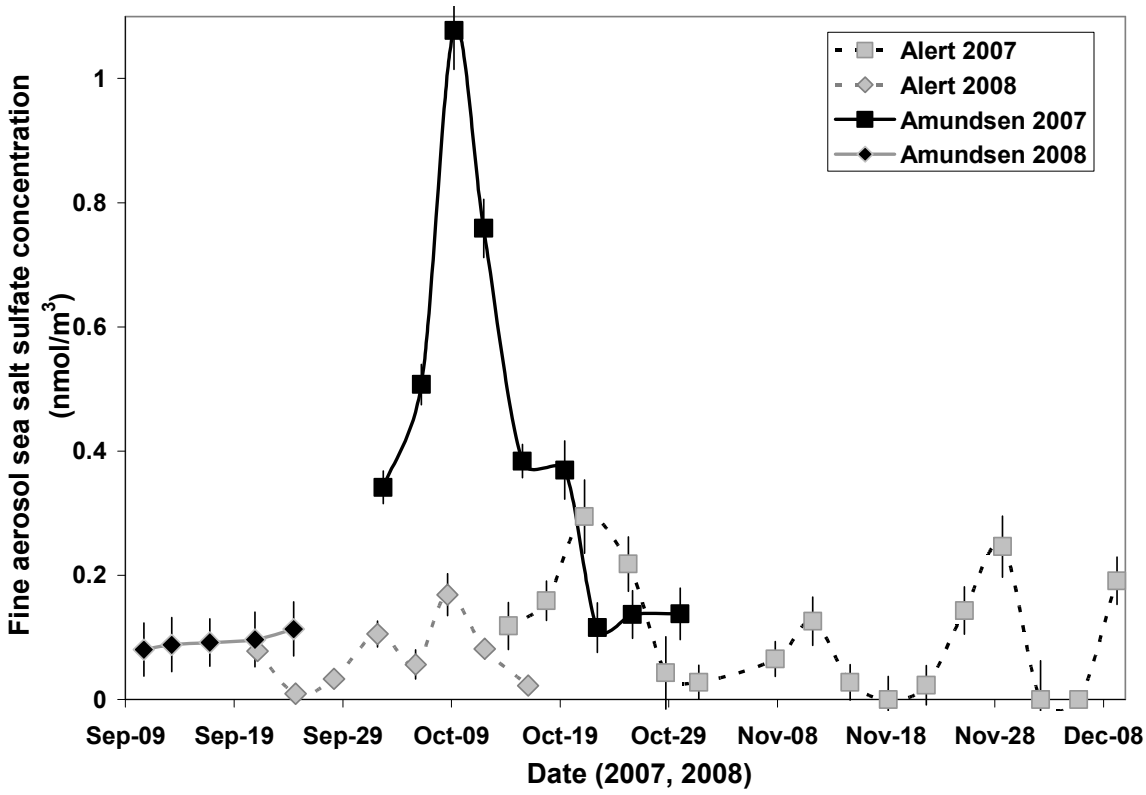

Figure 3.18 Sea salt sulfate concentrations in fine aerosol at Alert and on board the *Amundsen* in 2007 and 2008.

3.5 Lithospheric Influences

3.5.1 Crustal

Sirois and Barrie (1999) studied constituents of aerosols found at Alert between 1980 and 1995. They found that both local and long range transport influenced the crustal component of aerosols from Alert. Using aluminum as a tracer for crustal influence, they found that there were two seasonal peaks, one in the spring and another in September.

The peak in September is mainly from local dust (Sirois and Barrie, 1999). Aluminum was not analyzed for the samples collected during the SOLAS study, but two other components of local crustal composition were. The major source of calcium in aerosols at Alert is expected to be crustal (Sirois and Barrie, 1999; Jacobi et al., 2012). Magnesium is also crustal although it also has a large component that comes from sea salt.

Crustal components in aerosols are additional to the sea salt components. Therefore a comparison between positive non sea salt magnesium with positive non sea salt calcium (see Chapter 1.1 for calculations of non sea salt calculations) for the total aerosol filter should give insight to the ratio of these elements in the crustal component in aerosols. Samples collected at Alert show a linear relationship with a slope of approximately one for the NSS Ca^{2+}/NSS Mg^{2+} (see Figure 3.19). Sirois and Barrie (1999), using positive matrix factorization, found a larger ratio for crustal component (approximately 1.94). An excess of both magnesium and calcium relative to the sodium ratio in sea water was found in the positive matrix factorization sea salt component by Sirois and Barrie (1999) and therefore the calculated ratio from the crustal component in their study would not necessarily represent the NSS Ca^{2+}/NSS Mg^{2+} calculated in this thesis. A second possibility for the difference in the ratio may be due to the presence of frost flowers in this study. The calculated NSS component based on equation 1.1 is actually the non sea salt and the non frost flower component if the ratio of sea salt is preserved in frost flowers. As discussed in Section 3.3.7, most sea salt ions ratios are preserved in frost

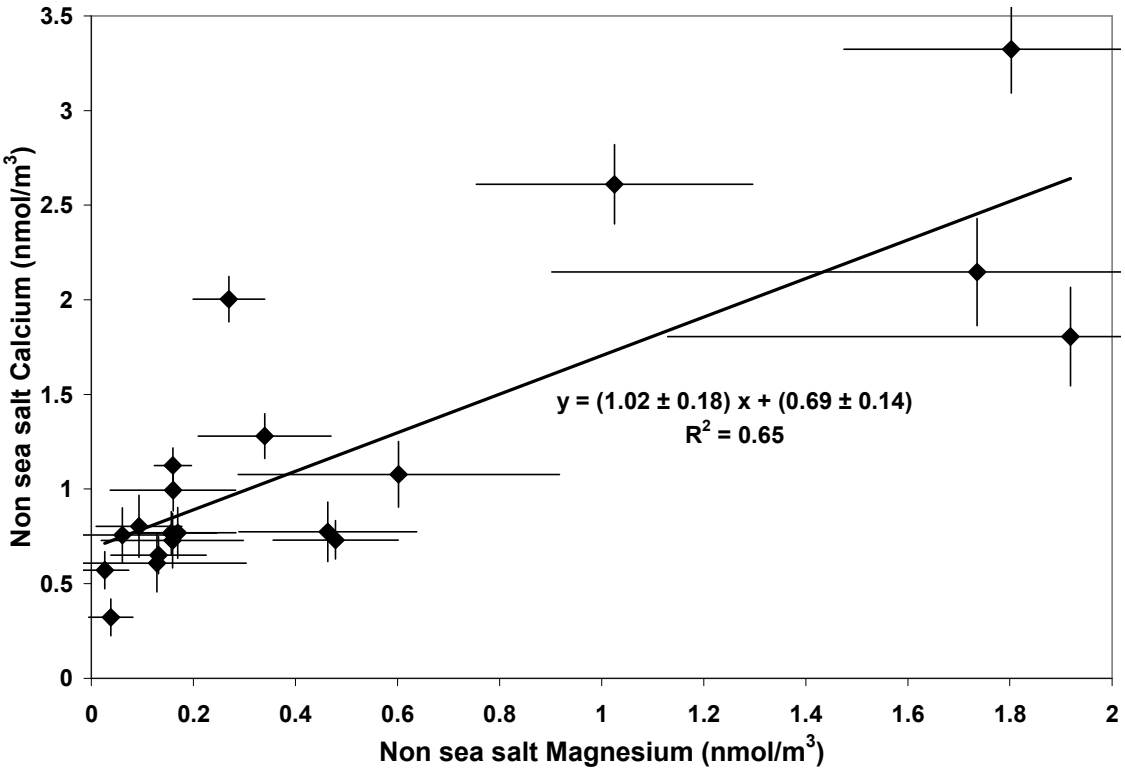

Figure 3.19 Non sea salt calcium versus non sea salt magnesium at Alert. Both NSS calcium and NSS magnesium are expected to be from a crustal component.

flowers. This would be true in the case of magnesium but calcium may be depleted in frost flowers since $CaCO_3 \cdot 6H_2O$ can precipitate out (see Section 3.3.7). The calcium contribution from frost flowers may therefore be overestimated which would lead to an underestimation of calcium from other sources such as the crustal component. The calcium/sodium ratio for frost flowers varies in the literature; some predict almost 100% Ca^{2+} depletion with the formation of sea ice and thus frost flowers (Sander et al., 2006; Piot and von Glasow, 2008 and references within) and others that measured calcium in frost flowers samples found excess calcium relative to the sea salt ratio (Douglas et al.,

2012). With such a large variability in Ca^{2+}/Na^{+} ratios, a frost flower correction similar to what was carried out for SO_4^{2-} (Section 3.3.3) cannot be conducted.

It may be more beneficial to study the total calcium found in aerosols compared to NSS magnesium since 79% of calcium in aerosols has been attributed to contributions from soil in the past (Sirois and Barrie, 1999). A strong correlation ($R^2 = 0.93$) between total calcium and NSS magnesium is observed (see Figure 3.20) with a slope of 2.21 closer to

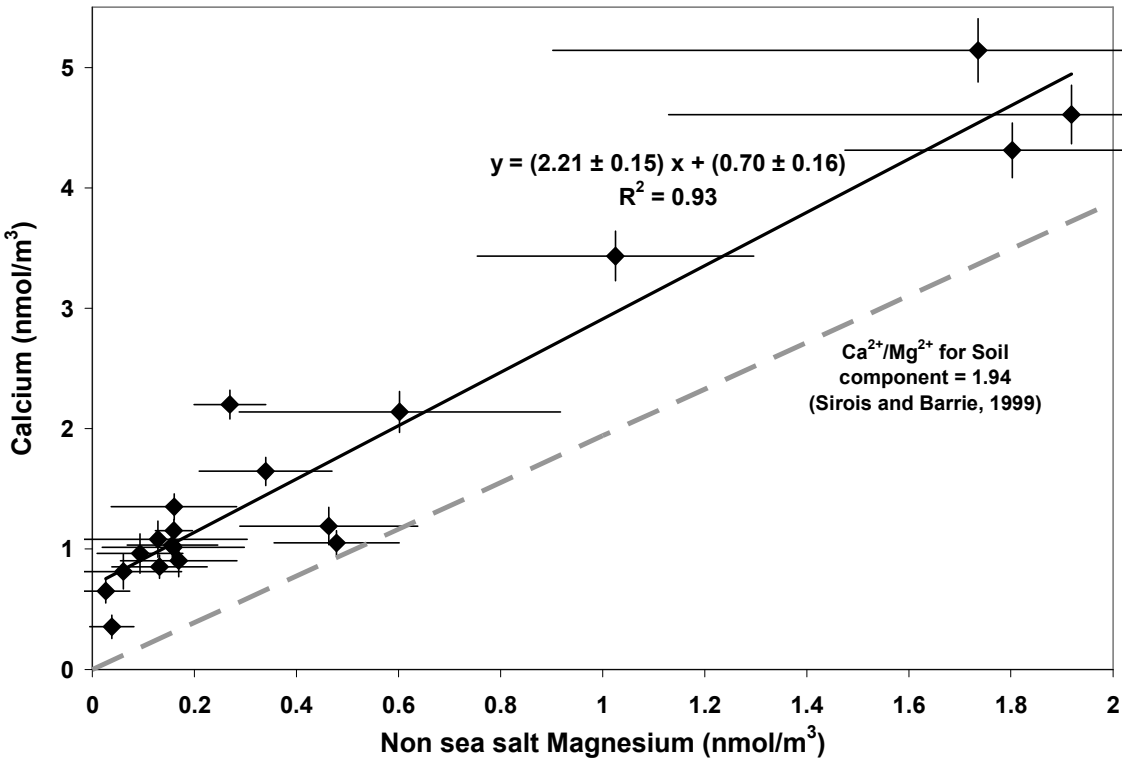

Figure 3.20 Calcium versus non sea salt magnesium at Alert. Both NSS calcium and NSS magnesium are expected to be from a crustal component. The Ca^{2+}/Mg^{2+} ratio for the soil component in aerosols found by Sirois and Barrie (1999) is plotted for comparison.

the ratio found by Sirois and Barrie (1999) than when comparing NSS Ca^{2+} and NSS Mg^{2+}. The larger ratio can be explained by the inclusion of sea salt calcium in this data set and that positive matrix factorization by Sirois and Barrie (1999) accounts for other sources of these ions.

In the Alert data an offset was observed between calcium and non sea salt magnesium. This may be attributed to an additional source of calcium at Alert that is not accounted for or the analysis techniques used in this thesis (Section 2.5). Calcium in the form of $CaCO_3$ from the skeletons of pelagic organism and coccoliths can be introduced into aerosols from sea spray which would lead to excess calcium (Hoornaert et al., 1996 and references within). Measurements for ions are for dissolvable ions in aqueous solution only, and may not be representative of the total amount of magnesium and calcium found in the soil component.

Calcium and non sea salt magnesium concentrations were calculated for samples taken on board the *Amundsen*. Because of the large sea salt component in aerosols collected on the *Amundsen*, propagated error (equation 2.7) for NSS magnesium (equation 1.1) was on the same order of magnitude as the concentrations (approximately 0.3 nmol/m^3) and/or NSS magnesium was found to be negative for the majority of the samples and therefore tests for crustal influence could not be conducted for *Amundsen* samples. It was noted, though, that total aerosol samples had a median of 1.58 nmol/m^3 non sea salt calcium (compared to 0.76 nmol/m^3 at Alert) and that this excess calcium is likely from $CaCO_3$ in

sea spray (Hoornaert et al., 1996) or from calcium in crustal components (Sirois and Barrie, 1999; Jacobi et al., 2012).

Although calcium and magnesium concentrations in aerosols are influenced by local crustal sources, aerosol sulfate concentrations are minimally influenced since sulfur content in soils is typically less than 1% and most is not in the form of sulfate (Norman et al., 1999). Norman et al. (1999) reported measurements for a single aliquot of local crustal material around Alert. The sample had low concentrations of sulfate (approximately 4.4 μg S/g soil) with a $\delta^{34}S$ value of approximately +5‰. Therefore aerosols formed from crustal sources are not expected to contribute greatly to the sulfur loading at Alert. Since long range transport of crustal material over a period of fifteen years was low in the Fall (Sirois and Barrie, 1999) and typically low concentrations of sulfate are found in soils, influences from long range crustal material on sulfate concentrations in aerosols during the Arctic fall on a regional level are expected to be minimal compared to sea salt, anthropogenic and biogenic sources.

3.5.2 Volcanic

Besides crustal sources, lithospheric influence can come from volcanic activities although at Alert this is expected to be minimal (Norman et al., 1999). The Smithsonian/United States Geological Survey Global Volcanism Program reported little to no volcanic

activity in and around the Arctic during the time of the SOLAS campaign (http://www.volcano.si.edu/reports/usgs/index.cfm?content=archive).

3.5.3 Smoking Hills

The Smoking Hills are located at 79°14`N 127°10`W where exposed bituminous shale in sea cliffs are spontaneously ignited. This releases SO_2, sulfuric acid mists and aerosols into the atmosphere (Freedman et al., 1990). This source of sulfur into the Arctic atmosphere is expected to be important on a local scale but not on a regional scale (Radke and Hobbs, 1989). Radke and Hobbs (1989) estimated a flux from the Smoking Hills of 4.5 ± 3.0 moles/s for SO_2 and a 0.2-0.26 kg/s flux for fine fraction (0.05-1.9 μm) aerosol consisting almost entirely of soluble sulfate. Sulfur and iron are the major components of the central nuclei of the droplet. If the whole mass of the aerosol was composed of sulfate this would lead to a flux of 2.1 – 2.7 moles/s. Concentrations of sulfur (both aerosol sulfate and SO_2 concentrations) collected on board the *Amundsen* within the vicinity of the Smoking Hills (October 22 – October 28, 2007) did not show significant elevated non sea salt sulfur concentrations compared to other locations in the Arctic (see Figure 3.21 for non sea salt sulfate). Influence from the Smoking Hills on non sea salt sulfate concentrations are masked by other sources of sulfate such as anthropogenic and biogenic.

The $\delta^{34}S$ values in the vicinity of the Smoking Hills, however, were clearly influenced. Shale from the Smoking Hills has $\delta^{34}S$ values that range between -30 to -40‰ (Rempillo

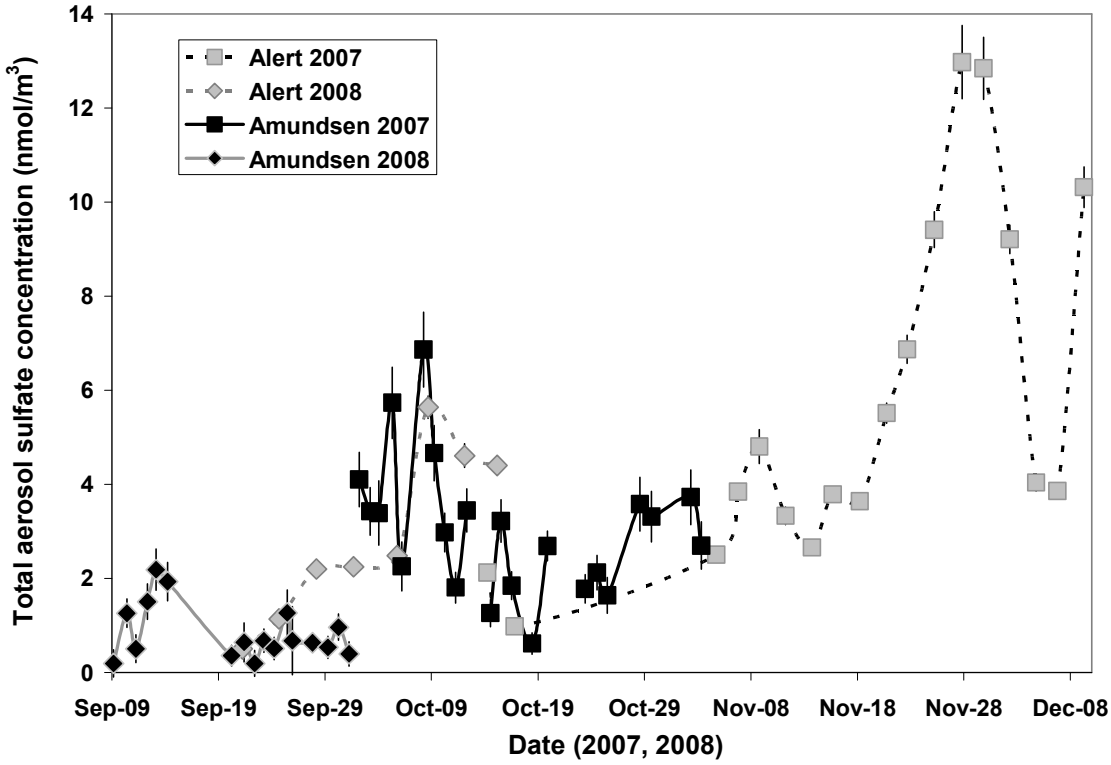

Figure 3.21 Non Sea salt sulfate concentrations in total aerosol at Alert and from the *Amundsen* in 2007 and 2008. Local smoke stack emissions can influence the *Amundsen* data.

et al., 2011). Size segregated aerosols collected within the vicinity of the Smoking Hills less than a size of 3 μm diameter had negative $\delta^{34}S$ values (see Appendix Figure B.2).

Negative $\delta^{34}S$ values were also found in the total aerosol and SO_2 samples during the same sampling periods. SO_2 along with the aerosols with size ranges between 0.95-1.5 μm and 0.49-0.95 μm had the most negative $\delta^{34}S$ values (as low as -21‰) indicating that at the time of sampling the aerosols of these size ranges were influenced the most by

emissions from the Smoking Hills. Volume distribution of aerosols measured directly over the Smoking Hills (Radke and Hobbs, 1989) dictate that the <0.49 μm aerosol size range measured for the SOLAS study should show the largest influence of sulfur loading from the Smoking Hills. The difference between the SOLAS study and the previous study by Radke and Hobbs (1989) is that the air mass influenced by the Smoking Hills had a chance to age. Aerosol growth can occur by the oxidation of SO_2 on existing aerosols and/or condensation of water as the aerosols travel across the ocean (Seguin et al., 2011). This would increase aerosol diameter size and change the volume distribution of the aerosols.

3.6 Biogenic and Anthropogenic Sulfur

Sulfate sources besides sea salt have already been introduced (frost flowers and lithospheric sources) but the majority of the remainder of sulfate is either from biogenic or anthropogenic sources (e.g., Li and Barrie, 1993; Norman et al., 1999; Sirois and Barrie, 1999). In many places of the world biogenic and anthropogenic sources contribute to most, if not all, the non sea salt sulfate (e.g., Wadleigh 2004; Seguin et al., 2011) and therefore the sum of biogenic and anthropogenic sulfate will be referred to as non sea salt sulfate in this thesis. Concentrations of non sea salt sulfate are displayed in Figure 3.21 and are comparable to previous studies in the Arctic for the time of year (Li and Winchester, 1989, Sirois and Barrie, 1999, Ricard et al., 2002; Quinn et al., 2009). Sulfur isotopes can be used to distinguish between biogenic and anthropogenic sources

(McArdle et al., 1998; Norman et al., 1999; Seguin, 2007) and will be done in this study with the exception of a few cases that will be discussed in Chapter 3.6.2.

3.6.1 Isotope Apportionment: Biogenic versus Anthropogenic

Sulfur isotope apportionment can be used to calculate anthropogenic and biogenic concentrations. Marine biogenic sulfur ($\delta^{34}S_{bio}$ = +18 ± 1.5 ‰; Calhoun, 1990; Patris et al., 2000) is isotopically significantly different than anthropogenic sulfur ($\delta^{34}S_{anthro}$ = +4.4 ± 0.4 ‰; Norman et al., submitted) at Alert (see Chapter 1.3). Assuming that biogenic and anthropogenic sulfur compose the majority of non sea salt sulfate the following equations hold true

$$SO_{4nss} \cdot \delta^{34}S_{nss} = SO_{4bio} \cdot \delta^{34}S_{bio} + SO_{4anthro} \cdot \delta^{34}S_{anthro} \quad \textbf{3.8}$$

and

$$SO_{4nss} = SO_{4bio} + SO_{4anthro} \quad \textbf{3.9}$$

where $\delta^{34}S_x$ indicates sulfur isotopic values and SO_{4x} indicates sulfur concentrations of biological (bio), anthropogenic (anthro) and non sea salt (nss) origin. This equation can be applied to both SO_2 and aerosol sulfate. Three Alert samples of SO_2 fall outside the anthropogenic constraints of $\delta^{34}S$ sulfate set by Norman et al. (submitted), but are still

higher than $\delta^{34}S$ values reported by Rempillo et al. (2011) in the Arctic. Anthropogenic sulfur concentrations are explored in greater detail in Chapter 4 and biogenic sulfur concentrations are studied in Chapter 5.

3.6.2 Apportionment Constraints

Isotopic apportionment for two sources can only occur if both end points (i.e., biogenic and anthropogenic sulfur) are known and if all other sources of sulfur have been accounted for. If these assumptions break down, isotope apportionment is not feasible. *Amundsen* samples had an end point for anthropogenic sulfur (or background sulfur) that was variable (Rempillo et al., 2011). This was due to the influence of the Smoking Hills (Chapter 3.5.3) and the discovery of low $\delta^{34}S$ values in both aerosol and SO_2 samples throughout the Arctic. Therefore instead of an exact endpoint for background sulfur a range was used which is explained in detail by Rempillo et al. (2011). This leads to a range in the concentrations for both biogenic and anthropogenic (background) sulfur instead of a single value. In this thesis, a single value of -5‰ (the midpoint of the anthropogenic/background range) is used for the anthropogenic endpoint for samples collected on board the *Amundsen*. A large uncertainty of 5‰ is used to account for the variability/range of the $\delta^{34}S$ values found by Rempillo et al. (2011). The variability of the $\delta^{34}S$ values for the end members is treated as an error associated with the isotope value and is used when determining propagated error (equation 2.7) for anthropogenic and biogenic concentrations (equation 3.8 and equation 3.9). The error and uncertainty of the anthropogenic/background $\delta^{34}S$ value is discussed by Rempillo et al. (2011). The

only time where the assumption of +5 ± 5‰ $\delta^{34}S$ value for background/anthropogenic does not hold true is when the *Amundsen* was in the area of the Smoking Hills (October 20-26th 2007). Sulfate from the Smoking Hills lowered the background $\delta^{34}S$ values during these times (see Appendix Figure B.2). Anthropogenic and biogenic sulfate contributions are not calculated at these times.

The variable $\delta^{34}S$ background values are not expected at Alert. $\delta^{34}S$ measurements for sulfate aerosol have been measured for weekly samples over a ten year period and a winter anthropogenic $\delta^{34}S$ value of +4.4 ± 0.4‰ (Norman et al., submitted) has been determined. No sulfate aerosol $\delta^{34}S$ value falls significantly below this value, and only three SO_2 $\delta^{34}S$ values did. A problem arises though when considering $\delta^{34}S_{nss}$ values when frost flowers are present. Frost flowers are not expected for the whole duration of the sampling period (see Figure 3.8 and Figure 3.9) and during the times of no frost flower contribution isotope analysis can be carried out to determine anthropogenic and biogenic sulfur concentrations according to equations 3.8 and 3.9.

The $\delta^{34}S_{nss}$ values were used to constrain frost flower concentrations, and thus the calculation of biogenic and anthropogenic sulfate concentrations cannot be directly applied when frost flowers are present. The minimum contribution of frost flowers was used to calculate sea salt sulfate (frost flower ratio = 0.017; see Chapter 3.3), this leads to a calculated non sea salt (and non frost flower) $\delta^{34}S$ value that, in most cases, tends to be the same as the anthropogenic endpoint. This value can be compared to the $\delta^{34}S_{nss}$ value

for the maximum frost flower contribution. The difference between these two values can be used as the error of the $\delta^{34}S_{nss}$ value. Propagated error (equation 2.7) was also calculated based on sea salt corrections associated with equation 3.1 for each sample. Error associated with $\delta^{34}S_{nss}$ will be taken as the greater of the two errors. This error will be carried over when using equations 3.8 and 3.9 and would be incorporated when calculating error associated with biogenic and anthropogenic sulfate concentrations.

3.7 Summary

Sulfate and $\delta^{34}S$ values were measured at Alert and on board the *Amundsen* in 2007 and 2008. Concentrations of sulfate in total aerosol were generally found to be higher on board the *Amundsen* due to the greater contribution of sea spray to aerosols on board the *Amundsen.*

Besides sea salt four other sources of sulfate are identified in the Arctic and include frost flowers, The Smoking Hills, biogenic and anthropogenic contributions.

Evidence of frost flowers contributing to aerosol ion loading was found at Alert. Frost flowers and sea salt contributions in aerosols can be distinguished from each other with the use of $\delta^{34}S$ values. This is the first time frost flower concentrations have been reported in aerosols. The distinction between frost flowers and sea salt sulfate allows for the calculation of non sea salt sulfate when contribution from frost flowers is present in aerosols. This was demonstrated with samples collected in 2007 at Alert.

Sea salt was found predominately in the large (> 3.0 μm) size range aerosols collected on board the *Amundsen* while at Alert sea salt sulfate is distributed throughout the size ranges. It was found that sea salt sulfate in the fine aerosols at both locations had similar concentrations for the majority of the study period which is consistent with long range transport. Elevated aerosol sea salt in the fine fraction was observed when sea ice cover was at a maximum and high oceanic productivity was present. This could potentially be associated with bubble bursting at the ocean surface.

Lithospheric influences on sulfate concentrations in aerosols were examined. Observed aerosol magnesium and calcium were consistent with crustal influences, although the influence from crustal material on aerosol sulfate concentrations is minimal. As described by Rempillo et al. (2011), the background $\delta^{34}S$ values are lower in the vicinity of the Smoking Hills, indicating that the Smoking Hills contributes to aerosols in the local area.

Isotope and biogenic and anthropogenic sulfate apportionment is discussed along with the assumptions that are used in this thesis. Biogenic and anthropogenic sulfur concentrations in aerosols are studied in Chapter Four and Five.

Chapter Four: Anthropogenic Sulfur

Anthropogenic influence on the Arctic atmosphere has been well documented for many years (e.g., Stonehouse, 1986; Sirois and Barrie, 1999). Sulfur concentrations are largest during winter and spring in the presence of Arctic Haze (Barrie and Bottenheim, 1991; Sirois and Barrie, 1999). Once polar sunrise occurs, oxidation of SO_2 and deposition of aerosols occurs leading to low loading of anthropogenic aerosols during the summer when the Arctic vortex is at a minimum (Raatz, 1991). A similar pattern is also seen with SO_2 (Barrie and Bottenheim, 1991) which can travel long distances before being oxidized to sulfate. Both anthropogenic SO_2 and aerosol sulfate were calculated using apportionment techniques explained in Chapter 3.6.

4.1 Aerosol Anthropogenic Sulfate

4.1.1 Location and Temporal Differences

Anthropogenic sulfur in the Arctic is expected to be predominantly from long range transport. If long range transport is of importance, similar trends in fine aerosols may be observed between the data sets collected at Alert and samples collected under clean air conditions on the *Amundsen*. Total and fine aerosol anthropogenic sulfate concentrations at Alert are displayed in Figure 4.1 and Figure 4.2. Concentrations of anthropogenic sulfate increased throughout the sampling period in both years at Alert. This is consistent

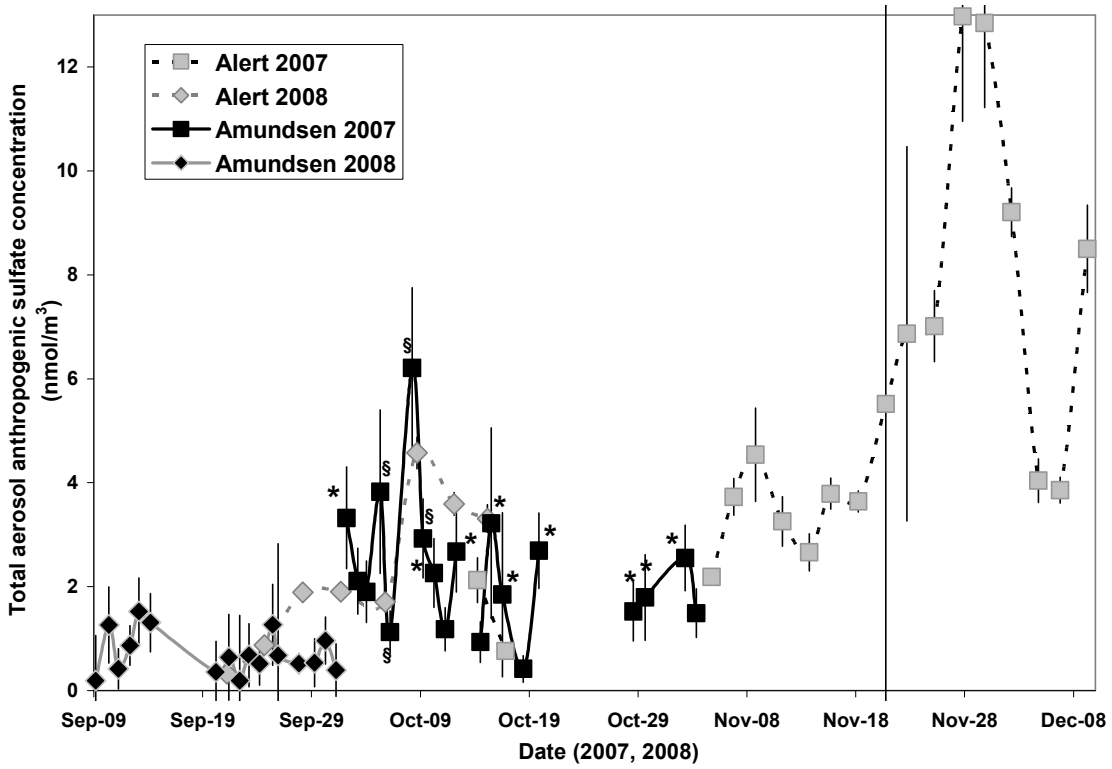

Figure 4.1 Anthropogenic sulfate concentrations in total aerosol at Alert and collected on board the *Amundsen* in 2007 and 2008. *Amundsen* data in 2007 marked with * identifies smoke stack emission events, § indicate samples in the 2007 *Amundsen* data set that did not have significant data to identify smoke stack emission events.

with the start of winter when sulfate associated with Arctic Haze is expected to accumulate. Samples collected at Alert in 2007 had more anthropogenic loading than 2008. Samples from 2007 were collected later in the season and thus higher concentrations are expected than in 2008.

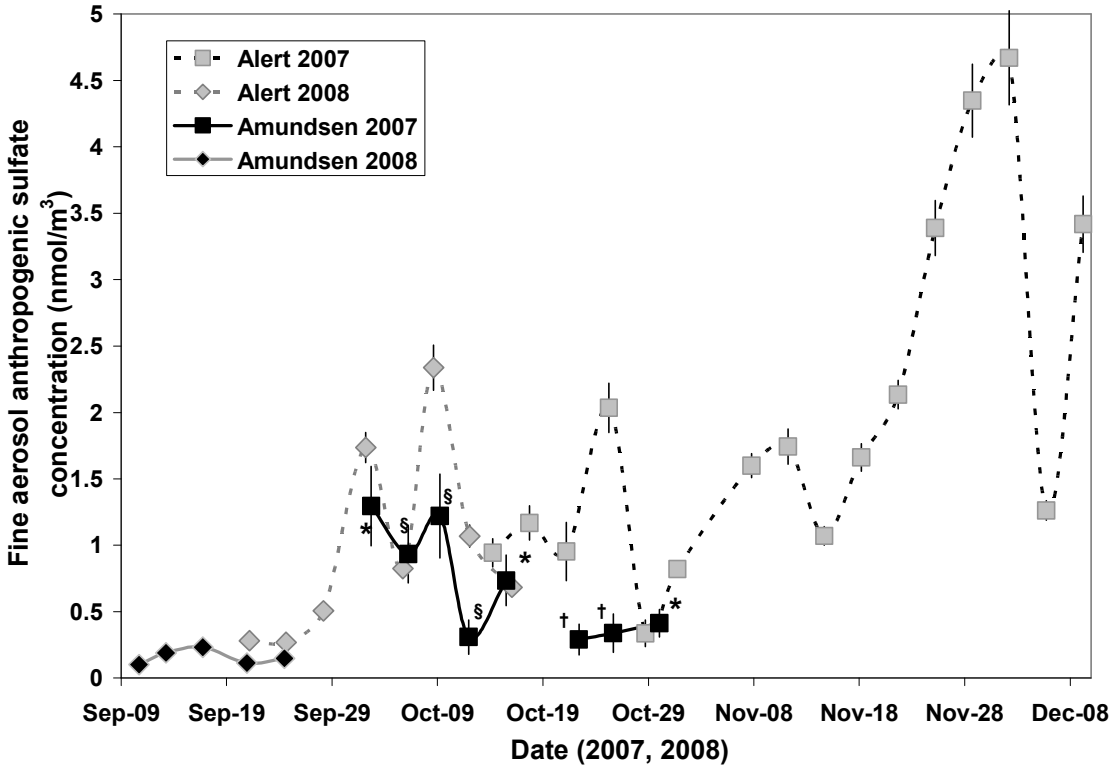

Figure 4.2 Anthropogenic sulfate concentrations in fine aerosol (<0.49µm) at Alert and collected on board the *Amundsen* in 2007 and 2008. *Amundsen* data in 2007 marked with * identifies smoke stack emission events, † are samples influenced by the Smoking Hills and possible smoke stack emissions and represent maximum contributions of anthropogenic sulfate, § indicate samples in the 2007 *Amundsen* data set that did not have significant CO_2 data to identify smoke stack emission events.

Long range transport and smoke stack emissions from the *Amundsen* can account for anthropogenic sulfate on board the *Amundsen* (Rempillo et al., 2011). It is possible that larger anthropogenic influences from smoke stack emissions in 2007 compared to 2008

may also have influenced the calculated anthropogenic sulfate concentrations on board the *Amundsen* as greater care to eliminate smoke stack emissions from the sampler was taken in 2008. Rempillo (2011) studied the possibility of smoke stack emissions affecting SO_2 concentrations on board the Amundsen using a CO_2 analyzer to mark when ship stack emissions were high. Rempillo (2011) found ten dates in 2007 that were considered "polluted" (i.e., high possible influence from smoke stack emissions). Not all days had continuous CO_2 measurements and categorization for samples influenced by smoke stack emissions could not be conducted during these sampling periods (Rempillo, 2011). In 2008, only 5 dates had enough CO_2 measurements to determine possible influence from smoke stack emissions and therefore no analysis for possible influence from smoke stack emissions was conducted for 2008 data. Total aerosol anthropogenic sulfate concentrations of samples that had possible influence from smoke stack emissions (Figure 4.1) were significantly different than the samples that were not influenced by smoke stack emissions collected on board the *Amundsen* in 2007 (p value = 0.007 for unequal variance, two tail t – test). A median concentration of 2.5 ± 0.6 (1σ) nmol/m^3 (average 2.4 nmol/m^3; n = 9) for anthropogenic sulfate from total aerosol samples in 2007 that had possible influence from the smoke stack emissions were higher than samples that did not have this influence; median 1.3 ± 0.6 (1σ) nmol/m^3 (average 1.3 nmol/m^3; n = 6). Size segregated samples, including fine aerosols, were collected over a longer time period. The same test that Rempillo (2011) carried out to test for influence of smoke stack emissions was also tested in this thesis for size segregated sampling periods in 2007. Possible smoke stack emissions could not be ruled out for any of the size segregated samples collected in 2007 (Figure 4.2).

Anthropogenic sulfate concentrations at Alert were significantly different than samples collected on board the *Amundsen* (p value < 0.01 for unequal variance, two tail t – test). Lower anthropogenic sulfate was observed on the *Amundsen* (Total aerosol median; 1.3 ± 1.2 (1σ) nmol/m^3) relative to Alert (Total aerosol median; 3.7 ± 3.3 (1σ) nmol/m^3). Samples on board the *Amundsen* were collected earlier in both seasons and thus a lower concentration of anthropogenic sulfate on board the *Amundsen* is expected when ship stack sulfate emissions are low. This is observed for total and fine aerosols (see Figure 4.1 and Figure 4.2). Anthropogenic sulfate concentrations for fine aerosols were similar when temporal overlap occurred between the sampling periods on board the *Amundsen* (median 0.3 ± 0.4 nmol/m^3, n = 7) and those from Alert (median 0.8 ± 0.6 nmol/m^3, n = 8). Differences in concentrations between the two sites were often smaller than the temporal variation in concentration seen at either site (see Figure 4.1 and 4.2). This is consistent with the hypothesis that anthropogenic sulfate concentrations are uniform throughout the Arctic if smoke stack emissions have minimal influence (Wasiuta et al., 2006; Norman et al., submitted). It is also noted that anthropogenic sulfate concentrations are in agreement between 2007 and 2008 at Alert (i.e., anthropogenic sulfate concentrations are within 20% for fine aerosols when sampling periods between the two years overlap from October 10 – 17). This is consistent with long term studies over the Arctic (Sirois and Barrie, 1999) where aerosol sulfate concentrations reflect seasonality rather than long term variations.

4.1.2 Size Segregated Samples

Anthropogenic sulfate from long range transport is expected to be mostly secondary (i.e., formed from the oxidation of SO_2) and thus anthropogenic sulfate is expected to be predominantly in the fine aerosol (Finlayson-Pitts and Pitts, 2000). Size segregated samples at Alert show that anthropogenic sulfate is mostly present in the fine aerosol (see Figure 4.3 for 2007 and Figure 4.4 for 2008). Over 70% of the anthropogenic sulfate

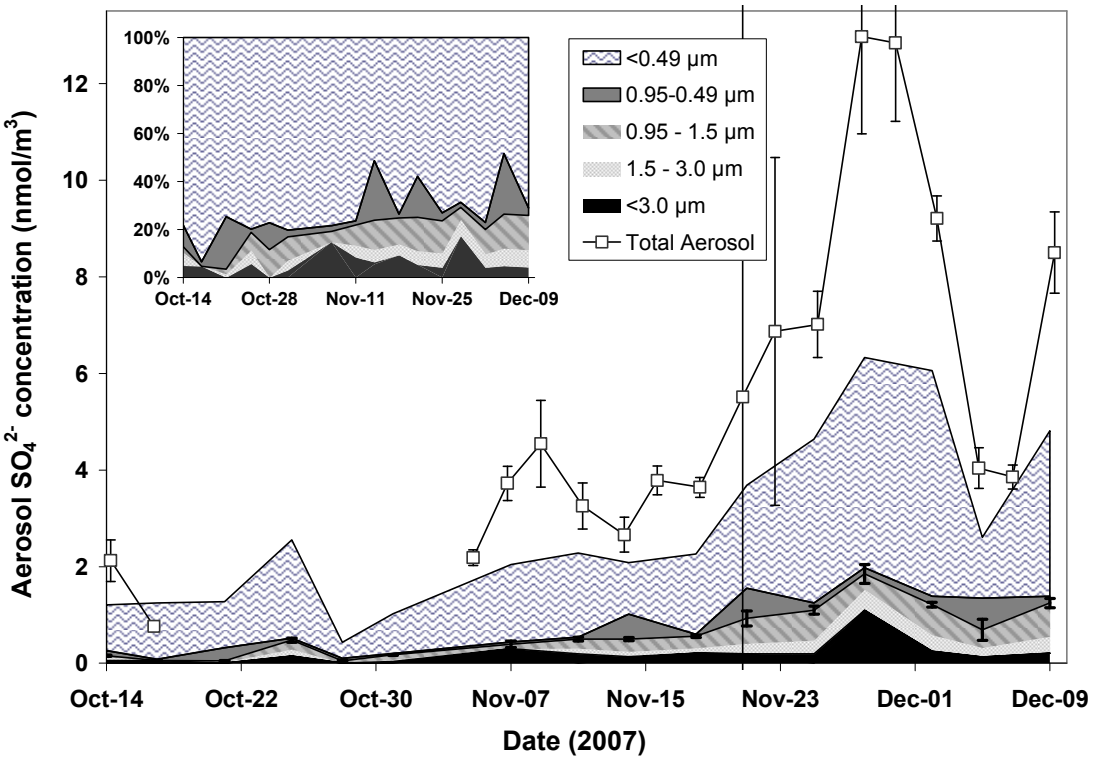

Figure 4.3 Anthropogenic sulfate in size segregated samples in 2007 at Alert. Error is shown on the total and 0.95 -1.5 µm size range aerosols. Percent contribution is displayed in the insert. Size segregated concentrations are cumulative.

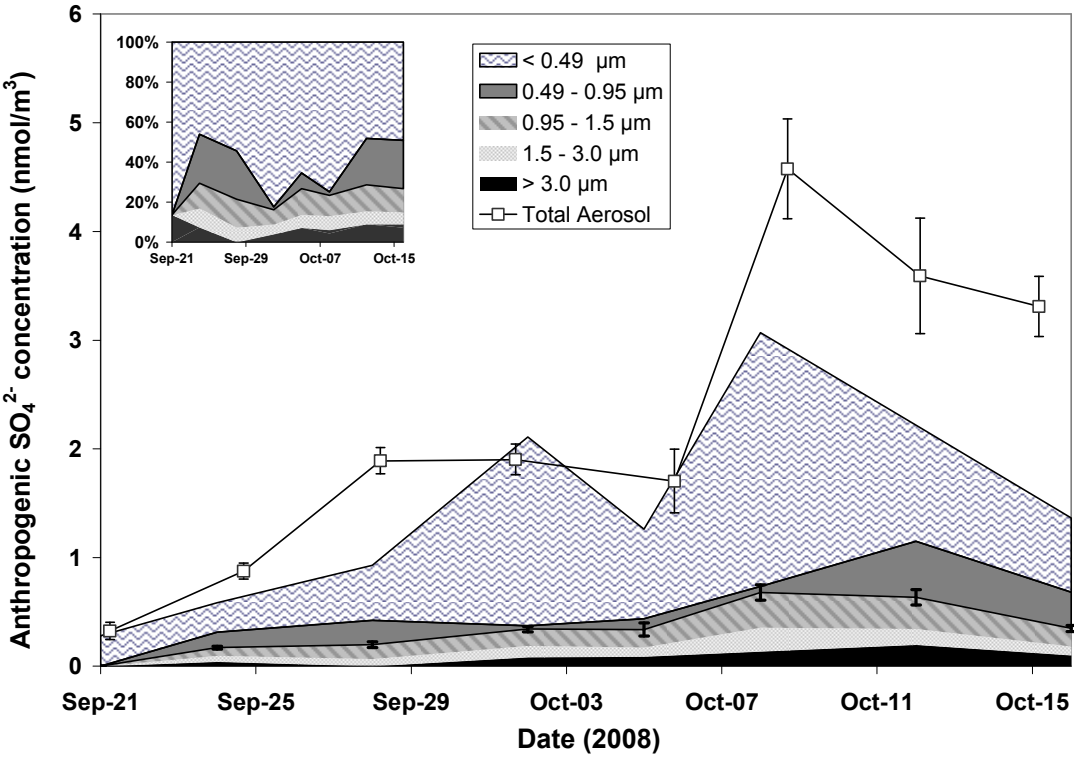

Figure 4.4 Anthropogenic sulfate in size segregated samples in 2008 at Alert. Error is shown on the total and 0.95 -1.5 µm size range aerosols. Percent contribution is displayed in the insert. Size segregated concentrations are cumulative.

loading is present in the two smallest size fractions (i.e., < 0.95 µm) at Alert at all times, and over 50% of the total anthropogenic sulfur load is found in aerosols < 0.49 µm in diameter for the majority of the sampling periods (Figure 4.3; Figure 4.4; Appendix C). The discrepancy between the sum of the fine aerosol concentrations of anthropogenic sulfate and that of total aerosol sulfate concentration in Figure 4.3 was discussed in Chapter 2.4.

The same size distribution characteristics were not observed for the *Amundsen* samples. Anthropogenic sulfur loading is spread through all size segregated samples (Figure 4.5 for 2007 and Figure 4.6 for 2008; and Appendix C). Although more error is associated with the *Amundsen* samples because of variable $\delta^{34}S_{anthro}$ from the Smoking Hills influence (see Chapter 3.5.3, Appendix C and Rempillo et al., 2011), it does not account for differences in the aerosol size profile where approximately 20% of the anthropogenic aerosol is in the fine fraction.

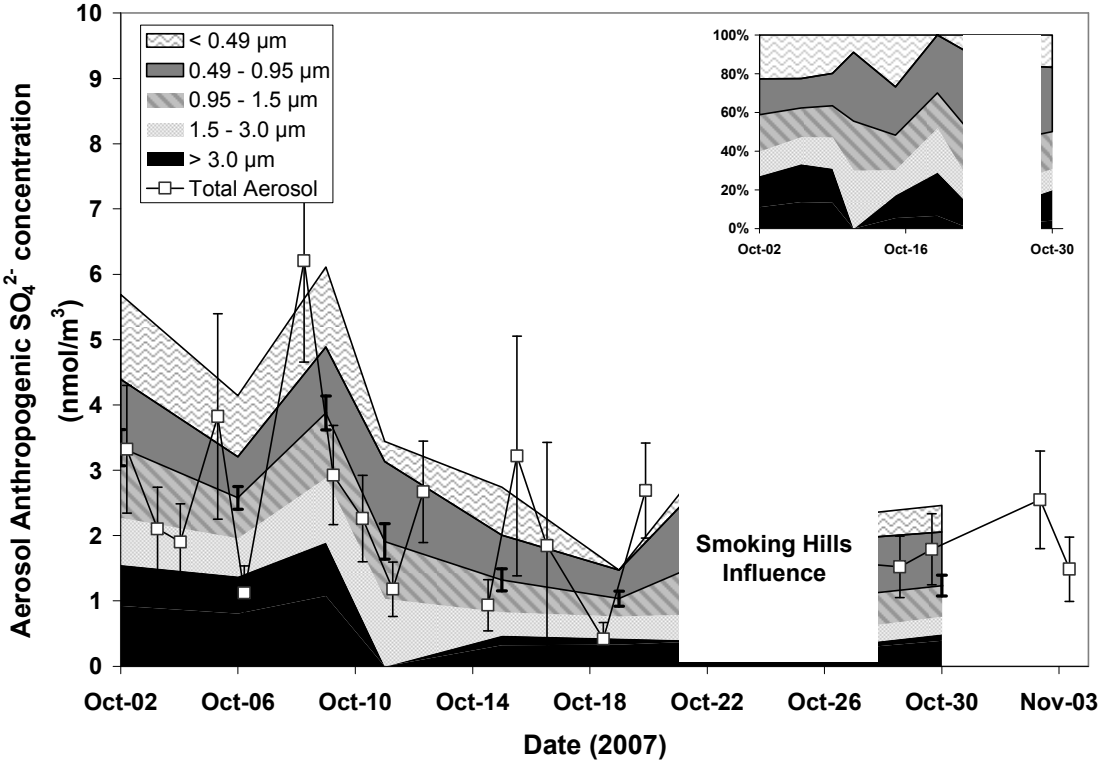

Figure 4.5 Anthropogenic sulfate in size segregated samples in 2007 from the *Amundsen*. Error is shown on the total and 0.95 -1.5 µm size range aerosols. Size segregated concentrations are cumulative.

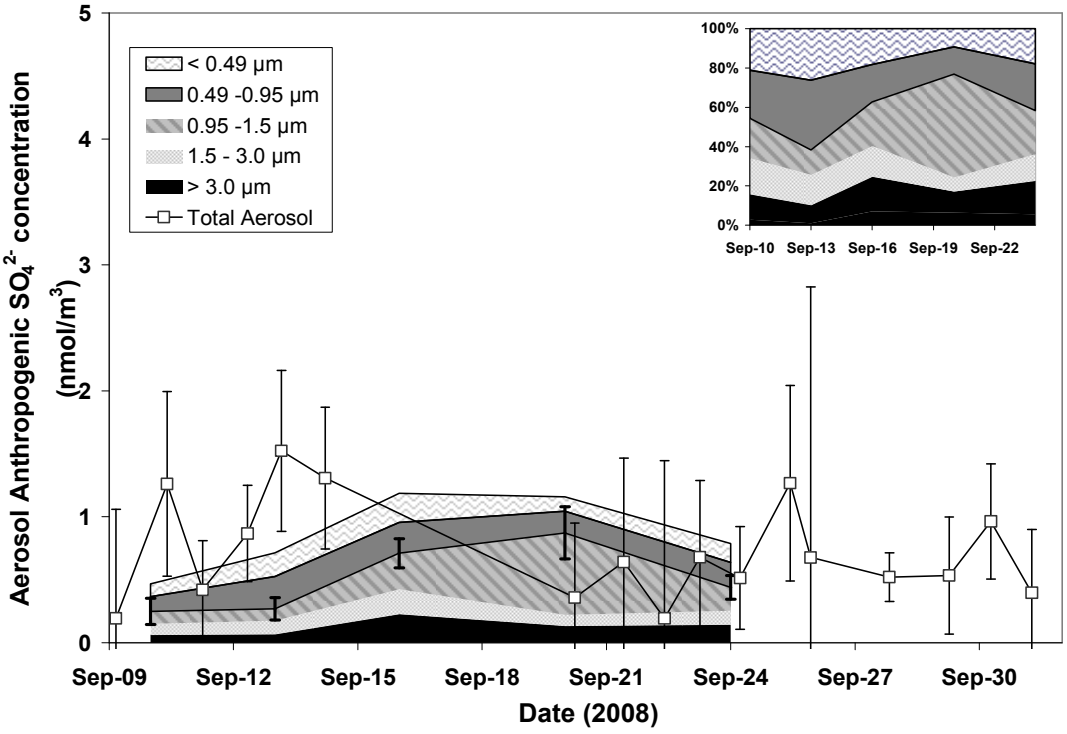

Figure 4.6 Anthropogenic sulfate in size segregated samples in 2008 from the *Amundsen*. Error is shown on the total and 0.95 -1.5 µm size range aerosols. Percent contribution is displayed in the insert. Size segregated concentrations are cumulative.

The larger size aerosols (i.e., > 0.49 µm) collected aboard *Amundsen* in 2007 had higher anthropogenic sulfate concentrations relative to Alert for overlapping sampling periods (Figure 4.3; Figure 4.5). It is likely that anthropogenic sulfur is associated with the larger size aerosols in 2007 on board the *Amundsen* when sulfur from the smoke stack was preferentially incorporated into the larger aerosols and/or the smoke emissions contained primary aerosols (> 0.49 µm in diameter).

Although the aerosols greater than > 0.49 μm in diameter collected on board the *Amundsen* in 2007 had elevated sulfate relative to Alert, the fine aerosol anthropogenic sulfate did not (Figure 4.2; Appendix C). This is consistent with long range transport of fine aerosols which could be representative of a well mixed sulfate reservoir in the Arctic atmosphere and with previous measurements in the Arctic (e.g., Quinn et al., 2009).

4.2 Anthropogenic SO_2

Anthropogenic SO_2 at Alert is displayed in Figure 4.7 and in Appendix C. Ten out of 11 samples of total, and thus anthropogenic, SO_2 concentrations in the 2007 sampling period before November 26, 2007 (see insert Figure 4.7) were not significantly different from zero (i.e., zero falls within propagated error) (see Appendix C). After November 26, 2007, an increase in anthropogenic SO_2 concentrations are observed (see insert of Figure 4.7) with 6 out the 7 samples after November 26, 2007 significantly larger than zero (median value 1.1 nmol/m^3). The rate of loss of SO_2 by oxidation depends on sunlight intensity along with presence of clouds and fog and important SO_2 oxidants (Finlayson - Pitts and Pitts, 2000). Gaseous oxidation of SO_2 would decrease with the onset of winter when OH concentrations decrease with less sunlight and would lead to increased SO_2 concentrations if aqueous oxidation of SO_2 along with SO_2 emission or production remained relatively constant over time. A similar increase in SO_2 concentrations was not observed for 2008 at Alert (see insert Figure 4.7). SO_2 concentrations in 2008 were higher (median 0.51 nmol/m^3) than samples collected before November 26, 2007 at Alert (Figure 4.7 insert). Back trajectories in 2008 (Appendix A.2) were varied but between

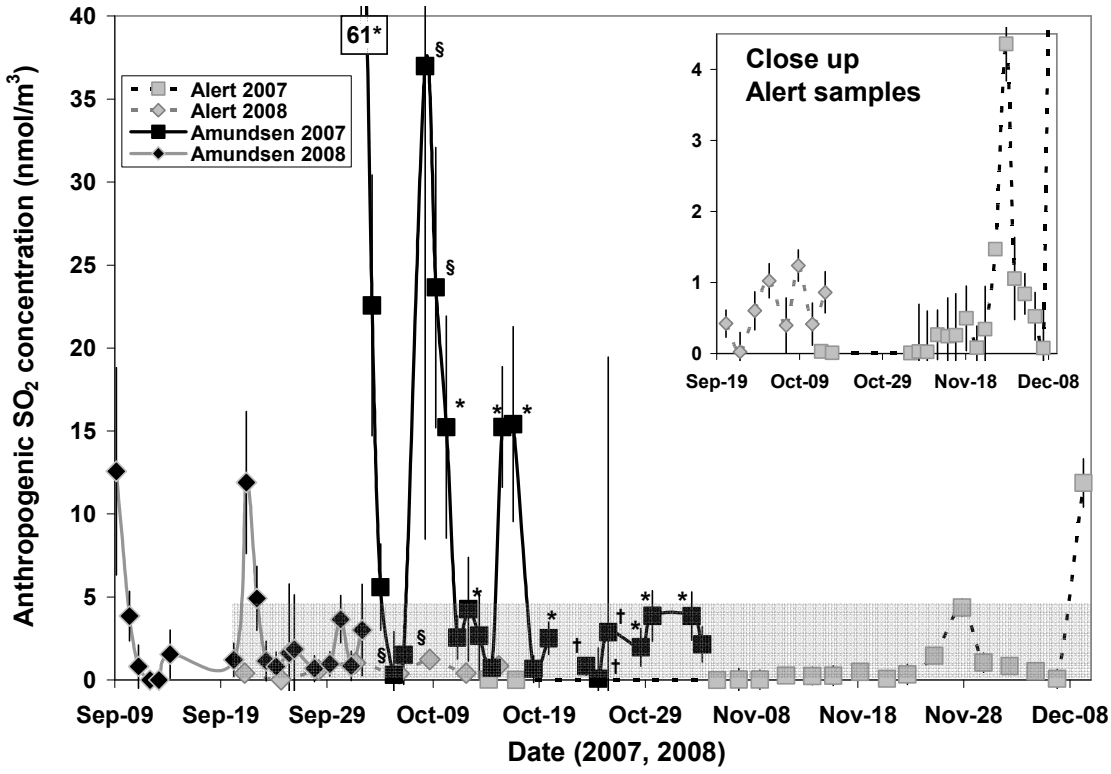

Figure 4.7 Anthropogenic SO_2 concentrations at Alert and from the *Amundsen* in 2007 and 2008. The insert shows a close up of Alert samples in the shaded area in the main diagram. *Amundsen* data in 2007 marked with * identifies smoke stack emission events, † are samples influenced by the Smoking Hills and represent maximum contributions of anthropogenic sulfate, § indicate samples in the 2007 *Amundsen* data set that did not have significant CO_2 data to identify smoke stack emission events.

September 29 – October 10 were predominately from the south. Back trajectories from 2007 (Appendix A.1) were primarily from the North and may explain the difference between the two years.

A possible artefact on SO_2 filters collected on board the *Amundsen*, from airborne sea salt, was identified that affected biogenic and anthropogenic apportionment. This was corrected for (Appendix F) and the results presented in this chapter have taken this into consideration. Concentrations of anthropogenic SO_2 on board the *Amundsen* were much greater than at Alert and were also much more variable (Figure 4.7). This is likely due to the local source of the smoke stack on board the *Amundsen*. Smoke stack emissions could increase the local SO_2 concentrations by over an order of magnitude (Figure 4.7). As explained in Section 4.1.1, Rempillo (2011) separated samples with high possibility from smoke stack emissions. The median concentration for anthropogenic SO_2 with possible smoke stack influence was 4.3 nmol/m^3 (n = 9) relative to samples that had little smoke stack influence (2.4 nmol/m^3; n = 10). Anthropogenic SO_2 concentrations above 6 nmol/m^3, with the exception of one sampling period, were either associated with times that CO_2 measurements indicated there was high possibility of smoke stack influence or times when CO_2 measurements were off line. The median value of anthropogenic SO_2 concentrations below 6 nmol/m^3 was 1.9 ± 1.4 (1σ) nmol/m^3 (n = 15). This is slightly higher than the median at Alert (0.4 ± 2.4 (1σ) nmol/m^3; n = 24), but is within the same order of magnitude and is likely influenced to some extent by smoke stack emissions. This demonstrates that even in areas where strong local sources are present (i.e., smoke stack emissions) samples representative of background levels can be approached, as long as appropriate sampling precautions are taken.

There were two instances at Alert where anthropogenic SO_2 concentrations exceeded 2 nmol/m^3; almost an order of magnitude greater than the remainder of the samples. These

dates, Nov 26-28 and Dec 7-10, 2007, started with low barometer pressure before increasing over the sampling period suggesting a front passed through. Back trajectories (see Appendix A.1) and weather station wind directions both showed high variability during these two sampling periods. Fine aerosol anthropogenic and biogenic sulfate concentrations during this time were also elevated (Figure 4.2, Figure 4.1 Figure 5.1 and Figure 5.2). Two possible explanations for these elevated concentrations are as follows. The first is local contamination from Alert. The sampling site is at a distance of approximately 6 km (Sirois and Barrie, 1999) from the Alert station and in most cases is upwind from the Alert station. With the variability of back trajectories and wind directions during the two sampling periods in question, it is possible that some local anthropogenic influence from the Alert station may have resulted in increased concentrations. In this case, little to no change in biogenic sulfate concentrations is expected. The second possibility may be mixing of the boundary layer and the free troposphere. As a front passes through during the sampling period, mixing can occur between the boundary layer and the free troposphere, concentrating pollutants closer to the surface. This is often referred to as boundary layer pumping and occurs in rotating air masses (Holton, 1992) and may explain the elevated sulfur concentrations measured near the surface during these times. This is the more likely scenario since DMS and its oxidation products, such as biogenic sulfate and SO_2 can be transported long distances in the free troposphere (Quinn and Bates, 2011 and references within) and were also elevated at this time (Chapter 5.1).

4.3 Indicators of Anthropogenic Influence in Aerosols

Many other aerosol ions can be used as tracers of anthropogenic influence. Savoie et al. (2002) used aerosol antimony and nitrate to determine anthropogenic sources over the North Atlantic. Metals including zinc, manganese, selenium, copper, lead and vanadium along with other ions such as K^+, I^-, H^+ and NH_4^+ have been used as indicators of anthropogenic aerosols in previous studies (Arimoto et al., 1992; Arimoto et al., 1995; Sirois and Barrie, 1999; Savoie et al., 2002); however each has its drawback. For instance, selenium has a marine biogenic source (Dudzinska-Huczuk and Bolalek, 2007) while manganese and vanadium have continental sources from dust (Savoie et al., 2002, Sirois and Barrie, 1999). Metal components are expected to be close to detection limits because of the variability of the filter blanks relative the contribution from aerosols (Seguin, 2007) and were not measured. Aerosol potassium, nitrate, and ammonium were detected with ion chromatography (Chapter 2.5) for the Alert and *Amundsen* samples.

Potassium has been used as a tracer of biomass burning (Andreae, 1983; Crutzen and Andreae, 1990). Sirois and Barrie (1999) linked potassium to a source of anthropogenic sulfur at Alert. However, the sea salt source of potassium must be taken into account before the remainder can be used as a tracer (equation 1.1). Non sea salt potassium was found in both the total (Figure 4.8) and fine aerosol (Figure 4.9) at Alert. Elevated potassium was also observed on board the *Amundsen* (Figure 4.8 and 4.9). Non sea salt potassium for other size segregated samples was not significantly different than zero (i.e., zero falls within propagated error) for the majority of samples (Chapter 2.5 and 2.8.1).

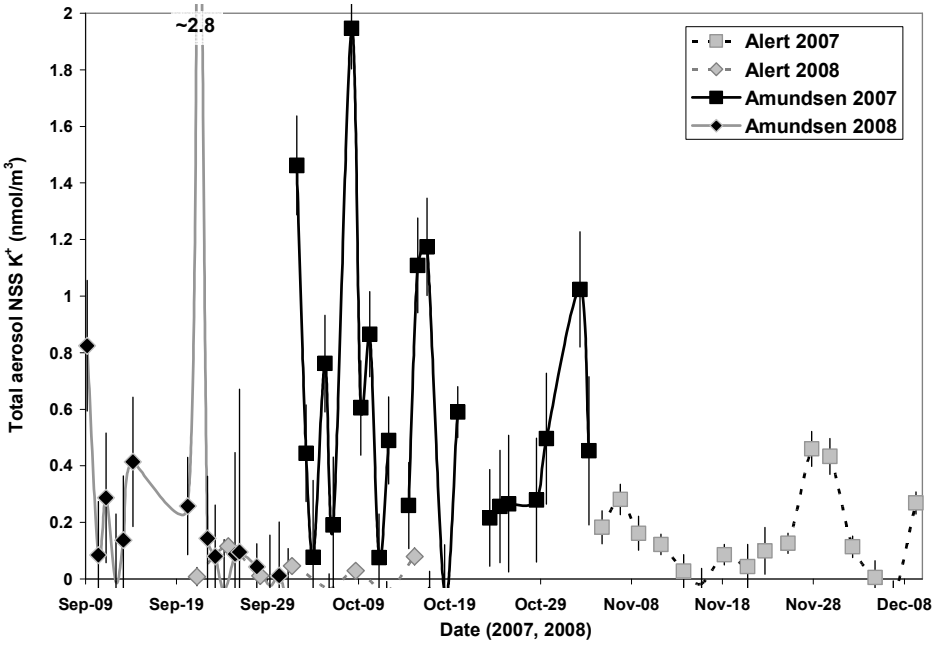

Figure 4.8 NSS K^+ concentrations at Alert and collected on board the *Amundsen* in 2007 and 2008 in total aerosol.

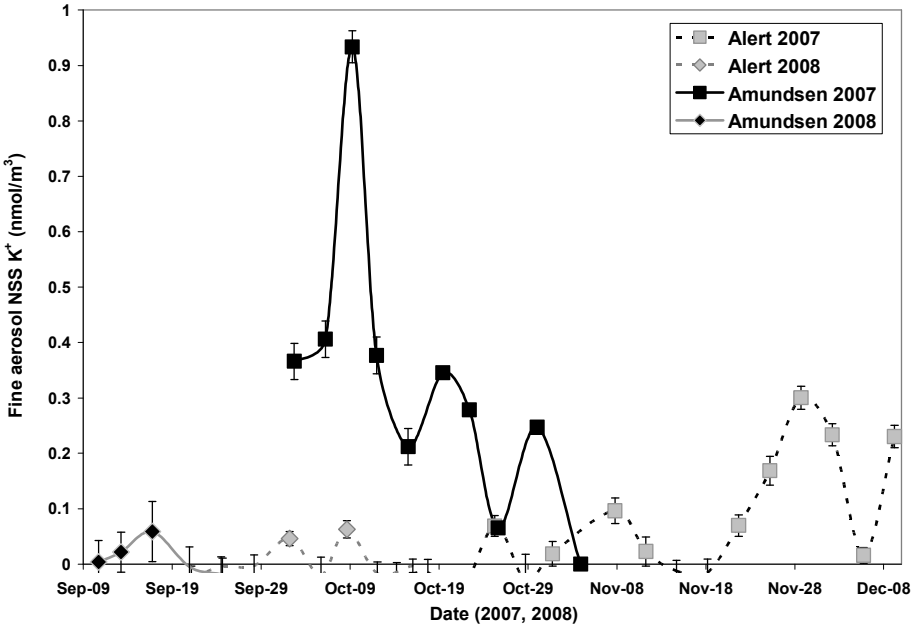

Figure 4.9 NSS K^+ concentrations at Alert and collected on board the *Amundsen* in 2007 and 2008 in fine aerosols (<0.49 µm in diameter).

Comparisons between anthropogenic sulfate and non sea salt potassium are shown in Figure 4.10. One point from the Amundsen is not included in the relationship since it is elevated in non sea salt potassium compared to other samples. Back trajectories during the this sampling period (Rempillo, 2011) and the position of the ship suggest that there was possible influence from the Thule Air Base (76º31 N 68°42 W) since the ship was within 100 km of the military station. Error on non sea salt potassium is large but trends for both locations are apparent. At Alert, non sea salt potassium concentrations in the fine and total aerosols were approximately equivalent. Since total includes the fine

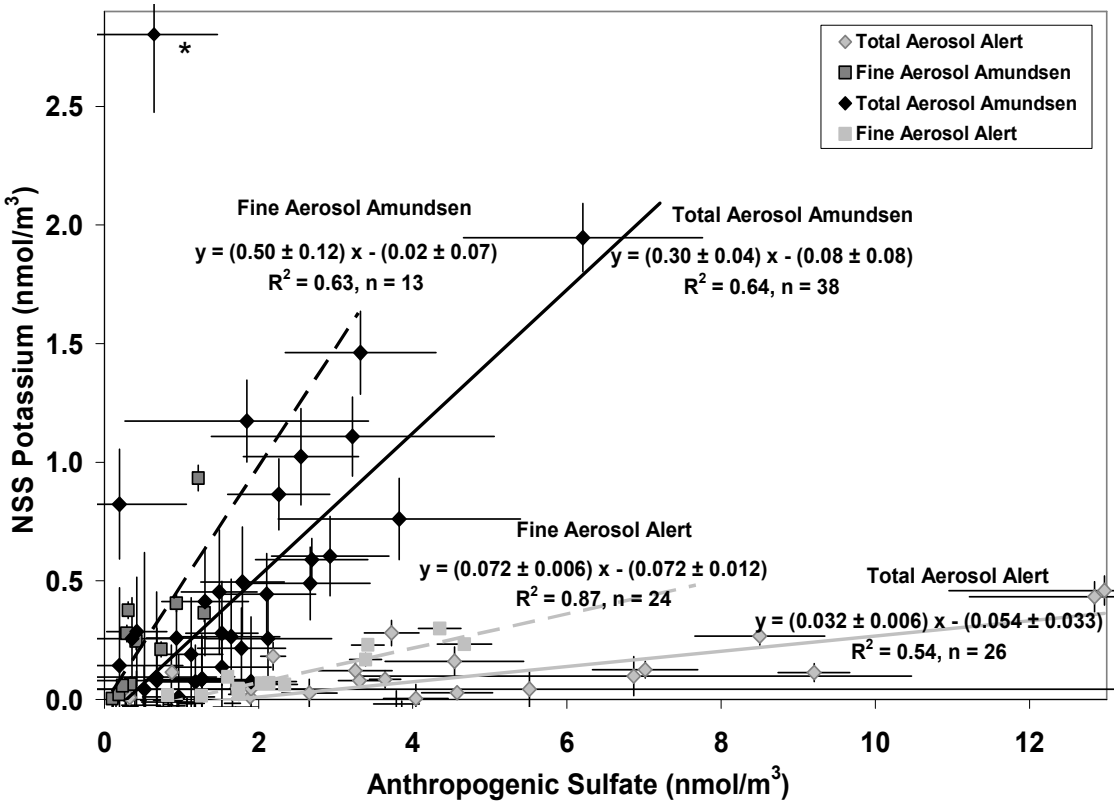

Figure 4.10 Comparison of non sea salt potassium and anthropogenic sulfate. Point marked with * is not included in relationship.

component this result indicates most of the potassium at Alert was found in the fine aerosol. This would be consistent with long range transport; larger aerosols emitted at the source containing potassium would be deposited closer to the source relative to smaller aerosols from the same source.

On board the *Amundsen*, non sea salt potassium was found in greater amounts in the total aerosol than the fine aerosol. This indicates a more local source on board the *Amundsen* than at Alert such as the *Amundsen*'s smoke stack emissions. Higher non sea salt potassium concentrations on board the *Amundsen* compared to Alert also support a local combustion source for larger aerosols. Total aerosol samples possibly influenced from smoke stack emissions (as explained in Chapter 4.1.1) from the *Amundsen* had larger concentrations of non sea salt potassium (median = 0.86 ± 0.39 nmol/m^3; n = 9), than those that were determined to have little influence (median 0.26 ± 0.16 nmol/m^3; n = 9). Although a correlation between non sea salt potassium and anthropogenic sulfate from samples effected by smoke stack emissions was expected, a low correlation was found (R^2 = 0.35). Smoke stack emissions would contain sulfur both as sulfur dioxide and sulfate. A relationship between non sea salt potassium and anthropogenic sulfate may not be observable within the vicinity of the smoke stack until sufficient uptake of anthropogenic sulfur occurs on the anthropogenic aerosol. A low correlation between anthropogenic sulfate and non sea salt potassium for *Amundsen* samples not affected my smoke stack emissions (R^2 = 0.29) was also observed. This low correlation is most likely due to non sea salt potassium for these samples being close to detection limit.

Li and Winchester (1989*b*) found a large non sea salt potassium contribution in aerosols between March and May 1986 at Barrow, Alaska. A strong relationship in the course aerosol mode (> 1 μm) was found between non sea salt sulfate and non sea salt potassium ($R^2 = 0.78$) during the Barrow campaign, with a weaker relationship ($R^2 = 0.39$) in the fine aerosol (< 1 μm). This is opposite to what was found at Alert. It is uncertain if this is due to seasonality (i.e., spring samples versus fall samples), or a more local source at Barrow during the Li and Winchester (1989*b*) study. Non sea salt potassium in aerosols has been observed for decades in the Arctic (Sirois and Barrie, 1999; Quinn et al., 2009) but the spatial distribution of non sea salt potassium contribution in aerosols in the Arctic has not been studied. The trends found in this study displayed in Figure 4.10 along with previous studies (i.e., Li and Winchester, 1989*b*) suggest ratios may differ across the Arctic. It would be interesting to examine aerosol non sea salt potassium and anthropogenic sulfate relationships in a larger spatial study to gain insights of sources and lifetimes of these components.

To further evaluate the possible biomass burning source in the Arctic a second tracer can be used. Ammonia is also produced during biomass burning (Hegg et al., 1988, Whitlow et al., 1994). It should be noted that ammonium may not accurately reflect atmospheric concentrations since it may not be preserved using the sampling and storage procedures used here (Dougle and Brink, 1996; McMurry, 2000; Schaap et al., 2004). Ammonium for *Amundsen* samples were measured in February 2009 (> 2 months after being processed in the lab and > 5 months after collection) while Alert aerosol ions where measured in Kingston, in January 2011 (> 6 months after being processed in the lab and >

2 years after collection) and therefore storage may have affected the reported ammonium concentrations. It is of interest to note that even though ammonium may not be preserved, relatively strong relationships were still observed.

A correlation between ammonium and anthropogenic sulfate aerosol concentrations was found with both samples collected at Alert and on board the *Amundsen*. The ammonium/anthropogenic sulfate ratio was observed to be 1.10 on board the *Amundsen* (see Figure 4.11) for total aerosols (R^2=0.66) and 1.12 for fine aerosols (R^2 = 0.80). Alert samples also showed strong correlations between anthropogenic sulfate and ammonium but with lower slopes (total aerosol, slope = 0.34, R^2 =0.78; fine aerosol slope = 0.48, R^2 = 0.93). Lower slopes at Alert may be a result of longer storage times for Alert samples. The slopes may not reflect true ratios in the atmosphere, and may be larger if ammonium was not preserved in storage. Although ratios may not be preserved in either data set, it is evident that anthropogenic sulfate and ammonium in aerosols in the Arctic are correlated.

This relationship between ammonium and anthropogenic sulfate is not observed with larger size fractionated (> 0.49 μm) aerosols on board the *Amundsen*, most likely due to the high error associated with anthropogenic sulfate, and ammonium concentrations being near the limit of detection for all other size fractions (> 0.49 μm). Ammonium was not measured for the larger size fractions (>0.49 μm) at Alert. If loss of ammonium is similar between both data sets during storage, a lower ammonium to anthropogenic sulfate slope is observed at Alert (slope = 0.34) compared to the *Amundsen* (slope =

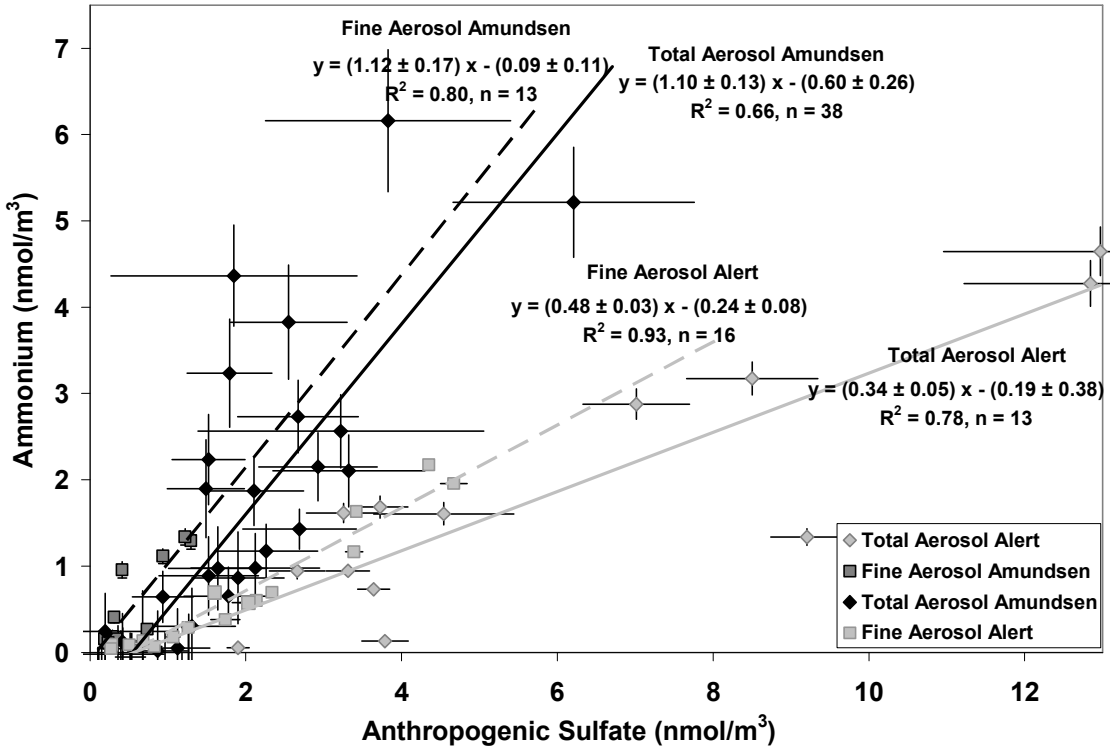

Figure 4.11 Comparison of ammonium and anthropogenic sulfate concentrations.

1.10) and is similar to trends for non sea salt potassium discussed previously. This continues to support the postulate that a biomass burning signature from remote sources at Alert is evident and a more local source on board the *Amundsen* contributes to the aerosol load. It is also consistent with aged aerosols at Alert relative to the aerosols collected on the *Amundsen*. This is supported by examining the samples possibly influenced by smoke stack emissions (as explained in Section 4.1.1). Samples with possible influence from smoke stack emissions had larger concentrations of aerosol ammonium (median 2.56 ± 1.05 (σ); n = 9) relative to those that did not (median 0.86 ± 0.66 nmol/m^3; n = 9) but the correlation between ammonium and anthropogenic sulfate

was weaker in samples that contained a possible influence from the smoke stack ($R^2 <$ 0.08, n = 9) than those that did not ($R^2 = 0.50$, n = 6). This finding supports that the ammonium and anthropogenic sulfate correlation is found in aged aerosols that have undergone long range transport.

Whitlow et al. (1994) studied the relationship of non sea salt potassium relative to ammonium in three different ice core samples and found that when non sea salt potassium was elevated so was ammonium associated with biomass burning. A strong relationship between non sea salt potassium and ammonium in the Alert data set is displayed in Figure 4.12. Although ratios may be affected by storage, a higher ratio of ammonium to non sea salt potassium at Alert is found relative to the *Amundsen*. Ammonium besides an indicator of biomass burning is also expected in aged aerosols associated with anthropogenic sources (ApSimon et al., 1994; Seinfeld and Pandis, 1998) and would be consistent with aged aerosols at Alert.

It was noted that elevated non sea salt potassium and ammonium occurred more often in 2007 than in 2008 on board the *Amundsen*. Possible sources of these biomass tracers may include incinerations on board the *Amundsen* itself. It was noted that in 2007 greater influences from the smoke stack emissions may have affected the samples (see Chapter 4.1.1; Rempillo, 2011). When examining non sea salt potassium and ammonium from samples that had high possibility of influence of smoke stack emissions with those of low influence, elevated concentration of both ions were found. This supports the thesis that non sea salt potassium observed on board the *Amundsen* is local and is emitted from the

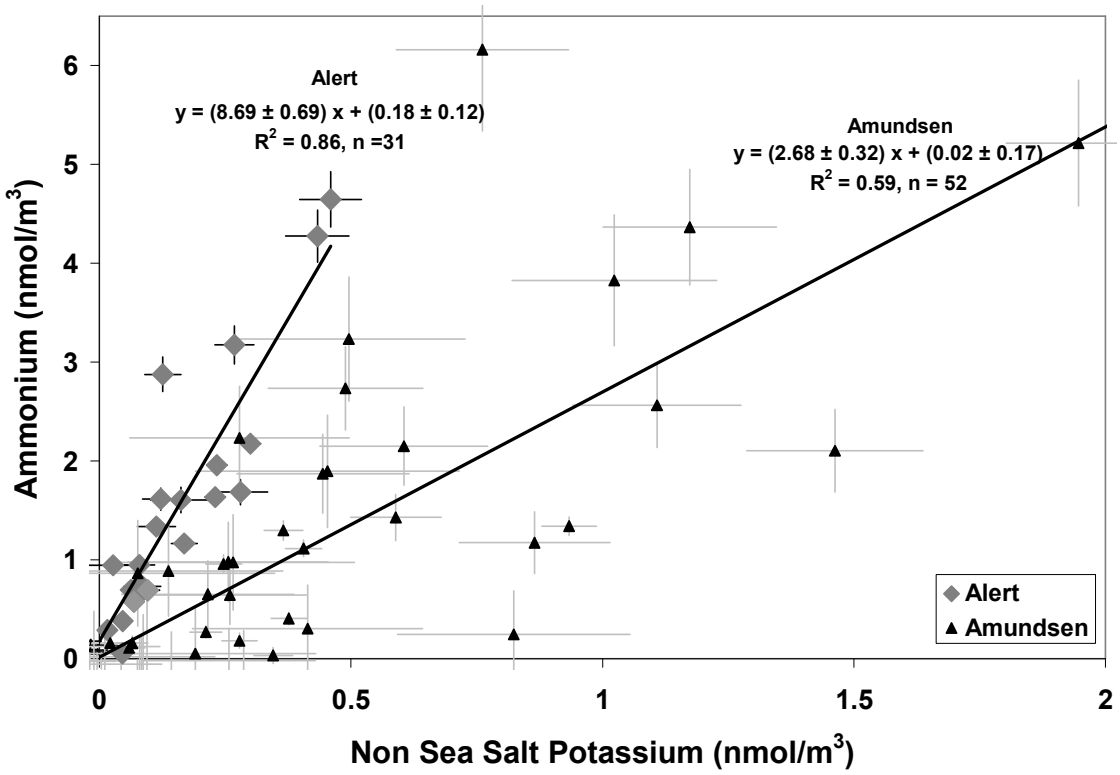

Figure 4.12 Comparison between ammonium and non sea salt potassium concentrations for total and fine aerosols collected at Alert and on the *Amundsen*.

ship's stack. A second possibility that the non sea salt potassium is from the Smoking Hills can be examined by comparing the concentration of non sea salt potassium to the $\delta^{34}S$ value of sulfate. As higher concentrations of non sea salt potassium are observed, the $\delta^{34}S$ value of the sulfate associated with it should approach the $\delta^{34}S$ value of the source material. The $\delta^{34}S$ values approach +3‰ which is consistent with ship emissions (Section 1.3) rather than SO_2 from combustion of shale from the Smoking Hills ($\delta^{34}S$ between -30 and -40‰).

4.3.1 Nitrate and Anthropogenic Sulfate in Aerosols

NO_3^- concentrations were compared to anthropogenic sulfate in the total and fine fractions for both data sets. A positive linear relationship ($R^2 = 0.58$) was observed between nitrate and anthropogenic sulfate in total aerosols but the correlation was not as strong in the fine aerosol ($R^2 = 0.28$) at Alert (see Figure 4.13). Total and fine aerosol collected on board the *Amundsen* also showed positive correlations ($R^2 = 0.32$, 0.62 respectively; Figure 4.13). The positive correlation indicates nitrate may be associated with anthropogenic aerosols, although the correlation is not strong. Although NO_3^- is not necessarily preserved under sampling conditions (Slanina et al., 2001; Schaap et al., 2004; Trebs et al., 2008), it is expected to be better preserved in colder weather (Schaap et al., 2004) and has been used as an anthropogenic indicator in previous studies (Barrie and Bottenheim, 1991; Yalcin and Wake, 2001). Nitrate is usually associated with anthropogenic aerosols, but the positive matrix factorization carried out by Sirois and Barrie (1999) at Alert placed it separately from anthropogenic sulfate. Sirois and Barrie (1999) rationalized that in the northern atmosphere there is a considerable fraction of atmospheric nitrogen oxide in the form of organic nitrate gases rather than in the form of aerosol nitrate. Therefore measurements of aerosol nitrate may not be representative of the total concentration of nitrogen oxides in the atmosphere. This may also be the case for this study, where fine aerosol NO_3^- at Alert is poorly correlated to anthropogenic sulfate.

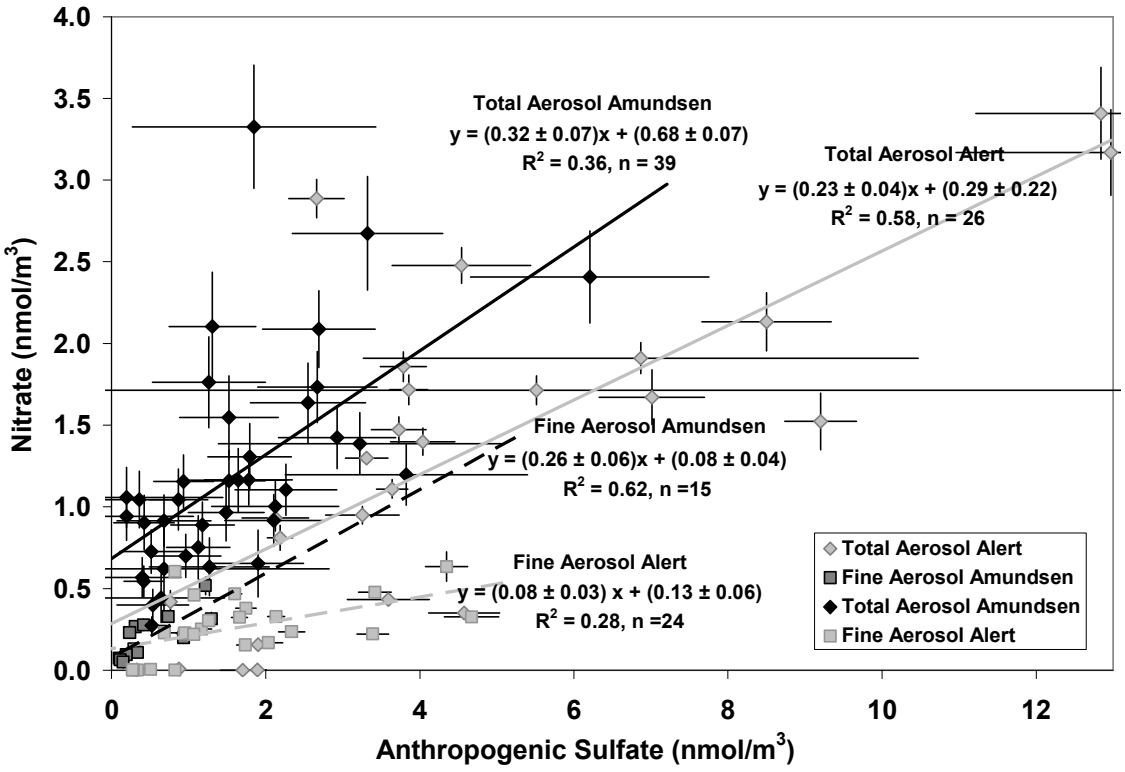

Figure 4.13 Comparison of nitrate and anthropogenic sulfate concentrations in aerosols.

Higher surface area on the smaller aerosols may lead to more gas phase exchange of nitrogen compounds. Differences in aerosol chemistry such as pH between larger aerosols and smaller aerosols (> 0.49 μm) may also explain the loss of nitrate relative to sulfate in the smaller aerosols at Alert. Another possibility exists, where emissions of anthropogenic NO_x are released at the source and products of its atmospheric oxidation (e.g. HNO_3) are preferentially taken up on larger aerosols due to differences in surface chemistry (such as pH and chemical composition; e.g. Karlsson and Ljungström, 1995; Weis and Ewing, 1999) between the large and small sized aerosols. Both of these

scenarios could potentially explain the fact there is a correlation between nitrate and sulfate in the total but not the fine (< 0.49 μm) aerosols at Alert.

4.3.2 Chloride Deficit

In the literature, chloride is associated with sea salt but during times of anthropogenic influence a chloride deficit relative to other sea salt ions is observed in particulate matter (Seinfeld and Pandis, 1998). This effect is seen often at lower latitudes where pollution is of greater importance (McInnes et al., 1994; Weis and Ewing, 1999; Sarin et al., 2010). A chloride deficit has been observed in polar aerosols before (Ricard et al., 2002; and Quinn et al., 2009) and is present at Alert for some samples (see Figure 3.2 from Chapter 3.2). All total aerosols samples collected on board the *Amundsen* had a chloride/sodium ratio within propagated error (~ 10%) of what is expected for sea salt (Rempillo, 2011) and therefore no chloride deficit is observed in the total aerosol samples. A chloride deficit is expected only with aged aerosol. Based on the interpretation of non sea salt potassium and potentially ammonium earlier in the chapter, aged aerosol is expected to be of importance at Alert. The dominance of sea salt (Chapter 3.4.1) aerosols within the vicinity of the *Amundsen* would mask the chloride deficit from aged aerosols.

The chloride deficit is calculated by the difference of the expected sea salt chloride concentration (based on sodium concentration and the sea salt ratio) and measured concentrations (see Chapter 1.1, equation 1.1). A relationship between non sea salt sulfate and chloride deficit is shown in Figure 4.14. Samples that are not influenced by

frost flowers (see Chapter 3.3.7) depict a relationship between non sea salt sulfate and the chloride deficit (Figure 4.14). One sample with a high chloride deficit (~13 nmol/m^3) was not included in the relationship (see * in Figure 4.14). This sample was the first sample in the 2007 season. Black material, most likely from the filter holder, was found on the filter before sampling and may have contaminated this sample.

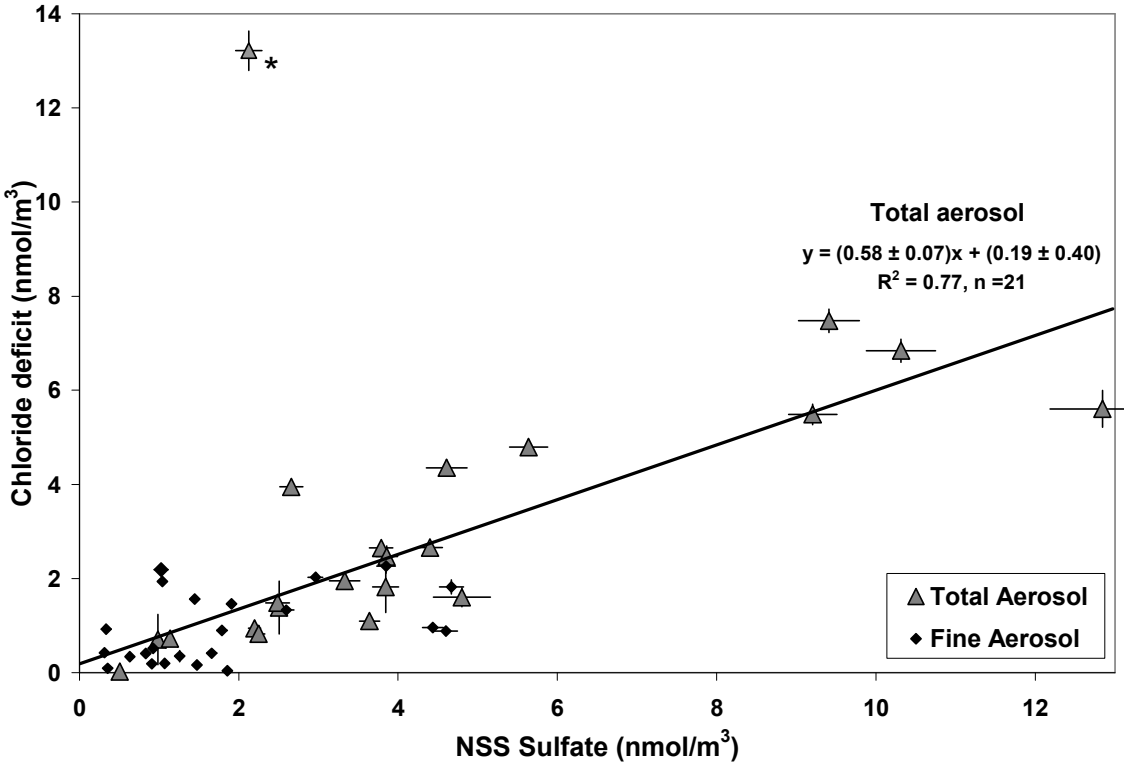

Figure 4.14 Comparison of chloride deficit and non sea salt sulfate concentrations in aerosols at Alert. Point marked with * is not included in the relationship. Three samples with large frost flower contributions are not displayed.

The remaining samples formed a strong relationship between non sea salt sulfate and chloride deficit ($R^2 = 0.77$). This is an indication of acidified aged marine aerosol. Ricard et al. (2002) found a relationship between chloride deficit and the sum of nitrate and excess non sea sulfate where excess non sea salt sulfate was calculated by subtracting ammonium from non sea salt sulfate (i.e., $NO_3^- + 2 \cdot NSS\ SO_4^{2-} - NH_4^+$). Formation of $HCl_{(g)}$ or $Cl_{2(g)}$ can occur in aerosols in the presence of sulfuric acid and/or HNO_3 (Singh, 1995; Ricard et al., 2002) and the calculation carried out by Ricard et al. (2002) incorporates the liberation of HCl from both acidic nitrogen and sulfur species. The relationship described in Figure 4.13 for Alert samples did not differ significantly when ammonium and nitrate were considered. This indicates that the chloride deficit at Alert is largely due to acidification of aerosols from H_2SO_4 rather than HNO_3.

This finding is important in the Arctic atmosphere, where once the sun sets for the winter, liberated HCl or other potential halogens (see Chapter 1.1) released from aerosols would not photolyze until spring. The spring and summer deficit of chloride has been observed for many years in Arctic aerosols associated with Arctic Haze (Ricard et al., 2002; Quinn et al., 2009). A deficit of chloride on aerosols just before and at the start of the dark period in the Arctic raises many questions about the destination of the liberated halogenated gases during the winter and what, if any, aerosol chemistry is occurring months before the return of photolysis in spring and the occurrence of ozone depletion events (Chapter 1.4.2).

4.4 Comparison between SO_2 and Sulfate

SO_2 is expected to oxidize to sulfate and be incorporated into/onto aerosols. This would lead to anthropogenic sulfate and anthropogenic SO_2 to be present in air masses influenced by anthropogenic sources. As air masses age, SO_2 would be oxidized to sulfate, decreasing the concentration of anthropogenic SO_2 while increasing the loading of aerosol sulfate in the air mass. Mixing of these anthropogenic air masses with clean air masses would lead to the dilution of both anthropogenic SO_2 and anthropogenic sulfate. If a positive correlation is observed between anthropogenic SO_2 and anthropogenic sulfate, it would support a situation where aerosols in polluted air masses have not had a chance to age. A negative correlation between SO_2 and sulfate would support aged air masses. Clean air mixing with anthropogenic influenced aged air masses may not show a correlation, but would be expected to have low SO_2 concentrations with variable sulfate concentrations throughout different sampling periods.

The correlation between SO_2 and total aerosol non sea salt sulfate is low at Alert (R^2 = 0.19) and on board the *Amundsen* (R^2 = 0.34). The low correlation supports clean air mixing with aged anthropogenic air masses. This is consistent with the postulate that long range transport is prevalent in the Arctic. The slightly stronger correlation on board the *Amundsen* may be due to some smoke stack emissions from the *Amundsen* having some influence on SO_2 and aerosol loading.

The fine aerosols (< 0.49 μm) have a longer lifetime than the larger aerosols and comprise a large surface area on which SO_2 may react (Chapter 1.1) and thus may be better to compare when studying the relationship between aerosols and SO_2 (Seguin, 2007). Comparing the SO_2 with fine aerosol concentrations does have some difficulties since sampling periods did not overlap exactly. This can be resolved by combining some of the SO_2 sampling periods. At Alert, the concentrations of SO_2 and non sea salt sulfate for fine aerosol are not correlated (R^2 =0.16). This indicates that even in the presence of aerosol anthropogenic sulfate, anthropogenic SO_2 may not be elevated. Once again this supports clean air mixing with aged air masses with anthropogenic influence and supports long range transport of aerosols at Alert.

Comparison of $\delta^{34}S$ values for SO_2 and non sea salt sulfate can give insight into the uptake of SO_2 onto aerosols. A 1:1 relationship between $\delta^{34}S$ values would indicate little to no isotope fractionation in the conversion between SO_2 and sulfate. A 1:1 would also indicate that SO_2 and sulfate was derived from similar sources; most likely that SO_2 that is present is taken up by surrounding aerosols. Figure 4.15 shows $\delta^{34}S$ values for SO_2 versus those for $\delta^{34}S_{nss}$ for fine and total aerosols at Alert. One sample above the mixing line may be due to underestimating frost flowers in the sample (Figure 4.15, marked with *). Another sample below the mixing line had the lowest $\delta^{34}S$ value recorded for SO_2 at Alert, which coupled with the difference between the sulfate $\delta^{34}S$ values, may signify a different source of SO_2 for that day. In most cases $\delta^{34}S$ values fall within 2‰ of the 1:1 line; indicating that the aerosol non sea salt sulfate found in both the total and fine aerosol

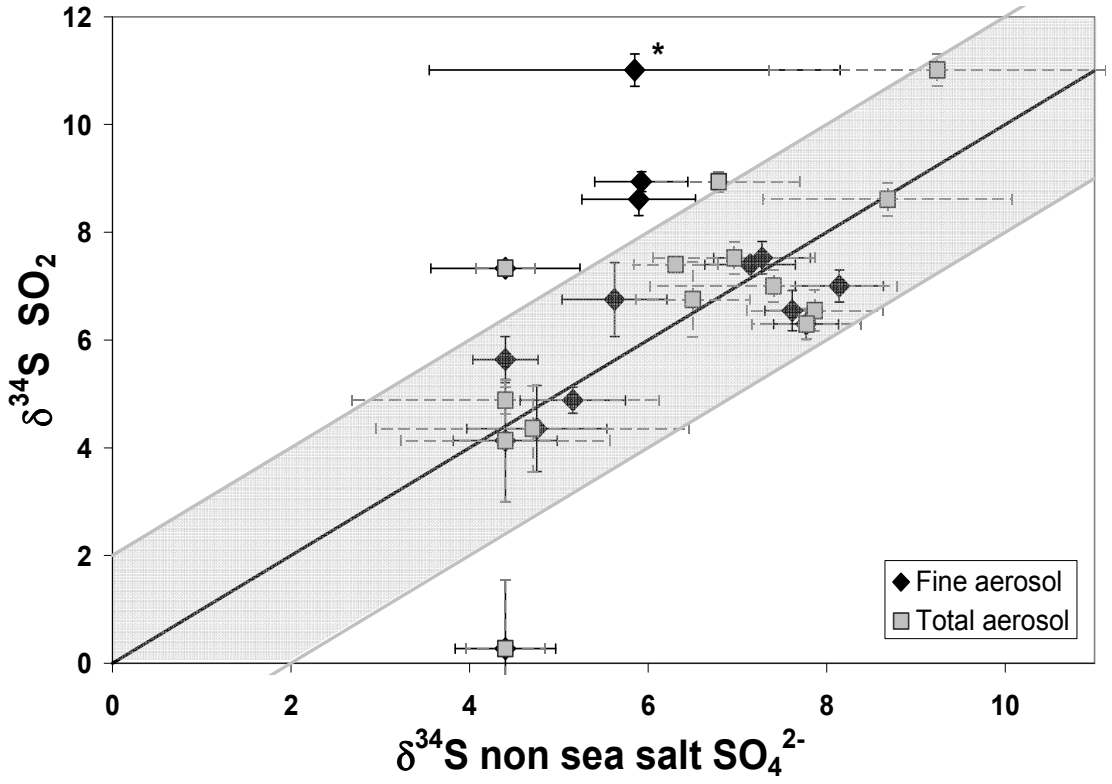

Figure 4.15 Comparison of $\delta^{34}S$ of SO_2 and $\delta^{34}S$ of non sea salt sulfate at Alert. Both total and fine aerosol $\delta^{34}S$ values are displayed. The 1:1 line ± 2‰ is illustrated for comparison. Sample that may underestimate frost flower (and underestimate $\delta^{34}S$ non sea salt SO_4^{2-}) is marked with *.

component at Alert is from the uptake of the SO_2 in the surrounding atmosphere. Larger aerosols are usually associated with more local sources since they tend to deposit at faster rates than fine aerosols. At Alert, though, isotope analysis suggests that all aerosols (not just the fine) are from long range transport and is consistent with the low concentrations of course aerosols what was described in Chapter 4.1.2.

4.5 Summary

Atmospheric anthropogenic sulfate concentrations are found to increase with the onset of Arctic Winter. Concentrations of anthropogenic sulfate are found to be relatively consistent during temporal overlap between the Alert and the *Amundsen* data set (fine aerosol 0.8 ± 0.6 nmol/m^3 and 0.3 ± 0.4 nmol/m^3 respectively); supporting the postulate that similar concentrations exist for this size fraction throughout the remote Arctic. At Alert, over 70% of the anthropogenic sulfate is present in size segregated aerosols smaller than 0.95 μm. The anthropogenic sulfate loading, in the *Amundsen* data set, is spread throughout the size segregated samples with approximately 20% of the anthropogenic sulfate found in the fine fraction aerosols (< 0.49 μm). These differences in aerosol size distribution for anthropogenic sulfate were attributed to smoke stack emissions from the *Amundsen*.

Anthropogenic SO_2 at Alert increased with the onset of winter in 2007 from below detection limits up to 11.8 nmol/m^3. Concentrations of anthropogenic SO_2 on board the *Amundsen* were greater than at Alert, more variable and were most likely due to the *Amundsen*'s smoke stack emissions. Samples collected on board the *Amundsen*, and determined to have little to no influence from smoke stack emissions, were within an order of magnitude relative to those samples collected at Alert (0.4 ± 2.4 nmol/m^3). There were two incidents when SO_2 concentrations were almost an order of magnitude larger than other SO_2 samples at Alert. Mixing between the boundary layer and the free troposphere at these times may explain the elevated SO_2 concentrations.

Long range transport to at Alert was evident from non sea salt potassium relationships with anthropogenic sulfate. Ammonium to anthropogenic sulfate and non sea salt potassium relationships were consistent with long range transport. Nitrate was correlated with anthropogenic sulfate in total aerosols but this was not observed in the fine aerosols (<0.49 μm). Differences in surface chemistry between smaller aerosols and larger aerosols may have affected the nitrate present in the samples. Either nitrate was preferentially lost from the smaller aerosols due to acidification during long range transport, or nitrogen species from the oxidation of NO_x, were preferentially taken up by the larger aerosols during transport.

A strong relationship ($R^2 = 0.77$) between the chloride deficit and anthropogenic sulfate in total aerosol samples was found for Alert but not in the *Amundsen* data set. This relationship supports the supposition that acidified aerosols are present in the Arctic during the onset of winter and that long range transport of aerosols is important at Alert. The observed chloride deficit raises questions about the resulting fate of halogenated gasses, such as $HCl_{(g)}$, that have been liberated from aerosols. With the approach of winter, these halogenated species may not photolyze until spring and the possible extent that these gasses would influence polar winter atmospheric chemistry is unknown.

Chapter Five: Biogenic Sulfur

Knowledge of biogenic SO_2 and aerosol biogenic sulfate concentrations in the Arctic is limited due to the large influence of the anthropogenic component of SO_2 and aerosol sulfate (see previous chapter). Charlson et al. (1987) proposed the idea that biogenic sulfur can play an important part of the natural climate feedback cycle (Chapter 1.5.1). Although climatic feedbacks are now known to be more complicated (Quinn and Bates, 2011) than the theory proposed by Charlson et al. (1987), there is still reason to study the biogenic contribution to the atmospheric sulfur budget. To understand the impact of anthropogenic influences on the atmosphere consideration of the natural influences must be taken into account.

Biogenic sulfur in the Arctic atmosphere comes from dimethylsulfide (DMS) released from oceans. DMS undergoes a series of oxidation processes in the atmosphere. Oxidation products consist of SO_2, methanesulfonic acid (MSA), sulfate and other intermediate trace products (i.e., MSIA, DMSO, $DMSO_2$; see Figure 1.3 in Chapter 1.5.3).

In this chapter, the oxidation products of DMS for two sampling stations are described and discussed. DMS measurements were conducted aboard the *Amundsen* during the SOLAS study but not at Alert. However, DMS oxidation products including SO_2, particulate MSA and sulfate were measured at both sampling sites. Note that the sole source of MSA in the Arctic is DMS oxidation (e.g., Li and Winchester, 1989*a*; Sirois

and Barrie, 1999). SO_2 and sulfate from biogenic sources can be separated from anthropogenic sulfur with the use of stable isotopes as explained in Chapter 3.6.1.

5.1 Aerosol Biogenic Sulfate

5.1.1 Location and Temporal Differences

Because of the presence of anthropogenic sulfate, biogenic aerosol sulfate measurements in the Arctic are few (Norman et al., 1999, Li and Barrie, 1993). Biogenic aerosol sulfate concentrations at Alert and on board the *Amundsen* are displayed in Figure 5.1 for total aerosol and Figure 5.2 for fine aerosols (<0.49 μm). Even with high error, some patterns are observed. Biogenic sulfate concentrations in the Arctic are low (approximately by an order of magnitude) compared to anthropogenic and sea salt sources (see Appendix C).

Total biogenic sulfate concentrations in 2007 at Alert were significantly different from zero for less than 50% of the sampling periods. The median value for total aerosol biogenic component at Alert was 0.00 ± 0.68 (1σ) nmol/m^3 in 2007 (fine aerosol 0.06 ± 0.29 (1σ) nmol/m^3). Aerosol samples (both total and fine) that contained biogenic sulfate that was significantly different than zero (i.e., propagated error did not pass through zero) occurred early in the season; before November 9, 2007. There were two time periods later in the 2007 sampling program when biogenic sulfate concentrations rose above the detection limit. These sampling periods occurred when biogenic SO_2 (Chapter 5.2) along

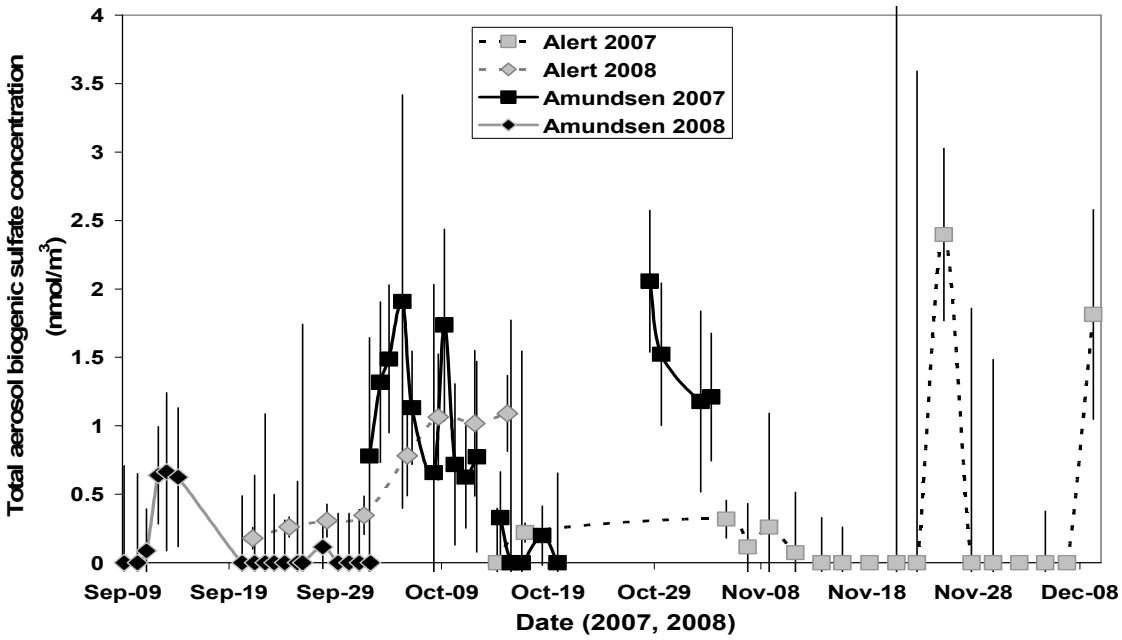

Figure 5.1 Biogenic sulfate concentrations in total aerosol at Alert and collected on board the *Amundsen* in 2007 and 2008.

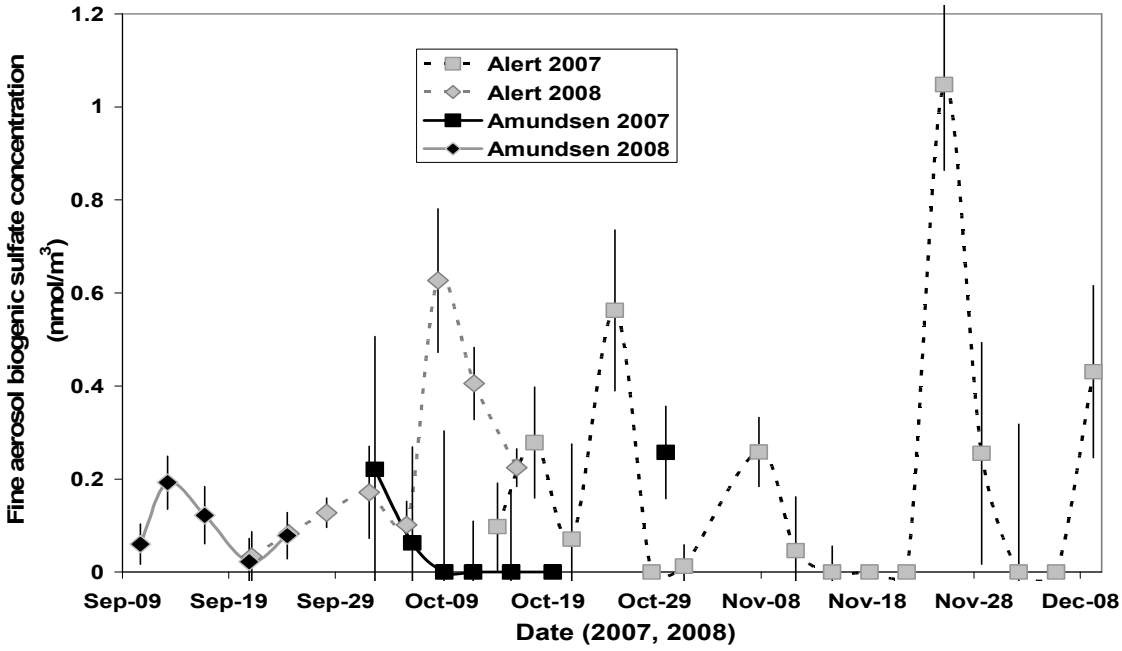

Figure 5.2 Biogenic sulfate concentrations in fine aerosol (<0.49 µm) at Alert and collected on board the *Amundsen* in 2007 and 2008

with anthropogenic sulfur (Chapter 4.2) were elevated and can be explained by mixing of the free troposphere and the boundary layer (see Chapter 4.2).

Biogenic sulfate in 2008 for both total and fine aerosols was usually significantly higher than zero with a median value of 0.56 ± 0.40 (1σ) nmol/m^3 for total and 0.15 ± 0.20 (1σ) nmol/m^3 for fine aerosols (< 0.49 μm). The larger values for 2008 than 2007 can be attributed to the samples being taken earlier in the season when biogenic sulfur is expected to be higher due to greater amounts of phytoplankton in the Arctic waters. The sea salt and frost flower sulfate components are less dominant in 2008 and will thus introduce less error associated with the non sea salt sulfate component and therefore result in lower source of error in 2008 than 2007 for biogenic sulfate. It is of interest to note that in 2008 the biogenic sulfate component rose during the sampling period. Norman et al. (1999) determined 36 ± 13% of non sea salt sulfate in September 1993 at Alert was from marine biogenic sources, before sharply decreasing in October. Samples measured in 2008 (i.e., between September 19th and October 18th) for this study also found similar percentages; total aerosols averaged 38 ± 8% and fine aerosols averaged 40 ± 19% non sea salt sulfate being biogenic in nature.

Concentrations of biogenic sulfate are found to be higher on average for samples collected on board the *Amundsen* compared to Alert. However this result is not significant (p value = 0.18 for unequal variance, two tail t – test for total aerosol between the *Amundsen* and Alert data sets) and errors associated with the calculation of biogenic

sulfate (Chapter 3.6) lead to high uncertainty for *Amundsen* samples. It is expected that biogenic sulfate is larger on board the *Amundsen* than at Alert due to the *Amundsen*'s proximity to the ocean and the source of biogenic sulfate. Samples were also collected earlier in the season on board the *Amundsen* relative to Alert; again leading to the expectation that the biogenic component is higher with the *Amundsen* data set. This expectation can not be proven with the data sets presented here since they are not significantly different. Additional measurements would be required to determine the spatial extent over which biogenic sulfate concentrations in the Arctic are uniform.

5.1.2 Size Segregated Samples

The biogenic sulfate component is usually found in the smaller aerosol sizes (Sciare et al., 2000; Wadleigh, 2004; Seguin et al., 2011) since submicron range aerosols have a larger total available reactive surface area relative to those of larger diameter (Seinfeld and Pandis, 1998). Larger diameter aerosols tend to have a shorter lifetime and are generally deposited more quickly than smaller aerosol size fractions.

Trends in biogenic sulfate are similar to those found for anthropogenic sulfate (Chapter 4.1.2) although error is much larger in the biogenic than anthropogenic component. At Alert, the majority of biogenic sulfate is found in the two smallest size fractions (see Figure 5.3 and Appendix C). Two measuring periods at Alert; November 26-28 and December 7-10, 2007 display elevated concentrations for biogenic sulfate calculated from apportionment. This occurs at the same time SO_2 concentrations were elevated at

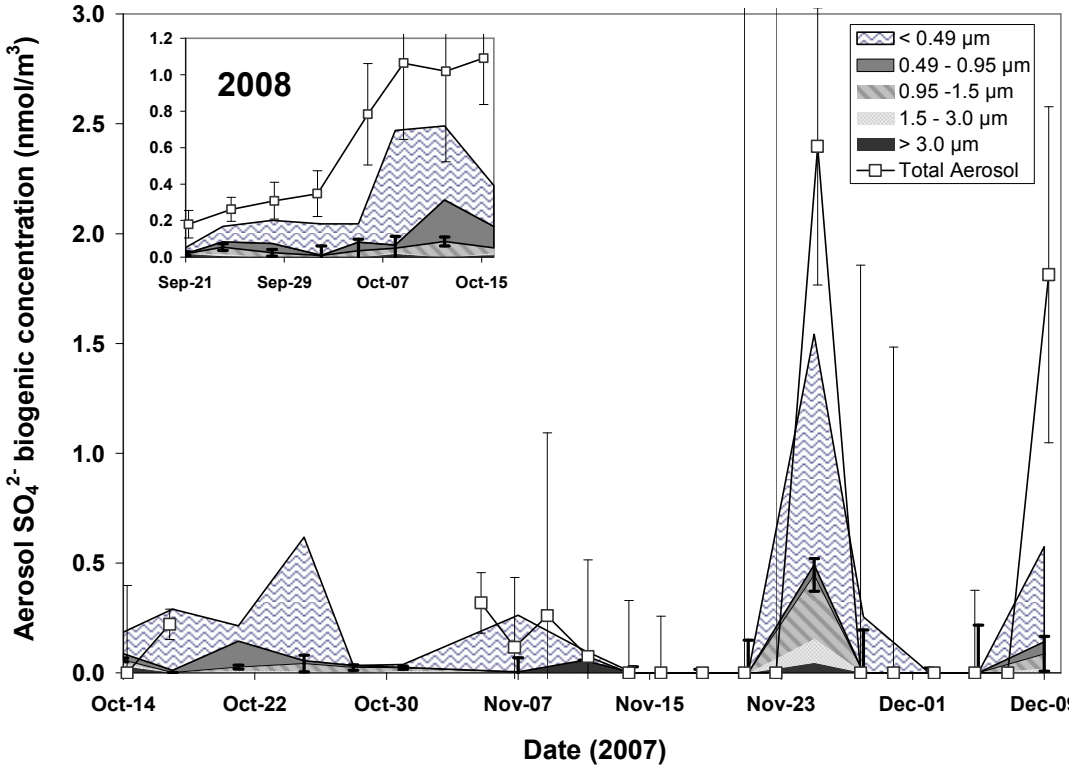

Figure 5.3 Biogenic sulfate in size segregated samples at Alert. Biogenic sulfate is calculated based on stable isotope techniques. Error is shown on the total and 0.95 - 1.5 µm size range aerosols. Size segregated concentrations are cumulative. The insert displays 2008 data.

Alert (Chapter 4.2) and may indicate pumping from the free troposphere and/or introduction of biogenic sulfur components from long range transport.

Biogenic sulfate collected on board the *Amundsen* is more widely distributed between the aerosol size fractions (see Figure 5.4 and Appendix C) than at Alert although biogenic sulfate on board the *Amundsen* in the size segregated samples are usually not significant

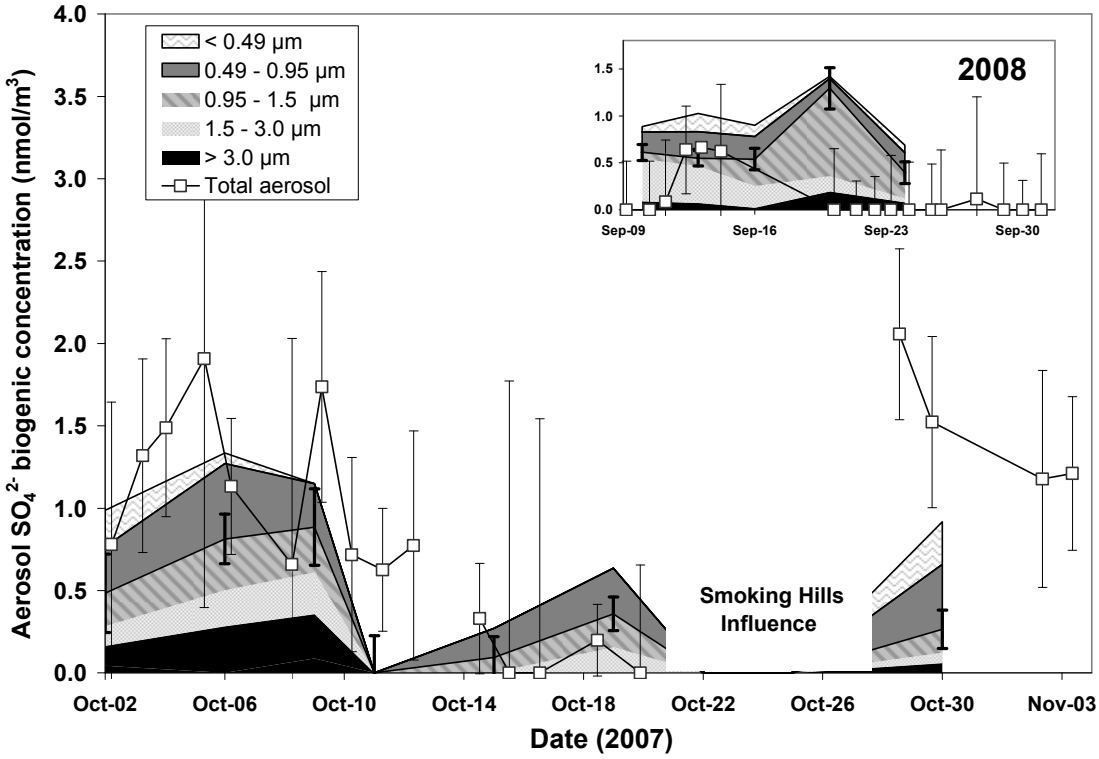

Figure 5.4 Biogenic sulfate in size segregated samples from the *Amundsen*. Biogenic sulfate is calculated based on stable isotope techniques. Sample of error is shown on the 0.95 -1.5 µm size range. Size segregated concentrations are cumulative. The insert displays 2008 data.

because of the high sea salt component and the variable anthropogenic $\delta^{34}S$ values discussed in Chapter 3.6.2.

Although others have studied isotope apportionment in the Arctic (Li and Barrie, 1993; Norman et al., 1999) the high proportion of biogenic sulfate at Alert found in the fine aerosol confirms biological sources of sulfate influence the fine aerosols. Fine aerosols

have a longer lifetime than larger aerosols and biogenic sulfate in the fine aerosol supports that long range transport of biogenic sulfur is of importance at Alert.

5.2 Biogenic SO_2

Biogenic SO_2 concentrations at Alert are displayed in Figure 5.5. In 2007, biogenic SO_2 concentrations were significantly different from zero on 5 occasions (out of 18 sampling periods) at Alert and no sampling period in 2007 on board the *Amundsen* had

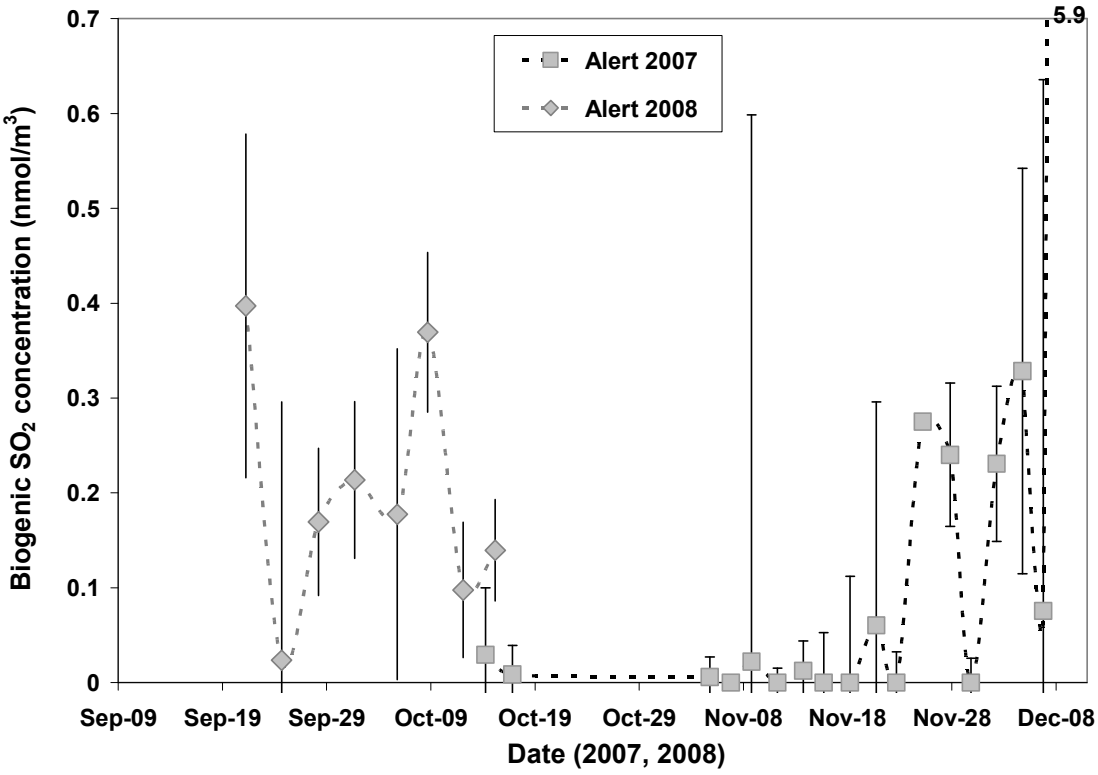

Figure 5.5 Biogenic SO_2 concentrations at Alert in 2007 and 2008. Note that the last sampling time (December 7 – 10, 2007) has a concentration of 5.9 nmol/m^3.

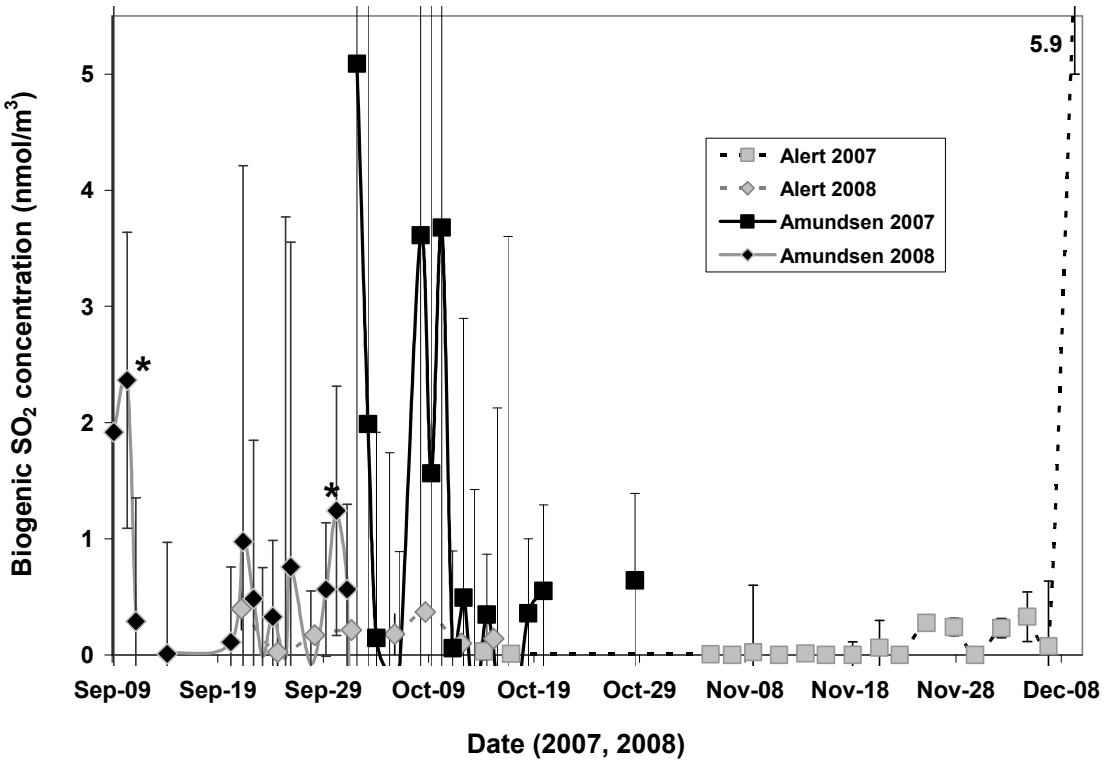

Figure 5.6 Biogenic SO_2 concentrations at Alert and collected on board the *Amundsen* in 2007 and 2008. Alert samples are displayed by themselves in Figure 5.5 for clarity. The two samples collected on board the *Amundsen* in 2008 that are significantly different than zero are marked with *.

concentrations significantly different than zero (see Figure 5.5 for Alert and Figure 5.6 for both sites). At Alert, biogenic SO_2 concentrations in 2007 only became significant late in the season (i.e., late November and December). There are a few reasons for this. SO_2, in general in 2007, increased in concentration later in the season, leading to the ability to measure SO_2 $\delta^{34}S$ values with more confidence such that apportionment of biogenic and anthropogenic SO_2 could be performed. Total SO_2 concentrations in

general increased (see Chapter 4.2) during this time of year and may signify a strong transport mechanism that brings both pollutants and biogenic components to the far north. By December, no sunlight reaches Alert and therefore if any DMS is present, oxidation would occur via abstraction pathways by the $NO_3\cdot$ radical (the only radical present in significant amounts in the absence of light) or by oxidation in the aqueous phase. Abstraction will preferentially produce SO_2 over MSA (Barnes et al., 2006). The sink of SO_2 in the atmosphere by homogenous $OH\cdot$ oxidation also decreases with the onset of winter. In addition, the heterogeneous oxidation sink for SO_2 may be reduced as winter progresses since pH (Martin 1984; Martin 1991; Seinfeld and Pandis, 1998) decreases through the winter in Arctic aerosols (Sirois and Barrie, 1999). The decrease in sinks for SO_2 in the Arctic atmosphere may also explain the increase in biogenic SO_2 with the onset of winter.

Biogenic SO_2 concentrations in 2008 are displayed in Figure 5.5 and Figure 5.6. Values for 2008 at Alert were significantly different from zero but were not significantly different than 2007 concentrations due to the lower error associated with SO_2 measurements in 2008 (median error in 2008 was 0.19 nmol/m^3 compared to median error of 0.39 nmol/m^3 in 2007).

It is interesting to compare data from the Arctic to those from the Antarctic where SO_2 is expected to mainly come from biogenic sources. SO_2 concentrations in Antarctica were measured to be 0.6 ± 0.5 nmol/m^3 (Jourdain and Legrand, 2001). The median value of biogenic SO_2 at Alert was 0.07 nmol/m^3 which is an order of magnitude smaller. It must

be noted that during one sampling period at Alert late in the season (December 7 – 10, 2007) biogenic SO_2 concentrations increased to approximately 5.9 nmol/m^3. This is one of the two sampling periods in 2007 (November 26-28 being the other) that may be affected by pumping from the free troposphere (see Chapter 5.1.2 and Chapter 4.2). Biogenic SO_2 concentrations measured on board the *Amundsen* are displayed in Figure 5.6. All data presented for the *Amundsen* data set has been corrected for the artefact introduced on the SO_2 filter during sampling (Appendix F). Large error is associated from biogenic SO_2 collected on board the *Amundsen* and all but two days were within propagated error of 0 nmol/m^3 (Figure 5.6). Therefore the only conclusion we can make is that median concentrations of biogenic SO_2 measured on the *Amundsen* are, at maximum, on the order of 1 nmol/m^3. Future studies with higher detection capabilities (e.g. longer collection periods) need to be conducted to gain additional insight on the spatial resolution of biogenic SO_2 in the Arctic.

5.3 Aerosol Methanesulfonic Acid

5.3.1 Location and Temporal Differences

Methanesulfonic acid (MSA) was measured in both the total aerosol and fine aerosol size segregated samples for Alert and on board the *Amundsen*. Methanesulfonic acid concentrations are displayed in Figure 5.7 for total aerosol and Figure 5.8 for fine aerosols. As with biogenic sulfate, methanesulfonic acid is expected to have higher concentrations earlier in the season when phytoplankton is present in the ocean waters.

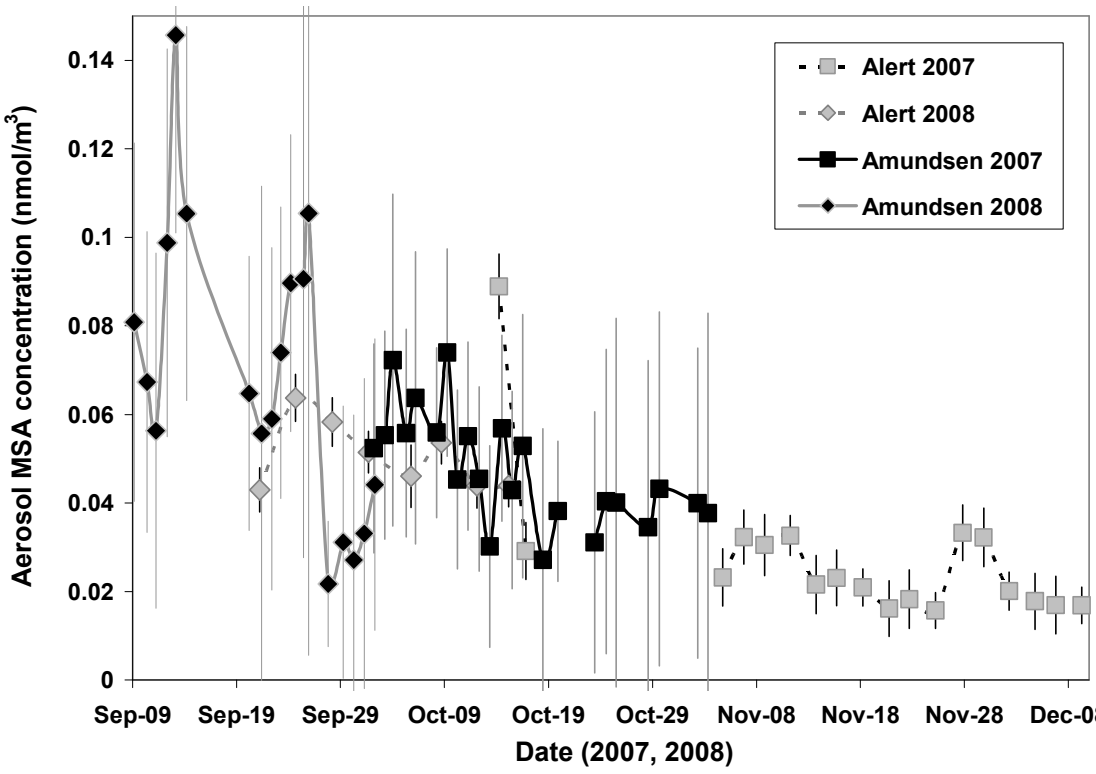

Figure 5.7 MSA concentrations in total aerosol at Alert and from the *Amundsen* in 2007 and 2008.

As illustrated in Figure 5.7 and Figure 5.8 a steady decrease with the onset of winter is seen which corresponds to what is expected. During the temporal overlap, total aerosol MSA concentrations on board the *Amundsen* were within error of concentrations at Alert (Figure 5.7). MSA concentrations in the fine aerosol are higher at Alert than on board the *Amundsen.* The *Amundsen* sampling took place directly on the ocean where DMS, the sole source of MSA in the Arctic, is produced and thus higher concentrations in aerosols at Alert is an interesting result. A correlation between fine aerosol MSA and DMS concentrations for the *Amundsen*, found by Rempillo et al. (2011), lead to the conclusion

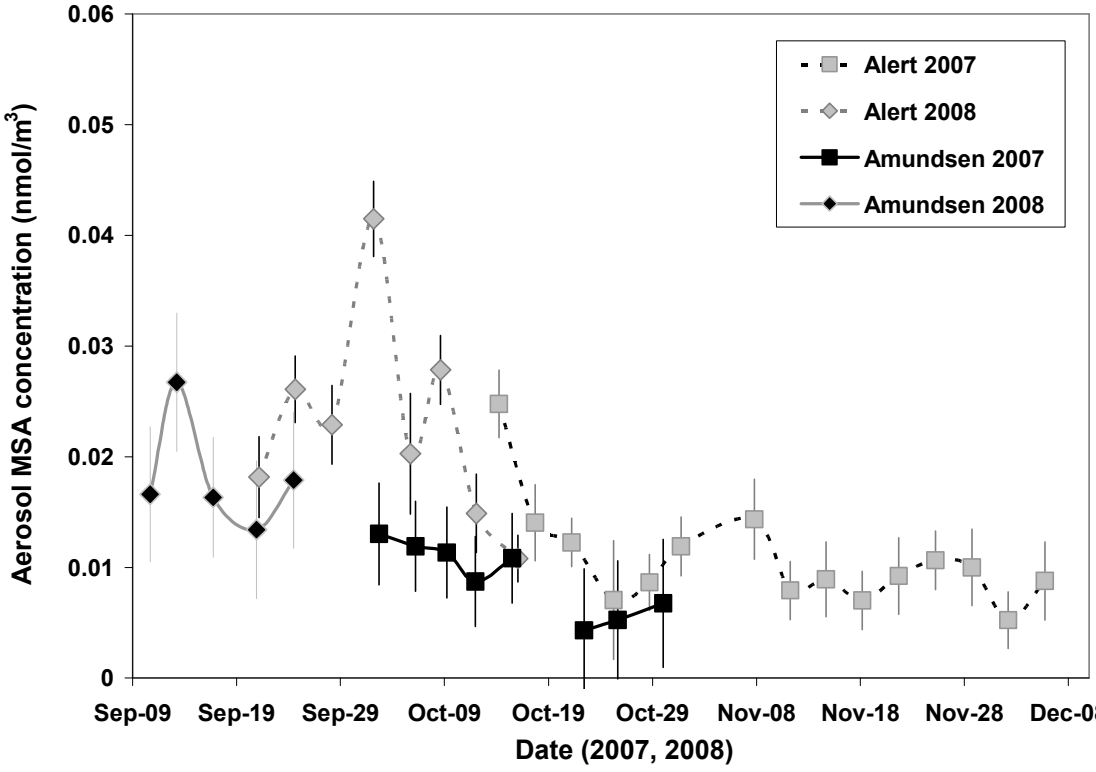

Figure 5.8 MSA concentrations in fine aerosol (< 0.49 µm) at Alert and from the *Amundsen* in 2007 and 2008.

that at least some proportion of DMS is oxidized locally. This would indicate that DMS lifetimes are short (although lifetimes of DMS are explained more in Chapter 6.4.3) and MSA is produced quickly. As the aerosols age, dry deposition occurs, leading to expected lower concentrations further away from the source. This conflicts with what is found at Alert, the inland station, where higher MSA is found in the fine aerosol. One possibility is that local/regional DMS production may be important in September at Alert as suggested by Sirois and Barrie (1999). The other possible explanation is that DMS oxidation occurs not only at the source of DMS as Rempillo et al., (2011) found, but also

during transport. It would be interesting to measure DMS at Alert coincident with its oxidation products to observe whether the source of MSA in Alert aerosols is local.

Average concentrations of MSA were slightly lower than previous studies but were within the observed range around the Arctic. Lower concentrations are due to seasonality since most studies were completed in the spring or the summer. Li and Winchester (1989*a*) measured an average concentration of MSA of 0.12 nmol/m^3 in total aerosol (submicron aerosol concentration ranged below detection limit up to 0.54 nmol/m^3, average 0.08 nmol/m^3) at Barrow between March 16 to May 6, 1986. Kerminen and Leck (2001) reported concentrations in accumulation mode aerosols of 0.03 - 1.1 nmol/m^3 over the Arctic Ocean in July 1996. Leck and Persson (1996*b*) found concentrations between 0.05 and 1.4 nmol/m^3 over open ocean between August and October 1991 with lower concentrations found later in the season and over pack ice (as low as 0.002 nmol/m^3). At Alert, previous MSA concentrations have ranged between 0.01 and 0.26 nmol/m^3 (Li et al., 1993; Norman et al., 1999), with highest concentrations in March/April and July/August. The measurements in this study, median of 0.031 ± 0.018 nmol/m^3 at Alert and 0.054 ± 0.026 nmol/m^3 from the *Amundsen*, correspond to the lower end of previous measurements and, as stated earlier, are most likely due to seasonality and location.

5.3.2 Size Segregated Aerosols

As found with non sea salt sulfate (Chapter 4.1.2 and Chapter 4.1.2), the distribution of MSA on aerosols may differ between sites. The *Amundsen* MSA size segregated temporal profile is displayed in Figure 5.9. Error for the 0.95 -1.5 µm size range is also displayed in the figure. As shown, error associated with the larger size fractions is large, and most often times concentrations are not significantly different from zero. The two finest aerosol size bins had significant non zero MSA concentrations (<0.49 µm and

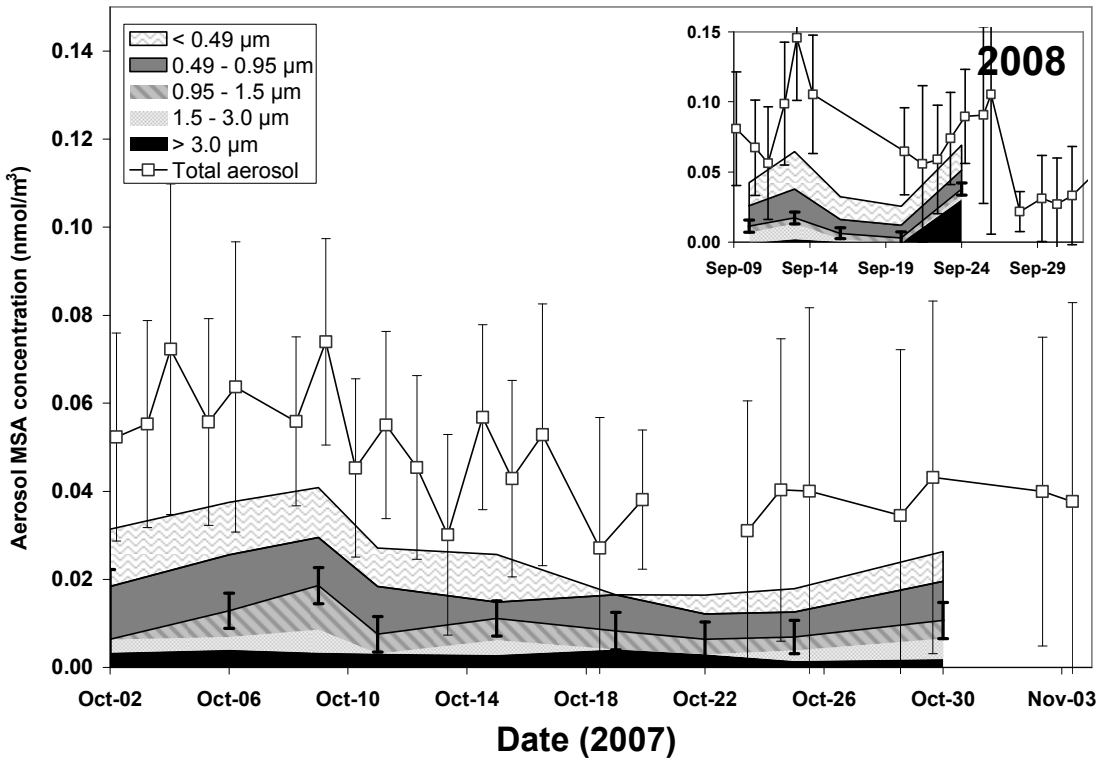

Figure 5.9 MSA in size segregated samples from the *Amundsen* for 2007 (and 2008, see insert). Sample of error is shown for total aerosol and the 0.95 -1.5 µm size range. Size segregated concentrations are cumulative.

0.49 – 0.95 μm) for the majority of the sampling periods. Averages for the 0.49 – 0.95 μm range were 0.010 ± 0.004 nmol/m^3 while < 0.49μm range had concentrations 0.013 ± 0.006 nmol/m^3. The MSA found on the fine aerosols is consistent with what other studies in the Arctic have found (Li and Winchester, 1989*a*; Leck and Persson, 1996*b*; Ricard et al., 2002). At Alert, MSA was only determined for total and fine aerosol and therefore a size segregated profile cannot be examined. Due to the issues of sampling discussed in Chapter 2.4.1, MSA cannot be directly quantitatively compared between the two high volume samplers at Alert. Qualitatively though, MSA measured on the fine aerosol is always less than half of that for the total MSA (Figure 5.7 and Figure 5.8).

5.3.3 MSA Biogenic Sulfate Ratios

Although MSA concentrations are of importance it is valuable to study the ratios between MSA and biogenic sulfate. These ratios can lead to insight about DMS oxidation pathways and conditions of DMS oxidation. In the southern Pacific, a relationship,

$$\mathbf{MSA/\ SO_4^{2-}{}_{nss} = -1.50 \cdot T + 42.2} \qquad \mathbf{5.1}$$

between temperature (T, in °C) and the MSA/non sea salt sulfate ratio (as a percent) was found (Bates et al., 1992*a*). During the Bates et al. (1992*a*) study, non sea salt sulfate concentrations were expected to be similar to those for biogenic sulfur due to the sampling location. Seguin (2007) found a similar relationship,

$$\mathbf{MSA/\ SO_4^{2-}{}_{bio} = -1.34 \cdot T + 37.2} \qquad \mathbf{5.2}$$

over the Atlantic with the MSA/biogenic sulfate ratio. The relationship though was not as strong as that of Bates et al. (1992*a*), most likely either due to the anthropogenic influence on oxidation of DMS (Seguin et al., 2010) or the possibility that some anthropogenic sulfate was included in the Bates et al. (1992*a*) study. This temperature relationship is not found in the Arctic. Molar ratios for MSA/non sea salt sulfate range between 0.002 and 0.085 at Alert with a median value of 0.010 and on board the *Amundsen* 0.008 and 0.420 (median 0.028). When only biogenic sulfate is considered, the MSA/biogenic sulfate ratio at both sites ranged between 0.007 and approached infinity (i.e., when biogenic sulfate was zero) with a median value of 0.24 at Alert (median = 0.28 on board the *Amundsen*). Ratios were similar between fine and total aerosols with no significant difference. These MSA/ non sea salt sulfate ratios are similar to those reported and reviewed by Li et al. (1993). The MSA/ biogenic sulfate values at Alert in this study are similar to the MSA/ non sea salt sulfate ratios found in the Antarctic where biogenic sulfate is the dominant source of non sea salt sulfate (see Li et al. (1993) for review of literature values). Values found in this work compared to previous Arctic MSA/ biogenic sulfate ratios found by Li and Barrie (1993) and Norman et al. (1999) are also comparable.

5.3.4 MSA Branching Ratio

In the literature the MSA and sulfate is usually compared using the MSA/ biogenic sulfate ratio. The issue with this is that as biogenic sulfate concentration approaches zero, the ratio approaches infinity. Another way to illustrate the relationship between the two components is to look at the fractional contribution of MSA over the total sulfur budget in the aerosol. This will be referred to as the molar MSA branching ratio (MSA_{BR}) given as

$$MSA_{BR} = \frac{MSA}{MSA + SO_{4\ bio}^{2-}} \qquad \textbf{5.3}$$

where MSA and $SO_4^{2-}{}_{bio}$ are the concentrations (in nmol/m^3) of their respective compounds. Figure 5.10 illustrates the MSA branching ratio of fine and total aerosols from the *Amundsen* and at Alert. Large uncertainty is associated with the branching ratio and minimum and maximum MSA_{BR} are displayed in Figure 5.10 with error bars. It is of interest to note that lower MSA branching ratios are found in 2008 in fine aerosols at both locations along with lower error associated with each measurement. Although the branching ratio appears to be high in total aerosols on board the *Amundsen* from 2008, error associated with the measurements may lead to much lower branching ratios.

With the onset of the Arctic winter MSA_{BR} approaches unity at Alert due to the small amount of biogenic sulfate relative to MSA. Measurements of total aerosol on board the

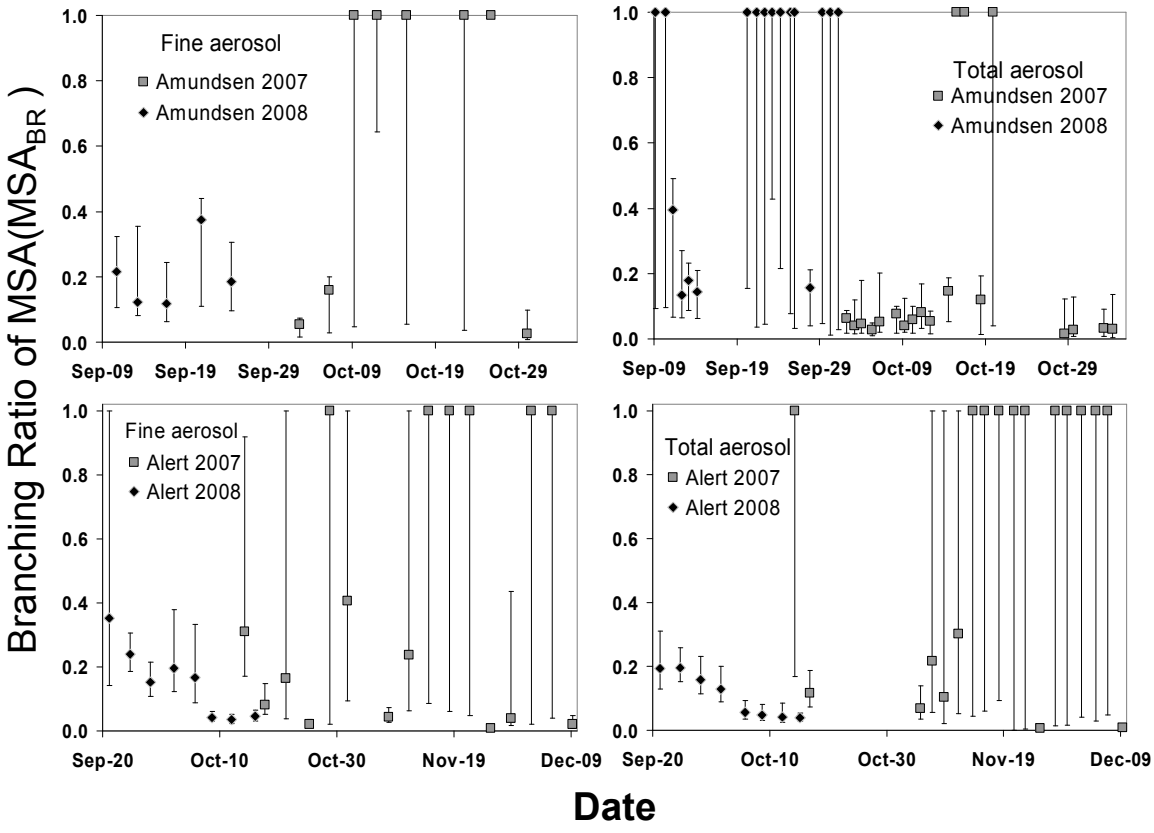

Figure 5.10 Molar branching ratios of MSA for fine and total aerosols. *Amundsen* data is on the top row, Alert is along the bottom. Minimum and maximum values are illustrated on the figure with error bars.

Amundsen had low MSA_{BR} ratios in 2007 prior to having a few extreme variations in the branching ratio between Oct 15th and 19th. The fine aerosol ratio increased before the total aerosol during this year although the different sampling times may be the cause of the difference. The MSA branching ratios can lead to insight on DMS oxidation pathways and will be explored further in Chapter 6.

5.4 Summary

There have been only a few previous measurements of biogenic sulfate in the Arctic (Li and Barrie, 1993; Norman et al., 1999). This study increased the knowledge of biogenic sulfate contributions in the Arctic. Median biogenic sulfate concentrations at Alert found in total aerosols were 0.15 ± 0.62 (1σ) nmol/m^3 and 0.20 ± 0.64 (1σ) nmol/m^3 for samples collected on board the *Amundsen*. Total aerosol biogenic sulfate had large error associated with the measurement because of the larger contribution of sea salt sulfate in the samples with over half the samples at Alert not being significantly different zero (zero fell within propagated error). Fine aerosol (<0.49 μm) concentration of biogenic sulfate was 0.19 ± 0.29 (1σ) nmol/m^3 at Alert and 0.15 ± 0.20 (1σ) nmol/m^3 from the samples collected on board the *Amundsen*. This is the first time that size segregated biogenic sulfate contributions in aerosols in the Arctic were studied. At Alert, the majority of biogenic sulfate is found in the two smallest size fractions (<0.49 μm, 0.49-0.95 μm).

Biogenic SO_2 was measured for the first time in the Arctic. Biogenic SO_2 concentrations at Alert were 0.07 nmol/m^3 (standard deviation = 1.15 nmol/m^3). An increase in biogenic SO_2 was observed with the onset of winter in 2007. In 2008, samples were collected earlier in the season and temporal variations were not observed.

Aerosol MSA was measured at Alert and on board the *Amundsen*. MSA concentrations decreased at both sites with the onset of winter. Concentrations of MSA in the fine aerosol was found to be higher at Alert than on board the *Amundsen* during similar

sampling periods and supports long range transport of DMS and MSA. MSA concentrations and MSA/non sea salt sulfate ratios are found to be within the range of previous studies conducted in the Arctic.

Chapter Six: DMS Oxidation in the Arctic Atmosphere

Oxidation of DMS occurs by $OH\cdot$, $NO_3\cdot$, $BrO\cdot$, $Cl\cdot$ and other atmospheric oxidants. Dependent on the reaction, DMS can either oxidize via the abstraction or addition pathway (Chapter 1.5.3) and will eventually form one of two end products: MSA (see Chapter 5.3) or sulfate (see Chapter 5.1). Biogenic SO_2 (Chapter 5.2) is an intermediate between DMS and the end product of sulfate. Modeling the oxidation of DMS (see Figure 6.1) can predict MSA branching ratios in the Arctic which in turn can be tested against the measurements presented in the previous chapter. The oxidation model can also be used for insight into DMS transport to and from the Arctic region. DMS concentrations are affected by removal from the boundary layer through oxidation or by transport (entrainment to the lower troposphere or advection in the surrounding boundary layer).

6.1 DMS Concentrations

DMS concentrations were measured on board the *Amundsen* and have been presented previously by Rempillo (2011) and Rempillo et al. (2011). Daily median concentrations in 2007 ranged from below detection limit (0.3 nmol/m^3) to 1.3 nmol/m^3 with a median value of 0.38 ± 0.34 (1σ) nmol/m^3. In 2008, daily averages ranged between below detection limit to 4.1 nmol/m^3 with a median concentration of 1.2 ± 0.9 (1σ) nmol/m^3. Periods of low to moderate DMS concentrations were punctuated by episodes where concentrations were an order of magnitude higher. The highest individual measurement

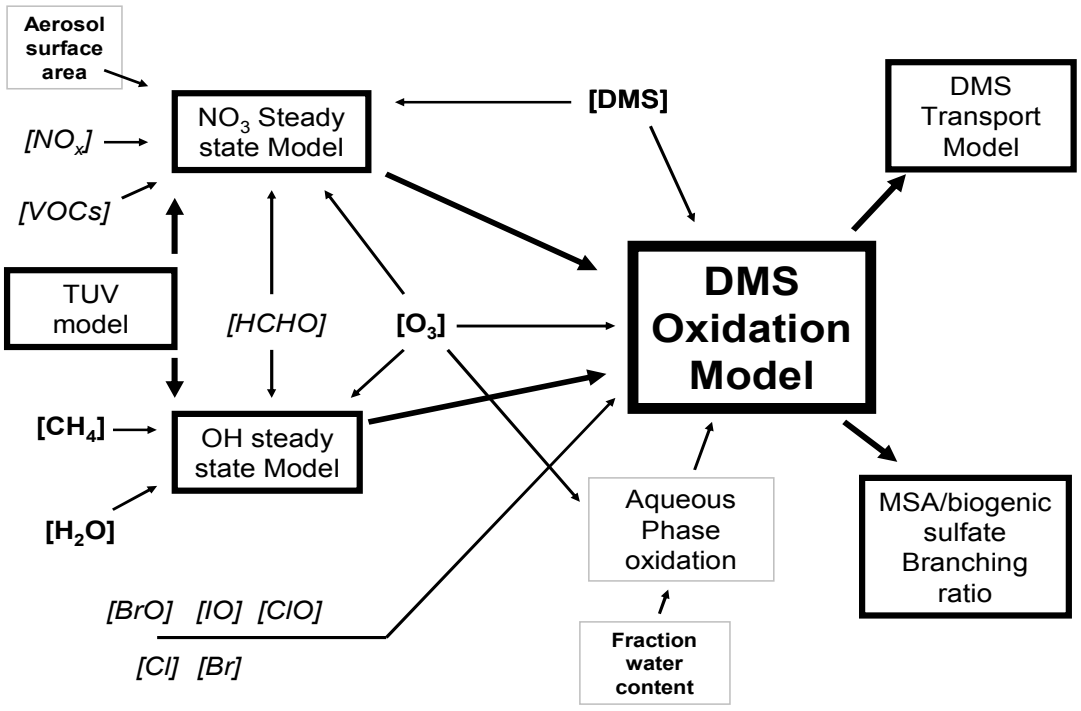

Figure 6.1 Flow chart of inputs and outputs of the DMS Oxidation Model used in this chapter. Models are boldly boxed. Italicized inputs indicate assumptions from previous studies were used; bold text inputs indicate concentrations were measured concurrently with this study; Inputs that are boxed in grey indicate that assumptions were made before values could be determined.

was taken on September 12, 2008 with a DMS concentration of 12.55 nmol/m^3. Two other peaks that reached over 12 nmol/m^3 occurred on September 15 and October 2, 2008. DMS concentrations measured in this study are on par with other studies where values ranged between 0.1 to 50 nmol/m^3 in the Arctic atmosphere (Ferek et al., 1995; Leck and Persson, 1996*b*; Sharma et al., 1999). Additional information of previous studies can be found in Rempillo (2011).

6.2 DMS Oxidation Model

The removal of DMS by oxidation (L_{Ox}) can be written as

$$L_{Ox} = [DMS](k_{OH:DMS}[OH\cdot] + k_{NO_3:DMS}[NO_3\cdot] + k_{BrO:DMS}[BrO\cdot] + ...) \quad 6.1$$

where [radical] is the radical concentration and $k_{i:DMS}$ is the rate coefficient between the oxidant and DMS (units molecules cm^{-3} s^{-1}). Other oxidants including Cl·, ClO·, Br·, IO· and O_3 also removes atmospheric DMS and are included in the model.

Radical concentrations were not measured during the SOLAS study but assumptions can be made for each oxidant (see Figure 6.1 for overview) in order to determine approximate values.

6.3 Radical Concentrations

6.3.1 OH· Concentrations

The hydroxyl radical (OH·) is one of the most important oxidants in the atmosphere. DMS can be oxidized by the OH· radical by either the addition or the abstraction pathway (see Chapter 1.5.3). As no OH· measurements were made, OH· radical concentrations during the SOLAS study must be estimated. The most dominant formation reaction over

continental mid-latitudes for OH· is the reaction of $O(^1D)$ with H_2O (Seinfeld and Pandis, 1998). This reaction is also believed to be the leading source of OH· in polar regions. Daytime average OH· concentrations have been measured in the Antarctic and found to be 3 x 10^5 molecules/cm^3 which is within 30% agreement of OH production from $O(^1D)$ + H_2O using the two major sinks of CO and CH_4 (Jefferson et al., 1998).

Recent studies have shown that OH· concentration may also be influenced by other processes. A campaign at the Summit Research Station (altitude of over 3000 m on the Greenland ice cap) found average summer OH· measurements at noon to be 8.4 x 10^6 molecules/m^3 (Sjostedt et al., 2007). The elevation (3000 m above sea level) would contribute to elevated OH· concentrations relative to sea level. Formaldehyde (HCHO), nitrous acid (HONO) and hydrogen peroxide (H_2O_2) were found to be elevated during that study and could also contribute significantly to the OH· concentration (Chen et al., 2007). These compounds along with others can be released from the snowpack which can significantly change the chemistry of the atmosphere in the boundary layer (Grannas et al., 2007 and references within). Edwards et al. (2011) found daily peaks of OH· concentrations of 1.16 ± (1.02) x 10^6 molecules/cm^3 over Hudson Bay in February and March 2008 and attributed 80% of the source to be from HCHO photolysis. Other processes that are unique to the polar regions tend to decrease OH· concentrations. Mao et al. (2010) found relatively low values (average: 5 x 10^5 molecules/cm^3) under sunlit conditions in surface air (defined as 0-1km) relative to a model they used to calculate OH· concentration. Low water vapour and solar elevation along with thick ozone columns decreases OH· concentrations in the Arctic, but had been factored within their

model. The model discrepancy at the surface was attributed to halogen chemistry, which can effectively remove OH· (Mao et al. 2010; Mahajan et al., 2010; Edwards et al., 2011). Summer measurements reported for the Hadley research station in Antarctic during the austral summer (January-February) were 3.9 x 10^5 molecules / cm^3 and the authors reported that the HO_x and halogen chemistry were closely coupled, indicating an important link between OH· concentration and halogen chemistry (Bloss et al., 2007; Bloss et al., 2010).

It can be illustrated with the large number of studies conducted in the Polar Regions, that there is a large range of OH· concentrations due to the diversity of formation pathways present under polar conditions. Although halogens are a driving influence in the spring (Edwards et al., 2011) the influence of these compounds on OH· concentrations later in the year (i.e., fall season) is not well studied. HCHO, HONO and H_2O_2 chemistry has also been studied in spring and summer months (Grannas et al., 2007; Sjostedt et al., 2007; Mao et al., 2010; Edwards et al., 2011) but fall data are sparse. Riedel et al. (2005) did a year round study on HCHO and H_2O_2 in Antarctica. Concentrations in the fall tended to be much lower than in the spring and summer but can still be of importance. Mabilia et al. (2007) determined formaldehyde to be 14.9 ± 3.5 nmol/m^3 at Ny-Alesund, Svalbard, in September, which is higher than fall values reported at Antarctica.

All of these processes effect the formation of OH· radicals, but only during the presence of light. As the days start to shorten in the fall, OH· concentrations will decrease due to the shortening of daylight and the increase in solar zenith angle: OH· concentration is

dependent on solar radiation especially at wavelengths between 290 and 319 nm where the quantum yield of $O(^1D)$ is significant in the troposphere.

High albedo from snow and ice in the Arctic can also effect OH· concentrations due to the reflectivity of the snow. Snow, besides being a source of some of the compounds effecting OH· concentrations, also affects albedo, often reflecting greater than 90% in the UV spectral region (Grannas et al., 2007). This can increase atmospheric photolysis in the Arctic so that it becomes similar to that at mid-latitudes and is very significant for UVA absorbing species such as NO_2, BrO, HONO and CH_2O (Grannas et al., 2007). Although this also occurs with UVB species, the long path through the ozone layer leads to a decrease of an order of magnitude of the photolysis rate of O_3 between the Arctic and the mid-latitudes (Lefer et al., 2001). The large albedo would be expected to have more influence over land where snow is present. Sampling on board the *Amundsen*, was done for the majority of the time in open seas, and although there were times where ice was present, the albedo would be much lower than those reviewed by Grannas et al. (2007).

6.3.1.1 Determination of OH· Concentrations

Seguin (2007) utilized a scaling factor to determine concentrations for OH· over the Atlantic. In the model calculated concentrations for OH· were based on the assumption that loss of OH· was relatively constant compared to the production from $O(^1D)$. Irradiance at different wavelengths was measured during the study and normalization wavelengths were found to be within ± 3% of each other. Seguin (2007) assumed that

this would carry over to the UVB region where O_3 is photolyzed. There is a possibility that a similar assumption could be carried out for this study (Rempillo et al., 2011) but some of the unique aspects of the Arctic expressed in Chapter 6.3.1 must be addressed to validate the assumptions in the model and to predict the variables needed for analysis. For example, photolysis of HCHO is an important part in the production of HO_x in the arctic troposphere. This production term can be the dominate source of OH· in the spring (Edwards et al., 2011).

Instead of the assumption described above, a box model was used here to determine OH· concentrations. OH· is short lived and can be assumed to be in steady state (see Appendix G.1). HO_2· can also be assumed to be in steady state (Appendix G.1). The major production and loss reactions for OH· and HO_2· that are used in this model are shown in Table 6.1 along with the rate constants associated with each reaction.

Measurements of relative humidity and temperature (Figure 2.3) from the meteorological station on board the *Amundsen* were used to calculate concentrations of water in the atmosphere. O_3 measurements performed on board the *Amundsen* have not yet undergone quality assurance and control (Abbatt, J., personal communications 2012) and therefore could not be used for this study. Instead O_3 concentrations from alternate stations in the Arctic were examined. Barrow (Alaska) is on the coast of the Arctic Ocean (71.32 ºN, 156.60 ºW, elevation 11 m) which is at a similar latitude to the location for the sampling performed for this study. Barrow is located at sea level and air masses are dominantly influenced by the Arctic Ocean. Therefore, daily average O_3

concentrations from Barrow measured by NOAA (http://ds.data.jma.go.jp/gmd/wdcgg/) were assumed to be similar to those aboard the *Amundsen*.

Rapid ozone loss in the Arctic (see Helmig et al., 2007) is associated with the spring polar sunrise period. These rapid ozone losses have not been observed in the fall and

OH Production			**k ($cm^3 molecule^{-1} s^{-1}$)**
	$O(^1D) + H_2O \rightarrow 2\ OH$	k_1	2.14×10^{-10}
	$O_3 + HO_2 \rightarrow OH + 2O_2$	k_2	$2.03 \times 10^{-16} (T/300)^{4.57} e^{(693/T)}$
	$NO + HO_2 \rightarrow OH + NO_2$	k_3	$3.45 \times 10^{-12} e^{(270/T)}$
OH loss			
	$CH_4 + OH \rightarrow HO_2$	k_4	$1.85 \times 10^{-12} e^{(-1690/T)}$
	$CO + OH \rightarrow H + CO_2$ $H + O_2 \rightarrow HO_2$	k_{5*}	- *fast*
	$HCHO + OH \rightarrow$ products	k_{6*}	$5.4 \times 10^{-12} e^{(135/T)}$
HO_2 production			
	$CO + OH \rightarrow H + CO_2$ $H + O_2 \rightarrow HO_2$	k_{5*}	- *fast*
	$HCHO + h\nu \rightarrow H + HCO$ $H + O_2 \rightarrow HO_2$ $HCO + O_2 \rightarrow HO_2 + CO$	j_{HCHO}	- *fast* *fast*
HO_2 loss			
	$O_3 + HO_2 \rightarrow OH + 2O_2$	k_2	*above*
	$NO + HO_2 \rightarrow OH + NO_2$	k_3	*above*
$O(^1D)$ concentration			
	$\frac{j_{O_3 \rightarrow O^1D}[O_3]}{(k_{O^1D:N_2}[N_2] + k_{O^1D:O_2}[O_2])}$	k_{N2}	$2.15 \times 10^{-11} e^{(110/T)}$
		k_{O2}	$3.2 \times 10^{-11} e^{(67/T)}$

Table 6.1 Major loss and production of OH· and HO_2· used in the box model to determine OH· concentrations in the Arctic atmosphere (Appendix G). k_{5*}, k_{6*} are the rate determining step of the complete reaction. Rate constants used in the model are the recommended values from IUPAC (2009). All other reactions are assumed to have minimal effect on OH· concentrations.

ozone concentrations stay relatively stable throughout the fall period (see Helmig et al., 2007 and references within). Daily average O_3 concentrations were taken since diurnal variations are expected to be less than 10% (Helmig et al., 2007). Although concentrations of ozone varies throughout the Arctic (e.g., Alert and Barrow yearly median values differ between 10 to 20%; Helmig et al., 2007), the data set from Barrow represents the best source of ozone data at this time.

OH· is affected by atmospheric CH_4 concentrations as shown in Table 6.1 and Appendix G. Daily CH_4 concentrations are relatively stable over large distances because of their long lifetimes (lifetime > 10 years; Seinfeld and Pandis, 1998). Measurements of CH_4 at Alert by Environment Canada and Barrow by NOAA will be used in the model (http://ds.data.jma.go.jp/gmd/wdcgg/) as no CH_4 measurements were available from aboard the ship. The median value for CH_4 concentrations for the sampling periods for 2007 and 2008 was 83 nmol/m^3 (5.0 x 10^{13} molecules/cm^3). It should be noted that the difference in CH_4 concentrations between the two sites was less than 5% at all times and was less than 1% for the majority of times. Therefore, Alert samples were used for CH_4 unless no reading was obtained for a given day, in which case, data from Barrow was used. CH_4 measurements for September 16, 2008 were unavailable at either site and therefore an average value based on data for September 15 and 17 was used.

Formaldehyde has been found to influence the OH· concentration in the Arctic in past studies (Grannas et al., 2007; Sjostedt et al., 2007; Mao et al., 2010; Edwards et al., 2011). Literature values for HCHO concentrations averaged 14.9 ± 3.5 nmol/m^3 in the

Arctic in September 2004 at Ny-Alesund, Svalbard (Mabilia et al., 2007). Most studies have focused on HCHO concentrations in the spring and summer (Grannas et al., 2007; Edward et al., 2011). Riedel et al. (2005) noted annual variation in HCHO concentrations in the Antarctic, and therefore spring samples may not be representative of the time period of this study. The average literature value measured by Mabilia et al. (2007) in the autumn of 2004 will be used as a plausible approximate value for concentrations in this study.

Effective photolysis rate coefficients for j_{O3} and j_{HCHO} can be calculated with the use of a radiation transfer model, specifically the Version 4.1 Tropospheric Ultraviolet and Visible (TUV) Radiation Model (http://cprm.acd.ucar.edu/Models/TUV). Quick TUV calculates photolysis rate coefficients for clear sky conditions. Inputs that are required are latitude, longitude, date, time of day, overhead ozone column, albedo, ground elevation and measurement elevation. All of these parameters were recorded during the *Amundsen* cruise except for ozone burden and albedo. The albedo is dependent on ice cover around the ship. For the purpose of this model, an albedo of 0.06 will be used for open water, while an albedo of 0.7 for frozen white ice (Perovich, 1996 and references within) will be used when the ship was surrounded by greater than 50% ice as recorded by visual observations. Ozone burden can be estimated based on satellite images (http://ozoneaq.gsfc.nasa.gov/OMIOzone.md) and is found to be approximately 300 DU based on images from the ozone monitoring instrument (OMI). A constant 300 DU was used throughout the sampling period. See Appendix G.2 for photolysis rate coefficients for j_{O3} and j_{HCHO} determined by the TUV model.

OH· concentrations were calculated each time atmospheric DMS concentrations were measured on board the *Amundsen*. Calculated concentrations from October 2 – 17, 2007 are displayed in Figure 6.2 and concentrations for 2008 are displayed in Figure 6.3. The inclusion of HCHO chemistry can account for a large percentage of OH· concentration in the Arctic atmosphere and percent difference between the inclusion of HCHO is displayed in Figure 6.2 and Figure 6.3 along with the calculated concentrations for the OH· model. Spikes in percent contribution are seen corresponding to sunrise and sunset (top of Figure 6.2 and Figure 6.3). Modeled OH· concentrations are in agreement with

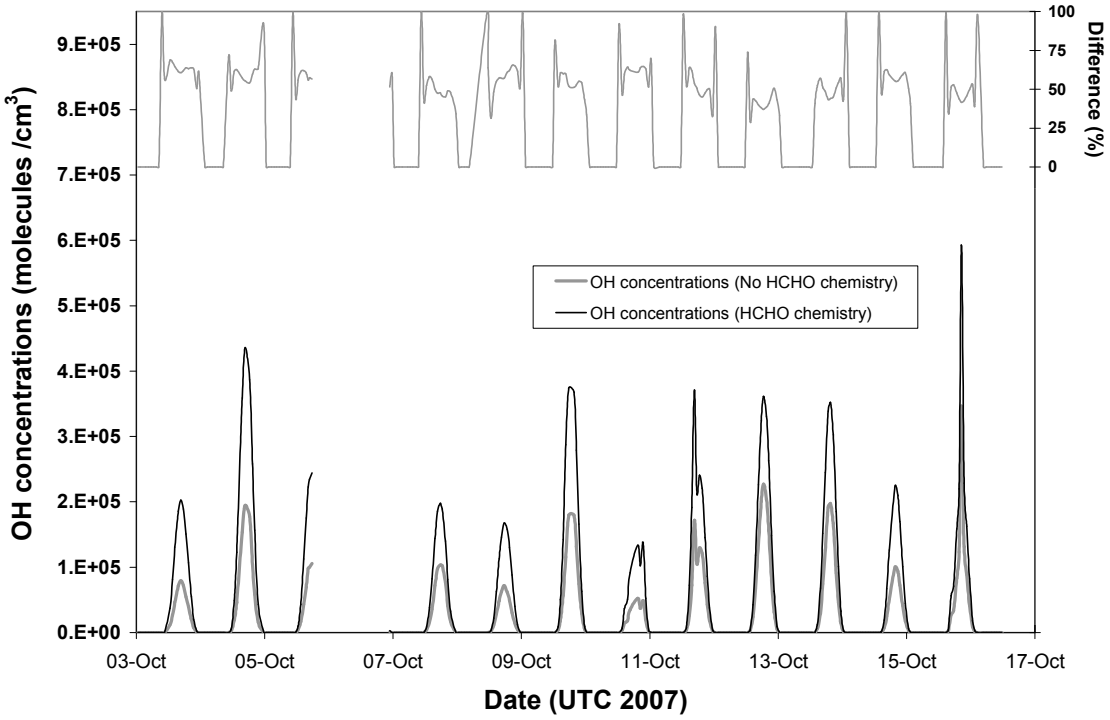

Figure 6.2 Modeled OH· concentrations between October 3 and October 17, 2007 with and without HCHO chemistry. Percent difference between the two runs is shown on the right axis.

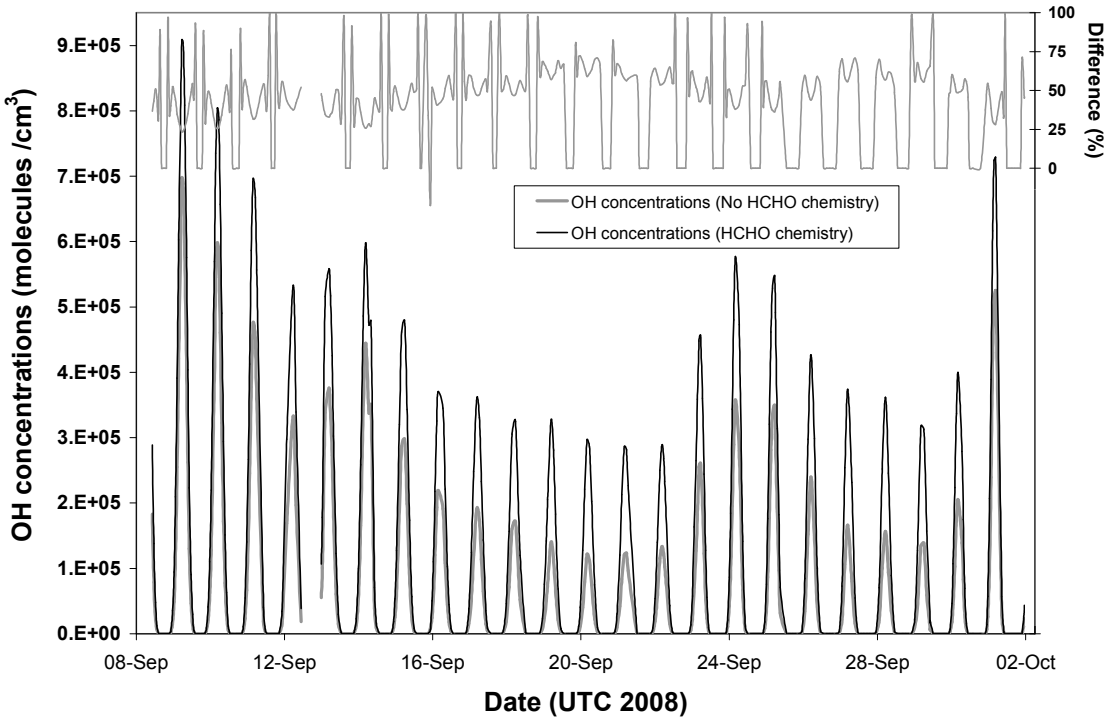

Figure 6.3 Modeled OH· concentrations in 2008 with and without HCHO chemistry. Percent difference between the two runs is shown on the right axis.

previous measurements in the Arctic (see Chapter 6.3.1), and since HCHO impacts OH· radical chemistry by more than a few percent, modeled OH· concentrations will include HCHO chemistry for the DMS model in Chapter 6.4.

6.3.2 NO_3· Concentrations

The NO_3· radical is also an important oxidizer for DMS (e.g., Barnes et al., 2006; Osthoff et al., 2009). Concentrations of NO_3· can be determined by equating production and loss

mechanisms assuming steady state of the $NO_3\cdot$ radical. $NO_3\cdot$ is associated with night NO_x from long range transport. During the day $NO_3\cdot$ will photodissociate quickly and will not be a significant pathway for DMS oxidation. This changes at night when $OH\cdot$ concentrations are minimal and the $NO_3\cdot$ radical lifetime increases. $NO_3\cdot$ is formed in the presence of NO_2 and O_3

$NO_2 + O_3 \rightarrow NO_3\cdot + O_2$ **6.2**

$NO_3\cdot$ is lost in the atmosphere by the reaction with NO and photolysis during the day with a short lifetime of approximately five seconds at noon in lower latitudes (Seinfeld and Pandis, 1998) and a slightly longer lifetime of approximately 10 seconds at local noon during this study (Appendix H; TUV calculation). At night, $NO_3\cdot$ concentrations will increase and other loss mechanisms must be considered.

One of the major losses of $NO_3\cdot$ at night is the reaction with DMS especially in remote areas (Seguin, 2007; Osthoff et al., 2009) (see Figure 6.4; Appendix H). $NO_3\cdot$ can also react with other volatile organic carbon (VOCs) especially alkenes and aldehydes. Most VOCs have sources from either anthropogenic or biogenic continental sources and will oxidize during transport resulting in negligible concentrations from their source regions (Stark et al., 2007). The presence of VOCs in the Arctic implies either long range transport and long life times or potential local sources (Gautrois et al., 2003; Mabilia et al., 2007). Although some organics were measured on board the *Amundsen* (Abbatt, J.,

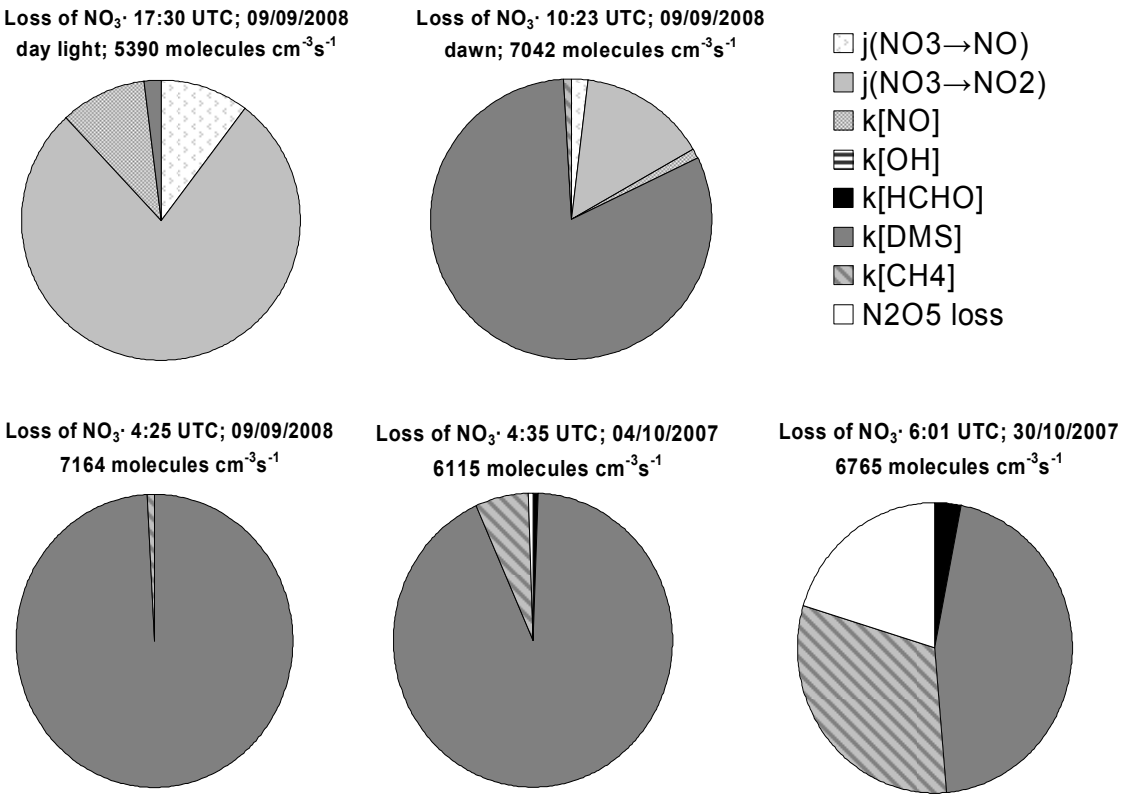

Figure 6.4 Percent loss of NO_3· by different pathways for 5 select times during the study. The top charts illustrate examples of NO_3· loss mechanisms during daylight and dawn. The bottom row illustrates examples of loss mechanisms as temperatures and DMS concentrations decrease with the onset of winter. Loss is calculated based on 0.88 nmol/m^3 of NO_x. Time series of the loss mechanisms is found in Appendix H.

personal communications 2012), most were below detection limit or do not readily react with NO_3·. Mabilia et al. (2007) measured a number of non-methane hydrocarbons and carbonyls near Ny-Alesund, Svalbard. Using values measured by Mabilia et al. (2007)

and rate constants for the compounds (IUPAC, 2009; Sander et al., 2011) it is determined that organics such as acetaldehyde and ethene account for less than 1% of the loss of $NO_3\cdot$ during this study. Formaldehyde also had a low contribution to $NO_3\cdot$ loss but could contribute 2-4% later in the season when lower DMS concentrations are present (see Figure 6.4; Appendix H). Isoprene measured at Ny-Alesund Svalbard was 1.0 ± 0.4 nmol/m^3 (Mabilia et al., 2007) and was attributed to local sources (lifetime < 10 hours; Solberg et al. 1996). Therefore, concentrations of isoprene at Svalbard are not representative of the Arctic as a whole.

It is of interest to note that even if isoprene is a tenth of what it is at Svalbard, it would contribute significantly, approximately 20%, of nighttime loss of $NO_3\cdot$ on board the *Amundsen*. However, based on the clean air masses observations by the University of Toronto (Abbatt, J., personal communications 2012), no VOCs besides DMS and formaldehyde will be included in the model.

$NO_3\cdot$ and N_2O_5 are usually in equilibrium in the night atmosphere (Osthoff et al., 2007). N_2O_5 can be lost from the atmosphere by heterogeneous reactions on aerosols which form HNO_3. The loss rate of N_2O_5 (from Osthoff, 2007) can be represented by

$$\mathbf{N_2O_5 + H_2O \rightarrow 2HNO_3, \quad k_{13} = \tfrac{1}{4} c \gamma S_{aerosol}} \qquad \mathbf{6.3}$$

where c is the mean molecular speed of N_2O_5 which ranged between 223 and 232 m/s on board the *Amundsen* dependent on the measured temperature. Mean molecular speed is determined from gas kinetic theory

$$c = \sqrt{\left(\frac{8RT}{\pi M}\right)} \qquad \textbf{6.4}$$

where R is universal rate constant, T is the temperature that was recorded on board the *Amundsen* and M is the molecular weight of N_2O_5 (Seinfeld and Pandis, 1998). The uptake coefficient, γ, of N_2O_5 on aerosols was set to 0.03, which is the value found for N_2O_5 onto liquid water at approximately -11°C (Sander et al., 2011 and references within). Surface area, $S_{aerosol}$, was calculated using aerosol size distribution measurements made by the University of Toronto (Chang, R. personal communications 2011). Measurements of aerosol size distributions (i.e., number density) in aerosol diameter bins were made using a Scanning Mobility Particle Sizer and are explained in detail by Chang et al. (2011). Surface area was determined by assuming particles are spherical. Surface area for each size bin was calculated based on the average diameter and the number of particles of that size bin. The surface area ($S_{aerosol}$) for each size bin was summed to obtain an aerosol surface area.

$$S_{aerosol} = 4\pi \sum_i r_i^2 n_i \qquad \textbf{6.5}$$

where i is the individual size bin, r_i is the radius of the mid value of each size bin and n_i is the number of aerosols found in that individual size bin. The Scanning Mobility Particle Sizer's size bins range approximately between 10 and 500 nm. Note that the surface areas of particles larger than 500 nm such as primary aerosols from sea salt are not included in these calculations and this omission may lead to a small underestimation of surface area. Contributions to surface area from larger aerosols (i.e., > 500 nm in diameter) are expected to be small relative to fine aerosols (< 500 nm in diameter; Seinfeld and Pandis, 1998).

Data corresponding to surface areas greater than 2.2 x 10^{-6} cm^2/cm^3 were removed as these were identified with smoke stack emissions from the ship. During these times and when no data was available from the Scanning Mobility Particle Sizer, the median surface area from the 2007 or 2008 data set was used in its place.

Assuming N_2O_5 is in equilibrium with $NO_3\cdot$ and NO_2, a ratio of N_2O_5 and $NO_3\cdot$ can be determined (i.e., $[NO_3]/[N_2O_5] = K/[NO_2]$, where K is the equilibrium constant) and the loss of $NO_3\cdot$ by the loss of N_2O_5 can be expressed as,

$$L_{NO_3 \text{ via } N_2O_5} = k_{13} K [NO_2][NO_3] \qquad \textbf{6.6}$$

where k_{13} is calculated from equation 6.3, K is the equilibrium constant of N_2O_5 and its reactants; $NO_3\cdot$ and NO_2. Depending on initial NO_x concentrations, N_2O_5 heterogeneous

reactions can account for over 10% of the losses at night of $NO_3\cdot$, see Appendix H for loss via N_2O_5 and for modeled N_2O_5 concentrations.

Nighttime $NO_3\cdot$ concentrations will increase with the onset of winter as DMS concentrations decrease (Rempillo, 2011). The lifetime of nighttime $NO_3\cdot$ also increases with the onset of winter and can be on the order of a few hours. It is noted that $NO_3\cdot$ reacts slowly with CH_4; IUPAC recommends a maximum rate constant of 1×10^{-18} $cm^3molecules^{-1}s^{-1}$ (IUPAC, 2009). If this rate constant is used along with CH_4 concentrations mentioned in Chapter 6.3.1.1, it can contribute significantly (approximately 20%) to the calculated loss of $NO_3\cdot$ at night (see Figure 6.4; Appendix H). This, along with the uncertainties of the organic concentrations, suggests the $NO_3\cdot$ loss mechanisms and thus $NO_3\cdot$ concentrations during the Arctic night when DMS concentrations are low are difficult to predict. The $NO_3\cdot + CH_4$ reaction rate, although a maximum, will be kept in the model, to represent not only the $NO_3\cdot + CH_4$ reaction, but also potential other unknown sinks that may occur and the uncertainty in the model.

NO_x concentrations are assumed to be relatively constant throughout the study period. Since there were no measurements of NO_x on board the *Amundsen*, it is uncertain how valid this assumption is. Anthropogenic influence from the south occurs in the winter and spring but is expected to be relatively low in the summer. Data from previous studies where Arctic NO_x was measured will be used to estimate the $NO_3\cdot$ concentration on board the *Amundsen*. Beine et al. (1996) measured NO_x concentrations at Svalbard (78º55 N, 11º53 E, 474 m above sea level) between February to May 1994. Median NO_x

concentrations in background air from the Arctic or Northern Atlantic regions during their campaign were approximately 0.88 nmol/m^3 (Beine et al., 1996). Liang et al. (2011) found background NO_x concentrations of approximately 1.1 nmol/m^3 in the spring (April 1-30th) over Northern Canada at altitudes between 0 and 12 km. Ridley and Orlando (2003) measured NO_x concentrations between 0.88-1.8 nmol/m^3 and night concentrations between 0.22-0.44 nmol/m^3 at Alert in spring 1993. It must be noted that previous studies were conducted in spring or summer and therefore may be affected by other factors that are not present in the fall.

Ozone depletion occurs when significant halogen chemistry occurs in the spring. These ozone depletion events can potentially affect other chemistry in the atmosphere (Simpson et al., 2007*a*). Ozone measurements were made in each of the studies above and were not significantly different than ozone concentrations in the Arctic during the SOLAS study. This indicates that NO_x chemistry during the above studies was not influenced by ozone depletion events and can be used to model fall concentrations in our study. To evaluate the full possible range in NO_x concentrations, values of 0.22, 0.88 and 1.8 nmol/m^3 can be used in the model to obtain a possible range of concentrations for $NO_3\cdot$. Rate constants and concentrations used in the $NO_3\cdot$ model are displayed in Table 6.2.

Modeled concentrations of $NO_3\cdot$ are displayed in Figure 6.5 for 2007 and Figure 6.6 for 2008. Modeled production and loss rates for $NO_3\cdot$ are found in Appendix H along with modeled N_2O_5 concentrations.

			k ($cm^3 molecule^{-1} s^{-1}$)
NO_3· Production			
	$NO_2 + O_3 \rightarrow NO_3\cdot + O_2$	k_7	$1.4 \times 10^{-13} e^{(-2470/T)}$
NO_3 Loss			
	$NO_3\cdot + h\nu \rightarrow NO_2 + O$	j	-
	$NO_3\cdot + h\nu \rightarrow NO + O_2$	j	-
	$NO_3\cdot + NO \rightarrow$ products	k_{10}	$1.8 \times 10^{-11} e^{(110/T)}$
	$NO_3\cdot + OH \rightarrow$ products	k_{11}	2.0×10^{-11}
	$NO_3\cdot + DMS \rightarrow$ products	$k_{DMS:NO3}$	$1.9 \times 10^{-13} e^{(520/T)}$
	$NO_3\cdot + HCHO \rightarrow$ products	k_9	5.5×10^{-16}
	$NO_3\cdot + CH_4 \rightarrow$ products	k_8	$< 1 \times 10^{-18}$
N_2O_5 Loss			
	$N_2O_5 +$ aerosol $\rightarrow$ products	k_{13}	$¼\ c\ \gamma\ S_{aerosol}$
Equilibrium constants			
	$NO_3\cdot + NO_2 \leftrightarrow N_2O_5$	K	$2.7 \times 10^{-27} e^{(11000/T)}$ *
NO_x Relationships			
	$[NO_2] + [NO] = [NO_x]$	$k_{NO:O3}$	$1.4 \times 10^{-12} e^{(-1310/T)}$
	$[NO] = \frac{j_{NO_2 \rightarrow NO}[NO_2]}{(k_{NO:O_3}[O_3])}$		

Table 6.2 Major loss and production of NO_3· used in the box model to determine NO_3· concentrations. Rate constants are the recommended values from IUPAC (2009). *Equilibrium constant is in units of $cm^3 molecule^{-1}$ (Sander et al., 2011).

Nighttime NO_3· concentrations estimated by Rempillo (2011) (1-10 x 10^6 molecules/cm^3) using values obtained from Wagner et al. (2000), fall within the range calculated here for 0.22 nmol/m^3 of NO_x. It is of note that a concentration of 1.8 nmol/m^3 for NO_x produces large amounts of NO_3· (on the order of 10^8 molecules/cm^3). Although this may be valid during the spring when anthropogenic influences are large (Barrie and Bottenheim, 1991; Ridley and Orlando, 2003), anthropogenic influence is not expected to be as large in the fall. Therefore, for test cases of DMS oxidation (in Chapter 6.4), the value of 1.8 nmol/m^3 will not be used and sensitivity tests using 0.22 and 0.88 nmol/m^3 are evaluated.

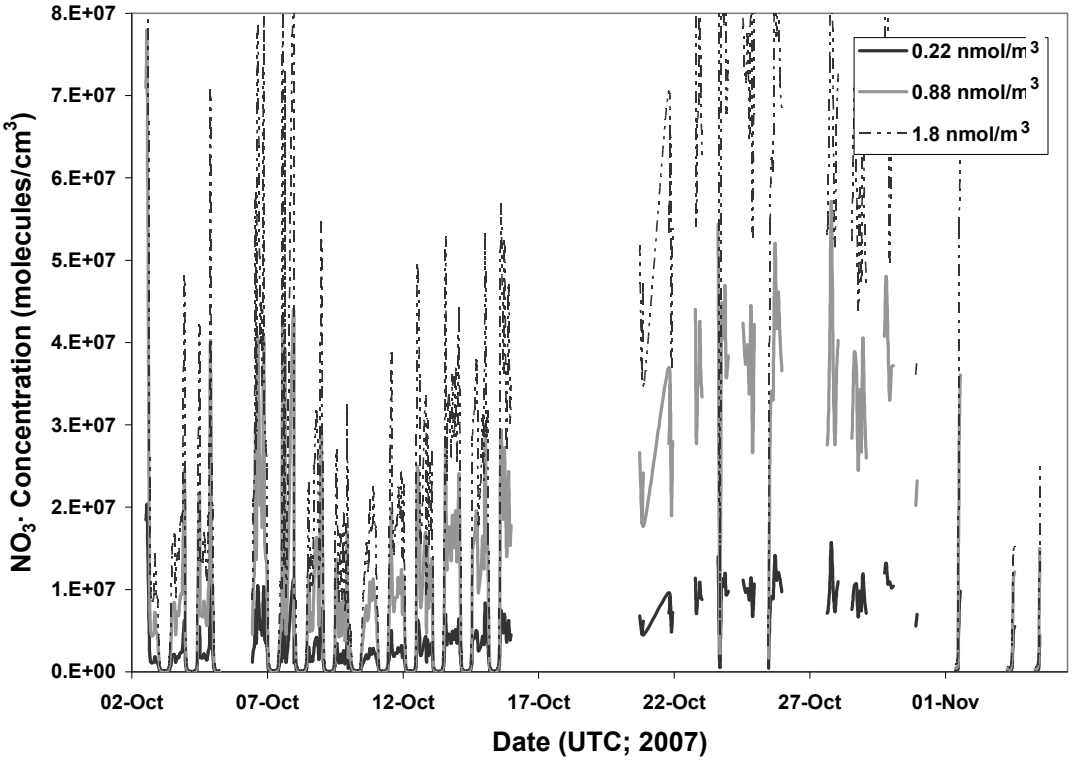

Figure 6.5 Modeled $NO_3\cdot$ concentrations for 2007 using the range of NO_x concentrations specified in the label.

Many of the rate constants in the model are dependent on temperature and it was noted that night time $NO_3\cdot$ concentrations started to increase as the temperatures decreased. At lower temperatures N_2O_5 losses start to become significant. The reaction of DMS and $NO_3\cdot$ remained the largest nighttime loss pathway for the $NO_3\cdot$ radical throughout the study period.

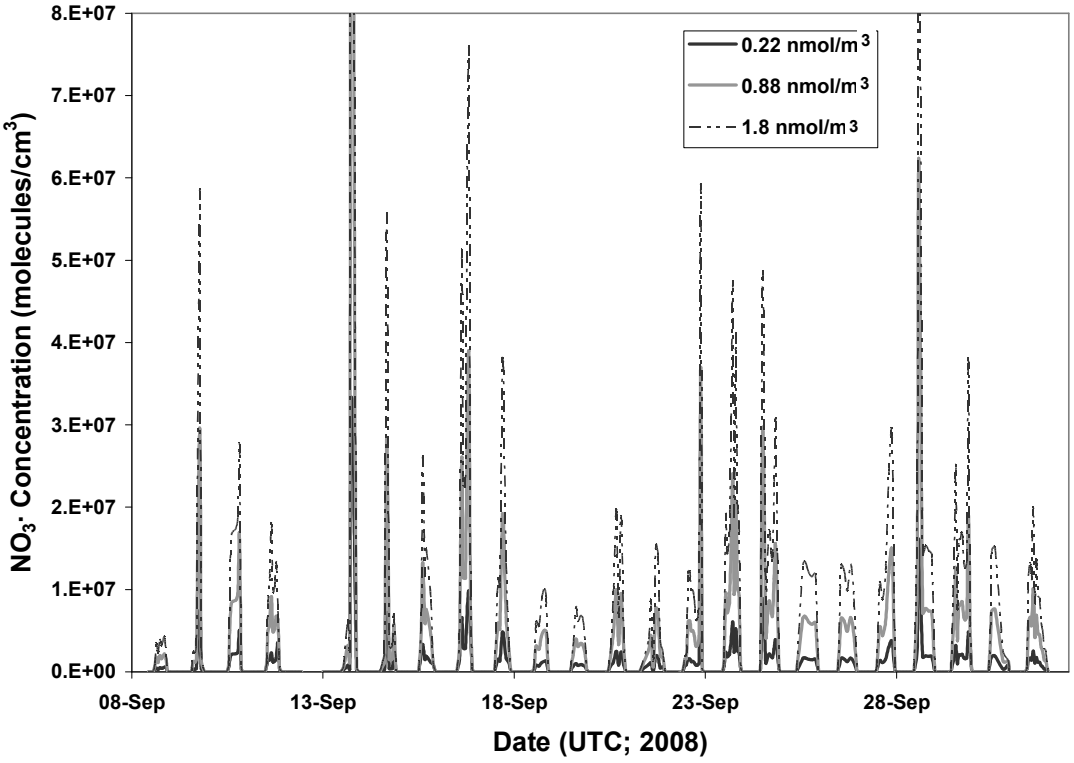

Figure 6.6 Modeled NO_3· concentrations for 2008 with specified NO_x concentrations.

6.3.3 Halogens

Halogens have been shown to play an important role in the oxidation of DMS (e.g., von Glasow and Crutzen, 2004). In the Arctic spring, these compounds are expected to be an important part of the oxidizing capacity of the atmosphere. Ozone depletion events have been observed in numerous studies and are anticorrelated most often with bromine compounds such as filterable bromide in aerosols (Barrie et al., 1988) or gaseous reactive bromine compounds (Simpson et al., 2007*b*). Gaseous iodine compounds have also been

observed in Arctic coastal regions (Mahajan et al., 2010). Chlorine chemistry may also play an important role in DMS oxidation. However, gaseous reactive halogen concentrations are expected to be larger in spring, relative to typical concentrations in fall (i.e., the sampling period presented in this thesis) (Simpson et al., 2007*b*). To determine maximum possible concentrations for gaseous forms of reactive halogen compounds in the fall, lower concentrations present in the literature for spring are considered (Table 6.3; Table 6.4).

Chlorine chemistry can be a potential source of DMS oxidation in the Arctic atmosphere. The Cl· radical is just as important, if not more important, than ClO· for DMS oxidation.

Reactive Halogen	Concentration (molecules/cm^3)	When/Where	Reference
Cl·	7.20×10^2	Southern ocean	Wingenter et al. (1999)
Cl·	$0.39 – 7.7 \times 10^4$	Spring/Alert	Jobson et al. (1994)
ClO·	$2 – 16 \times 10^7$	Spring /Alert *	Wayne et al. (1995)
ClO·	1000 x Cl·	Modeled unpolluted marine boundary layer†	Vogt et al. (1996) Vogt (1996)
BrO·	$0.8 – 1.3 \times 10^6$ $1.3 – 2.7 \times 10^6$ $2.65 – 8.0 \times 10^6$	Spring (ODE) /Arctic Localized Coastal (ODE) Arctic Spring no ODE	Zhao et al. (2008)
BrO·	2.65×10^7	Spring/Arctic	Edwards et al. (2011)
BrO·	$1 – 6 \times 10^9$	Spring/Alert *	Wayne et al (1995)
BrO·	$0.2 – 4.0 \times 10^7$	45ºN	Vogt et al. (1999)
Br·	$0.30 – 6.1 \times 10^7$	Spring/ Alert	Jobson et al. (1994)
IO·	$0.2 – 4.0 \times 10^7$	45ºN	Vogt et al. (1999)
IO·	2.65×10^7	Spring/Arctic	Edwards et al. (2011)

* based on values of Cl· or Br· from Jobson et al., (1994)
† temperature = 293K, relative humidity = 76%, photolysis rates calculated for 1 April 45° N

Table 6.3 Summary of literature concentrations used in estimating reactive halogen concentrations in Arctic fall for the DMS oxidation model.

Jobson et al. (1994) used relative rates of hydrocarbon degradation in the atmosphere to predict a concentration between 0.39 – 7.7 x 10^4 molecules/cm^3 for the Cl· radical at Alert. Wayne et al. (1995) predicted a ClO· concentration between 2 – 16 x 10^7 molecules /cm^3 based on the work completed by Jobson et al. (1994) at Alert (Table 6.3). Models found in literature for the Arctic atmosphere during ozone depletion events have used a value of 1 x 10^4 molecules/cm^3 for the Cl· concentration (e.g., Ariya et al., 2002; Stephens et al., 2012). This will be taken as an upper sensitivity test for the model presented here (Table 6.4) but it must be noted that these values are used in spring when anthropogenic influences are higher which would lead to increased Cl· concentrations (Karlsson and Ljungström, 1995; Simpson et al., 2007*b*).

Concentrations calculated by Wingenter et al. (1999) determined a Cl· radical concentration of 720 atoms/cm^3 in the clean marine boundary layer in the southern ocean (Table 6.3). The ratio of ClO·/Cl· has been modeled to be on the order of 1000 (Vogt, 1996; Vogt et al., 1996). Based on this ratio and the Cl· concentration found by Wingenter et al. (1999), a concentration of 7.2 x 10^5 molecules/cm^3 (i.e., 1000 x 720 molecules/cm^3) for ClO· is determined This will be used for the lower bound of Cl· concentrations in this study (see Table 6.4). Although Cl· and ClO· concentrations are expected to be low in the Arctic Fall, a non zero value is taken for the lower limit. Since a chlorine deficit is observed in aged aerosols in this study (see Chapter 4.3.2), gaseous halogen components are expected to be important to atmospheric chemistry in the Arctic Fall.

molecules/cm^3	Low Halogen (LH)	High Halogen (HH)
Cl·	7.20 x 10^2	1.00 x 10^4
ClO·	7.20 x 10^5	2.00 x 10^7
Br·	2.65 x 10^2	2.65 x 10^5
BrO·	2.65 x 10^4	2.65 x 10^7
IO·	2.65 x 10^4	2.65 x 10^7

Table 6.4 Daytime concentrations of halogens that will be used in two scenarios for the DMS oxidation model. See text and Table 6.3 for source of numbers. Concentrations are in molecules/cm^3. Night time concentrations for all species are set to zero.

BrO· and IO· chemistries are also of interest in the Arctic not just because of the ozone depletion events that BrO· can cause (Barrie et al., 1988) but because of its impact on OH· concentrations (Liao et al., 2011, Edwards et al. 2011). Autumn concentrations for these compounds are expected to be less than that for spring and early summer (Saiz-Lopez et al., 2007) and therefore an upper bound sensitivity test for the DMS oxidation model using the lower concentrations from spring is conducted. Measurements of BrO· and IO· are quite often below the detection limit of current instruments even in the spring and summer; the detection limit is approximately 2.65 x 10^7 molecules/cm^3 for long path Differential Optical Absorption Spectroscopy (LP-DOAS) and chemical ionization mass spectrometry (Saiz-Lopez et al., 2007; Mahajan et al., 2010; Liao et al., 2011). Hence modeled concentrations for these halogen compounds will be considered.

Edwards et al. (2011) modeled concentrations of Br and I compounds assuming nighttime Arctic concentrations of 8.0 molecules/cm^3 and 4.5 x 10^7 molecules/cm^3 of Br_2 and I_2

respectively which translated to a concentration of BrO· and IO· of about 2.65 x 10^7 molecules/cm^3 during the day (approximately their limit of detection). Zhao et al. (2008) used a three dimensional model to study the Arctic spring atmosphere. Enhanced BrO· concentrations in the Arctic ranged between 8.0 x 10^5 and 1.3 x 10^6 molecules/cm^3 during ozone depletion events in the spring (Table 6.3). High BrO· simulated production near the surface of the Arctic Ocean predicted concentrations ranging between 1.3 x 10^5 – 2.7 x 10^5 molecules/cm^3 at coastal regions. Average BrO· concentrations in areas where ozone depletion events were not predicted were usually between 2.65 x 10^4 and 8.0 x 10^4 molecules/cm^3. Zhao et al. (2008) linked frost flowers and tropospheric BrO· in the model that was first introduced by Kaleschke et al. (2004). Although frost flowers are also present in the Arctic during fall, there is no evidence of elevated BrO· associated with them and therefore frost flowers will not be considered a source of halogens in this thesis. Jobson et al. (1994) calculated bromine radical concentrations between 0.30 - 6.1 x 10^7 molecules/cm^3 at Alert, which Wayne et al. (1995) used to determine BrO· concentrations between 1- 6 x 10^9 molecules/cm^3. The two scenarios for BrO· concentrations for this study will be taken as 1. the minimum from the Zhao et al. (2008) study for minimum contributions (Table 6.4) and 2. an upper sensitivity test of 2.65 x 10^7 molecules/cm^3 from Edwards et al. (2011) and the detection limit of LP-DOAS (see Table 6.4). It is noted though that BrO· concentrations are expected to be much smaller than this upper limit when this study was conducted because elevated BrO· concentrations are associated with spring (Chapter 1.4.2).

Br· concentrations are predicted to be two orders of magnitudes smaller than the BrO· concentration (Platt and Hönninger, 2003): because of a lack of data for this halogen radical in the Arctic fall, this assumption will be used in the DMS oxidation model (Table 6.4).

Measurements of IO· are sparse in the Arctic (Mahajan et al., 2010) but are expected to be on the same order of magnitude as BrO· (Edwards et al., 2011). Vogt et al. (1999) modeled IO· concentrations and found daytime concentrations between 0.2 - 4.0 x 10^7 molecules/cm^3 under conditions representative of 45 ºN. This was on par with concentrations of BrO· at 45 °N as modeled in the same study. For the purpose of the model presented here, IO· concentrations will be kept at the same concentration as BrO· (Table 6.4).

Diurnal variability is observed with reactive halogen species since X_2 and XOH are photolyzed to produce X· and XO· (X = Cl, Br or I). Daytime concentrations of halogens for the DMS oxidation model are displayed in Table 6.4. Two test studies for halogen concentrations will be conducted for the model including low halogens (LH) and high halogen (HH) concentrations. Night concentrations for all the halogen species in the model are set to zero. A step function for halogen chemistry is assumed in the model where halogen chemistry concentrations are assumed to be constant during the day, and once modeled OH· concentrations are zero at local night, the reactive halogen species are also assumed to have a concentration of zero.

6.4 Loss of DMS by Oxidation

The rate of loss of atmospheric DMS by oxidation can be calculated based on equation 6.1. Rate constants for the reaction of DMS with different oxidants are displayed in Table 6.5. Every time DMS was measured, the model was run to determine the loss rate of DMS by each of the oxidants (Figure 6.7 (2007); Figure 6.8 (2008)). An example of a 24 hour period is displayed in Figure 6.9 to illustrate the diurnal pattern and importance of each of the oxidants throughout the day. NO_x concentrations were held at 0.22nmol/m^3 (5pptv) for both day and nighttime conditions and low halogen concentrations (see Table 6.4) were considered for this particular example (Figure 6.7,

Reaction	k ($cm^3 molecule^{-1} s^{-1}$) (T = temperature in K)	Notes
DMS + OH·	$k_{abstraction} + k_{addition}$	
$k_{abstraction}$	$1.2 \times 10^{-11} e^{(-280/T)}$	
$k_{addition}$	$\frac{8.2\times10^{-39}[O_2]e^{(5376/T)}}{1+1.05\times10^{-5}\frac{[O_2]}{[M]}e^{(3644/T)}}$	$[O_2]/[M]$ = fraction of O_2 in atmosphere
DMS + NO_3·	$1.9 \times 10^{-13} e^{(530/T)}$	
DMS + Cl·	3.5×10^{-10}	
DMS + ClO·	$2.1 \times 10^{-15} e^{(340/T)}$	
DMS + Br·	$9.0 \times 10^{-11} e^{(-2390/T)}$	
DMS + BrO·	$1.4 \times 10^{-14} e^{(950/T)}$	
DMS + IO·	$2.4 \times 10^{-12} e^{(-1470/T)}$	
DMS + O_3 (gas phase)	$<1.5 \times 10^{-19}$	
DMS + O_3 (aqueous phase)	5.1×10^{8}	* k in $M^{-1}s^{-1}$ see text

Table 6.5 Rate constants for DMS oxidation. All gas phase reaction rate constants are recommended by NASA in the Chemical Kinetics and Photochemical Data for use in Atmospheric Studies (Sander et al., 2011). Aqueous phase DMS +O_3 rate constant is in $M^{-1}s^{-1}$ measured by Gershenzon et al. (2001) at a temperature of 274K.

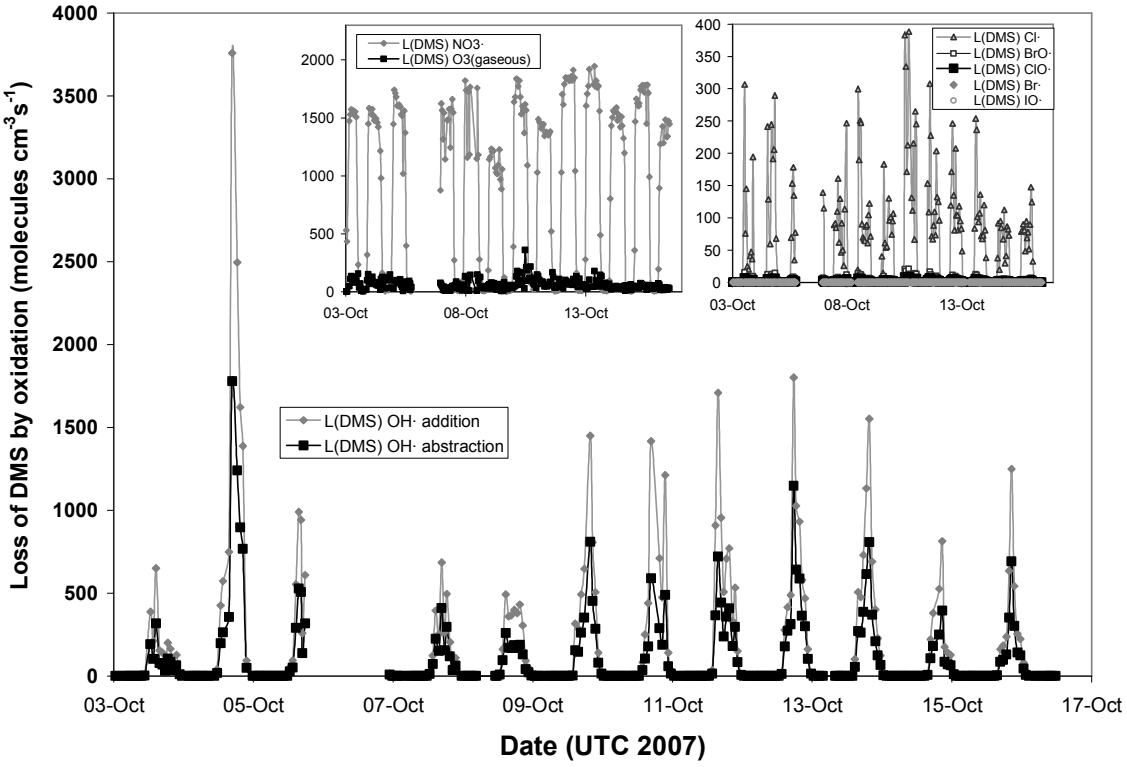

Figure 6.7 Rate of loss of DMS by oxidation for 2007. Concentrations for NO_x are 0.22 nmol/m^3 (5 ppt of NO_x) and low halogen concentrations (see Table 6.4) are considered. Inserts show loss of DMS from the reactions of NO_3· and $O_{3(g)}$ (left) and by halogen chemistry (right).

Figure 6.8, Figure 6.9). Liquid water content was considered low (3.0×10^{-11} cm^3/cm^3) for the aqueous phase oxidation of DMS (see Chapter 6.5) displayed in Figure 6.9.

Daily averages of DMS oxidation rates were calculated and displayed in Figure 6.10 for 2007 and Figure 6.11 for 2008. Daily averages are important when considering end products (Chapter 6.5) and transport mechanisms (Chapter 6.6), since lifetime of both

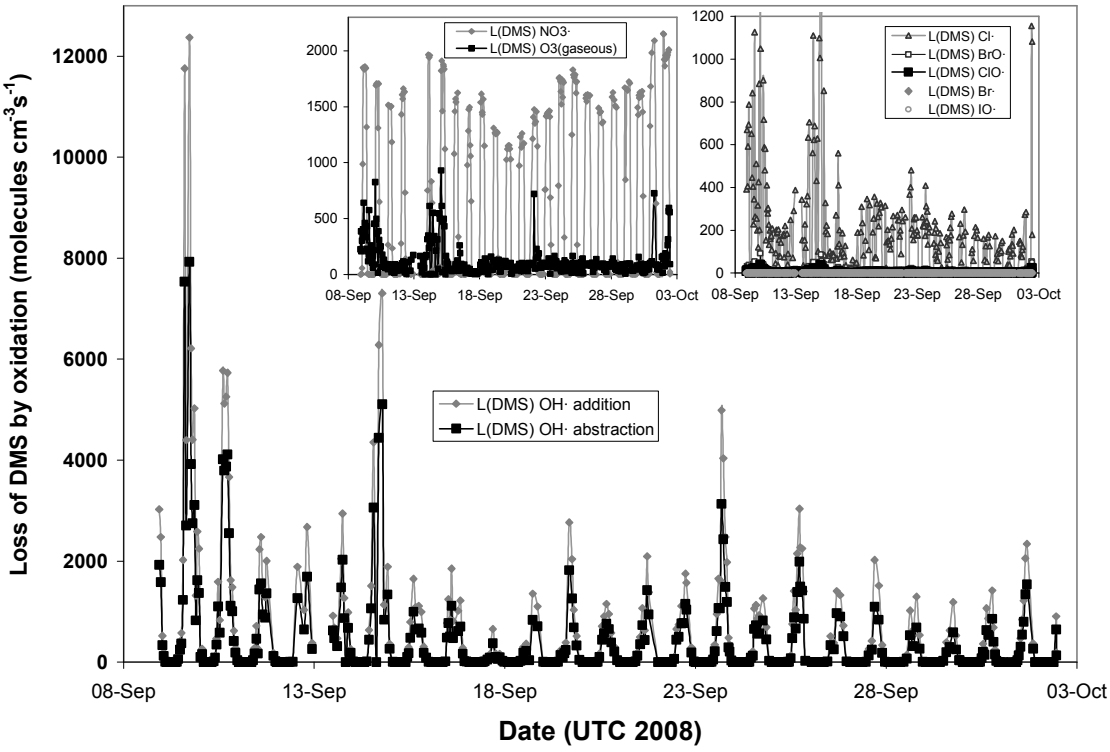

Figure 6.8 Rate of loss of DMS by oxidation for 2008. Concentrations for NO_x are 0.22 nmol/m^3 (5 ppt of NO_x), and low halogen concentrations (see Table 6.4) are considered. Inserts show loss of DMS from the reactions of NO_3· and $O_{3(g)}$ (left) and by halogen chemistry (right).

DMS and its end products are expected to be greater than a few hours (lifetime of DMS calculated in Chapter 6.6.6; Discussion of long range transport of biogenic sulfur components in Chapter 5).

When solar zenith angle increases (both on a daily cycle and seasonal cycle) the contribution of OH· to DMS oxidation decreases (refer to Figure 6.9; inserts of

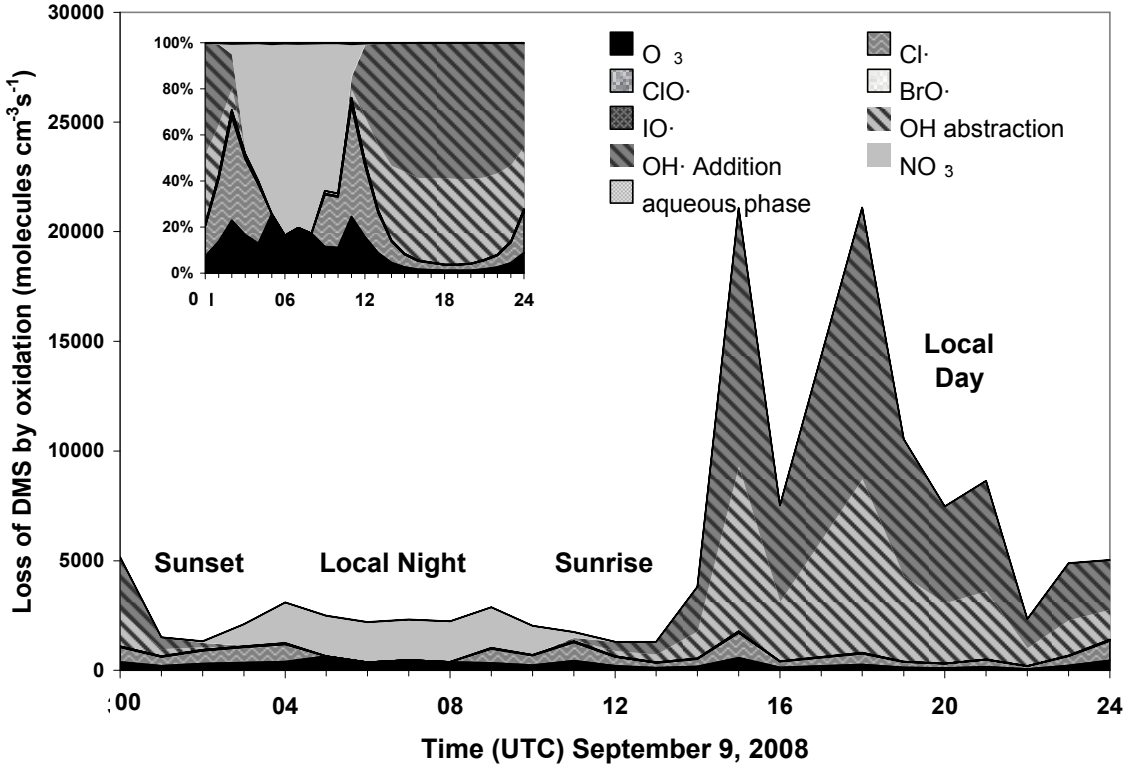

Figure 6.9 Time series of DMS loss by oxidants for September 9, 2008. Concentrations for NO_x are 0.22 nmol/m^3 (5 ppt of NO_x) and low halogen concentrations (see Table 6.4) are considered. Aqueous phase oxidation is based on the lower limit of liquid water content (Chapter 6.4.1). Rate of loss at each time point is additive. Insert shows percent contribution of each oxidant.

Figure 6.10 and Figure 6.11) relative to the total DMS oxidation. The influence of the contribution of OH· is also dependent on sea ice cover, sampling time relative to local time and the position of the ship. Although an overall decrease is observed in Figure 6.10 and Figure 6.11, a clearer decrease would have been observed if the measurement platform had remained in a stationary position throughout the sampling period. The

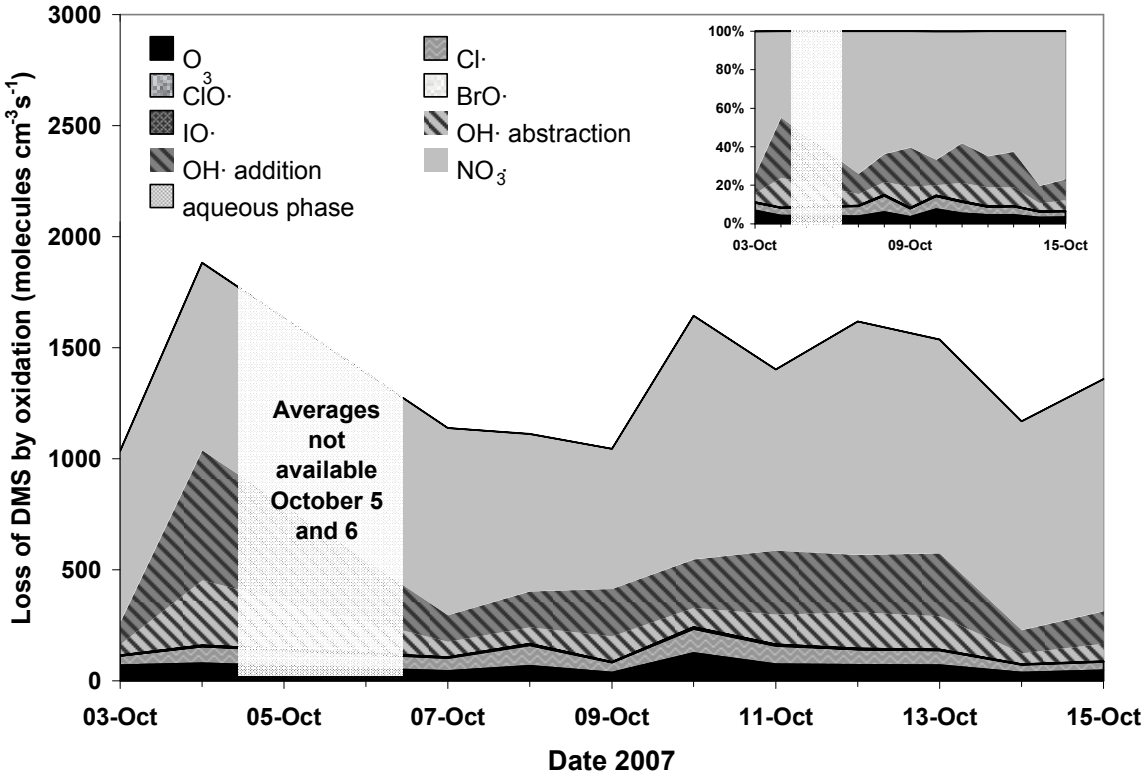

Figure 6.10 Rate of loss of DMS by oxidation for 2007 averaged daily. Concentrations for NO_x are 0.22 nmol/m^3 (5 ppt of NO_x) and low halogen concentrations (see Table 6.4) are considered. Aqueous phase oxidation is based on lower limit of liquid water content (Chapter 6.4.1). Average rate of loss displayed for each day are additive. Insert shows percent contribution.

reaction of DMS with NO_3· in almost all instances accounts for the largest daily loss of DMS (see Figure 6.10 and Figure 6.11). Another important feature to note is the chlorine radical, although quite low (720 moleclues/cm^3), is still an important part of the oxidation model especially during sunrise and sunset (Figure 6.9). It is interesting to note that the

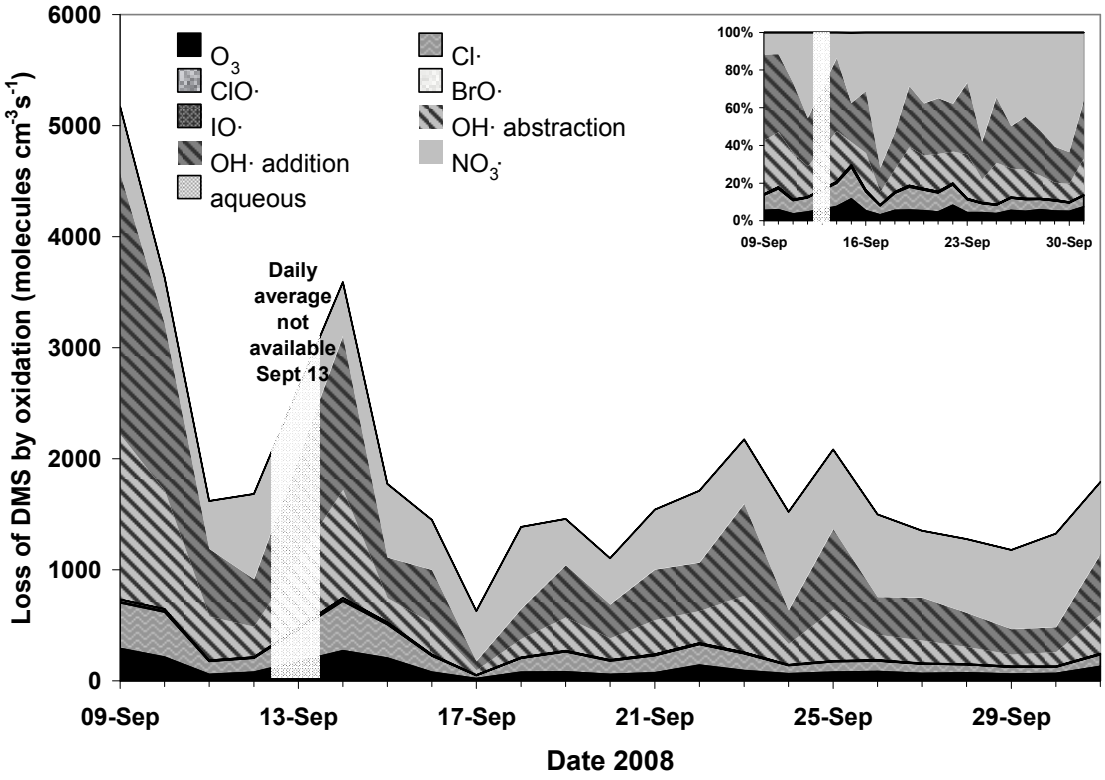

Figure 6.11 Rate of loss of DMS by oxidation for 2008 averaged daily. Concentrations for NO_x are 0.22 nmol/m^3 (5 ppt of NO_x), and low halogen concentrations (see Table 6.4) are considered. Aqueous phase oxidation is based on lower limit of liquid water content (Chapter 6.4.1). Rate of loss displayed is cumulative. Insert shows percent contribution.

oxidation of DMS by O_3 also is an important feature. This reaction is slow and is not thought to be important in the atmosphere (e.g., Gershenzon et al., 2001). Even with a slow rate constant (see Table 6.5), between 5-10% is expected to oxidize from gaseous O_3 with the model presented here (inserts of Figure 6.10 and Figure 6.11). The rate constant is a maximum value and thus the rate may be slower then actually calculated,

but it does illustrate that with low concentrations of radicals, seemingly unimportant reactions start to contribute to the overall rate. The rate of loss of DMS by oxidation mentioned until now has all been gas phase chemistry and it is worthy to note that heterogeneous oxidation of DMS may also be significant.

6.4.1 Aqueous Oxidation of DMS

Aqueous oxidation of DMS has been found to be important in many previous works (Zhu et al., 2006; Gershenzon et al., 2001; von Glasow and Crutzen, 2004). DMS is not very soluble in water and has a low Henry's Law constant, but DMS can react rapidly with $OH\cdot$ and O_3 in the aqueous phase. In the case of O_3 the rate coefficient can be more than 10^6 times faster than the gas phase and can be a significant source of DMS oxidation in tropospheric clouds where the lifetime of DMS from aqueous oxidation is predicted to be as low as 5.4 days (Gershenzon et al., 2001; Barnes et al. 2006). The aqueous O_3 reaction with DMS results in the formation of DMSO which will further oxidize to MSA.

Following the approach by Gershenzon et al. (2001), if liquid and gas phase are in equilibrium the liquid water concentration of a compound can be expressed as

$$[X_{solution}]=H_x\cdot P_x \qquad 6.7$$

where concentration is in $mol \cdot L^{-1}$, Henry's law coefficient is in $M \cdot atm^{-1}$ and P is the partial pressure of the gas in question. Henry's law coefficients can be determined for both DMS and ozone using the formula given by Gershenzon et al. (2001)

$$H_{DMS(mol \cdot L^{-1} atm^{-1})} = 0.48\ e^{3730 \cdot (1/T - 1/T_0)} \quad \textbf{6.8}$$

and

$$H_{O_3 (mol \cdot L^{-1} atm^{-1})} = 0.0107\ e^{2330 \cdot (1/T - 1/T_0)} \quad \textbf{6.9}$$

where T is the temperature (in Kelvin) and T_0 is equal to 298 K. The rate of oxidation of DMS by O_3 in aqueous form can be expressed as

$$Ox_{aqueous(mol \cdot L^{-1} s^{-1})} = k_{aqueous(L \cdot mol^{-1} s^{-1})} \cdot H_{O_3 (mol \cdot L^{-1} atm^{-1})} \cdot P_{O_3 (atm)} \cdot H_{DMS(mol \cdot L^{-1} atm^{-1})} \cdot P_{DMS(atm)} \quad \textbf{6.10}$$

where k is the aqueous rate constant (Table 6.5) that was determined by Gershenzon et al. (2001). Units are displayed in brackets behind each component and it is of note that this reaction is in liquid. Water liquid content in the atmosphere must be taken into consideration when translating oxidation of DMS in the aqueous phase to a rate loss in the atmosphere.

The amount of DMS loss from aqueous oxidation is strongly dependent on the liquid water content. Gershenzon et al. (2001) tested a scenario of oxidation in tropospheric clouds by using a value for fractional liquid water content of 3 x 10^{-7} cm^3/cm^3. Barnes et al. (2006) drew attention to the fact that fractional liquid water content can range greatly in the atmosphere between 5 x $10^{-7}cm^3/cm^3$ (tropospheric clouds) to 3 x 10^{-11} cm^3/cm^3 (sea salt aerosols). The lower assumption is most likely similar to conditions that were found on board the *Amundsen* except under foggy conditions. The loss of DMS in the atmosphere due to O_3 oxidation in aqueous solution can be calculated as

$$L(DMS)_{aqueous(molecule \cdot cm^{-3}s^{-1})} = Ox_{aqueous(molecule \cdot cm^{-3}s^{-1})} \cdot lw_{(cm^3 cm^{-3})} \qquad \textbf{6.11}$$

where *lw* is the fractional liquid water content in the atmosphere. The addition of the liquid phase oxidation to the model using the average fraction liquid water of 3.0 x 10^{-11} cm^3/cm^3 only accounts on average 0.02% of the modeled loss of DMS. An increase of an order of magnitude of the fractional liquid water content raises the average to 0.2% of the total modeled loss of DMS. Later in the sampling season, when temperatures were lower the aqueous loss mechanism can account for up to 1% of DMS loss. If the fractional liquid water content expected in tropospheric clouds from Gershenzon et al. (2001) is used in the model (likely representative of fog events), the aqueous oxidation of DMS accounts for, on average, 55% of the DMS oxidized in the atmosphere and up to 92% later in the season.

Although water freezes at 0ºC, water can be super cooled in atmospheric aerosols (Seinfeld and Pandis, 1998), leading to liquid water in clouds at temperatures lower than freezing. Ion concentrations in aerosols will also lower the freezing point. The majority of the clouds at approximately -10ºC would contain super cooled liquid (Seinfeld and Pandis, 1998). As temperature decreases, the liquid water content would decrease as ice becomes more important. The calculation for aqueous DMS oxidation does not take the freezing of water into account, and would therefore be an upper limit (especially at lower temperatures).

6.4.2 Model Sensitivity

Large uncertainties exist in the DMS oxidation model. NO_x concentrations were not measured on board the *Amundsen* and in the Arctic atmosphere there can be considerable variations (see Chapter 6.3.2). Halogen chemistry is relatively unknown in the Arctic atmosphere since many of the compounds are below detection limits of present day instruments (see Section 6.3.3). Also mentioned above, the liquid content of the atmosphere can change the oxidation rate of DMS greatly, especially in fog events.

Sensitivity tests were conducted. They are named based on what assumptions were made in the model. The first two letters of the model run/sensitivity test indicate high (HN 0.88 nmol/m^3) or low (0.22 nmol/m^3) NO_x conditions. The middle two letters represent low (LH) or high (HH) reactive halogen species present in the atmosphere (see Table 6.4). The last two letters in the model name represents if cloud (CC) liquid water content was

used (3.0×10^{-7} cm^3/cm^3) or the lower concentration (3.0×10^{-11} cm^3/cm^3) expected in sea salt aerosols (0C) was assumed. For example, the base scenario is named LNLH0C since NO_x concentrations were set to 0.22 $nmol/m^3$ NO_x, low halogen chemistry was assumed and no cloud chemistry was considered. The naming convention is summarized in Table 6.6.

Different model sensitivity tests were carried out (see Table 6.6) and displayed for 2007 in Figure 6.12 (note that the scaling on the y-axis differs for individual scenarios). The DMS oxidation in the base run is approximately 8 times slower than the fastest run (high NO_x, halogens and fraction liquid content). Although this is a large difference, the different test scenarios predict DMS oxidation rate within an order of magnitude of each other.

	NO_x ($nmol\ m^{-3}$)	Halogen	Liquid content (cm^3/cm^3)
Base (LNLH0C)	0.22	LH	3.0×10^{-11}
HNLH0C	0.88	LH	3.0×10^{-11}
LNHH0C	0.22	HH	3.0×10^{-11}
LNHHCC	0.22	LH	3.0×10^{-7}
HNHH0C	0.88	HH	3.0×10^{-11}
HNHHCC	0.88	HH	3.0×10^{-7}

Table 6.6 Sensitivity inputs for Oxidation Model. First two letters of model run indicate high (HN; 0.88nmol/m^3) or low NO_x (LN; 0.22 nmol/m^3), the middle two letters represent low or high halogen input (see Table 6.4) and the last two letters indicate if cloud (CC) liquid water content were used 3.0×10^{-7} cm^3/cm^3 or the lower concentration expected in sea salt aerosols; (0C) 3.0×10^{-11} cm^3/cm^3.

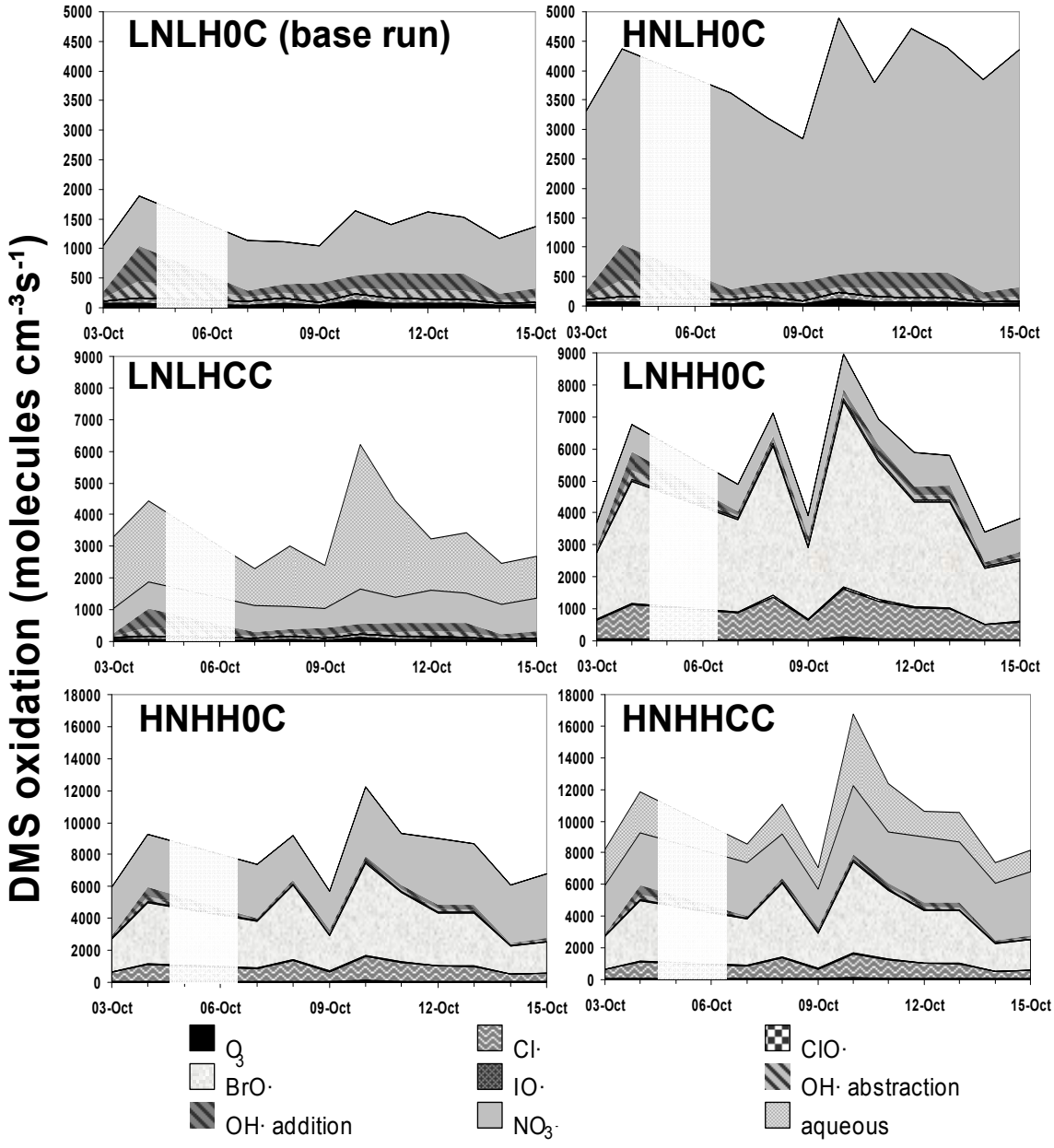

Figure 6.12 Sensitivity tests for the oxidation model in 2007. See Table 6.6 for definition of the different sensitivity scenarios. Note the different scales on the y-axis on the second and third row.

The most important halogen for DMS oxidation in the modeled high halogen scenarios is BrO· (Figure 6.12), which agrees with literature (von Glasow and Crutzen, 2004; Barnes et al., 2006), although it is noted that Cl· is also of importance (Figure 6.12). It must be noted that there is much uncertainty in the halogen concentrations and that with the liberation of chlorine from the aerosol phase (see Chapter 4.3.2), the chlorine radical may impact the chemistry to a greater degree than BrO·. In times of high halogen concentrations, such as the Arctic spring, DMS oxidation would be dominated by the DMS + BrO· reaction (60% or greater) and DMS + Cl· reaction (approximately 20%) and

OH· oxidation would only be a minor component (see Figure 6.12; LNHH0C). NO_x chemistry will also influence DMS oxidation and could potentially account for 80% of DMS oxidation during the fall (see Figure 6.12; HNLH0C).

6.4.3 Lifetime of DMS in the Arctic

Kerminen and Leck (2001) found that DMS concentrations over the frozen Arctic Ocean decreased with time since contact with the open ocean. Although concentrations decreased in their study, atmospheric DMS was detectable over 72 hours after an airmass's last contact with the open sea (Kerminen and Leck, 2001), supporting the concept that DMS in the Arctic can be transported great distances before being oxidized. The lifetime of DMS,

$$\tau = (k_{OH:DMS}[OH\cdot] + k_{NO_3:DMS}[NO_3\cdot] + k_{BrO:DMS}[BrO\cdot] + ...)^{-1} \quad \textbf{6.12}$$

in this study was calculated to be, on average for the base model (LNLH0C) 6.1 days (0.65 days for HNHHCC). This would be consistent with literature lifetimes reported for the high Arctic of 2.5 to 8 days calculated using a photochemical box model (Sharma et al., 1999) or 59 hours computed with a pseudo-Lagrangian model (Nilsson and Leck, 2002).

6.5 Modeled Branching Ratios for DMS Oxidation

6.5.1 MSA_{BR} Model Inputs

Final products of DMS oxidation are MSA or biogenic sulfate (see Chapter 5). The percent yield of SO_2 from DMS has ranged between 39 to 98% in past studies (Faloona, 2009 and references within). To model the MSA branching ratio, the formation rate of MSA relative to the total formation of the end products (i.e., MSA + biogenic sulfate) is considered for DMS oxidation. Assuming no loss from deposition, and that intermediates react quickly, the rate of formation of the end products will equal the loss of DMS by oxidation (equation 6.1). Percent yield of MSA (*f*) and thus the branching ratio is dependent on the initial oxidation mechanism that DMS undergoes. The total MSA branching ratio can then be modeled as follows

$$MSA_{Br:Model} = \frac{(f_{OH}k_{OH:DMS}[OH\cdot] + f_{NO_3}k_{NO_3:DMS}[NO_3\cdot] + f_{BrO}k_{BrO:DMS}[BrO\cdot] + ...)}{(k_{OH:DMS}[OH\cdot] + k_{NO_3:DMS}[NO_3\cdot] + k_{BrO:DMS}[BrO\cdot] + ...)} \quad \textbf{6.13}$$

where [radical] is the oxidant concentration and $k_{radical:DMS}$ is the rate coefficient between the oxidant and DMS (units molecules cm^{-3} s^{-1}) and $f_{radical}$ is the fractional yield of MSA for the reaction of DMS + radical. Branching ratios (and thus fractional yields) for the different oxidation pathways have been studied (for reviews see Barnes et al., 2006; Faloona, 2009) and are dependent on the initial DMS oxidation mechanism. The summary of molar ratios for MSA and sulfate formation for the DMS oxidation pathways modeled here is displayed in Table 6.7 and discussed below.

Reaction	Percent Yield of MSA	Percent Yield of Sulfate	Notes
DMS + OH· (addition)	100%	0% **	Addition reaction, DMSO approximately 100% yield
DMS + OH· (abstraction)	0%	100%	
DMS + NO_3·	0%	100%	Low MSA production in literature; assume that sulfate is formed
DMS + Cl·	55%	45%	Branching ratio of abstraction and addition pathway (IUPAC, 2009)
DMS + XO· (X=Cl, Br, I)	100%	0% **	DMSO approximately 100% yield
DMS + Br·	0%	100%	assumed
DMS + $O_{3(g)}$	100%	0% **	Assumed; DMSO approximately 100% yield
DMS + $O_{3(aq)}$	100%	0%	Gaseous reaction assumed to act similar to aqueous phase oxidation

Table 6.7 Molar branching ratio of MSA and sulfate used to determine branching ratio for modeled DMS oxidation. Percent yields are taken from Barnes et al. (2006) and references within unless otherwise stated (see text). Reactions that yield $DMSO_{(g)}$ (represented by **) are assumed to further oxidize 100% to form MSA (this assumption is studied further in Section 6.5.3).

DMS oxidation by OH· can occur by the abstraction or addition oxidation pathways (Chapter 1.5.3). Yields of the final products (MSA and sulfate) of DMS from OH· oxidation are not only dependent on which initial oxidation mechanism occurs (abstraction/addition) but also on intermediate steps (Chapter 1.5.3). Change in temperature, humidity, and aerosol and trace gas (e.g. O_3, NO) concentrations can also affect the percent yield of the final products (Bandy et al., 1992; Berresheim et al., 1995; von Glasow and Crutzen, 2004). For example, when temperatures decrease, the addition pathway from OH· oxidation increases (Berresheim et al., 1995; Sander et al., 2011) from 33% of total OH· oxidation at 295K to 50% at 285K (Barnes et al., 2006 and references within). The decomposition of the reaction intermediate CH_3SO_2 to form SO_2 is also temperature dependent and SO_2 formation would be slower at lower temperatures, further reducing the yield of SO_2 at lower temperatures (Yin et al., 1990). DMSO, $DMSO_2$ and MSA are major products of the addition mechanism (prevalent at lower temperatures) while SO_2 is known to be the major product of the abstraction mechanism (which is favoured at higher temperatures) (Plane, 1989; Berresheim et al., 1995; Davis et al., 1998; von Glasow and Crutzen, 2004). The branching ratio of DMS + OH· to produce SO_2 has been studied previously and molar yields of approximately 70-80% SO_2 under typical atmospheric conditions have been reported (Barnes et al., 2006 and references within). This is approximately the same as the branching ratio of addition and abstraction at 298K.

Davis et al. (1998) modeled the major products of the abstraction pathway as SO_2 (70%) and SO_3 (1%); both react further to yield sulfate. MSA yield for the abstraction pathway

was found to be low (less than 0.35%; Davis et al., 1998). Therefore an assumption that DMS oxidation by OH· abstraction will yield 100% sulfate (Table 6.7) has been made.

The addition pathway of the DMS + OH· reaction produces close to unity of DMSO (Barnes et al., 2006 and references within; Sander et al., 2011). DMSO is highly soluble in water (Henry's law coefficient at 298 K = 9.9 x 10^4 M atm^{-1} (no information on temperature dependence is available); Sander et al., 2011) which leads to the dominance of aqueous oxidation over gas phase oxidation of DMSO (Barnes et al., 2006). The lifetime of gaseous DMSO with respect to OH· was calculated to be on the order of 25 hours for one Antarctic study (Berresheim et al., 1998). However, the observed lifetime for gaseous DMSO was approximately two hours (Berresheim et al., 1998; Davis et al., 1998). This led to the conclusion that aerosol scavenging and deposition onto snow and ice surfaces was a major loss of DMSO in the polar atmosphere (Berresheim et al., 1998).

Oxidation of DMSO by OH·, NO_3· and halogen radicals in both the gas and aqueous phase yields both $DMSO_2$ and MSIA in the gas phase and in aerosols (Barnes et al., 2006). Both of these are highly soluble in water (Henry's law coefficient greater than 10^7 M atm^{-1}; Barnes et al., 2006). The aqueous oxidation of $DMSO_2$ will yield MSA although the lifetime of $DMSO_2$ is expected to be larger than the lifetime of many aerosols in the atmosphere (Barnes et al., 2006). The lifetime of MSIA due to aqueous oxidation in the atmosphere is less than an hour (Barnes et al., 2006) with the major oxidation product being MSA (Bardouki et al., 2003; Barnes et al., 2006). Homogenous oxidation of MSIA by OH· would result in SO_2 formation as the major product (Yin et

al., 1990; Kukui et al., 2003; Barnes et al., 2006) with only minor formation of MSA (Davis et al., 1999; von Glasow and Crutzen, 2004) although it has been noted that other studies have found SO_2 yields from gaseous MSIA oxidation to be small (5-10%; Barnes et al., 2006 and references within). Aqueous phase oxidation rates of DMSO and MSIA are at least comparable with gas phase reactions and in the presence of clouds can be thousands of times higher (Barnes et al., 2006). Therefore, the overall SO_2 yield from the addition pathway is expected to be small since heterogeneous oxidation of DMSO and MSIA is expected to be prevalent when aerosols are present (Berresheim et al., 1998; Mihalopoulos et al., 2007; Grey et al., 2011). One hundred percent conversion of DMS + OH· to DMSO was used in the model for the addition pathway. It will be assumed that DMSO oxidation will yield 100% MSA and 0% sulfate based on the rationale explained above. Test scenarios for MSA/sulfate as the final products in an 80/20 and 60/40 mix for DMSO oxidation were also conducted for the model runs with low liquid water content (i.e., 3.0×10^{-11} cm^3/cm^3). These results are discussed Section 6.5.3.

Reported values for the DMS + NO_3· branching ratio in the literature suggest minimal MSA concentrations (Barnes et al., 2006 and references within) and therefore the branching ratio will be modeled as 100% sulfate (Table 6.7). The Cl· + DMS pathway has been found to produce approximately 39% SO_2 and 52% DMSO at 293K (Barnes et al., 2006) which is similar to the branching ratio for the Cl· abstraction (45%; IUPAC, 2009) and addition pathways (55%; IUPAC, 2009). BrO·, ClO· and IO· reactions with DMS produce DMSO (Barnes et al. 2006). Little is known about Br· and O_3 gaseous phase products either because of complex side reactions in the case of Br· (Barnes et al.,

2006) or low yields and interferences (Sander et al. 2011). For the purposes of this study Br· will be considered an abstraction pathway and produce 100% sulfate. The O_3 aqueous reaction with DMS produces DMSO and therefore the O_3 gaseous reaction is assumed to also produce DMSO. As stated above, DMSO in the atmosphere can react with OH·, NO_3· and halogen radicals to produce MSIA and $DMSO_2$ (see Chapter 1.5.3 and Barnes et al., 2006). DMSO is also highly soluble in water and the aqueous phase oxidation rate of DMSO by OH· radicals is comparable if not greater than that of the gas phase reaction (Barnes et al., 2006). For the purpose of this thesis; 100% MSA formation from DMSO oxidation will be assumed, although test scenarios of MSA/sulfate branching ratios 80/20 and 60/40 as final products are conducted (see Section 6.5.3).

6.5.2 MSA_{BR} Model Output

The modeled branching ratio, MSA_{BR}, (equation 6.13) is displayed in Figure 6.13 for 2007 and Figure 6.14 for 2008 for the different oxidation model runs introduced in Section 6.4.2. Higher branching ratios are present when NO_x was low. Higher branching ratios are present when halogens and/or liquid phase oxidation are included in the model (top four lines in Figure 6.13 and Figure 6.14). It is of interest to note that elevated MSA_{BR} of approximately 0.8 are modeled when clouds and/or elevated halogens are present which corresponds to an MSA/biogenic sulfate ratio of 4. This would be a large ratio compared to MSA/non sea salt sulfate ratios that have been previously measured in the Polar Regions (see Li et al., 1993 for review) and range between 0.07 and 0.77 which is significantly less than 4 found in the models that include cloud and/or elevated halogen

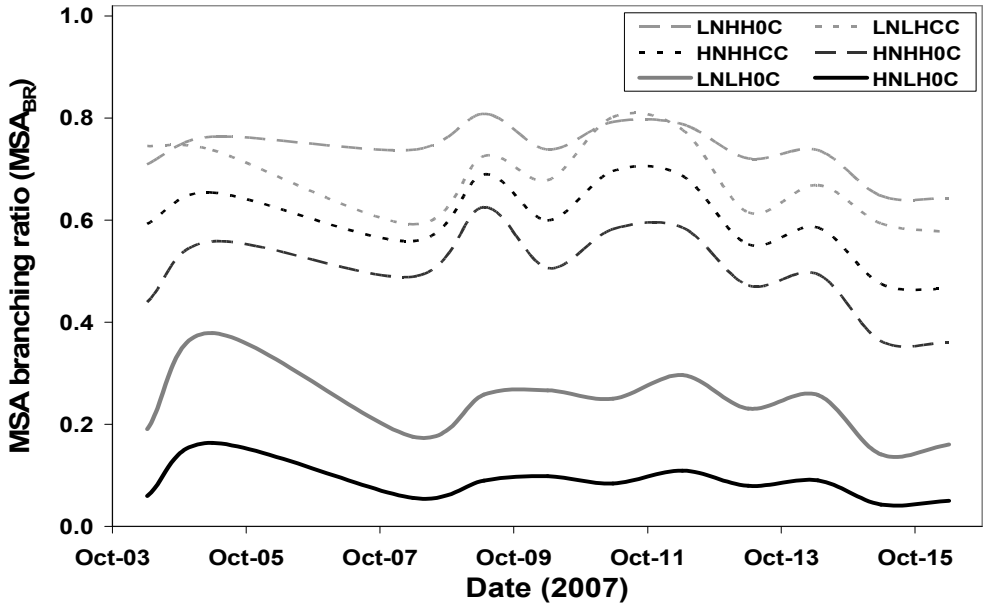

Figure 6.13 Modeled MSA branching ratios for 2007. Sensitivity tests are also displayed. See Table 6.6 for definitions of sensitivity tests.

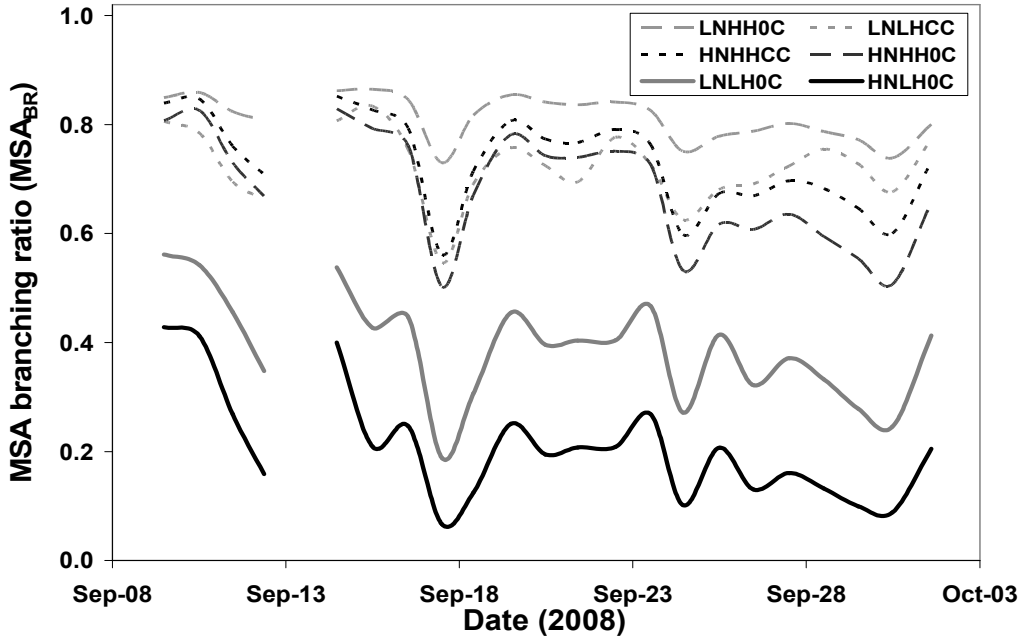

Figure 6.14 Modeled MSA branching ratios for 2008. Sensitivity tests are also displayed. See Table 6.6 for definitions of sensitivity tests.

chemistry. This mismatch between these modeled scenarios for MSA_{BR} and measurements reported by others may indicate that halogen and cloud oxidation of DMS is not important relative to $NO_3\cdot$ oxidation. There have only been a limited number of studies that examined MSA relative to biogenic sulfate in the Arctic and therefore these elevated ratios may have been masked before because of the inclusion of anthropogenic sulfate.

6.5.3 Sensitivity of DMSO Branching Ratio

As discussed in Section 6.5.1, the oxidation of DMSO + $OH\cdot$ can occur both in the gas and aqueous phase (Barnes et al., 2006). The phase of this reaction can influence the overall branching ratio of DMS oxidation. Although SO_2 can be formed (Section 6.5.1) from the oxidation of DMSO, this reaction is assumed to be small except when low aerosol loading occurs in the atmosphere. Two sensitivity tests were performed where DMSO was assumed to oxidize to yield 20% and 40% sulfate; the remainder of DMSO is oxidized to MSA (Figure 6.15). The sensitivity test illustrates that if DMSO oxidizes to sulfate, the MSA_{BR} decreases (equation 6.13).

In Figure 6.15, the MSA_{BR} branching ratio is distinctly higher when halogens are high (LNHH0C versus LNLH0C) irrespective of the DMSO branching ratio.

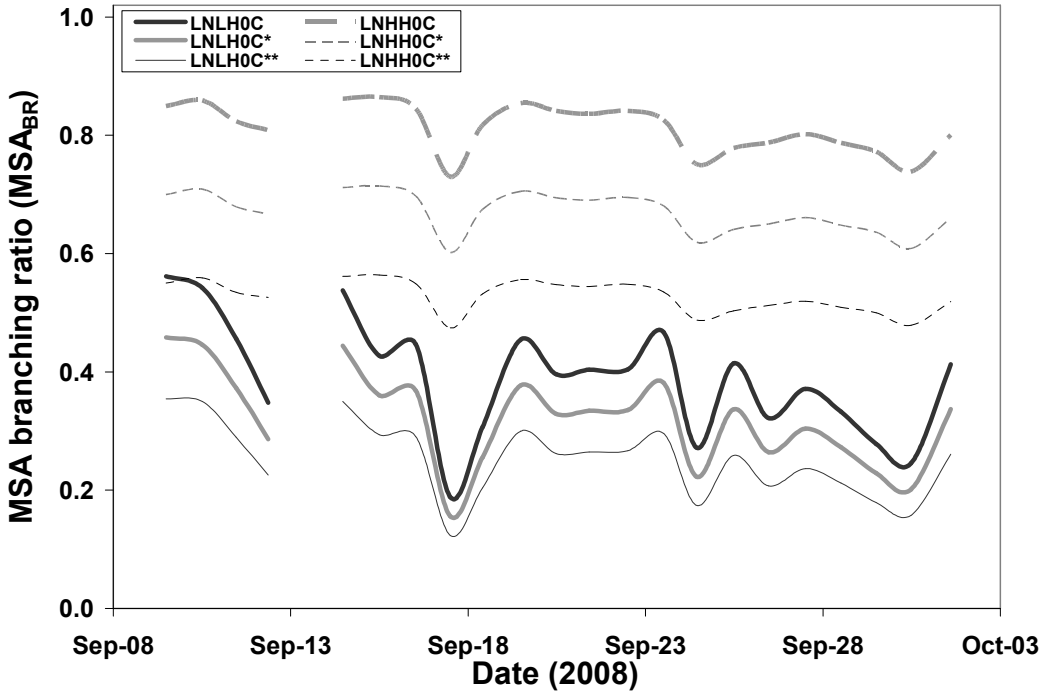

Figure 6.15 DMSO sensitivity tests on modeled MSA branching ratios. Tests of 100% yield of MSA for two models (LNLH0C, LNHH0C) are compared to 20/80 (*) and 40/60 (**) sulfate/MSA yields.

6.5.4 Modeled versus Measured MSA_{BR}

The measured branching ratio of MSA and biogenic sulfate (MSA_{BR}) was introduced in Chapter 5.3.4 (equation 5.3) and can be compared to the modeled results ($MSA_{BR:Model}$; equation 6.13). The MSA branching ratio found on board the *Amundsen* from Chapter 5.3.4 is displayed along with the modeled runs in Figure 6.16 for 2007. Total aerosol MSA_{BR} are low until October 15th and follow the branching ratios of the modeled run for low halogen and cloud oxidation and high NO_x levels (HNLH0C). This is consistent

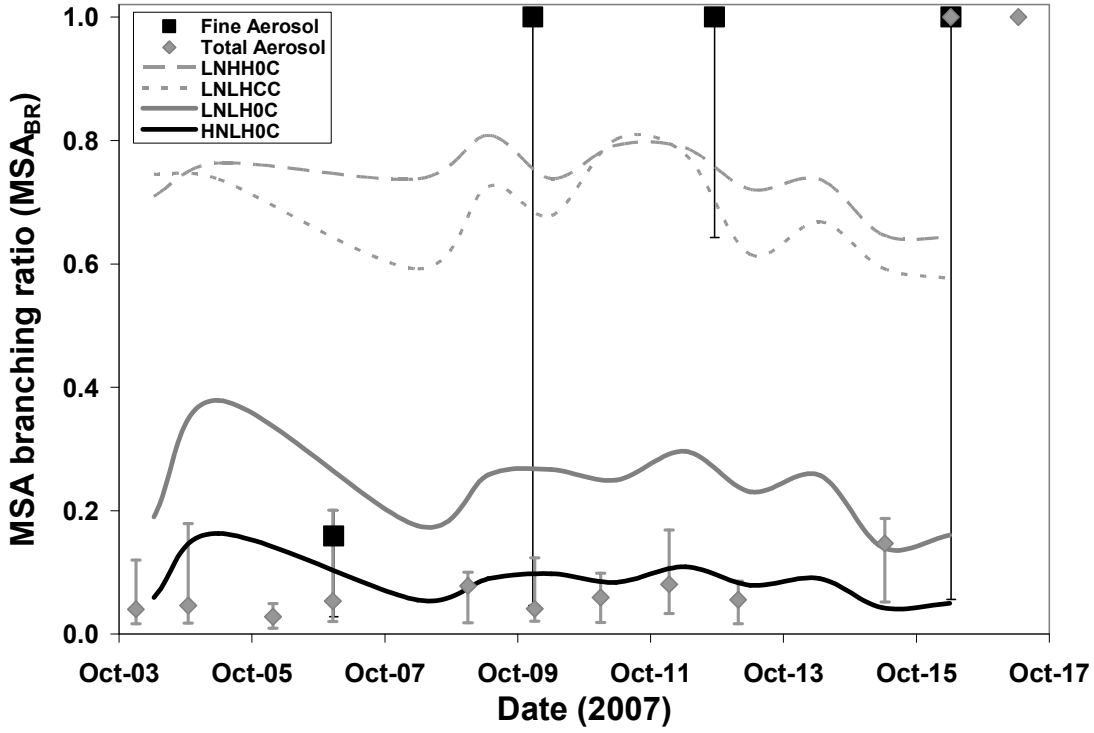

Figure 6.16 Modeled MSA branching ratios (equation 6.13) compared to 2007 MSA branching ratios (equation 5.3) in aerosols collected on board the *Amundsen*. Total and fine aerosols are displayed.

with a scenario in which NO_3· oxidation is more important than halogen or cloud oxidation. The results for the fine aerosols display much more variability and have higher MSA_{BR} than total aerosols although error associated with this measurement is very large (see Figure 6.16 and Chapter 5.3.4). Some total and fine aerosols have elevated MSA_{BR} ratios (see Figure 6.16) that cannot be explained by the models even when considering error associated with the measurements. This indicates that the MSA_{BR} and/or DMS oxidation was impacted in some way that is not captured in the model. This

could include processes that occurred during transport such as a fog event or an episode where elevated reactive halogens were present in the atmosphere.

The MSA branching ratio for 2008 on board the *Amundsen* is displayed in Figure 6.17. Fine aerosols in 2008 fall within the range of the two modeled runs of low halogen and aqueous oxidation. MSA_{BR} for total aerosols had large error associated with the values, but if error is taken into consideration the branching ratio could also potentially fall within the range of low halogen and aqueous oxidation. In both years it is of interest to note that the model predicting low levels of halogens and aqueous oxidation is the best fit for the data. This conclusion excludes samples when $MSA_{BR} = 1$ in 2007. This trend can also be extrapolated to Alert (see Chapter 5.3.4). Although no DMS oxidation model was carried out for Alert due to a lack of DMS data there, low ratios earlier in the season are consistent with low halogen concentrations and minimal aqueous DMS oxidation. Higher MSA_{BR} were possibly measured with the onset of winter at both locations, although at the same time, errors associated with these measurements were large (see Figure 5.10 in Chapter 5.3.4; Figure 6.16; Figure 6.17). Comparison between model and measurements indicate that $NO_3\cdot$ oxidation of DMS is more important than halogen and gaseous oxidation earlier in the fall. As winter approaches and MSA_{BR} ratios approach unity, oxidation from in cloud processes or halogen chemistry may become more important to the MSA/biogenic sulfate branching ratio.

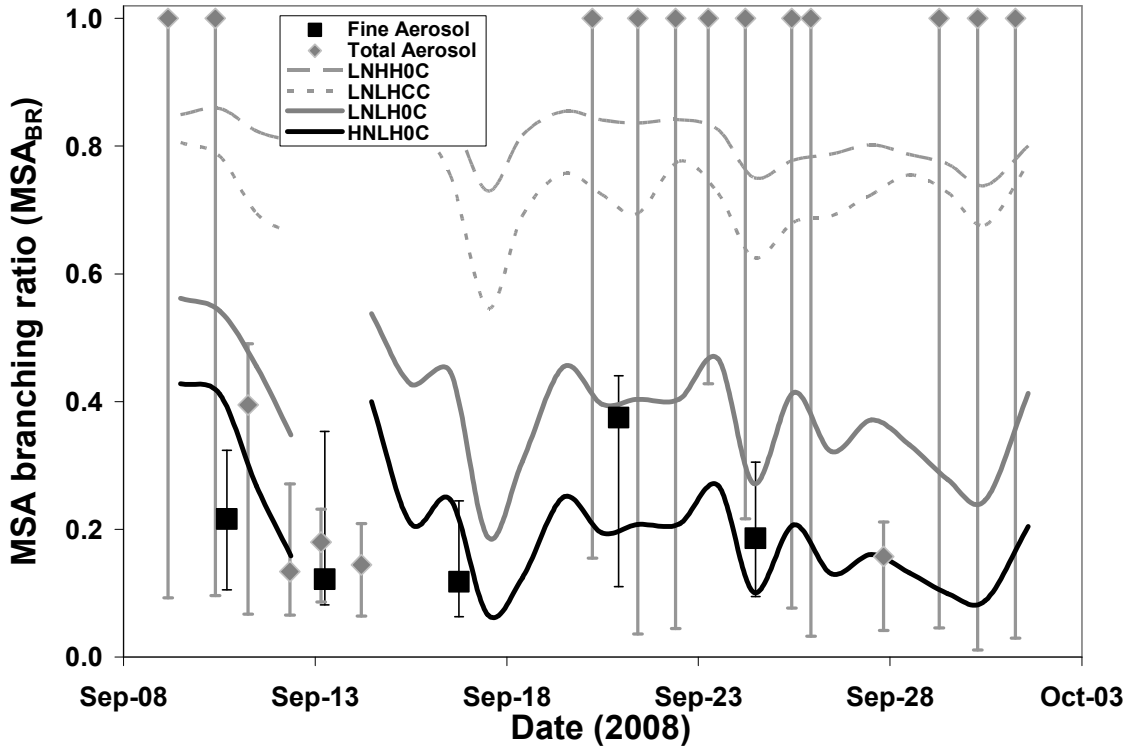

Figure 6.17 Modeled MSA branching ratios (equation 6.13) compared to 2008 MSA branching ratios (equation 5.3) in aerosols collected on board the *Amundsen*. Total and fine aerosols are displayed.

6.6 DMS Transport Model

6.6.1 Modeled Temporal Changes in DMS Concentrations

Transport of DMS in the marine boundary layer has been identified as an important process. Modeling the change in DMS may give insight to the magnitude of this important flux. Production and loss mechanisms are considered when modelling the

change of DMS concentration in the atmosphere. Flux of DMS (Chapter 1.5.2) from the ocean surface is considered as the sole source of DMS. Oxidation of DMS (Chapter 6.4) is considered a loss mechanism.

Therefore, without taking DMS transport into consideration, the change of DMS concentrations can be modeled with the following equation (Andreae et al., 1985)

$$\frac{d[DMS]}{dt} = \frac{F_{DMS}}{BLH} - L_{Ox} \qquad 6.14$$

where d[DMS]/dt is the modeled change of DMS over time, F_{DMS} is the flux of DMS from the ocean surface, BLH is the boundary layer height, and L_{Ox} is defined in equation 6.1. Boundary layer height was not measured during the study but is expected to be shallow (e.g. Mahajan et al. 2010; Kerminen and Leck, 2001) and a value of 100 m is assumed for the basic model run. Sensitivity of boundary layer for the model is discussed in Section 6.6.5.

This model does not take into consideration DMS transport. Transport can include venting to, or from, the free troposphere and/or horizontal transport (e.g., Conley et al., 2009). This modeled change in DMS along with measured DMS concentrations is used to give insight into transport in Section 6.6.6.

6.6.2 DMS Flux

The DMS flux between the ocean and the atmosphere (Chapter 1.5.2) depends on its Henry's law coefficient, as well as the temperature, wind speed and the concentration of DMS in the ocean (Liss and Merlivat, 1986; Wanninkhof, 1992; Nightingale et al., 2000). DMS concentrations in water, measured by the Levasseur research group from University of Laval, were used by Rempillo (2011) to determine DMS flux between October 10 – 13 and 23 – 24, 2007 in the Northwest Passage (Figure 6.18) and September 23 – 26, 2008 (Figure 6.19) in the Baffin Bay region. Details for calculations can be found in Chapter 1.5.2. DMS flux in 2007 was modified for the presence of sea ice; Rempillo et al. (2011) corrected flux for the fraction of open water.

Rempillo (2011) conducted sensitivity tests using other flux parameterizations from Liss and Merlivat (1986) and Wanninkhof (1992) and found the Nightingale et al. (2000) parameterization to fall between the other two calculations. Huebert et al. (2004) found the Nightingale et al. (2000) parameterization to be the best parameterization when fitting direct measurements of DMS flux. A new parameterization for DMS has been determined (e.g., Yang et al., 2011) that may represent DMS flux at larger wind speeds (> 10 m/s) but at low speeds tends to over predict flux (Elliott, 2009; Yang et al., 2011). The Nightingale et al. (2000) parameterization fell within the 95% confident level best fit line of data collected by Ho et al. (2011) for $^{3}He/SF_6$ dual tracer experiments. Winds speeds for the Ho et al. (2011) experiment ranged between 5 and 17 m/s and were similar to wind speeds that were used for flux calculations on board the *Amundsen* (median = 6.0

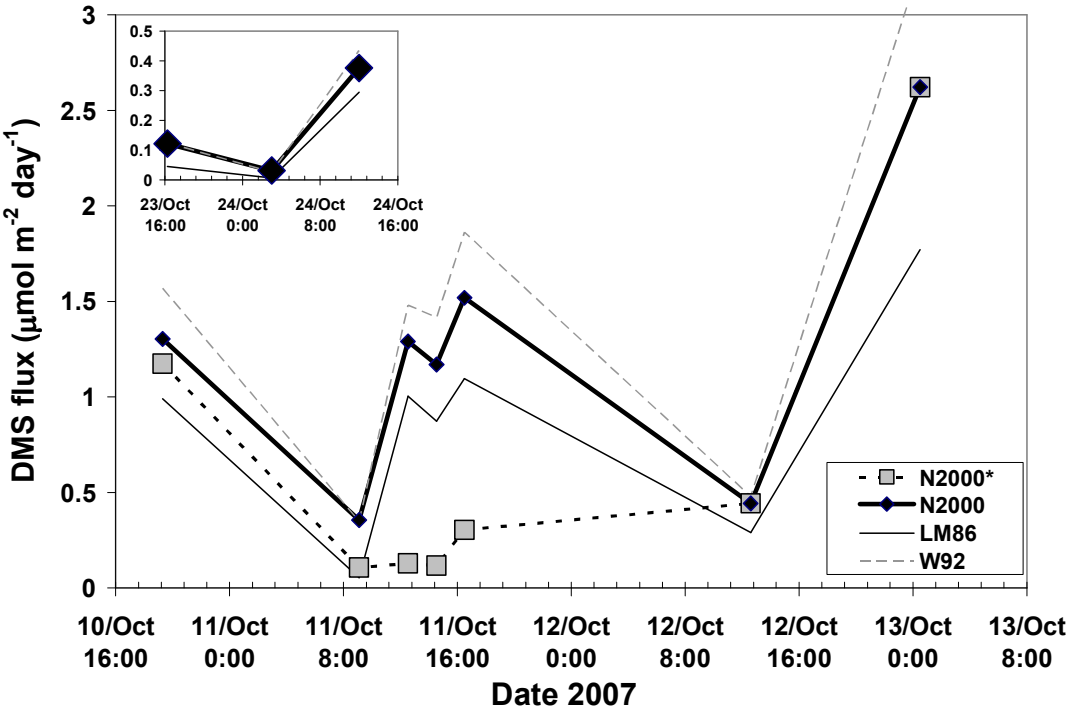

Figure 6.18 Calculated DMS flux between October 10 and 13th, 2007 (insert between October 23-24) using N2000 (Nightingale et al., 2000), LM86 (Liss and Merlivat, 1986) and W92 (Wanninkhof, 1992) parameterization. Corrections for flux because of sea ice conditions is shown for the Nightingale parameterization (N2000*) between October 10 and 13th. DMS flux is calculated by Rempillo (2011).

± 2.6 m/s). Therefore the Nightingale et al. (2000) parameterization will be considered for flux calculations in this thesis.

The DMS flux calculated by Rempillo (2011) using the parameterization of Nightingale et al. (2000) is displayed in Figure 6.18 for 2007 in the Northwest Passage and Figure 6.19 for 2008 in the Baffin Bay region. The magnitude of DMS flux falls between the

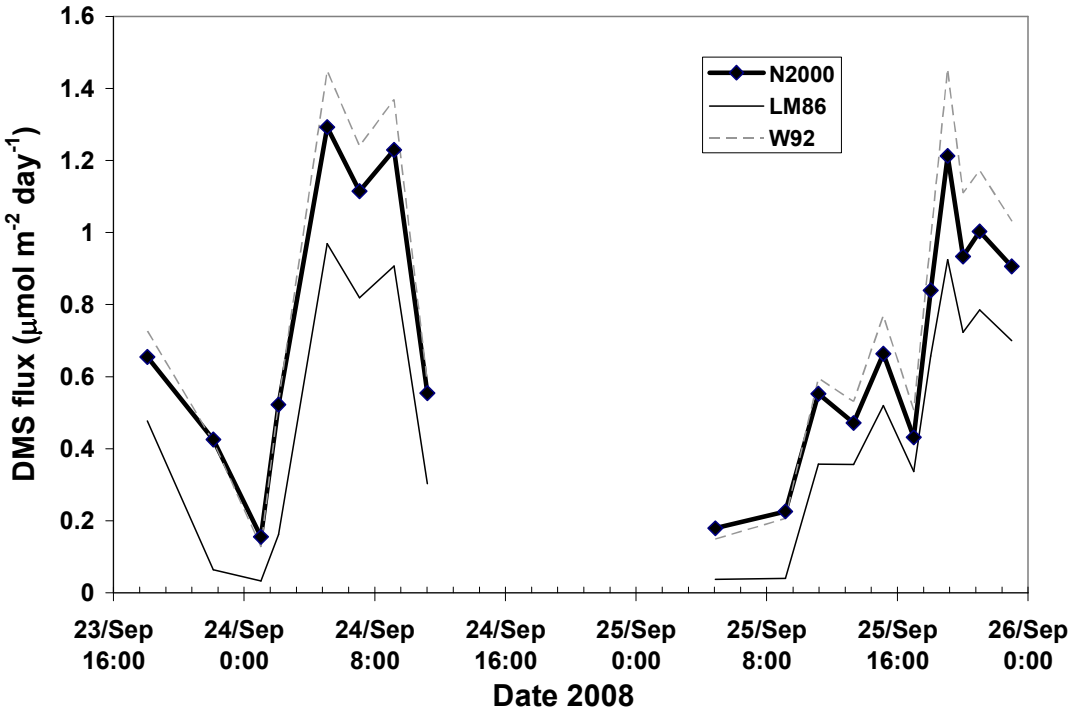

Figure 6.19 DMS flux between September 23 and 26th, 2008 using N2000 (Nightingale et al., 2000), LM86 (Liss and Merlivat, 1986) and W92 (Wanninkhof, 1992) parameterization. No sea ice was observed on board the *Amundsen* during this time period. DMS flux is calculated by Rempillo (2011).

extremes of the predicted values of 3.11 (summer) and 0 $\mu molm^{-2}d^{-1}$ (winter) calculated by Erickson et al. (1990) for the North Pacific region (65° - 80° N). DMS flux in this study was found to be less than previous studies that measured DMS flux in the Arctic (Bates et al., 1987; Leck and Persson, 1996*a*; Sharma et al., 1999) and Rempillo et al. (2011) attributed this to seasonality.

6.6.3 Temporal Considerations

The calculation for the change of DMS over time (equation 6.14) assumes that air mass history remains the same between each measurement. Atmospheric DMS concentrations were measured at least once every two hours during times when DMS flux calculations were available and changes in the air mass history due to the movement of the *Amundsen* or the surrounding air parcel are assumed to be minimal between measurements.

The flux, using DMS surface water concentrations, were calculated by Rempillo et al. (2011) when both DMS surface water concentrations and wind speed measurements were available. The loss of DMS by oxidation (L_{Ox}) was modeled in Chapter 6.4 each time a measurement of atmospheric DMS was obtained. To integrate equation 6.14, temporal variations in the two measurements must be taken into consideration. Flux was assumed to be linear between each calculation and was computed only when coincident atmospheric and ocean DMS concentrations were measured. Changes in DMS concentrations were not calculated for the October 23 – 24, 2007 period because of the limited number of flux calculations (3) and atmospheric DMS concentration measurements (7) during this time.

6.6.4 Changes in DMS Concentrations: Modeled versus Measured

The rate of change of atmospheric DMS concentrations for the base model (boundary layer height = 100 m, flux calculated using Nightingale et al. (2000) parameterization,

L_{Ox} = LNLH0C) is displayed in Figure 6.20 for 2007 and Figure 6.21 for 2008. This can be compared to rates of change of measured atmospheric DMS. The change of atmospheric DMS concentrations was determined by

$$\left(\frac{d[DMS]}{dt}\right)_{measured} = \frac{[DMS]_{t_{i-1}} - [DMS]_{t_i}}{t_{i-1} - t_i} \qquad \textbf{6.15}$$

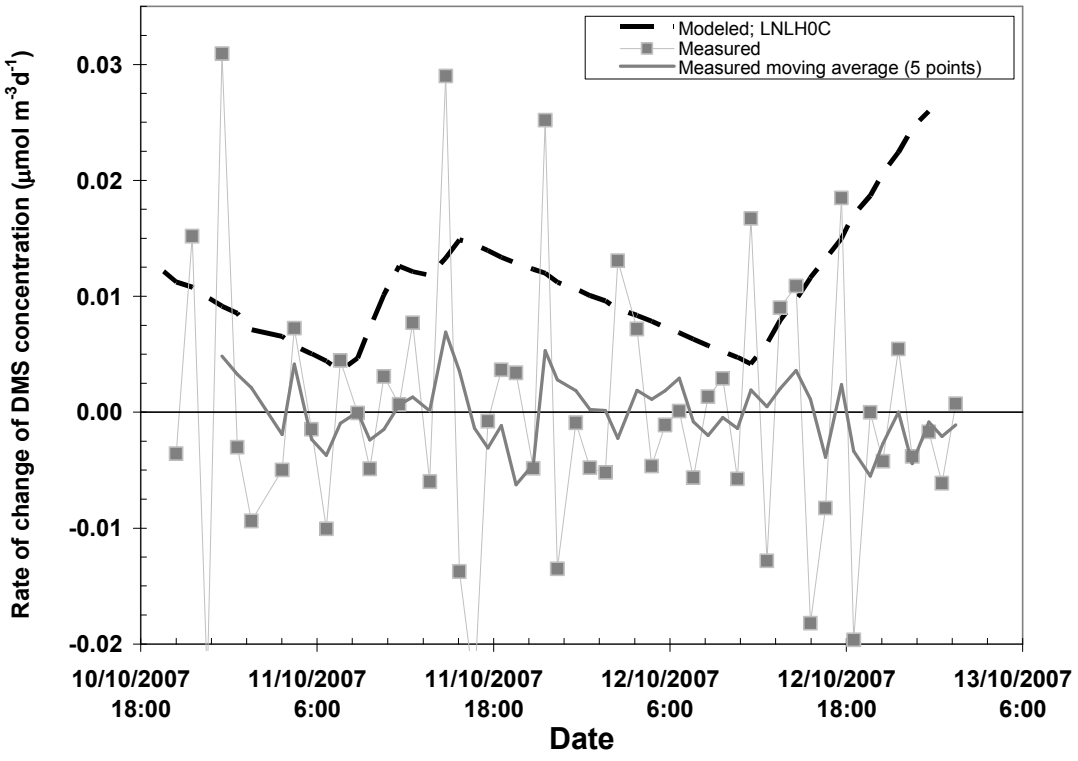

Figure 6.20 Modeled rate of change of DMS concentration (equation 6.14) compared to measured changes in DMS (equation 6.15) for 2007 data. A 5 point moving average of the measured data is also displayed.

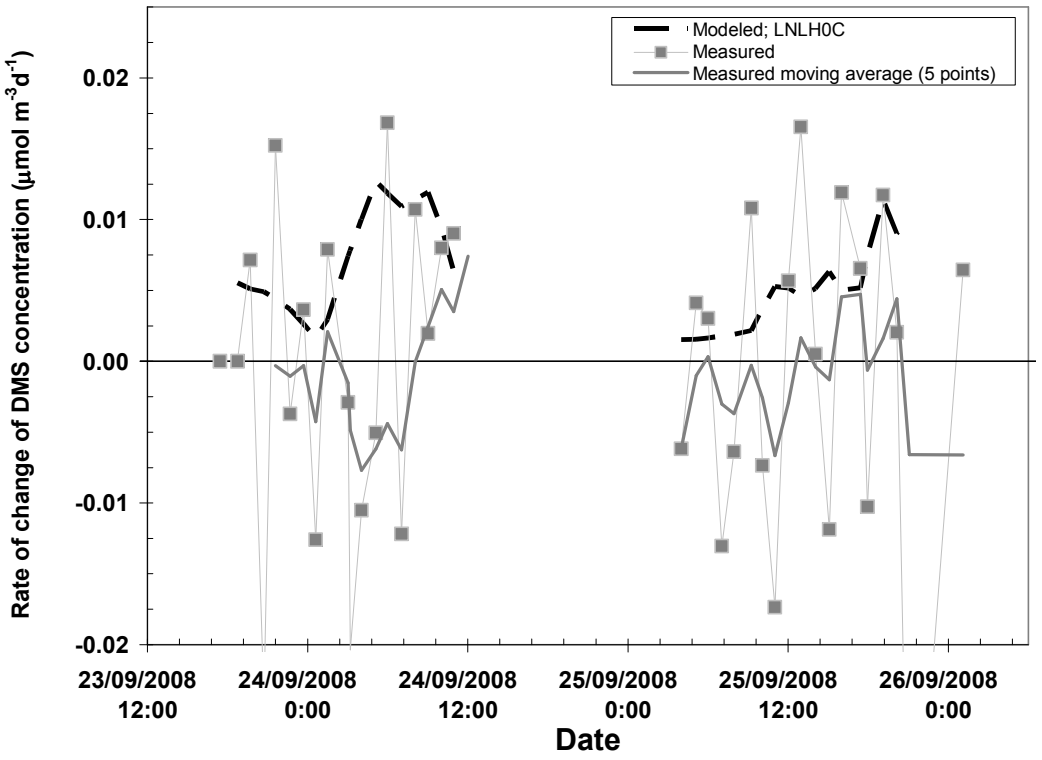

Figure 6.21 Modeled rate of change of DMS concentration (equation 6.14) compared to measured changes in DMS (equation 6.15) for 2008 data. Base model is displayed. A 5 point moving average of the measured data is also displayed for measurements.

where $[DMS]_t$ is the DMS concentration measured at the time (t_i) that is displayed in Figure 6.20 (2007) or Figure 6.21 (2008) and $[DMS]_{t_{i-1}}$ is the previous measurement of atmospheric DMS concentration taken at time t_{i-1}. Atmospheric DMS measurements were made more frequently than DMS water samples so data points are available prior to each t_i.

The modeled change in DMS is larger than the measured median values and is always larger than a 5 point average of the measured DMS changes (see Figure 6.20, Figure 6.21, Table 6.8). The observed changes in DMS concentrations from the base model are positive (Figure 6.20, Figure 6.21), which would lead to a continuous increase of DMS in the atmosphere if no other loss mechanism (such as transport; Chapter 6.6.6) is taken into consideration.

6.6.5 Sensitivity of Modeled Temporal Changes in DMS Concentrations

Flux parameterization, boundary layer height and the rate of loss by oxidation can effect the modeled temporal changes in DMS concentration. Flux parameterization was discussed in Section 6.6.2. The oxidation rate of DMS was discussed in Section 6.4.2 (also see Table 6.8).

The boundary layer height was not measured in this campaign, but a value of 100 m was used in the base model based on models and observations for the Arctic described elsewhere in literature (Kermin and Leck, 2001; Ludén et al., 2010; Mahajan et al. 2010). Others have measured, calculated or modeled larger boundary layer heights in the Arctic (e.g., Andreae et al., 1985; Sharma et al., 1999; Nilsson and Leck, 2002; Edwards et al., 2011) and based on these, test scenarios of 400 and 1000 m were run and are displayed in Figure 6.22 (see Table 6.8, third column, for median values). Changing the boundary layer height from 100 m to 400 m resulted in a factor of approximately four decrease in the change of DMS concentration.

BLH (m)	L_{Ox}	Modeled change in DMS (nmol m^{-3} day^{-1}) median ± σ	(min/max)	% negative	Transport of DMS (nmol m^{-3} day^{-1}) median ± σ	(min/max)	% negative
100	LNLH0C	8.1 ± 5.0	(1.5 / 25.9)	0	10.0 ± 13.2	(-21.0 / 53.0)	28
	LNLH0C*	4.4 ± 5.4	(0.9 / 25.9)	0	7.0 ± 13.6	(-27.9 / 53.0)	33
	HNLH0C	7.7 ± 5.2	(0.8 / 25.3)	0	9.2 ± 13.3	(-21.4 / 53.0)	29
	LNHH0C	7.4 ± 5	(0.7 / 25.5)	0	9.4 ± 13.5	(-23.6 / 52.8)	29
	LNLHCC	7.7 ± 5.1	(1.3 / 25.9)	0	9.7 ± 13.3	(-21.9 / 53.0)	28
	HNHHCC	6.3 ± 5.1	(-0.3 / 24.7)	1	8.4 ± 13.6	(-24.9 / 52.8)	30
	L_{Ox} = 0	8.4 ± 5.0	(1.8 / 26.2)	0	10.2 ± 13.2	(-20.8 / 53.0)	25
400	LNLH0C	1.9 ± 1.3	(0.2 / 6.3)	0	3.6 ± 12.2	(-28.6 / 45.5)	39
	LNLH0C*	0.9 ± 1.4	(0.1 / 6.3)	0	1.8 ± 12.3	(-29.0 / 45.5)	41
	HNLH0C	1.4 ± 1.4	(-0.6 / 6)	9	3.2 ± 12.2	(-29.0 / 45.5)	40
	LNHH0C	1.2 ± 1.5	(-1.7 / 5.9)	24	2.7 ± 12.5	(-31.2 / 45.3)	43
	LNLHCC	1.4 ± 1.3	(-0.1 / 6.2)	5	3.3 ± 12.3	(-29.5 / 45.5)	40
	HNHHCC	0.8 ± 1.5	(-1.9 / 5.2)	32	2.1 ± 12.6	(-31.6 / 45.3)	44
	L_{Ox} = 0	2.1 ± 1.3	(0.4 / 6.5)	0	3.8 ± 12.2	(-28.4 / 45.5)	38
1000	LNLH0C	0.6 ± 0.5	(-0.2 / 2.4)	10	1.9 ± 12.1	(-30.1 / 44.0)	44
	LNLH0C*	0.2 ± 0.6	(-0.2 / 2.4)	18	1.2 ± 12.2	(-30.3 / 44.0)	45
	HNLH0C	0.2 ± 0.7	(-0.9 / 2.3)	38	1.5 ± 12.2	(-30.5 / 44.0)	47
	LNHH0C	0.1 ± 1.0	(-2.5 / 1.9)	47	1.3 ± 12.5	(-32.7 / 43.8)	44
	LNLHCC	0.2 ± 0.6	(-0.5 / 2.3)	28	1.4 ± 12.2	(-31.0 / 44.0)	46
	HNHHCC	-0.7 ± 1.0	(-3.2 / 1.4)	81	0.4 ± 12.6	(-34.0 / 43.8)	48
	L_{Ox} = 0	0.8 ± 0.5	(0.2 / 2.6)	0	2.1 ± 12.1	(-29.9 / 44.0)	41

Table 6.8 Sensitivity tests for modeled changes in DMS concentrations and Net Transport of DMS. LNLH0C* is the modeled scenario that includes ice cover in the flux calculation. No DMS oxidation was considered in the L_{Ox} = 0 scenarios. LNLH0C at 100 m is considered the base scenario.

In the LNLH0C scenario for DMS oxidation, the model run with a boundary layer height of 1000 m has instances when the change of DMS over time becomes negative (Table 6.8). This would indicate a net decrease of DMS over time during these times (i.e., a net sink). The median value for the LNLH0C remains positive for all boundary layer heights modeled (Table 6.8). Comparing the 100, 400 and 1000 m boundary layer height

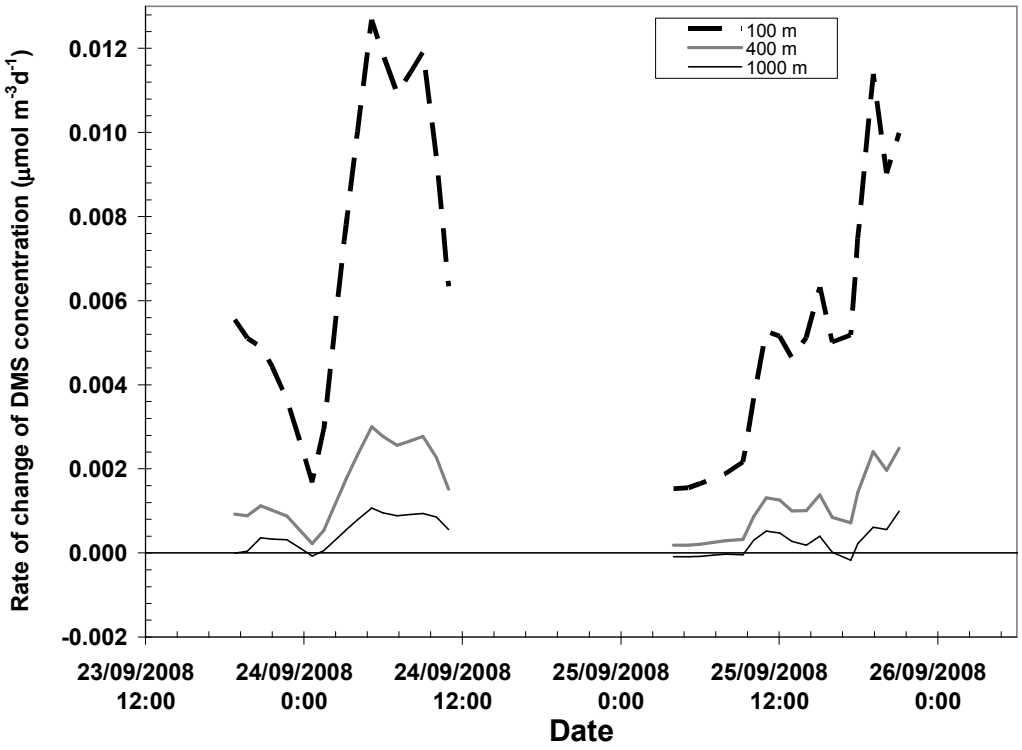

Figure 6.22 Sensitivity test for boundary layer height for modeled rate of change of DMS concentrations (equation 6.14). DMS oxidation is based on LNLH0C.

modeled scenarios, the median change in DMS shown in Table 6.8 is influenced greater by the boundary layer height than by the oxidation (L_{Ox}).

The modeled DMS oxidation rate (L_{Ox}) also affected the modeled temporal changes in DMS concentrations (Table 6.8). Sensitivity tests are shown in Table 6.8 and in Figure 6.23 for 2008. Boundary layer height is kept consistent at 100 m in Figure 6.23. If no oxidation is considered ($L_{Ox} = 0$; Table 6.8), the average rate of change of modeled DMS is 2% greater than the base model (LNLH0C) at 100 m. When considering the fastest

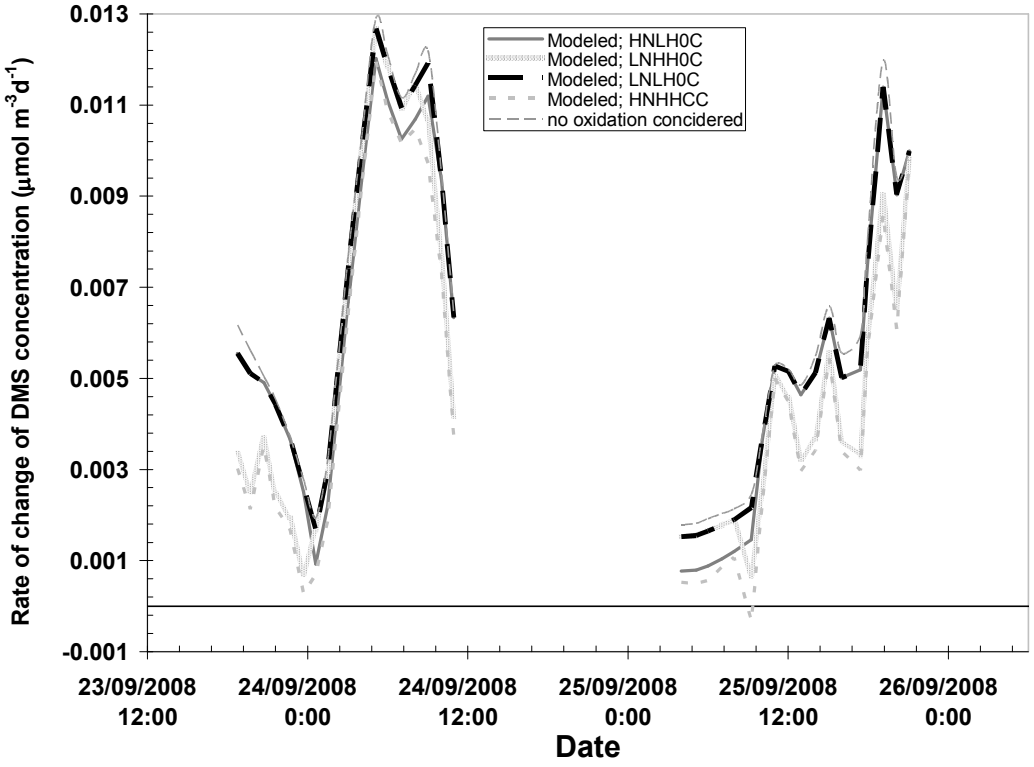

Figure 6.23 Sensitivity test for modeled rate of change of DMS concentrations (equation 6.14) when varying L_{Ox}. Boundary layer height is 100 m.

rate of oxidation modeled (HNHHCC), the average rate of change of DMS is 22% less than the base model. As the boundary layer height increases, the difference between the LNLH0C and other oxidation scenarios increases. For example, the median change of DMS in the HNHHCC scenario at a boundary layer height of 400 m is 76% less than the LNLH0C scenario (see Figure 6.24; Table 6.8).

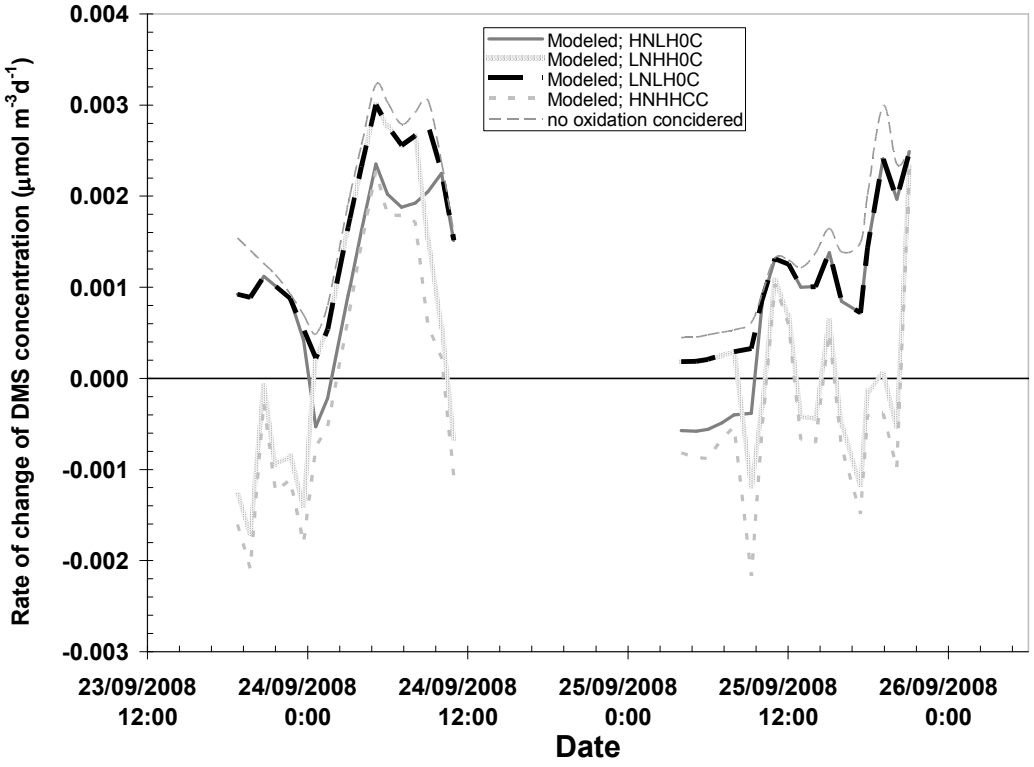

Figure 6.24 Sensitivity test for modeled rate of change of DMS concentrations (equation 6.14) when varying L_{Ox}. Boundary layer height is 400 m.

6.6.6 DMS Transport in the Arctic

The flux from the Arctic Ocean can be an order of magnitude greater than the rate of oxidation, even with the highest modeled rate of oxidation (scenario HNHHCC). If no other loss of DMS occurred, this would lead to net increase of DMS concentrations over time in the vicinity of the measurement platform.

Differences between measured and modeled changes in DMS concentrations are observed (Figure 6.20 (2007) and Figure 6.21(2008)) suggesting vertical and/or horizontal transport was important during the campaigns. In a region where production of DMS is greater than loss by oxidation, either DMS transport out of the region must occur or DMS concentrations will increase. Similarly if production of DMS is less than the oxidation loss, DMS transport into the region must be important or DMS concentrations decrease. The modeled changes in DMS concentrations (i.e., equation 6.14) do not take into consideration net transport of DMS into or out of the region. The measured change of DMS concentrations (equation 6.15) incorporates all influences on DMS, i.e.,

$$\left(\frac{d[DMS]}{dt}\right)_{measured} = \frac{F_{DMS}}{BLH} - L_{O_x} - T_{Net} \qquad \textbf{6.16}$$

where L_{Ox} is the loss of DMS by oxidation and T_{Net} is the net transport out of (or into) the system. By comparing the modeled change of DMS to the measured change of DMS, some measure of net transport can be obtained, i.e.,

$$T_{net} = \left(\frac{d[DMS]}{dt}\right)_{modelled} - \left(\frac{d[DMS]}{dt}\right)_{measured} \qquad \textbf{6.17}$$

Transport of DMS in the Arctic can include venting to (or from) the free troposphere (Lundén et al., 2010; Conley et al., 2009) and horizontal transport (Kerminen and Leck,

2001; Nilsson and Leck, 2002). The net transport of DMS is shown in Figure 6.25 (2007) and Figure 6.26 (2008). A positive (negative) net transport value indicates that the local region is a source (sink) of DMS and is shown for the various boundary layer height conditions and oxidation scenarios in Table 6.8 (right hand side). Net transport was generally positive throughout the study period, although negative transport was observed (Figure 6.25 and Figure 6.26; Table 6.8). Measurements collected on board the

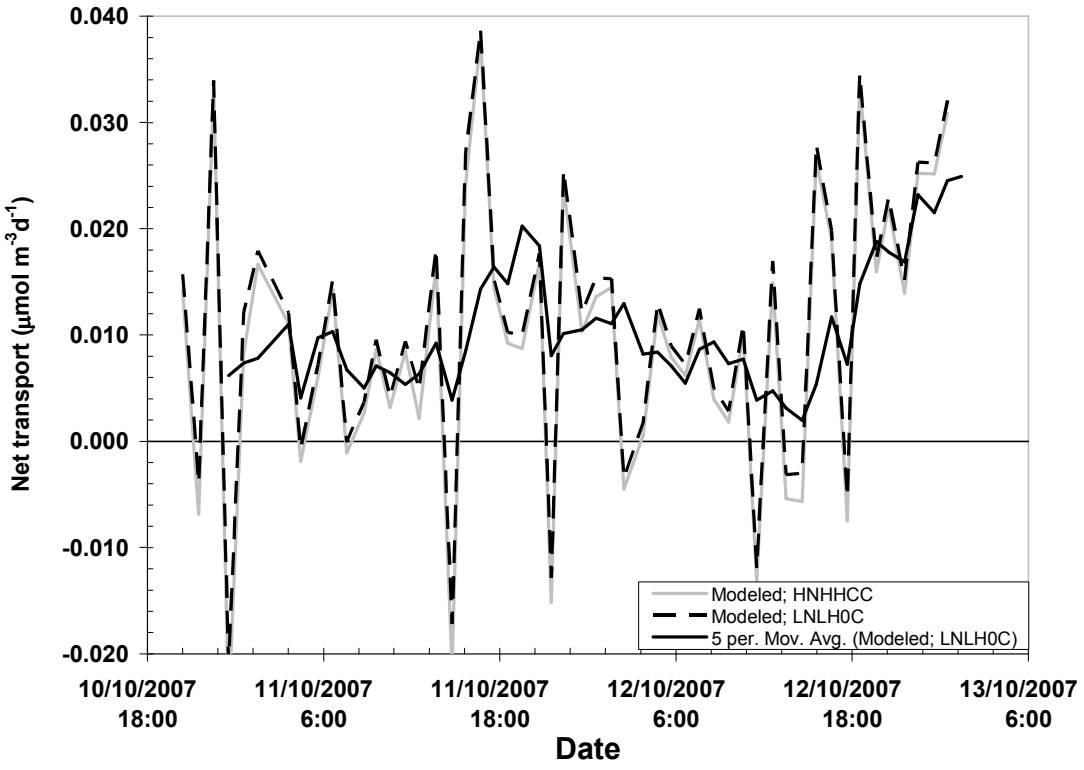

Figure 6.25 Net transport of atmospheric DMS into (negative) and out of (positive) of the local region around the *Amundsen* for 2007. Sensitivity tests for different L_{Ox} values are shown. Boundary layer is set at 100m. A 5 point moving average is also displayed.

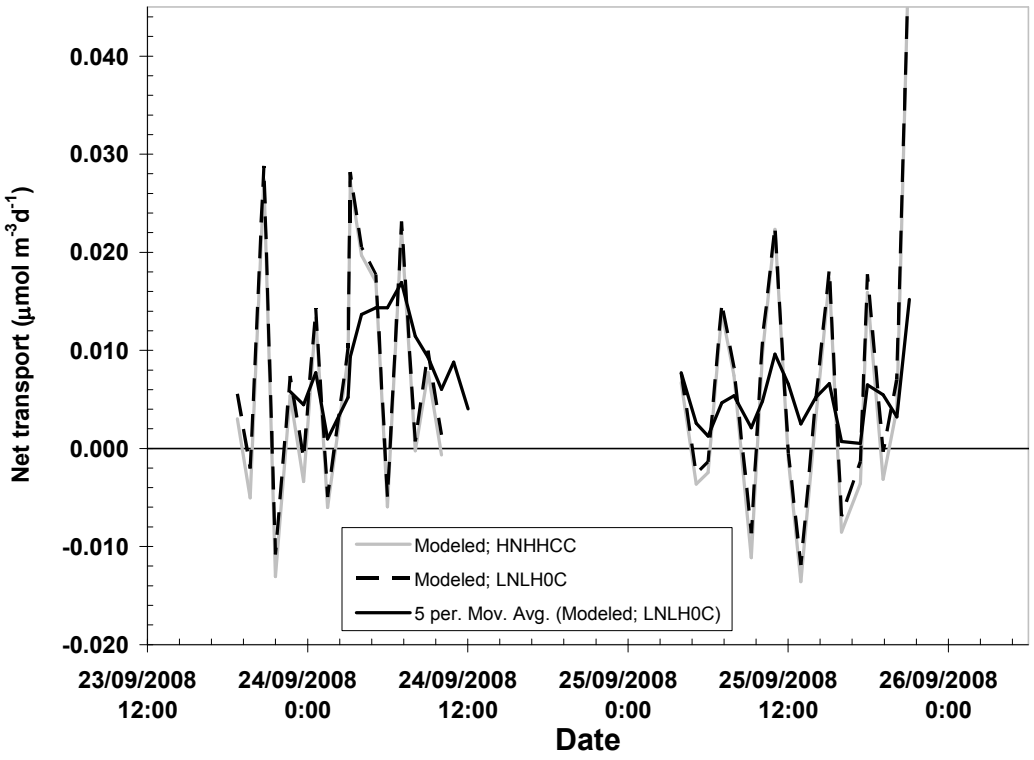

Figure 6.26 Net transport of atmospheric DMS into (negative) and out of (positive) of the local region around the *Amundsen* for 2008. Sensitivity tests for different L_{Ox} values are shown. Boundary layer is set at 100 m. A 5 point moving average is also displayed.

Amundsen support the Arctic Ocean is a net source of atmospheric DMS in the vicinities of the Northwest Passage and Baffin Bay.

Sensitivity tests for boundary layer height and oxidation scenarios were explored. The net transport average did not differ by more than 10% when boundary layer height was set to 100 m and when different oxidation scenarios were tested (see Figure 6.25 (2007),

Figure 6.26 (2008), Table 6.8). A sensitivity test, using the flux calculated by Rempillo et al. (2011), when ice is present, decreased the median value of transport by approximately 30% (Table 6.8).

The results for the boundary layer sensitivity tests for the transport model are displayed in Figure 6.27. As the boundary layer increases in height, the modeled net transport value decreases. The change in net transport due to difference in boundary layer height is small relative to the variations between each modeled point. However, median net transport

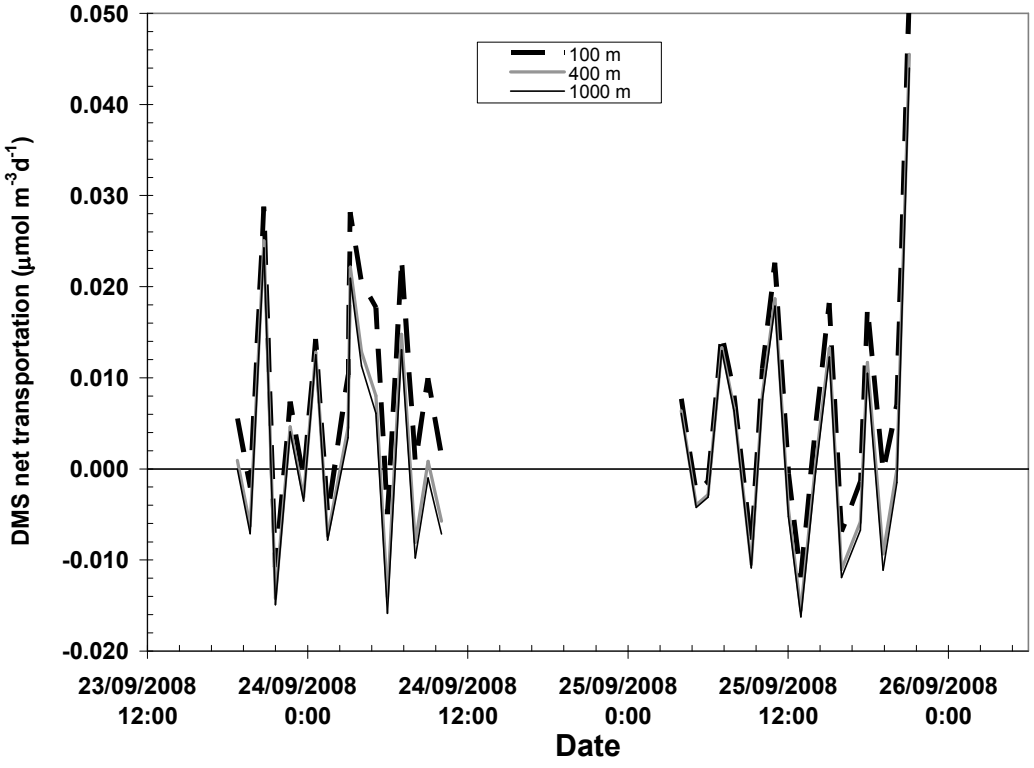

Figure 6.27 Sensitivity tests for DMS net transport when considering different boundary layer heights.

decreases as boundary layer height increases; decreasing by a factor of three as the boundary layer height increases from 100 m ($T_{Net} \approx 10$ nmol/m^3) to 400 m ($T_{Net} \approx 3.6$ nmol/m^3). A change between 100m and 400m for modeled boundary layer leads to an overall decrease of 64% in the median value of the net transport of DMS. There are instances of negative net transport modeled in all scenarios; approximately 30% of the modeled points for the 100 m boundary layer height scenario (40% for the 400 m boundary layer height) were negative (Table 6.8). Therefore there are instances where the atmosphere around the *Amundsen* acted as a net sink. However, net median transport is positive for all scenarios tested (Table 6.8), indicating that during the *Amundsen* campaign, Arctic waters acted as a net source of DMS into the atmosphere.

A positive net transport is in agreement with conclusions made throughout the thesis. DMS and thus MSA and biogenic sulfate are most likely not representative of the local DMS oxidation conditions, since DMS can be transported before being oxidized. Local DMS oxidation in the Arctic may become of importance in foggy conditions, in times when large amounts of halogen radicals are present (such as spring) or high pollution events. Measurements of DMS oxidation products are typically representative of regional scale conditions in the Arctic rather than local conditions.

6.7 Summary

Three models were discussed in this chapter. The oxidation model was used to determine the rate of loss of DMS from oxidation in the Arctic. The MSA_{BR} model was used to test

the sensitivity of the MSA/sulfate ratio under different oxidation schematics and to compare the results with the measurements found in this study. The third model, the transport model, studied the importance of transport of DMS into and out of the Arctic region.

6.7.1 Oxidation Model

OH· concentrations in the Arctic were modeled using a steady state model. HCHO chemistry increased the OH· concentration by approximately 50% and was included when considering OH· concentrations in the Arctic. Modeled OH· concentrations were within the range of previous measurements of OH· concentrations in the Polar Regions.

A steady state model was used to determine nitrate radical concentrations. DMS contributes to the greatest loss of nighttime nitrate. Aqueous loss of N_2O_5 can contribute up to 20% of nighttime loss of the nitrate radical. The lifetime of nighttime NO_3· increases with the onset of winter and can be on the order of a few hours. This can lead to difficulties in predicting NO_3· loss mechanisms during the Arctic night, since loss mechanisms which are assumed to be small under conditions at lower latitudes may start to become significant. This is apparent especially when DMS, one of the major losses of NO_3·, has low atmospheric concentrations.

Model results indicate DMS was determined to be largely oxidized by OH· and NO_3· during the Arctic fall season although BrO· may be important during times when reactive

halogens are present (such as the Arctic spring). The chlorine radical can be an important DMS oxidation mechanism especially during sunrise and sunset. This is true even when low concentrations (720 moleclues/cm^3) of Cl· are present. From the oxidation model, between 5-10% of DMS could potentially be oxidized by gaseous O_3. Aqueous oxidation of DMS may also play an important role in DMS oxidation. A median lifetime for DMS based on oxidation mechanisms was determined to be 6.1 days during the study.

6.7.2 MSA_{BR} Model

The MSA branching ratio (MSA_{BR}) was modeled using the oxidation model. The model suggests that during the campaign, nitrate radical oxidation of DMS is more important than aqueous and halogen oxidation. Elevated halogen and aqueous oxidation terms in the model lead to an increase in MSA_{BR}; while elevated nitrogen chemistry led to a decrease in MSA_{BR}. Low MSA_{BR} values were observed leading to the conclusion that nitrate is important for DMS oxidation in the high Arctic during the onset of winter.

Sensitivity tests were carried out on the DMSO branching ratio. DMSO branching ratios were less important to the MSA_{BR} than the overall oxidation mechanisms studied here.

It is interesting that there were instances where measured MSA_{BR} values were larger than predicted by the model. These elevated MSA_{BR} points may indicate that the MSA_{BR} and/or DMS oxidation was impacted during transport in some way that is not captured in the model.

6.7.3 Transport Model

Changes in DMS concentrations were used to determine net transport of DMS into and out of the region around the *Amundsen.* Median net transport of DMS was positive in the region of the *Amundsen*, indicating a net source of DMS during these campaigns. The net transport was found to be negative approximately 30% of the time (assuming a 100 m boundary layer height), illustrating that at times, the area can also act as a net sink. The median net transport was influenced by the boundary layer height (an increase in boundary layer height decreases the net transport) and the modeled DMS oxidation loss mechanisms. In all modeled scenarios, the median net transport was found to be positive although modeled results varied by over a factor of 20. The presence of ice affected the flux of DMS which in turn decreased the modeled net transport of DMS by approximately 30%. If Arctic waters become more ice free in the future, DMS flux and net transport would be expected to increase. The net transport term supports the concept that measurements of DMS oxidation products, such as MSA and biogenic sulfate, are representative of regional rather than local conditions in the Arctic.

Chapter Seven: Conclusions and Recommendations

This work was conducted as part of the Arctic SOLAS program where the goal was to study the interactions between gases emitted from the Arctic Ocean to the atmosphere. The findings presented here are used to define the importance of DMS oxidation and sulfate loading in the Arctic atmosphere on both regional and local scales. This study is the first to investigate the spatial variation in atmospheric biogenic sulfur in the Arctic. Size segregated aerosol samples and SO_2 samples were collected at Alert, Nunavut (82º30 N, 62º30 W) and on board the icebreaker CCGS *Amundsen*, in the fall of 2007 and 2008. Atmospheric DMS concentrations were measured concurrently on board the *Amundsen.* Apportionment with tracer ions and isotopes were used to distinguish between biogenic sulfur and sulfur from other sources.

7.1 Frost Flowers

A novel way to distinguish between frost flower and sea salt contributions in aerosols with the use of stable isotopes is introduced. This method, combining isotope analysis and a constraint on the sulfate to sodium ratio in frost flowers is the first time that $\delta^{34}S$ values are used to quantify frost flower contributions separately from those of sea salt even in the presence of non sea salt sulfate. The frost flower correction can be used in other applications such as precipitation and ice core analysis if the $\delta^{34}S$ value is measured. This method will advantageous in areas with low variability of $\delta^{34}S_{nss}$ values, such as in Antarctica, where the distinction between frost flowers and sea salt sulfate is

required. Future studies using this method of distinguishing between frost flowers and sea salt (of both ice cores and aerosols) could lead to possible additional information on the temporal variation of frost flower SO_4^{2-}/Na^+ ratios.

Frost flower contributions to aerosol loading were typically found in the larger size aerosols (> 3.0 μm) in this study. This is congruent with the concept that aerosols containing a frost flower signature are local and are primary aerosols. Sulfate loading in aerosols derived from frost flowers reached 2.3 nmol/m^3 at Alert during the study period. Frost flower contributions are not found in aerosols from the *Amundsen*, in part due to the large sea salt contribution on board the *Amundsen*. This is the first time frost flower concentrations in aerosols are reported quantitatively and separately from sea salt contributions.

7.2 Sea Salt Sulfate

Sea salt components dominated soluble ion concentrations in aerosols from the *Amundsen*. Size segregated samples show that the majority of sea salt was in the large size aerosols (i.e., > 60% of sulfate is in aerosols greater than 1.5 μm in diameter). Sea salt sulfate was present at Alert, but concentrations were not as large and a higher percent contribution was found in the smaller aerosols. Sea salt sulfate in the fine aerosol (< 0.49 μm) had a median concentration of 0.07 ± 0.08 nmol/m^3 at Alert and 0.13 ± 0.30 nmol/m^3 for samples collected on board the Amundsen . The consistency between the sea salt concentration in fine aerosols at the two sites suggests sea salt aerosols are aged and

supports long range transport of sea salt components in the Arctic atmosphere. Elevated fine aerosol sea salt sulfate on board the *Amundsen* was observed when sea ice cover was high and wave action was not a factor. The fact that fine aerosol sea salt sulfate was found in areas of high ice cover suggests these aerosols could potentially be associated with bubble bursting at the ocean surface and this aspect of sea salt aerosols would be of interest for further study. If sea ice is of importance for fine aerosol sea salt sulfate loading, changes in sea ice may influence aerosol loading. Since aerosols of this size range can be transported great distances, this in turn could influence the sulfate loading of aerosols undergoing long range transport in the Arctic.

7.3 Sulfur from the Smoking Hills

The influence of emissions from the Smoking Hills was found in $\delta^{34}S$ values for aerosol sulfate and SO_2 in their vicinity, although elevated atmospheric sulfur concentrations were not observed. SO_2 along with size ranges between 0.95 – 1.5 μm and 0.49 – 0.95 μm displayed the most influence from The Smoking Hills. The aerosols that were strongly influenced by the Smoking Hills in this study had larger diameters than previously measured aerosols released from the Smoking Hills (Radke and Hobbs, 1989) and can be attributed to aerosol growth, e.g., from SO_2 oxidation on existing aerosols. Future studies looking at the influence of the Smoking Hills can use $\delta^{34}S$ values as tools for apportionment because of the large negative $\delta^{34}S$ value relative to other sulfate sources in the Arctic.

7.4 Anthropogenic Sulfate

Concentrations of non sea salt sulfate at Alert (0.5 to 13 nmol/m^3) and from the aerosols collected on board the *Amundsen* (0.2 to 6.9 nmol/m^3) are within the same concentration range as previous studies that have measured non sea salt sulfate in the Arctic. $\delta^{34}S$ values are used to apportion anthropogenic and biogenic contributions of non sea salt sulfate. Future studies must consider isotope apportionment around local sources in the Arctic cautiously since local sources can influence the calculated $\delta^{34}S_{nss}$ value.

Anthropogenic sulfate increased as the onset of winter was approached which is consistent with the increase of influence from Arctic Haze. Similar anthropogenic sulfate concentrations (total aerosol; 0.2 -13.0 nmol/m^3) were observed at Alert and from the *Amundsen* congruent with a reservoir of anthropogenic sulfate that is well mixed in the Arctic atmosphere. Over 70% of the anthropogenic sulfate at Alert is found in aerosols less than 0.95 μm in diameter. Samples collected on board the *Amundsen* had only approximately 20% of anthropogenic aerosol in the fine fraction. Larger aerosol sizes (>0.95 μm) collected on *Amundsen* had greater amounts of anthropogenic sulfate (0.5 – 3.9 nmol/m^3 median = 1.2 nmol/m^3) relative to Alert (median = 0.5 nmol/m^3), while fine aerosol concentrations (< 0.49 μm) were relatively similar during temporal overlap at the two locations (on the order of 0.1 – 1.0 nmol/m^3 during this period). This is consistent with long range transport and represents a well mixed sulfate reservoir in the Arctic atmosphere.

Ammonium, nitrate and non sea salt potassium were all correlated with anthropogenic sulfate at both locations. Smoke stack emissions are a plausible explanation for non sea salt potassium on board the *Amundsen* because of the elevated non sea salt potassium found when CO_2 concentrations indicated a high possibility of smoke stack emission influence on the sample. At Alert, the non sea salt potassium is likely to be from long range transport since most is found in the fine aerosol fraction. Non sea salt potassium (along with ammonium) is usually associated with biomass burning. The plausible source from smoke stack emissions on board the *Amundsen* may suggest that besides biomass burning non sea salt potassium and ammonium in the Arctic could also be from anthropogenic sources. Studies to determine the persistent source of non sea salt potassium in the Arctic atmosphere, with, perhaps, the aid of black carbon measurements (a strong indicator of biomass burning; Finlayson-Pitts and Pitts, 2000), are recommended. Ammonium/anthropogenic sulfate and NSS Potassium/anthropogenic sulfate ratios are smaller at Alert than on board the *Amundsen*. This is likely due to long range transport since aerosols at Alert have had more time to interact with gaseous sulfur components. Caution to preserve ammonium and nitrate during sample storage would be beneficial for future work with aerosols. Studies on the ion ratios around the Arctic may yield additional spatial information on the contribution of non sea salt potassium and ammonium in the Arctic.

A chloride deficit relative to sea salt in aerosols is observed at Alert. A strong relationship ($R^2 = 0.77$) between anthropogenic sulfate and chloride deficit is observed in total aerosol. This deficit is due to the acidification of aerosols from H_2SO_4 and not

HNO_3 since there is a strong correlation between sulfate and the measured chloride deficit. A deficit of chloride in aerosols indicates removal of chlorine compounds to the gaseous phase. Campaigns and modeling studies to determine the persistence and concentrations of gaseous reactive compounds containing chlorine in the Arctic fall are highly recommended. Because of the low detection limit of bromide in this study, it is uncertain if it, like chloride, also experiences a deficit relative to sea salt. Studies to compare aerosol bromide relative to anthropogenic sulfate in the Arctic are also highly recommended due to the reactivity of bromine compounds in the Arctic atmosphere.

7.5 SO_2 Concentrations

Approximately 90% of SO_2 at Alert was from anthropogenic sources during the study. Anthropogenic concentrations of SO_2 ranged from below detection limits up to 11.8 nmol/m^3 at Alert (median 0.4 ± 2.4 (1σ) nmol/m^3). Concentrations of SO_2 at Alert were lower than those from the *Amundsen.* The local source of the smoke stack on board the *Amundsen* is likely the cause of some of the elevated SO_2 on the *Amundsen.* Samples collected on board the *Amundsen*, and determined to have little to no influence from smoke stack emissions had a median value of 2.4 nmol/m^3. When concentrations of SO_2 on board the *Amundsen* were low, concentrations were within the same order of magnitude as SO_2 concentrations at Alert. This supports that even in areas of strong local sources; samples can represent background levels as long as appropriate sampling precautions are taken. Local SO_2 sources in future studies must be taken into account when measuring low SO_2 concentrations in remote areas such as the Arctic.

The SOLAS campaign is the first study to determine biogenic SO_2 concentrations in the Arctic. Median values of biogenic SO_2 at Alert, 0.07 ± 1.15 (1σ) nmol/m^3, were an order of magnitude smaller than SO_2 concentrations found in Antarctica. Biogenic SO_2 measured on board the *Amundsen* for the majority of sampling periods (30 out of 32 samples) was not significantly different than zero. A high volume sampler wired to an instantaneous measurement (such as wind direction, CCN, CO_2, SO_2 etc.) that can detect possible conditions when interference from local sources (i.e., the ship stack emissions) occurs is recommended in the future so that the high volume samplers can be turned off during all high contamination events. Longer sampling times and less contamination from local sources would result in higher sensitivity in biogenic SO_2 concentrations. Additional measurements of biogenic SO_2 in the Arctic taking the above precautions to reduce local anthropogenic SO_2 influences is recommended so that spatial information on biogenic SO_2 in the Arctic can be studied in further detail.

Sea salt contamination on the cellulose acetate filters collected on board the *Amundsen* during snow events and/or other processes lead to episodes of high sulfur that may have interfered with SO_2 measurements. It is recommended that the elluent from the cellulose acetate filters is measured for chloride and sodium in future studies and that tests for the adsorption of different gasses containing chlorine on the cellulose acetate filters be carried out.

7.6 MSA

MSA concentrations, in general, decreased with the onset of winter (~ 0.10 nmol/m^3 in September down to ~ 0.02 nmol/m^3 in December) and were similar at both Alert (median = 0.031 ± 0.018 (1σ) nmol/m^3) and on board the *Amundsen* (median = 0.054 ± 0.026 (1σ) nmol/m^3). Concentrations of MSA are within the observed range of previous studies around the Arctic (0.002 – 1.4 nmol/m^3) although concentrations were on the lower end of what had been reported previously. This is most likely due to seasonality since most studies were completed in the spring or the summer. The Arctic SOLAS campaign is the first to measure biogenic sulfate in size segregated aerosols in the Arctic. Biogenic sulfate is found predominantly in the fine aerosols at Alert. MSA/biogenic sulfate ratios were variable with a median value of 0.24 at Alert and 0.28 for samples collected on board the *Amundsen*.

7.7 DMS Oxidation

Three different models were used to the predict rate of oxidation of DMS, explain the observed MSA_{BR} (fraction of MSA over total aerosol sulfur) and to determine the importance of DMS transport in the Arctic.

Oxidation Model: A DMS oxidation model was constructed to determine the rate of DMS oxidation in the Arctic. A median lifetime for DMS based on oxidation mechanisms was determined to be 6.1 days during the study although decreases to 0.65

days under a different modeling scenario when NO_x and halogen concentrations are increased and cloud aqueous oxidation is considered. Modeled OH· concentrations increased by approximately 50% when HCHO was included in the steady state model. The nitrate radical model suggested that the primary sink of NO_3· radicals in the Arctic is DMS oxidation. It is recommended that nitrate radical concentrations along with the loss mechanisms in the Arctic, especially with the onset of winter be studied further in order to gain insight on the influence of NO_x chemistry in the Arctic atmosphere during this time the year.

Halogen and aqueous chemistry were also included in the model and contributed 2 – 7% of total DMS oxidation when low halogen concentrations were used in the model. If halogen concentrations were held high in the model, 81% of the DMS was determined to be oxidized from halogens with the majority of the oxidation coming from BrO·. It would be beneficial to study halogen chemistry during the onset of winter with instrumentation that can detect halogens below current detection limits. Aqueous oxidation of DMS may be of importance during fog events, especially later in the season. The distribution of liquid across the different aerosol size fractions along with temperature and relative humidity are needed to be study the importance of aqueous oxidation of DMS in more detail, especially during fog events. In the Arctic, liquid water versus ice in aerosols could potentially affect DMS oxidation and should be a focus of a future study. A year round study of DMS oxidation, or more generally the oxidizing potential of the atmosphere in the Arctic atmosphere, may be of interest when considering the lifetime of DMS and VOCs in the atmosphere during different seasons.

MSA_{BR} Model: The MSA_{BR} was modeled and compared to measured results. Oxidation of DMS by $NO_3\cdot$ for the majority of the fall season is more important than halogen oxidation of DMS, since elevated halogen used in the models leads to a higher MSA branching ratio (0.61 – 0.84) than measured MSA branching ratios (0.24 at Alert, 0.28 for samples collected on board the *Amundsen*). In instances when the measured MSA_{BR} approaches unity aqueous and/or halogens may become more important. Additional concurrent measurements of MSA_{BR} and radicals that oxidize DMS (such as $OH\cdot$, $NO_3\cdot$, $BrO\cdot$, $Cl\cdot$, etc.) are of importance so that the observed MSA_{BR} can be understood. A sensitivity test for DMSO branching ratios was carried out and DMSO branching ratios were found to have less influence on the modeled MSA_{BR} relative to the sensitivity tests from the different oxidation mechanisms tested. A more detailed model of the branching ratio of DMSO along with other DMS oxidation intermediates (e.g., $DMSO_2$, MSIA, SO_2) may be of use to fine tune the MSA_{BR} model. Both heterogeneous and homogenous oxidation of DMSO, under ambient atmospheric conditions should be studied to determine final oxidation products.

A MSA peak in spring at Alert in past studies had been attributed to long range transport of DMS oxidation products (Li et al., 1993). Scenarios of the DMS oxidation model predict an elevated MSA branching ratio during times of high halogen oxide radical concentrations, which occurs during the spring. This may also contribute to an elevated MSA concentration that has been observed in the spring and therefore the year round study may give more insight into this phenomenon.

Transport Model: Transport of DMS in the Arctic was modeled and was found to be important (based model computed a median net transport of 10.0 ± 13.2 (1σ) nmol m^{-3} day^{-1} of DMS out of the region). In all modeled scenarios a median net positive transport was determined, indicating that the regions around the *Amundsen* were a net source of DMS. This supports that measurements of DMS and DMS oxidation products are representative of regional scale conditions in the Arctic rather than local conditions and agrees with the majority of findings in this thesis. In all modeled scenarios, there are incidences where the region around the *Amundsen* acted as sink of DMS. Variability in the measured changes of DMS was larger than the modeled changes of DMS and modeled DMS transport is highly dependent on these measurements. The variations of changes of measured DMS atmospheric concentrations effects the calculated DMS transport term on a much finer time scale than any of the other inputs into the model. Measurements of boundary layer height, radical and oxidant concentrations and meteorological conditions along side DMS measurements in both the surface water and atmosphere must be carried out at a much smaller time scale then what was carried out in this study. Fluctuation of DMS concentrations in the atmosphere must be studied in detail if DMS transport and concentrations are to be understood in the remote atmosphere.

References

Abbatt, J. (2012), Personal Communications, Department of Chemistry, University of Toronto.

Alvarez-Aviles, L., W. R. Simpson, T. A. Douglas, M. Sturm, D. Perovich and F. Domine (2008), Frost flower chemical composition during growth and its implications for aerosol production and bromine activation, *Journal of Geophysical Research 113*, D21304.

Andreae, M. O. (1983), Soot Carbon and excess Fine Potassium – Long-Range Transport of Combustion derived Aerosols, *Science 220*, 1148 – 1151.

Andreae, M. O., R. J. Ferek, F. Bermond, K. P. Byrd, R. T. Engstrom, S. Hardin, P. D., Houmere, F. LeMarrec, H. Raemdonck and R. B. Chatfield (1985), Dimethyl Sulfide in the Marine Atmosphere, *Journal of Geophysical Research 90(D7),* 12891 – 12900.

Andrews, J.E., P. Brimblecombe, T. D. Jickells, P. S. Liss, and B. Reid (2004), *An Introduction to Environmental Chemistry (2nd Ed),* Blackwell Publishing. Cornwall.

ApSimon, H. M., B. M. Barker and S. Kayin (1994), Modelling Studies of the Atmospheric Release and Transport of Ammonia in Anticyclonic Episodes, *Atmospheric Environment 28,* 665 – 678.

Arimoto, R., R.A. Duce, D. L. Savoie and J. M. Prospero (1992), Trace Elements in Aerosol Particles from Bermuda and Barbados: Concentrations, Sources and Relationships to Aerosol Sulfate, *Journal of Atmospheric Chemistry 14,* 439 – 457.

Arimoto, R., R. A. Duce, B. J. Ray, W. G. Ellis Jr, J. D. Culle and J. T. Merrill (1995), Trace elements over the North Atlantic, *Journal of Geophysical Research 100,* 1199 – 1213.

Ariya, P. A., A. Khalizov and A. Gidas (2002), Reactions of Gaseous Mercury with Atomic and Molecular Halogens: Kinetics, Product Studies and Atmospheric Implications, *The Journal of Physical Chemistry A 106,* 7310 – 7320.

Baltensperger U. and M. Furger (2008), Aerosol chemistry in Remote Locations, from *Environmental chemistry of Aerosols,* ed. I. Colbeck, 217 – 252.

Bandy, A. R., D. L. Scott, B. W. Blomquist, S. M. Chen and D. C. Thornton (1992), Low Yields of SO_2 from Dimethyl Sulfide Oxidation in the Marine Boundary Layer, *Geophysical Research Letters 19,* 1125 – 1127.

Bardouki, H., H. Berresheim, M. Vrekoussis, J. Sciare, G. Kouvarakis, K. Oikonomou, J. Schneider and N. Mihalopoulos (2003), Gaseous (DMS, MSA SO_2 H_2SO_4 and DMSO) and particulate (sulfate and methanesulfonate) sulfur species over the northeastern coast of Crete, *Atmospheric Chemistry and Physics 3*, 1871 – 1886.

Barnes, I., J. Hjorth, and N. Mihalopoulos (2006), Dimethyl Sulfide and Dimethyl Sulfoxide and Their Oxidation in the Atmosphere, *Chemical Reviews 106*, 940 – 975.

Barrie, L. A. (1986), Arctic Air Chemistry: An Overview, from *Arctic air pollution,* ed. B. Stonehouse, Cambridge University Press, Cambridge, 5 – 23.

Barrie L. A. and J. W. Bottenheim (1991), Sulphur and Nitrogen Pollution in the Arctic Atmosphere, from *Pollution of the Arctic Atmosphere*, ed. W.T. Sturges, Elsevier Science Publishers, New York, 155 – 183.

Barrie L. A., R. M. Hoff and S. M. Daggupaty (1981), The Influence of Mid-Latitudinal Pollution Sources on Haze in the Canadian Arctic, *Atmospheric Environment 15*, 1407 – 1419.

Barrie L.A., J. W. Bottenheim, R. C. Schnell, P. J. Crutzen and R. A. Rasmussen (1988) Ozone destruction and photochemical reactions at polar sunrise in the lower Arctic atmosphere, *Nature 334,* 138 – 141.

Barrie, L. A., S. M. Li, D. L. Toom, S. Landsberger and W. Sturges (1994), Lower tropospheric measurements of halogens, nitrates and sulphur oxides during Polar Sunrise Experiment 1992, *Journal of Geophysical Research 99,* 25453 – 25467.

Bates, T.S., J. D. Cline, R. H. Gammon and S. R. Kelly-Hansen (1987), Regional and Seasonal Variations in the Flux of Oceanic Dimethylsulfide to the Atmosphere, *Journal of Geophysical Research 92*, 2930 – 2938.

Bates, T. S., J. A. Calhoun and P. K. Quinn (1992*a*), Variations in the Methanesulfonate to Sulfate Molar Ratio in Submicrometer Marine Aerosol Particles Over the South Pacific Ocean, *Journal of Geophysical Research 97*, 9859 – 9865.

Bates, T. S., B. K. Lamb, A. Guenther, J. Dignon and R.E. Stoiber (1992*b*), Sulfur Emissions to the Atmosphere from Natural Sources, *Journal of Atmospheric Chemistry 14,* 315 – 337.

Beaudon, E. and J. Moore (2009), Frost flower chemical signature in winter snow on Vestfonna ice cap, Nordaustlandet, Svalbard, *The Cryosphere 3*, 147 – 154.

Beine, H. J., M. Engardt, D. A. Jaffe, O. Hov, K. Holmen and F. Stordal (1996), Measurements of NOx and aerosol particles at the Ny-Alesund Zeppelin mountain station on Svalbard: Influence of regional and local pollution sources, *Atmospheric Environment 30,* 1067 – 1079.

Berresheim, H., P. H. Wine and D. D. Davis (1995), Sulfur in the atmosphere, from *Composition, Chemistry, and Climate of the Atmosphere,* ed. H. B. Singh, Van Nostrand Reinhold, New York, 251 – 307.

Berresheim, H., J. W. Huey, R. P. Thorn, F. L. Eisele, D. J. Tanner and A. Jefferson (1998), Measurements of dimethyl sulphide, dimethyl sulfoxide, dimethyl sulfone, and aerosol ions at Palmer Station, Antarctica, *Journal of Geophysical Research 103(D1),* 1629 – 1637.

Blanchet, J. P. and É. Girard (1995), Water vapour-temperature feedback in the formation of continental Arctic air: its implication for climate, *The Science of the Total Environment 160/161*, 793 – 802.

Bloss, W. J., J. D. Lee, D. E. Heard, R. A. Salmon, S. J. B. Bauguitte, H. K. Roscoe and A. E. Jones (2007), Observations of OH and HO_2 radicals in coastal Antarctica, *Atmospheric Chemistry and Physics 7,* 4171 – 4185.

Bloss, W. J., M. Camredon, J. D. Lee, D. E. Heard, J. M. C. Plane, A. Saiz-Lopez, S. J. B. Bauguitte, R. A. Salmon and A. E. Jones (2010), Coupling of HO(x), NO(x) and halogen chemistry in the Antarctic Boundary Layer, *Atmospheric Chemistry and Physics 10,* 10187 – 10209.

Bottenheim, J. W., J. D. Fuentes, D. W. Tarasick and K. G. Anlauf (2002), Ozone in the Arctic lower troposphere during winter and spring 2000 (ALERT2000), *Atmospheric Environment 36*, 2535 – 2544.

Burridge, C.C. (2009), *Isotope tracing of atmospheric aerosols in the sub Arctic Pacific,* Masters of Science Dissertation, Memorial University of Newfoundland.

Calhoun, J.A. (1990), *Chemical and Isotopic Methods for Understanding the Natural Marine Sulfur Cycle,* Doctor of Philosophy Dissertation, Department of Chemistry, University of Washington.

Chang, R. (2011), Personal Communication, Department of Chemistry, University of Toronto.

Chang, R. Y. W., S. J. Sjostedt, J. R. Pierce, T. N. Papakyriakou, M. G. Scarratt, S. Michaud, M. Levasseur, W. R. Leaitch, and J. P. D. Abbatt (2011), Relating atmospheric and oceanic DMS levels to particle nucleation events in the Canadian Arctic, *Journal of Geophysical Research 116*, D00S03.

Charlson, R. J., J. E. Lovelock, M. O. Andreae and S. G. Warren (1987), Oceanic Phytoplankton, atmospheric sulfur, cloud albedo, climate, *Nature 326*, 655 – 661.

Charlson, R. J., T. L. Anderson and R. E. McDuff (1992), The Sulfur Cycle, from *Global Biogeochemical cycles,* ed. S.S. Butcher, R. J. Charlson, G. H. Orians and G. V. Wolfe, Academic Press, London.

Chen, G., L. G. Huey, J. H. Crawford, J. R. Olson, M. A. Hutterli, S. Sjostedt, D. Tanner, J. Dibb, B. Lefer, N. Blake, D. Davis and A. Stohl (2007), An assessment of the polar HOx photochemical budget based on 2003 Summit Greenland field observations, *Atmospheric Environment 41,* 7806 – 7820.

Cheng, M. H., P. K. Hopke, L. Barrie, A. Rippe, M. Olson and S. Landsberger (1993), Qualitative Determination of Source Regions of Aerosol in Canadian High Arctic, *Environmental Science and Technology 27*, 2063 – 2071.

Conley, S. A., I. Faloona, G. H. Miller, D. H. Lenschow, B. Blomquist and A. Bandy (2009), Closing the dimethyl sulfide budget in the tropical marine boundary layer during the Pacific Atmospheric Sulfur Experiment, *Atmospheric Chemistry and Physics 9,* 8745 – 8756.

CRC Handbook of Chemistry and Physics (83rd ed.) (2002), ed. D. R. Lide, CRC Press, New York.

Crutzen P. J and M. O. Andreae (1990), Biomass Burning in the Tropics: Impact on Atmospheric Chemistry and Biogeochemical Cycles, *Science 250*, 1669 – 1678.

Davis, D., G. Chen, P. Kasibhatla, A. Jefferson, D. Tanner, F. Eisele, D. Lenschow, W. Neff and H. Berresheim (1998), DMS oxidation in the Antarctic marine boundary layer: Comparison of model simulations and field observations of DMS, DMSO, $DMSO_2$, $H_2SO_{4(g)}$, $MSA_{(g)}$, and $MSA_{(p)}$, *Journal of Geophysical Research 103(D1)*, 1657 – 1678.

Davis, D., G. Chen, A. Bandy, D. Thornton, F. Eisele, L. Mauldin, D. Tanner, D. Lenschow, H. Feulberg, B. Huebert, J. Health, A. Clarke, and D. Blake (1999), *Journal of Geophysical Research 104*, 5765 – 5784.

DIONEX Corporation (1997), *Determination of Trace Anions in High-Purity Waters Using Direct Injection and Two-Step Isocratic Ion Chromatography,* Application Note 114.

DIONEX Corporation (2003), *Product Manual; IONPAC® AS14 Guard Column and IONPAC® AS14 Analytical Column,* Document No.031199, Revision 06.

Douglas, T., M. Sturm, W. Simpson, S. Brooks, S. Lindberg, and D. Perovich (2005), Elevated mercury measured in snow and frost flowers near Arctic sea ice leads, *Geophysical Research Letters 32*, L04502, doi:10.1029/2004GL022132.

Douglas, T. A., F. Domine, M. Barret, C. Anastasio, H. J. Beine, J. Bottenheim, A. Grannas, S. Houdier, S. Netcheva, G. Rowland, R. Staebler and A. Steffen (2012), Frost flowers growing in the Arctic ocean-atmosphere–sea ice–snow interface: 1. Chemical composition, *Journal of Geophysical Research 117*, D00R09.

Dougle, P. G. and H. M. Brink (1996), Evaporative Losses of Ammonium Nitrate in Nephelometry and Impactor Measurements, *Journal of Aerosol Science 27*, *Suppl., 1,* S511 – S512.

Draxler, R. R. and G. D. Rolph, (2011). HYSPLIT (HYbrid Single-Particle Lagrangian Integrated Trajectory) Model access via NOAA ARL READY, Website http://www.arl.noaa.gov/ready/hysplit4.html, NOAA Air Resources Laboratory, Silver Spring, MD.

Dudzinska-Huczuk, B. and J. Bolalek (2007), Particulate Selenium in the Baltic Sea Atmosphere, *Water, Air and Soil Pollution 179,* 29 – 41.

Eaton, J. J. (2006), *Source Apportionment of Sulphate Aerosols and Gaseous Sulphur Dioxide over the NW Atlantic during the Spring SABINA Cruise 2003 using Stable Isotopes,* Masters of Science Dissertation, Memorial University of Newfoundland.

Edwards, P., M. J. Evans, R. Commane, T. Ingham, D. Stone, A. S. Mahajan, H. Oetjen, J. R. Dorsey, J. R. Hopkins, J. D. Lee, S. J. Moller, R. Leigh, J. M. C. Plane, L. J. Carpenter, and D. E. Heard (2011), Hydrogen oxide photochemistry in the northern Canadian spring time boundary layer, *Journal of Geophysical Research 116*, D22306.

Elliott, S. (2009), Dependence of DMS global sea-air flux distribution on transfer velocity and concentration field type, *Journal of Geophysical Research, 114,* G02001, doi:10.1029/2008JG000710.

Else, B. G. T., T. N. Papakyriakou, R. J. Galley, W. M. Drennan, L. A. Miller, and H. Thomas (2011), Wintertime CO_2 fluxes in an Arctic polynya using eddy covariance: Evidence for enhanced air –sea gas transfer during ice formation *Journal of Geophysical Research 116,* C00G03, doi:10.1029/2010JC006760.

Environment Canada (2011), *National Climate Data and Information Archive* http://www.climate.weatheroffice.gc.ca.

Erickson, D. J., S. J. Ghan and J. E. Penner (1990), Global Ocean-to-Atmosphere Dimethyl Sulfide Flux, *Journal of Geophysical Research 95*, 7543 – 7552.

Faloona, I. (2009), Sulfur processing in the marine atmospheric boundary layer: A review and critical assessment of modeling uncertainties, *Atmospheric Environment 43*, 2841 – 2854.

Ferek, R. J., P. V. Hobbs, L. F. Radke, J. A. Herring, W. T. Sturges and G. F. Cota (1995), Dimethyl sulfide in the Arctic atmosphere, *Journal of Geophysical Research 100*, *D(12),* 26093 – 26104.

Finlayson-Pitts, B. J. and J. N. Pitts Jr. (2000), *Chemistry of the upper and lower atmosphere*, Academic Press, San Diego, CA.

Fisheries and Oceans Canada (2010), *Key Findings from International Polar Year 2007-2008 at Fisheries and Oceans Canada: Executive Summary*, Ottawa, Communications Branch of Fisheries and Oceans Canada.

François, F., W. Maenhaut, J. L. Colin, R. Losno, M. Schulz, T. Stahlschmidt, L. Spokes and T. Jickells (1995), Intercomparison of Elemental Concentrations in Total and Size-Fractionated aerosol samples collected during the Mace Head Experiment, April 1991, *Atmospheric Environment 29*, 837 – 849.

Freedman, B., V. Zobens, T. C. Hutchinson and W. I. Gizyn, 1990, Intense, Natural Pollution Affects Arctic Tundra Vegetation at the Smoking Hills, Canada, *Ecology, 71,* 392 – 503.

Fritz, J. S. and D. T. Gjerde (2000), *Ion Chromatography,* Wiley-Vch, Weinheim, Germany.

Gabric, A. J., B. Qu, P. Matrai and A. C. Hirst (2005), The simulated response of dimethylsulfide production in the Arctic Ocean to global warming, *Tellus 57B*, 391 – 403.

Gautrois, M., T. Brauers, R. Koppmann, F. Rohrer, O. Stein, and J. Rudolph (2003), Seasonal variability and trends of volatile organic compounds in the lower polar troposphere, *Journal of Geophysical Research 108(D13),* 4393, doi:10.1029/2002JD002765.

Gershenzon, M., P. Davidovits, J. T. Jayne, C. E. Kolb and D. R. Worsnop (2001), Simultaneous Uptake of DMS and Ozone on Water, *The Journal of Physical Chemistry A 105,* 7031 – 7036.

Giesemann, A., H.-J. Jäger, A. L. Norman, H. R. Krouse, and W. A. Brand (1994), Online Sulfur-Isotope Determination Using an Elemental Analyzer Coupled to a Mass Spectrometer, *Analytical Chemistry 66*, 18, 2816 – 2819.

Grannas, A. M., A. E. Jones, J. Dibb, M. Ammann, C. Anastasio, H. J. Beine, M. Bergin, J. Bottenheim, C. S. Boxe, G. Carver, G. Chen, J. H. Crawford, F. Dominé, M. M. Frey, M. I. Guzmán, D. E. Heard, D. Helmig, M. R. Hoffmann, R. E. Honrath and L. G. Huey (2007), An overview of snow photochemistry: evidence, mechanisms and impacts, *Atmospheric Chemistry & Physics 7,* 4329 – 4373.

Grey, B. A., Y. Wang, D. Gu, A. Bandy, L. Mauldin, A. Clarke, B. Alexander and D. D. Davis (2011), Sources, transport, and sinks of SO_2 over the equatorial Pacific during the Pacific Atmospheric Sulfur Experiment, *Journal of Atmospheric Chemistry 68,* 27 – 53.

Haddad, P. R. and P. E. Jackson (1990), *Ion Chromatography: principles and applications*, Elsevier, New York.

Hara, K., K. Osada, M. Hayashi, K. Matsunaga and Y. Iwasaka, (1997), Variation of Concentrations of Sulfate, Methanesulfonate and Sulfur Dioxide at Ny-ålesund in 1995/96 Winter, *Proceedings of the NIPR Symposium on Polar Meteorology and Glaciology 11*., 127 – 137.

Hara, K., K. Osada, M. Hayashi, K. Matsunaga, T. Shibata, Y. Iwasaka and K. Furuya (1999), Fractionation of inorganic nitrates in winter Arctic troposphere: Coarse aerosol particles containing inorganic nitrates, *Journal of Geophysical Research 104(D19),* 23671 – 23680.

Hara, K., K. Osada, M. Kido, M. Hayashi, K. Matsunaga, Y. Iwasaka, T. Yamanouchi, G. Hashida and T. Fukatsu (2004), Chemistry of sea-salt particles and inorganic halogen species in Antarctic regions: Compositional differences between coastal and inland stations, *Journal of Geophysical Research 109*, D20208.

Haywood J. and O. Boucher (2000), Estimates of the Direct and Indirect Radiative Forcing Due to Tropospheric Aerosols: A review, *Reviews of Geophysics, 38*, 515 – 543.

Hegg, D. A., L. F. Radke, P. V. Hobbs, and P. J. Riggan (1988), Ammonia emissions from biomass burning, *Geophysical Research Letters 15,* 335 – 337.

Helmig, D., S. J. Oltmans, D. Calson, J. F. Lamarque, A. Jones, C. Labuschagne, K. Anlauf and K. Hayden (2007), A review of surface Ozone in the Polar Regions, *Atmospheric Environment 41,* 5138 – 5161.

Ho, D. T., R. Wanninkhof, P. Schlosser, D. S. Ullman, D. Hebert, and K. F. Sullivan (2011), Toward a universal relationship between wind speed and gas exchange: Gas transfer velocities measured with $^3He/SF_6$ during the Southern Ocean Gas Exchange Experiment, *Journal of Geophysical Research 116*, C00F04, doi:10.1029/2010JC006854.

Holton, J. R. (1992), *An Introduction to Dynamic Meteorology, 3rd ed.*, Academic Press, Inc, Toronto.

Hoornaert, S., H. van Malderen and R. van Grieken (1996), Gypsum and Other Calcium-Rich Aerosol Particles above the North Sea, *Environmental Science and Technology 30,* 1515 – 1520.

Huebert, B. J., B. W. Blomquist, J. E. Hare, C. W. Fairall, J. E. Johnson and T. S. Bates (2004), Measurement of the sea-air DMS flux and transfer velocity using eddy correlation, *Geophysical Research Letters 31,* L23113, doi:10.1029/2004GL021567.

International Union of Pure and Applied Chemistry (IUPAC) Subcommittee for Gas Kinetic Data Evaluation (2009), *Evaluated Kinetic Data* (http://www.iupac-kinetic.ch.cam.ac.uk/).

Jacobi, H. W., D. Voisin, J. L. Jaffrezo, J. Cozic, and T. A. Douglas (2012), Chemical composition of the snowpack during the OASIS spring campaign 2009 at Barrow, Alaska, *Journal of Geophysical Research 117*, D00R13, doi:10.1029/2011JD016654.

Jefferson, A., D. J. Tanner, F. L. Eisele and H. Berresheim (1998), Sources and sinks of H_2SO_4 in the remote Antarctic marine boundary layer, *Journal of Geophysical Research 103(D1)*, 1639 – 1645.

Jobson, B. T., H. Niki, Y. Yokouchi, J. Bottenheim, F. Hopper and R. Leaitch (1994), Measurements of C_2-C_6 hydrocarbons during the Polar Sunrise 1992 Experiment: Evidence for Cl atom and Br atom chemistry, *Journal of Geophysical Research 99(D12),* 25355 – 25368.

Johnson M. S., K. L. Feilberg, P. von Hessberg and O. J. Nielsen (2002), Isotopic processes in atmospheric chemistry, *Chemical Society Reviews 31*, 313 – 323.

Jonsell, U., M. E. Hansson, C. M. Morth and P. Torssander (2005), Sulfur isotopic signals in two shallow ice cores from Dronning Maud Land, Antarctica, *Tellus 57B*, 341 – 350.

Jourdain, B., and M. Legrand (2001), Seasonal variations of atmospheric dimethylsulfide, dimethylsulfoxide, sulfur dioxide, methanesulfonate, and non-sea-salt sulfate aerosols at Dumont d'Urville (coastal Antarctica) (December 1998 to July 1999), *Journal of Geophysical Research 106*, 14391 – 14408.

Kaleschke, L., A. Richter, J. Burrows, O. Afe, G. Heygsterm J. Notholt, A. M. Rankin, H. K. Roscoe, J. Hollwedel, T. Wagner and H. W. Jacobi (2004), Frost flowers on sea ice as a source of sea salt and their influence on tropospheric halogen chemistry, *Geophysical Research Letters 31*, L16114.

Karlsson, R. and E. Ljungström (1995), Nitrogen dioxide and sea salt particles-A laboratory study, *Journal of Aerosol Science 26,* 39 – 50.

Kaufman, Y., D. Tanré and O. Boucher (2002), A Satellite View of Aerosols in the climate system, *Nature 419*, 215 – 223.

Kerminen, V. M. and C. Leck (2001), Sulfur chemistry over the central Arctic Ocean during the summer: Gas-to-particle transformation, *Journal of Geophysical Research 106(D23),* 32087 – 32099.

Kukui, A., D. Borissenko, G. Laverdet, and G. Le Bras (2003), Gas-phase reactions of OH radicals with dimethyl sulfoxide and methane sulfinic acid using turbulent flow reactor and chemical ionization mass spectrometry, *The Journal of Physical Chemistry A 107,* 5732 – 5742.

Kunasek, S. A., B. Alexander, E. J. Steig, E. D. Sofen, T. L. Jackson, M. H. Thiemens, J. R. McConnell, D. J. Gleason and H. M. Amos (2010), Sulfate sources and oxidation chemistry over the past 230 years from sulfur and oxygen isotopes of sulfate in a West Antarctic ice core, *Journal of Geophysical Research 115*, D18313.

Laskin, A., D. J. Gaspar, W. Wang, S. W. Hunt, J. P. Cowin, S. D. Colson, B. J. Finlayson-Pitts (2003), Reactions at Interfaces As a Source of Sulfate Formation in Sea – Salt Particles, *Science 301,* 340 – 344, DOI: 10.1126/science.1085374.

Leck, C. and C. Persson (1996*a*), The central Arctic Ocean as a source of dimethyl sulphide Seasonal variability in relation to biological activity, *Tellus 48B,* 156 – 177.

Leck, C. and C. Persson (1996*b*), Seasonal and short-term variability in dimethyl sulfide, sulfur dioxide and biogenic sulfur and sea salt aerosol particles in the marine boundary layer during summer and autumn, *Tellus 48B,* 272 – 299.

Leck, C. and E. K. Bigg (2005), Biogenic particles in the Surface Microlayer and overlaying Atmosphere in the Central Arctic Ocean during Summer, *Tellus 57B*, 305 – 316.

Lefer, B. L., S. R. Hall, L. Cinquini and R. E. Shetter (2001), Photolysis frequency measurements at the South Pole during ISCAT‐98, *Geophysical Research Letters 28,* 3637 – 3640.

Levasseur, M., S. Sharma, G. Cantin, S. Michaud, M. Gosselin and L. A. Barrie (1997), Biogenic sulfur emissions from the Gulf of St. Lawrence and assessment of its impact on the Canadian East Coast, *Journal of Geophysical Research 102,* 28025 – 28039.

Lewis, E. R. and S. E. Schwartz (2004), *Sea salt aerosol production. Mechanisms, methods, measurements, and models,* American Geophysical Union, Washington, D.C.

Li, S. M. and J. W. Winchester (1989*a*), Geochemistry of Organic and inorganic ions of late winter arctic aerosols, *Atmospheric Environment 23,* 2401 – 2415.

Li, S. M. and J. W. Winchester (1989*b*), Resolution of Ionic Components of Late Arctic Aerosols, *Atmospheric Environment, 23* 2387 – 2399.

Li, S. M. and L. A. Barrie (1993), Biogenic Sulfur Aerosol in the Arctic Troposphere Contributions to Total Sulfate, *Journal of Geophysical Research 98*, 20613 – 20622.

Li, S. M., L. A. Barrie, R. W. Talbot, R. C. Harriss, C. I. Davidson and J. L. Jaffrezo (1993), Seasonal and Geographic Variations of Methanesulfonic acid in the Arctic Troposphere, *Atmospheric Environment 27A*, 3011 – 3024.

Liang, Q., J. M. Rodriguez, A. R. Douglass, J. H. Crawford, J. R. Olson, E. Apel, H. Bian, D. R. Blake, W. Brune, M. Chin, P. R. Colarco, A. da Silva, G. S. Diskin, B. N. Duncan, L. G. Huey, D. J. Knapp, D. D. Montzka, J. E. Nielsen, S. Pawson, D. D. Riemer, A. J. Weinheimer, and A. Wisthaler (2011), Reactive nitrogen, ozone and ozone production in the Arctic troposphere and the impact of stratosphere-troposphere exchange, *Atmospheric Chemistry and Physics 11,* 13181 – 13199.

Liao, J., L. G. Huey, D. J. Tanner, N. Brough, S. Brooks, J. E. Dibb, J. Stutz, J. L. Thomas, B. Lefer, C. Haman and K. Gorham (2011), Observations of hydroxyl and peroxyl radicals and the impact of BrO at Summit, Greenland in 2007 and 2008, *Atmospheric Chemistry and Physics 11,* 8577 – 8591.

Light, B., G. A. Maykut and T. C. Grenfell (2003), Effects of Temperature on the microstructure of first-year Arctic sea ice, *Journal of Geophysical Research 108(C3),* 3051.

Liss, P. S. and L. Merlivat (1986), Air-gas exchange rates: introduction and synthesis, from *The Role of Air-Sea Exchange in Geochemical Cycling*, ed. P. Buat-Menard, 113 – 127.

Lovelock, J. E., R. J., Maggs and R. A. Rasmussen (1972), Atmospheric Dimethyl Sulphide and the Natural Sulphur Cycle, *Nature 237*, 452 – 453.

Ludén, J., G. Svensson, A. Wisthaler, M. Tjernström, A. Hansel and G. Leck (2010), The vertical distribution of atmospheric DMS in the high Arctic summer, *Tellus 62B*, 160 – 171.

Mabilia, R., V. Di Palo, C. Cassardo, C. Ciuchini, A. Pasini and M. Possanzini (2007), Measurements of lower Carbonyls and Hydrocarbons at Ny-Alesund, Svalbard, *Annali Di Chimica 97,* 1027 – 1037.

Mahajan, A. S., M. Shaw, H. Oetjen, K. E. Hornsby, L. J. Carpenter, L. Kaleschke, X. Tian-Kunze, J. D. Lee, S. J. Moller, P. Edwards, R. Commane, T. Inghan, D. E. Heard and J. M. Plane (2010), Evidence of reactive iodine chemistry in the Arctic boundary layer, *Journal of Geophysical Research 115*, D20303.

Maidment, D.R. (ed.), (1993), *Handbook of Hydrology*, McGraw-Hill, New York.

Mao, J., D. J. Jacob, M. J. Evans, J. R. Olson, X. Ren, W. H. Brune, J. M. St. Clair, J. D. Crounse, K. M. Spencer, M. R. Beaver, P. O. Wennberg, M. J. Cubison, J. L. Jimenez, A. Fried, P. Weibring, J. G. Walega, S. R. Hall, A. J. Weinheimer, R. C. Cohen, G. Chen, J. H. Crawford, C. McNaughton, A. D. Clarke, L. Jaeglé, J. A. Fisher, R. M. Yantosca, P. Le Sager and C. Carouge (2010), Chemistry of hydrogen oxide radicals (HO_x) in the Arctic troposphere in spring, *Atmospheric Chemistry and Physics 10,* 5823 – 5838.

Martin, L. R. (1984), Kinetic Studies of Sulfite Oxidation in Aqueous Solution, from *SO_2, NO and NO_2 Oxidation Mechanisms: Atmospheric Considerations*, ed. J. G. Calvert, Acid Precipitation Series Volume 3, Butterworth Publishers, Toronto, 63 – 100.

Martin, L. R. (1991), Aqueous Sulfur(IV) Oxidation Revisited, from *Environmental Oxidants, Advances in Environmental Science and Technology vol. 28*, ed. J. O Nriagu and M. S. Simmons, John Wiley & Sons, Inc., New York, 221 – 268.

Martin, S., R. Drucker and M. Fort (1995), A laboratory study of frost flower growth on the surface of young sea ice, *Journal of Geophysical Research 100(C4),* 7027 – 7036.

Martin, S., Y. Yu and R. Drucker (1996), The temperature dependence of frost flower growth on laboratory sea ice and the effect of the flowers on infrared observations of the surface, *Journal of Geophysical Research 101(C5),* 12111 – 12125.

McArdle, N., P. Liss and R. Dennis (1998), An isotopic study of atmospheric sulphur at three sites in Wales and at Mace Head, Eire, *Journal of Geophysical Research 103,* 31079 – 31094.

McInnes, L.M., D. S. Covert, P. K. Quinn and M. S. Germani (1994), Measurements of Chloride Depletion and Sulfur Enrichment in Individual Sea-Salt Particles collected from the Remote Marine Boundary-Layer, *Journal of Geophysical Research 99,* 8257 – 8268.

McMurry, P.H. (2000), A review of atmospheric aerosol measurements, *Atmospheric Environment 34,* 1959 – 1999.

Mihalopoulos, N., V. M. Kerminen, M. Kanakidou, H. Berresheim and J. Sciare (2007), Formation of particulate Sulfur species (sulfate and methanesulfonate) during summer over the Eastern Mediterranean: A modelling approach, *Atmospheric Environment 41*, 6860 – 6871.

Minikin A., D. Wagenbach, W. Graf and J. Kipfstuhl (1994), Spatial and seasonal variations of the snow chemistry at the central Filchner-Ronne Ice Shelf, Antarctica, *Annals of Glaciology 20*, 283 – 290.

Minikin, A., M. Legrand, J. Hall, D. Wagenbach, C. Kleefeld, E. Wolff, E. C. Pasteur and F. Ducroz (1998), Sulfur-containing species (sulfate and methanesulfonate) in coastal Antarctic aerosol and precipitation*, Journal of Geophysical Research 103(D9),* 10975 – 10990.

Morin, S., G. M. Marion, R. von Glasow, D. Voisin, J. Bouchez and J. Savarino (2008) Precipitation of salts in freezing seawater and ozone depletion events: a status report, *Atmospheric Chemistry and Physics 8*, 7317 – 7324.

Newman, L. (1981), Atmospheric Oxidation of Sulfur Dioxide: A Review as viewed from Power Plant and smelter Plume Studies, *Atmospheric Environment 15*, 2231 – 2239.

Nielsen, H. (1974), Isotopic composition of the major contributors to atmospheric sulfur, *Tellus 26*, 213 – 220.

Nightingale P. D., G. Malin, C. S. Law, A. J. Watson, P. S. Liss, M. I. Liddicoat, J. Boutin, and R. C. Upstill-Goddard (2000), In situ evaluation of air-sea gas exchange parameterizations using novel conservative and volatile tracers, *Global Biogeochemical Cycles 14*, 373 – 387.

Nilsson, E. D. and C. Leck (2002), A pseudo-Lagrangian study of the sulfur budget in the remote Arctic marine boundary layer, *Tellus 54B*, 213 – 230.

Norman, A. L., L. A. Barrie, D. Toom-Sauntry, A. Sirois, H. R. Krouse, S. M. Li, and S. Sharma (1999), Sources of aerosol sulphate at Alert: Apportionment using stable isotopes, *Journal of Geophysical Research 104,* 11619 – 11631.

Norman, A. L. and M. A. Wadleigh (2007), Dimethyl Sulphide (DMS) and its oxidation to Sulphur Dioxide Downwind of an Ocean Iron Fertilization Study, SERIES: A Model for DMS Flux, from *Air Pollution Modeling and its Application XVII,* Ed. C. Borrego and A-L. Norman, Springer, New York, 237 – 244.

Norman, A. L., W. Belzer and L. Barrie (2004), Insights into the biogenic contribution to total sulphate in aerosol and precipitation in the Faser Valley afforded by isotopes of sulphur and oxygen, *Journal of Geophysical Research 109,* DO5311.

Norman, A. L., O. Rempillo, K. Alam, S. Sharma, D. Toom-Sauntry, A. Siaw, S. L. Gong, S. Howell, E. Chan, J. Yackel, and L. A. Barrie (submitted), Aerosol Sulphate from DMS in the Arctic: Evidence for a Biotic Feedback to Warming?, *Nature*.

Nriagu, J. O., R. D. Coker, and L. A. Barrie (1991), Origin of Sulphur in Canadian Arctic Haze from Isotope Measurements, *Nature 349*, 142 – 145.

Obbard, R. W., H. K. Roscoe, E. W. Wolff, and H. M. Atkinson (2009), Frost flower surface area and chemistry as a function of salinity and temperature, *Journal of Geophysical Research 114,* D20305.

Osthoff, H. D., R. Sommariva, T. Baynard, A. Pettersson, E. J. Williams, B. M. Lerner, J. M. Roberts, H. Stark, P. D. Goldan, W. C. Kuster, T. S Bates, D. Coffman, A. R. Ravishankara and S. S. Brown (2006), Observation of daytime N_2O_5 in the Marine Boundary Layer during New England Air Quality Study–Intercontinental Transport and Chemical Transformation 2004, *Journal of Geophysical Research 111,* D23S14.

Osthoff, H. D., M. J. Pilling, A. R., Ravishankara and S. S. Brown (2007), Temperature dependence of the NO_3 absorption cross-section above 298 K and determination of the equilibrium constant for $NO_3 + NO_2 \leftrightarrow N_2O_5$ at atmospherically relevant conditions, *Physical Chemistry Chemical Physics 9*, 5785 – 5793.

Osthoff, H. D., T. S. Bates, J. E. Johnson, W. C. Kuster, P. Goldan, R. Sommariva, E. J. Williams, B. M. Lerner, C. Warneke, J. A. de Gouw, A. Pettersson, T. Baynard, J. F. Meagher, F. C. Fehsenfeld, A. R. Ravishankara and S. S. Brown (2009), Regional variation of the dimethyl sulfide oxidation mechanism in the summertime marine boundary layer in the Gulf of Maine, *Journal of Geophysical Research 114*, D07301.

Pacyna, J. M. (1991), Chemical Tracers of the Origins of Arctic Air Pollution, from *Pollution of the Arctic Atmosphere*, ed W.T. Sturges, Elsevier Science Publishers, New York, 97 – 122.

Patris, N., R. J. Delmas, and J. Jouzel (2000), Isotopic signatures of sulfur in shallow Antarctic ice cores, *Journal of Geophysical Research 105,* 7071 – 7078.

Patris, N., R. J. Delmas, M. Legrand, M. De Angelis, F. A. Ferron, M. Stièvenard, M. and J. Jouzel (2002), First sulfur isotope measurements in central Greenland ice cores along the preindustrial periods, *Journal of Geophysical Research 107,* D000672.

Perovich, D. K. (1996), *The Optical Properties of Sea Ice*, Monograph 96-1, US Army Corps of Engineers; Cold Regions Research & Engineering Laboratory, Office of Naval Research.

Perovich, D. K. and J. A. Richter-Menge (1994), Surface characteristics of lead ice, *Journal of Geophysical Research 99(C8),* 16341 – 16350.

Perovich, D., W. Meier, J. Maslanik and J. Richter-Menge (2011), Sea Ice from *Arctic Report Card: 2011*, http://www.arctic.noaa.gov/reportcard.

Piot, M., and R. von Glasow (2008) The potential importance of frost flowers, recycling on snow, and open leads for ozone depletion events, *Atmospheric Chemistry and Physics 8*, 2537 – 2467.

Plane, J. M. C. (1989), Gas-Phase Atmospheric Oxidation of Biogenic Sulfur Compounds: A review, from *Biogenic Sulfur in the Environment* ed. E. Saltzman and W. J. Cooper ACS Symposium Series; American Chemical Society, Washington, 405 – 423.

Platt, U. and G. Hönninger (2003), The role of halogen species in the troposphere, *Chemosphere 52,* 325 – 388.

Quinn P. K. and T. S. Bates (2011), The case against climate regulation via oceanic phytoplankton sulphur emissions, *Nature 480*, 51 – 56.

Quinn P. K., G. Shaw, E. Andrews, E. G. Dutton, T. Ruoho-Airola and S. L. Gong (2007), Arctic haze: current trends and knowledge gaps, *Tellus 59*, 99 – 114.

Quinn P. K., T. S. Bates, K. Schulz and G. E. Shaw (2009), Decadal trends in aerosol chemical composition at Barrow, Alaska: 1976 – 2008, *Atmospheric Chemistry and Physics 9,* 8883 – 8888.

Raatz, W. E. (1991), The Climatology and Meteorology of Arctic Air Pollution, from *Pollution of the Arctic Atmosphere*, ed W.T. Sturges, Elsevier Science Publishers, New York, 13 – 42.

Radke, L. F. and P. V. Hobbs (1989), Arctic hazes in summer over Greenland and the North American Arctic. III. A contribution from the natural burning of carbonaceous materials and pyrites, *Journal of Atmospheric Chemistry 9*, 161 – 167.

Rankin, A. M., and E. W. Wolff (2003), A year-long record of size-segregated aerosol composition at Halley, Antarctica, *Journal of Geophysical Research 108(D24*), 4775.

Rankin, A. M., E. W. Wolff and S. Martin (2002), Frost Flowers: Implications for tropospheric chemistry and ice core interpretation, *Journal of Geophysical Research 107(D23),* 4683.

Rees, C. E., W. J. Jenkins, and J. Monster (1978), Sulphur Isotopic Composition of Ocean Water Sulfate, *Geochimica et Cosmochimica Acta 42,* 377 – 381.

Rempillo, O. T. (2011), *Dimethyl Sulfide and Aerosol Sulfate in the Arctic Atmosphere*, Doctor of Philosophy Thesis, Department of Physics and Astronomy, University of Calgary.

Rempillo, O. T. (2012), Personal Communication, Department of Physics and Astronomy, University of Calgary.

Rempillo, O. T., A. M. Seguin, A. L. Norman, M. Scharratt, S. Michaud, R. Chang, S. Sjostedt, J. Abbatt, B. Else, T. Papakyriakou, S. Sharma, S. Grasby and M. Levasseur (2011), DMS air-sea fluxes and biogenic sulfur as a source of new aerosols in the Arctic fall, *Journal of Geophysical Research 116,* D00S04.

Ricard, V., J. L. Jaffrezo, V. M. Kerminen, R. E. Hillamo, K. Teinilä, and W. Maenhaut (2002), Size distributions and modal parameters of aerosol constituents in northern Finland during the European Arctic Aerosol Study, *Journal of Geophysical Research 107*(*D14*), 4208.

Richardson, C. (1976), Phase relationships in sea ice as a function of temperature, *Journal of Glaciology 17,* 507 – 519.

Ridley, B. A. and J. J. Orlando (2003), Active Nitrogen in Surface Ozone Depletion Events at Alert during Spring 1998, *Journal of Atmospheric Chemistry 44,* 1 – 22.

Riedel, K., W. Allan, R. Weller and O. Schrems (2005), Discrepancies between formaldehyde measurements and methane oxidation model predictions in the Antarctic troposphere: An assessment of other possible formaldehyde sources, *Journal of Geophysical Research 110*, D15308.

Roscoe, H. K., B. Brooks, A. V. Jackson, M. H. Smith, S. J. Walker, R. W. Obbard, and E. W. Wolff (2011), Frost flowers in the laboratory: Growth, characteristics, aerosol, and the underlying sea ice, *Journal of Geophysical Research 116,* D12301.

Roth, E., R. Létolle, C. M. Stevens, and F. Robert (2006), Isotope Effects in the Atmosphere, from *Isotope Effects in Chemistry and Biology,* ed. A. Kohen and H. H. Limbach, CRC Press; Taylor & Francis Group, Boca Raton, Florida, 387 – 416.

Saiz-Lopez, A., A. S. Mahajan, R. A. Salmon, S. J. B. Bauguitte, A. E. Jones, H. K. Roscoe and J. M. Plane (2007), Boundary Layer Halogens in Coastal Antarctica, *Science 317*, 348 – 351.

Saltzman, E.S., G.W. Brass and D.A. Price (1983), The Mechanism of Sulfate Aerosol Formation: Chemical and Sulfur Isotopic Evidence, *Geophysical Research Letters 10,* 513 – 516.

Saltzman, E. S., D. B. King, K. Holmen, and C. Leck (1993), Experimental determination of the diffusion coefficient of dimethylsulfide in water, *Journal of Geophysical Research 98(C9),* 16481 – 16486.

Sander, R., W. C., Keene, A. A. P. Pszenny, R. Arimoto, G. P. Ayers, E. Baboukas, J. M. Cainey, P. J. Crutzen, R. A. Duce, G. Hönninger, B. J. Huebert, W. Maenhaut, N. Mihalopoulos, V. C. Turekian and R. Van Dingenen (2003), Inorganic bromine in the marine boundary layer: a critical review, *Atmospheric Chemistry and Physics 3*, 1301 – 1336.

Sander, R., J. Burrows and L. Kaleschke (2006), Carbonate precipitation in brine – a potential trigger for tropospheric ozone depletion events, *Atmospheric Chemistry and Physics 6*, 4653 – 4658.

Sander, S. P., J. Abbatt, J. R. Barker, J. B. Burkholder, R. R. Friedl, D. M. Golden, R. E. Huie, C. E. Kolb, M. J. Kurylo, G. K. Moortgat, V. L. Orkin and P. H. Wine (2011), *Chemical Kinetics and Photochemical Data for Use in Atmospheric Studies, Evaluation No. 17*, JPL Publication 10-6, Jet Propulsion Laboratory, Pasadena, http://jpldataeval.jpl.nasa.gov.

Sarin, M., A. Kumar, B. Srinivas, A. K. Sudheer and N. Rastogi (2010), Anthropogenic sulphate aerosols and large Cl-deficit in marine atmospheric boundary layer of tropical Bay of Bengal, *Journal of Atmospheric Chemistry 66,* 1 – 10.

Savoie, D. L., R. Arimoto, W. C. Keene, J. M. Prospero, R. A. Duce, and J. N. Galloway (2002), Marine biogenic and anthropogenic contributions to non-sea-salt sulfate in the marine boundary layer over the North Atlantic Ocean, *Journal of Geophysical Research 107,* 4356 – 4377.

Schaap, M., G., Spindler, M. Schulz, K. Acker, W. Maenhaut, A. Berner, W. Wieprecht, N. Streit, K. Müller, E. Brüggemann, X. Chi, J. P. Putaud, R. Hitzenberger, H. Puxbaum, U. Baltensperger and H. ten Brink (2004), Artifacts in the sampling of nitrate studied in the "INERCOMP" campaigns of EUROTRAC-AEROSOL, *Atmospheric Environment 38*, 6487 – 6496.

Sciare, J., E. Baboukas, M. Kanakidou, U. Krischke, S. Belviso, H. Bardouki and N Mihalopoulos (2000), Spatial and temporal variability of atmospheric sulfur-containing gases and particles during the Albatross campaign, *Journal of Geophysical Research 105,* 14433 – 14448.

Seguin, A.M. (2007), *Inferences from Atmospheric Sulphur using Stable Isotopes over the NW Atlantic*, Masters of Science Thesis, Department of Chemistry, University of Calgary.

Seguin, A. M., A. L. Norman, S. Eaton, M. Wadleigh and S. Sharma (2010), Elevated biogenic sulphur dioxide concentrations over the North Atlantic, *Atmospheric Environment 44,* 1139 – 1144.

Seguin, A. M., A. L. Norman, S. Eaton and M. Wadleigh (2011), Seasonality in size segregated biogenic, anthropogenic and sea salt sulfate aerosols over the North Atlantic, *Atmospheric Environment 45,* 6947 – 6954.

Seinfeld, J. H. and S. N. Pandis (1998), *Atmospheric Chemistry and Physics: From Air Pollution to Climate Change,* John Wiley & Sons, Toronto.

Sharma, S., L. A. Barrie, D. Plummer, J. V. McConnel, P. C. Brickell, M. Levasseur, M. Gosselin and T. S. Bates (1999), Flux estimation of Oceanic Dimethyl Sulfide around North America, *Journal of Geophysical Research 104*, 21327 – 21342.

Shaw, G. E. (1991), Physical Properties and Physical Chemistry of Arctic Aerosols, from *Pollution of the Arctic Atmosphere*, ed. W. T. Sturges, Elsevier Science Publishers, New York, 123 – 154.

Sherman, L. S., J. D. Blum, T. A. Douglas, and A. Steffen (2012), Frost flowers growing in the Arctic ocean–atmosphere–sea ice–snow interface: 2. Mercury exchange between the atmosphere, snow, and frost flowers, *Journal of Geophysical Research 117*, D00R10, doi:10.1029/2011JD016186.

Simpson, W. R., D. Carlson, G. Honninger, T. A. Douglas, M. Sturm, D. Perovich and U. Platt (2007*a*), First-year sea-ice contact predicts bromine monoxoide (BrO) levels at Barrow, Alaska better than potential frost flower contact, *Atmospheric Chemistry and Physics 7*, 621 – 627.

Simpson W. R., R. von Glasow, K. Riedel, P. Anderson, P. Ariya, J. Bottenheim, J. Burrows, L. J. Carpenter, U. Frieß, M. E. Goodsite, D. Heard, M. Hutterli, H. W. Jacobi1, L. Kaleschke, B. Neff, J. Plane, U. Platt, A. Richter, H. Roscoe, R. Sander, P. Shepson, J. Sodeau, A. Steffen, T. Wagner and E.Wolff (2007*b*), Halogens and their role in polar boundary-layer ozone depletion, *Atmospheric Chemistry and Physics 7,* 4375 – 4418.

Singh, H.B (1995), Halogens in the atmospheric environment, from *Composition, Chemistry, and Climate of the Atmosphere,* ed. H. B. Singh, Van Nostrand Reinhold, New York, 216 – 250.

Sirois, A., and L. A. Barrie (1999), Arctic lower tropospheric aerosol trends and composition at Alert, Canada: 1980–1995, *Journal of Geophysical Research 104(D9),* 11599 – 11618.

Sjostedt, S. J., L. G. Huey, D. J. Tanner, J. Peischk, G. Chen, J. E. Dibb, B.Lefer, M. A. Hutterli, A. J. Beyersdorf, N. J. Blake, D. R. Blake, D. Sueper, T. Ryerson, J. Burkhart and A. Stohl (2007), Observations of hydroxyl and the sum of peroxy radicals at Summit, Greenland during summer 2003, *Atmospheric Environment 41*, 5122 – 5137.

Slanina, J., H. M. ten Brink, R. P. Otjes, A. Even, P. Jongejan, A. Khlystov, A. Waijersljpelaan, M. Hu and Y. Lu (2001), The continuous analysis of nitrate and ammonium in aerosols by the steam jet aerosol collector (SJAC): extension and validation of the methodology, *Atmospheric Environment 35*, 2319 – 2330.

Solberg, S., C. Dye, N. Schmidbauer, A. Herzog and R. Gehrig (1996), Carbonyls and Nonmethane Hydrocarbons at Rural European Sites from the Mediterranean to the Arctic, *Journal of Atmospheric Chemistry 25,* 33 – 66.

Solomon, S., D. Qin, M. Manning, R. B. Alley, T. Bernsten, N. L. Bindoff, Z. Chen, A. Chidthaijsong, J. M. Gregory, G. C. Hegerl, M. Heimann, B. Hewitson, B. J. Hoskins, F. Joos, J. Jouzel, V. Kattsov, U. Lohmann, T. Matsuno, M. Molina, N. Nicholls, J. Overpeck, G. Raga, V. Ramaswamy, J. Ren, M. Rusticucci, R. Somerville, T. F. Stocker, P. Whetton, R. A. Wood and D. Wratt (2007), *Technical Summary in Climate Change 2007. The Physical Science Basis. Contribution of Working Group I to the Fourth Assessment Report of the Intergovernmental Panel on Climate Change*, ed. S. Solomon, D. Qin, M. Manning, Z. Chen, M. Marquis, K. B. Averyt, M. Tignor and H. L. Miller, Cambridge University Press, Cambridge.

Stark, H., S. S. Brown, P. D. Goldan, M. Aldener, W. C. Kuster, R. Jakoubek, F. C. Fehsenfeld, J. Meagher, T. S. Bates and A. R. Ravishankara (2007), Influence of Nitrate Radical on the Oxidation of Dimethyl Sulfide in a polluted Marine Environment, *Journal of Geophysical Research 112*, D10S10.

Stephens, C. R., P. B. Shepson, A. Steffen, J. W. Bottenheim, J. Liao, L. G. Huey, E. Apel, A. Weinheimer, S. R. Hall, C. Cantrell, B. C. Sive, D. J. Knapp, D. D. Montzka and R. S. Hornbrook (2012), The relative importance of chlorine and bromine radicals in the oxidation of atmospheric mercury at Barrow, Alaska, *Journal of Geophysical Research 117*, D00R11, doi:10.1029/2011JD016649.

Stonehouse, B, (ed.) (1986), *Arctic Air Pollution*, Cambridge University Press, Cambridge.

Tisch Environmental, Inc (2004), *Series 230 High Volume Cascade Impactors; Multi-Stage Particulate Size Fractionator,* Operations Manual, http://www.tisch-env.com.

Thode, H.G. (1991), Sulphur Isotopes in Nature and the Environment: An Overview, from *Stable Isotopes; Natural and Anthropogenic Sulphur in the Environment, Scope 43,* ed. H. R. Krouse and V.A. Grinenko, John Wiley and Sons, Toronto, 1 – 26.

Trebs, I., M. O. Andrae, W. Elbert, O. Mayol-Bracero, L. Soto-Garcia, Y. Rudich, A. H. Falkovich, W. Maenhaut, P. Artaxo, R. Otjes and J. Slanina (2008), Aerosol inorganic composition at a tropical site: discrepancies between filter-based sampling and a semi-continuous method, *Aerosol Science and Technology 42,* 255 – 269.

Turner, J. and G.J. Marshall (2011) *Climate Change in the Polar Regions*, Cambridge University Press, Cambridge.

Vogt R. (1996), Iodine Compounds in the Atmosphere, from *Reactive Halogen Compounds in the Atmosphere,* ed. P. Fabian and O. N. Singh, Springer, New York, 113 – 128.

Vogt, R., P. J. Crutzen and R. Sander (1996), A mechanism for halogen release from sea-salt aerosol in the remote marine boundary layer, *Nature 383,* 327 – 330.

Vogt, R., R. Sander, R. von Glasow and P. J. Crutzen (1999), Iodine Chemistry and its Role in Halogen Activation and Ozone Loss in the Marine Boundary Layer: A Model Study, *Journal of Atmospheric Chemistry 32,* 375 – 379.

von Glasow, R. and P. J. Crutzen (2004), Model study of multiphase DMS oxidation with a focus on halogens, *Atmospheric Chemistry and Physics 4*, 589 – 608.

von Glasow, R. (2008), Pollution meets Sea Salt, *Nature Geoscience 1,* 292 – 293.

Wadleigh, M. A. (2004), Sulphur isotopic composition of aerosols over the western North Atlantic Ocean, *Canadian Journal of Fishery and Aquatic Sciences 61,* 817 – 925.

Wagenbach, D., F. Ducroz, R. Mulvaney, L. Keck, A. Minikinm, M. Legrand, J. S. Hall, and E. M. Wolff (1998), Sea-salt aerosol in coastal Antarctic regions, *Journal of Geophysical Research 103(D9),* 10961 – 10974.

Wagner, T., C. Otten, K. Pfeilsticker, I. Pundt and U. Platt (2000), DOAS moonlight observation of atmospheric NO_3 in the Arctic winter, *Journal of Geophysical Research 27,* 21, 3441 – 3444.

Wanninkhof, R. H. (1992), Relationship between gas exchange and wind speed over the ocean, *Journal of Geophysical Research 97*, 7373 – 7391.

Wasiuta, V., Norman, A. L., and S. Marshall (2006), Spatial patterns and seasonal variation of snowpack sulphate isotopes of the Prince of Wales Icefield, Ellesmere Island, Canada, *Annals of Glaciology 43*, 390 – 396.

Wayne, R. P., G. Poulet, P. Biggs, J. P. Burrows, R. A. Cox, P. J. Crutzen, G. D. Hayman, M. E. Jenkin, G. Le Bras, G. K. Moortgat, U. Platt and R. N. Schindler (1995), Halogen Oxides: Radicals, sources and reservoirs in the laboratory and in the Atmosphere, *Atmospheric Environment 29,* 2677 – 2881.

Wedding, J. B., T. C. Carney and R. K. Stevens (1980), Ambient Aerosol Sampling: Problems, Goals and Wind Tunnel Test Results of Hi-Volume Samplers, *Environment International 3,* 259 – 264.

Wedding, J. B., Y. J. Kin and J. P. Lodge Jr. (1986), Interpretation of Selected EPA Field Data on Particulate Matter Samplers: Rubidoux and Phoenix II, *Journal of the Air Pollution Control Association 36,* 164 – 170.

Weeks, W.F. (2010), *On Sea Ice*, University of Alaska Press, Fairbanks, Alaska.

Weis, D. D. and G. E. Ewing (1999), The Reaction of Nitrogen Dioxide with Sea Salt Aerosol, *Journal of Physical Chemistry A 103,* 4865 – 4873.

Whitby, K. B. (1978), Physical Characteristics of Sulfur Aerosols, *Atmospheric Environment 12*, 135 – 159.

Whitlow, S., P. Mayewski, J. Dibb, G. Holdsworth and M. Twickler (1994), An Ice-core-based Record of biomass burning in the Arctic and Sub-Arctic, 1750-1980, *Tellus Series B- Chemical and Physical Meteorology 46,* 234 – 242.

Wingenter, O. W., D. R. Blake, N. J. Blake, B. C. Sive, F. S Rowland, E. Atlas and F. Flocke (1999), Tropospheric hydroxyl and atomic chlorine concentrations, and mixing timescales determined from hydrocarbon and halocarbon measurements made over the Southern Ocean, *Journal of Geophysical Research 104,* 21819 – 21828.

Yalcin, K. and C. Wake (2001), Anthropogenic signals recorded in an ice core from Eclipse Icefield, Yukon Territory, Canada, *Geophysical Research Letters 28,* 4487 – 4490.

Yang, M., B. W. Blomquist, C. W. Fairall, S. D. Archer and B. J. Huebert (2011), Air-sea exchange of dimethylsulfide in the Southern Ocean: Measurements from SO GasEx compared to temperate and tropical regions, *Journal of Geophysical Research 116,* C00F05, doi: 10.1029/2010JC006526.

Yin, F., D. Grosjean, J. H. Seinfeld (1990), Photooxidation of Dimethyl Sulfide and Dimethyl Disulfide I: Mechanism Development, *Journal of Atmospheric Chemistry 11*, 309 – 364.

Zemmelink, H.J. (2003), *Dimethyl Sulphide: Measuring Emissions from the ocean to the atmosphere*, Doctor of Philosophy Dissertation, University of Groningen.

Zhao, T. L., S. L. Gong, J. W. Bottenheim, J. C. McConnell, R. Sander, L. Kaleschke, A. Richter, A. Kerkweg, K. Toyota and L. A. Barrie (2008), A three-dimensional model study on the production of BrO and Arctic boundary layer ozone depletion, *Journal of Geophysical Research 113*, D24304.

Zhu, L., A. Nenes, P. H. Wine and J. M. Nicovich (2006), Effects of aqueous organosulfur chemistry on particulate methanesulfonate to non–sea salt sulfate ratios in the marine atmosphere, *Journal of Geophysical Research 111*, D05316.

APPENDIX A: AIR MASS BACK TRAJECTORIES

The National Oceanic and Atmospheric Administration (NOAA) Hybrid Single Particle Lagrangian Integrated Trajectory (HYSPLIT) model can be used to determine the most probable location of the origin of an air mass (Draxler and Rolph, 2011). The model can be found on the World Wide Web at http://www.arl.noaa.gov/ready/hysplit.html. This appendix displays the HYSPLIT model run for each sampling period of size segregated samples at Alert. During each sampling period, 48 hour duration back trajectories starting every 12 hours are displayed. Model vertical velocity was used for vertical motion. Global Data Assimilation System (GDAS) was chosen for the meteorological data grid input. The HYSPLIT model was run with height of the back trajectory set to 0 m above ground level. HYSPLIT back trajectories for the *Amundsen* data set were reported by Rempillo (2011) and are not presented here.

A.1. Fall 2007: Alert air mass back trajectories modeled with HYSPLIT for each size segregated sampling time period

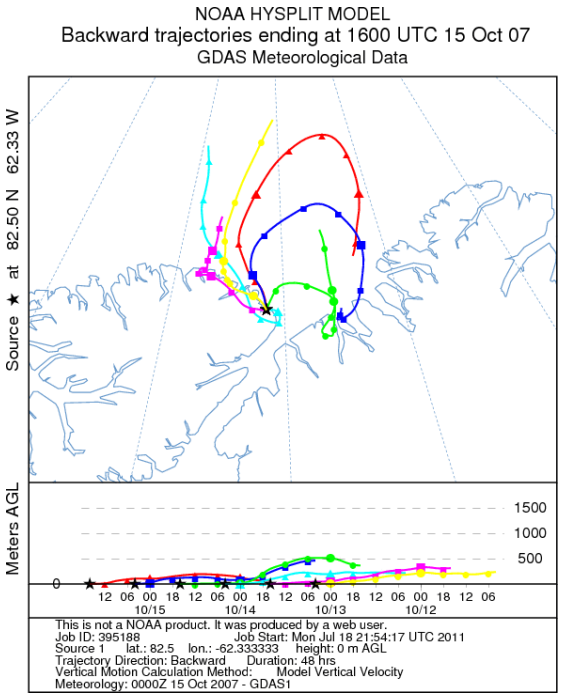

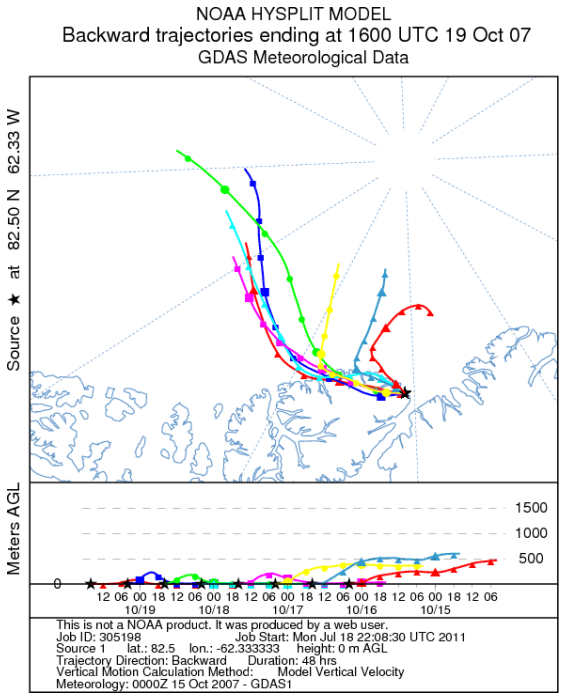

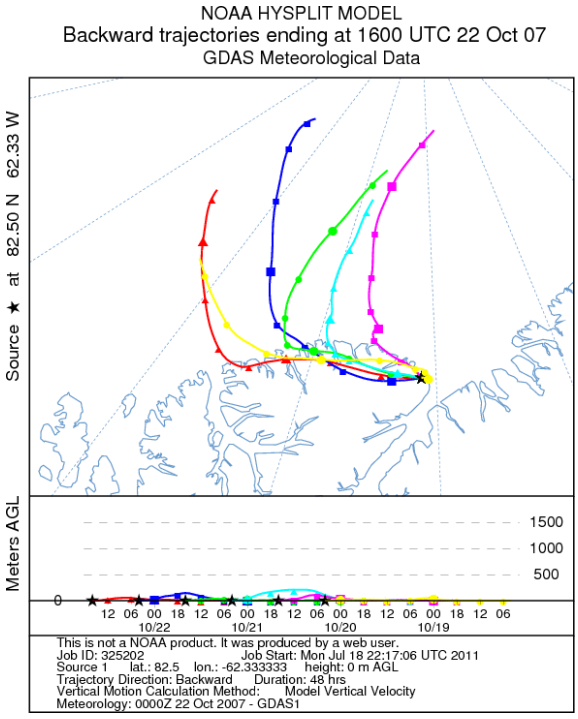

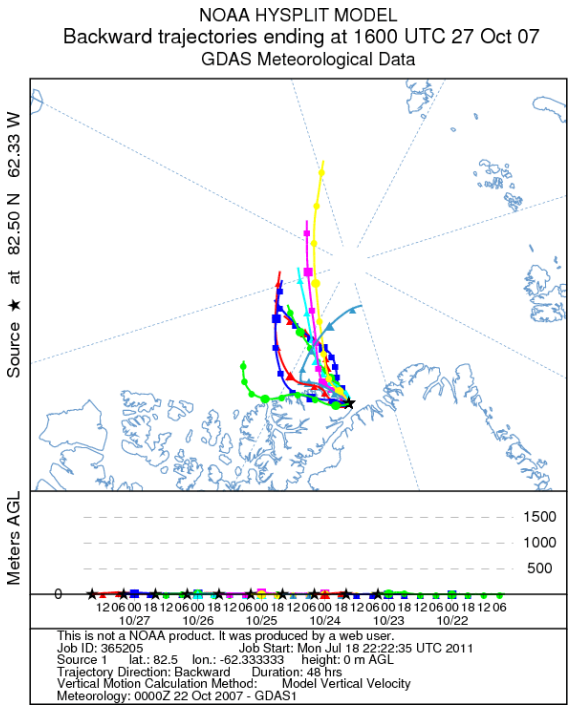

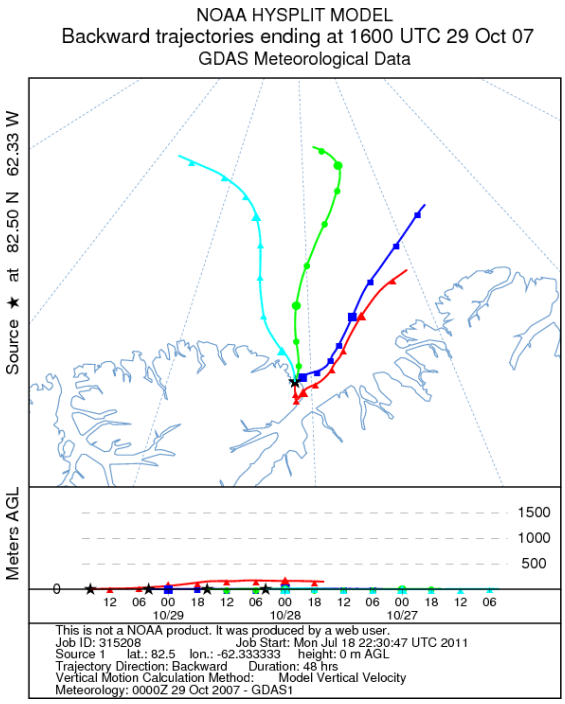
NOAA HYSPLIT MODEL
Backward trajectories ending at 1600 UTC 29 Oct 07
GDAS Meteorological Data
Source ★ at 82.50 N 62.33 W
Meters AGL
1500
1000
500
0
12 06 00 18 12 06 00 18 12 06 00 18 12 06
10/29 10/28 10/27
This is not a NOAA product. It was produced by a web user.
Job ID: 315208 Job Start: Mon Jul 18 22:30:47 UTC 2011
Source 1 lat.: 82.5 lon.: -62.333333 height: 0 m AGL
Trajectory Direction: Backward Duration: 48 hrs
Vertical Motion Calculation Method: Model Vertical Velocity
Meteorology: 0000Z 29 Oct 2007 - GDAS1

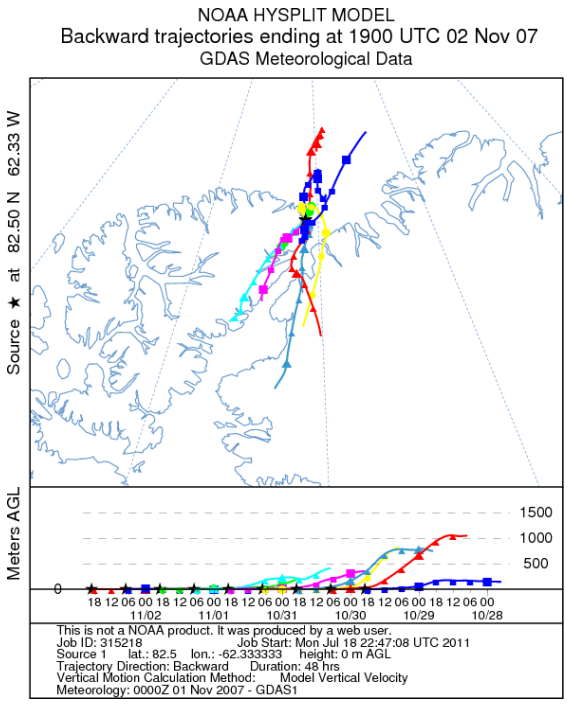
NOAA HYSPLIT MODEL
Backward trajectories ending at 1900 UTC 02 Nov 07
GDAS Meteorological Data
Source ★ at 82.50 N 62.33 W
Meters AGL
1500
1000
500
0
18 12 06 00 18 12 06 00 18 12 06 00 18 12 06 00 18 12 06 00
11/02 11/01 10/31 10/30 10/29 10/28
This is not a NOAA product. It was produced by a web user.
Job ID: 315218 Job Start: Mon Jul 18 22:47:08 UTC 2011
Source 1 lat.: 82.5 lon.: -62.333333 height: 0 m AGL
Trajectory Direction: Backward Duration: 48 hrs
Vertical Motion Calculation Method: Model Vertical Velocity
Meteorology: 0000Z 01 Nov 2007 - GDAS1

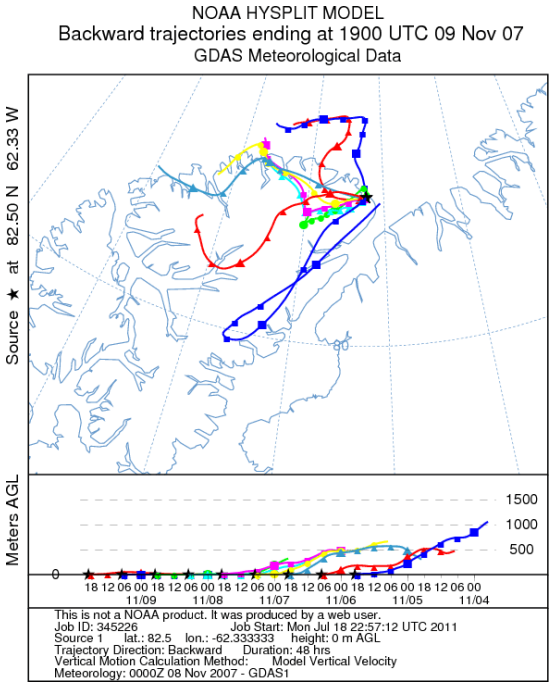
NOAA HYSPLIT MODEL
Backward trajectories ending at 1900 UTC 09 Nov 07
GDAS Meteorological Data
Source ★ at 82.50 N 62.33 W
Meters AGL
1500
1000
500
0
18 12 06 00 18 12 06 00 18 12 06 00 18 12 06 00 18 12 06 00
11/09 11/08 11/07 11/06 11/05 11/04
This is not a NOAA product. It was produced by a web user.
Job ID: 345226 Job Start: Mon Jul 18 22:57:12 UTC 2011
Source 1 lat.: 82.5 lon.: -62.333333 height: 0 m AGL
Trajectory Direction: Backward Duration: 48 hrs
Vertical Motion Calculation Method: Model Vertical Velocity
Meteorology: 0000Z 08 Nov 2007 - GDAS1

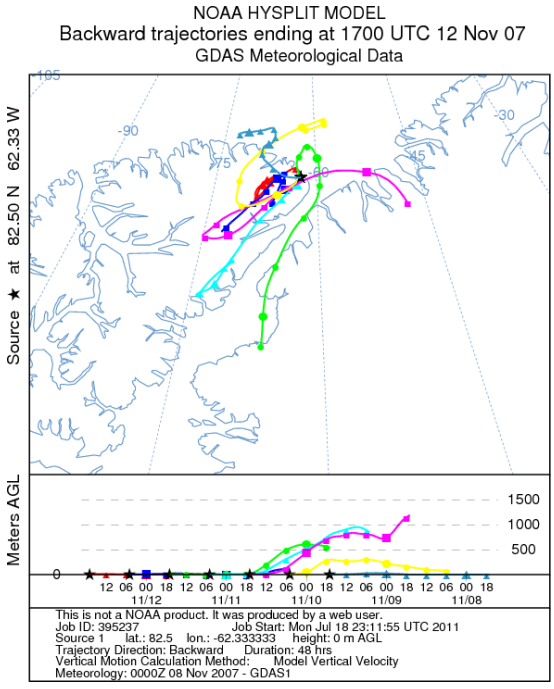
NOAA HYSPLIT MODEL
Backward trajectories ending at 1700 UTC 12 Nov 07
GDAS Meteorological Data
Source ★ at 82.50 N 62.33 W
Meters AGL
1500
1000
500
0
12 06 00 18 12 06 00 18 12 06 00 18 12 06 00 18 12 06 00 18
11/12 11/11 11/10 11/09 11/08
This is not a NOAA product. It was produced by a web user.
Job ID: 395237 Job Start: Mon Jul 18 23:11:55 UTC 2011
Source 1 lat.: 82.5 lon.: -62.333333 height: 0 m AGL
Trajectory Direction: Backward Duration: 48 hrs
Vertical Motion Calculation Method: Model Vertical Velocity
Meteorology: 0000Z 08 Nov 2007 - GDAS1

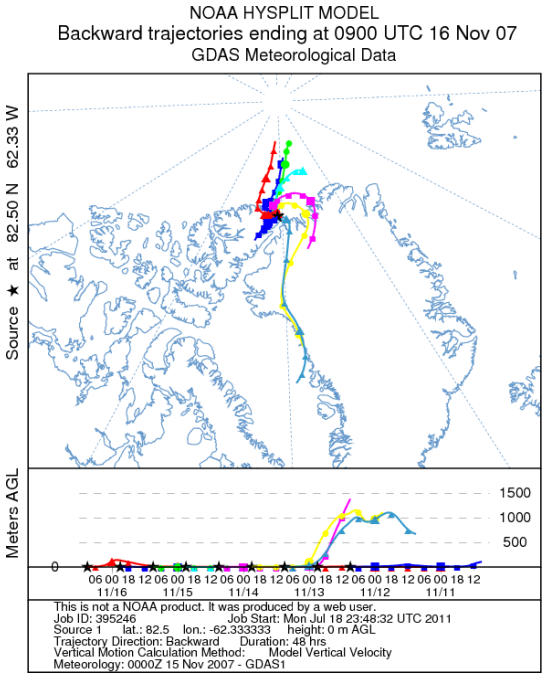
NOAA HYSPLIT MODEL
Backward trajectories ending at 0900 UTC 16 Nov 07
GDAS Meteorological Data
Source ★ at 82.50 N 62.33 W
Meters AGL
1500
1000
500
0
06 00 18 12 06 00 18 12 06 00 18 12 06 00 18 12 06 00 18 12 06 00 18 12
11/16 11/15 11/14 11/13 11/12 11/11
This is not a NOAA product. It was produced by a web user.
Job ID: 395246 Job Start: Mon Jul 18 23:48:32 UTC 2011
Source 1 lat.: 82.5 lon.: -62.333333 height: 0 m AGL
Trajectory Direction: Backward Duration: 48 hrs
Vertical Motion Calculation Method: Model Vertical Velocity
Meteorology: 0000Z 15 Nov 2007 - GDAS1

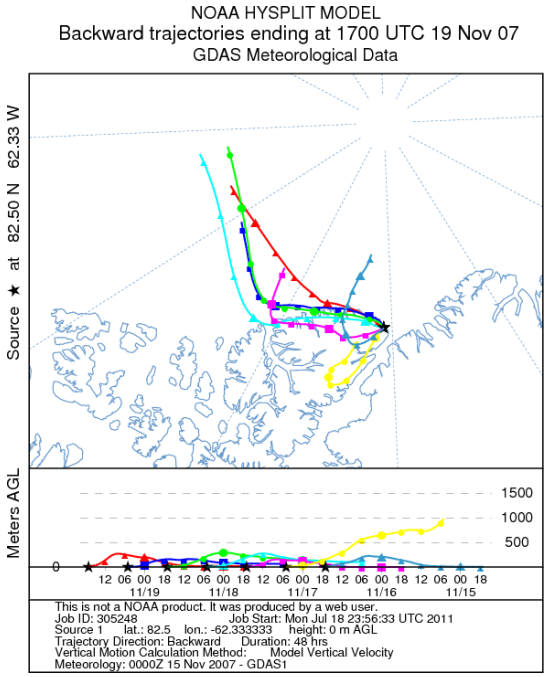
NOAA HYSPLIT MODEL
Backward trajectories ending at 1700 UTC 19 Nov 07
GDAS Meteorological Data
Source ★ at 82.50 N 62.33 W
Meters AGL
1500
1000
500
0
12 06 00 18 12 06 00 18 12 06 00 18 12 06 00 18 12 06 00 18 12 06 00 18
11/19 11/18 11/17 11/16 11/15
This is not a NOAA product. It was produced by a web user.
Job ID: 305248 Job Start: Mon Jul 18 23:56:33 UTC 2011
Source 1 lat.: 82.5 lon.: -62.333333 height: 0 m AGL
Trajectory Direction: Backward Duration: 48 hrs
Vertical Motion Calculation Method: Model Vertical Velocity
Meteorology: 0000Z 15 Nov 2007 - GDAS1

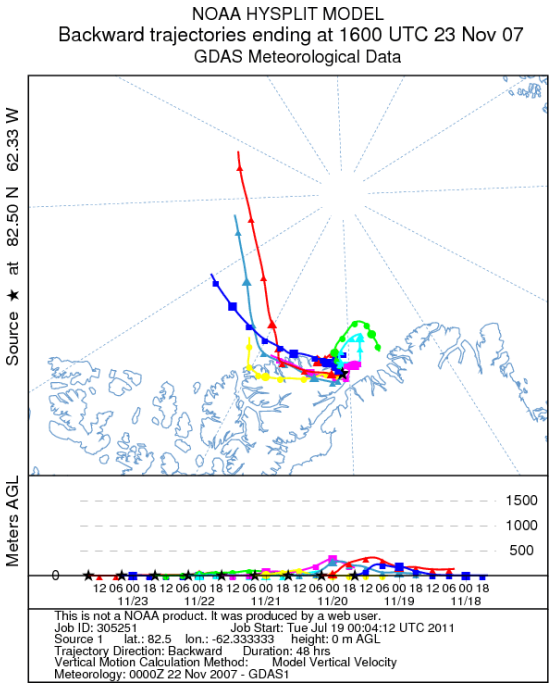
NOAA HYSPLIT MODEL
Backward trajectories ending at 1600 UTC 23 Nov 07
GDAS Meteorological Data
Source ★ at 82.50 N 62.33 W
Meters AGL
1500
1000
500
0
12 06 00 18 12 06 00 18 12 06 00 18 12 06 00 18 12 06 00 18 12 06 00 18
11/23 11/22 11/21 11/20 11/19 11/18
This is not a NOAA product. It was produced by a web user.
Job ID: 305251 Job Start: Tue Jul 19 00:04:12 UTC 2011
Source 1 lat.: 82.5 lon.: -62.333333 height: 0 m AGL
Trajectory Direction: Backward Duration: 48 hrs
Vertical Motion Calculation Method: Model Vertical Velocity
Meteorology: 0000Z 22 Nov 2007 - GDAS1

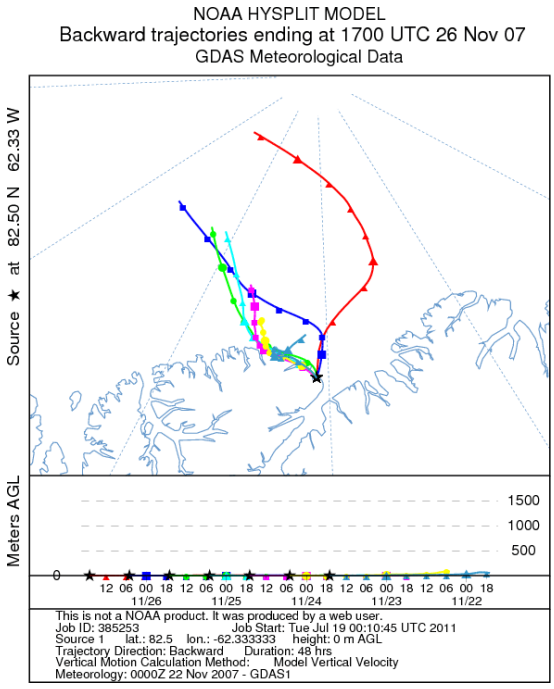
NOAA HYSPLIT MODEL
Backward trajectories ending at 1700 UTC 26 Nov 07
GDAS Meteorological Data
Source ★ at 82.50 N 62.33 W
Meters AGL
1500
1000
500
0
12 06 00 18 12 06 00 18 12 06 00 18 12 06 00 18 12 06 00 18 12 06 00 18
11/26 11/25 11/24 11/23 11/22
This is not a NOAA product. It was produced by a web user.
Job ID: 385253 Job Start: Tue Jul 19 00:10:45 UTC 2011
Source 1 lat.: 82.5 lon.: -62.333333 height: 0 m AGL
Trajectory Direction: Backward Duration: 48 hrs
Vertical Motion Calculation Method: Model Vertical Velocity
Meteorology: 0000Z 22 Nov 2007 - GDAS1

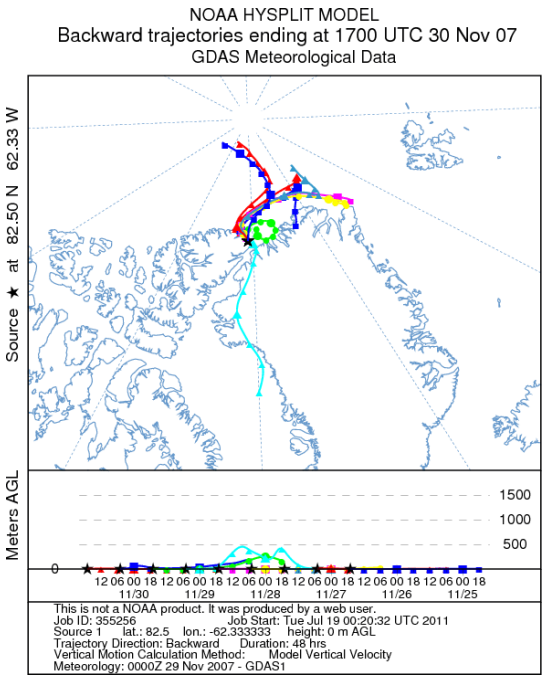
NOAA HYSPLIT MODEL
Backward trajectories ending at 1700 UTC 30 Nov 07
GDAS Meteorological Data
Source ★ at 82.50 N 62.33 W
Meters AGL
1500
1000
500
0
12 06 00 18 12 06 00 18 12 06 00 18 12 06 00 18 12 06 00 18 12 06 00 18
11/30 11/29 11/28 11/27 11/26 11/25
This is not a NOAA product. It was produced by a web user.
Job ID: 355256 Job Start: Tue Jul 19 00:20:32 UTC 2011
Source 1 lat.: 82.5 lon.: -62.333333 height: 0 m AGL
Trajectory Direction: Backward Duration: 48 hrs
Vertical Motion Calculation Method: Model Vertical Velocity
Meteorology: 0000Z 29 Nov 2007 - GDAS1

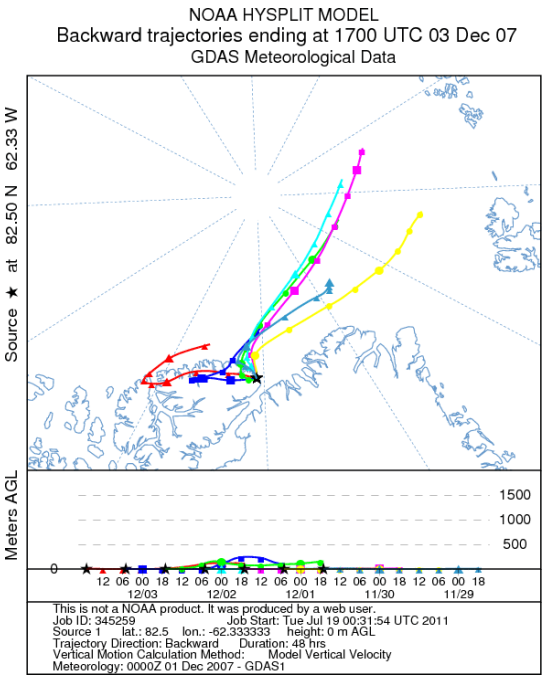
NOAA HYSPLIT MODEL
Backward trajectories ending at 1700 UTC 03 Dec 07
GDAS Meteorological Data
Source ★ at 82.50 N 62.33 W
Meters AGL
1500
1000
500
0
12 06 00 18 12 06 00 18 12 06 00 18 12 06 00 18 12 06 00 18 12 06 00 18
12/03 12/02 12/01 11/30 11/29
This is not a NOAA product. It was produced by a web user.
Job ID: 345259 Job Start: Tue Jul 19 00:31:54 UTC 2011
Source 1 lat.: 82.5 lon.: -62.333333 height: 0 m AGL
Trajectory Direction: Backward Duration: 48 hrs
Vertical Motion Calculation Method: Model Vertical Velocity
Meteorology: 0000Z 01 Dec 2007 - GDAS1

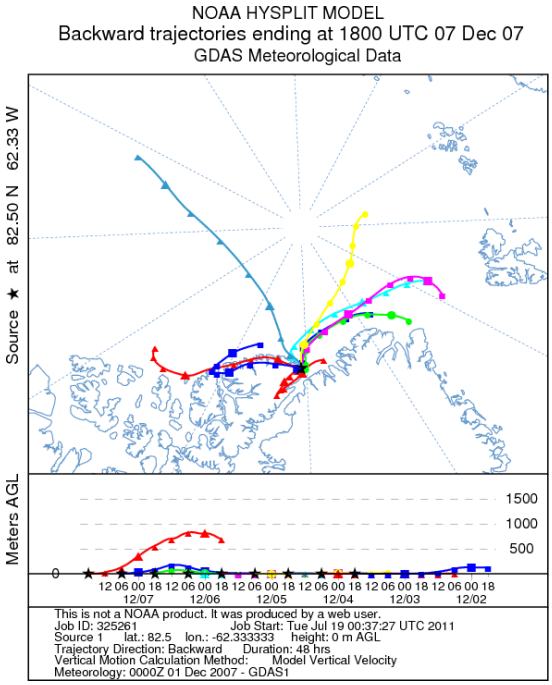
NOAA HYSPLIT MODEL
Backward trajectories ending at 1800 UTC 07 Dec 07
GDAS Meteorological Data
Source ★ at 82.50 N 62.33 W
Meters AGL
1500
1000
500
0
12 06 00 18 12 06 00 18 12 06 00 18 12 06 00 18 12 06 00 18 12 06 00 18
12/07 12/06 12/05 12/04 12/03 12/02
This is not a NOAA product. It was produced by a web user.
Job ID: 325261 Job Start: Tue Jul 19 00:37:27 UTC 2011
Source 1 lat.: 82.5 lon.: -62.333333 height: 0 m AGL
Trajectory Direction: Backward Duration: 48 hrs
Vertical Motion Calculation Method: Model Vertical Velocity
Meteorology: 0000Z 01 Dec 2007 - GDAS1

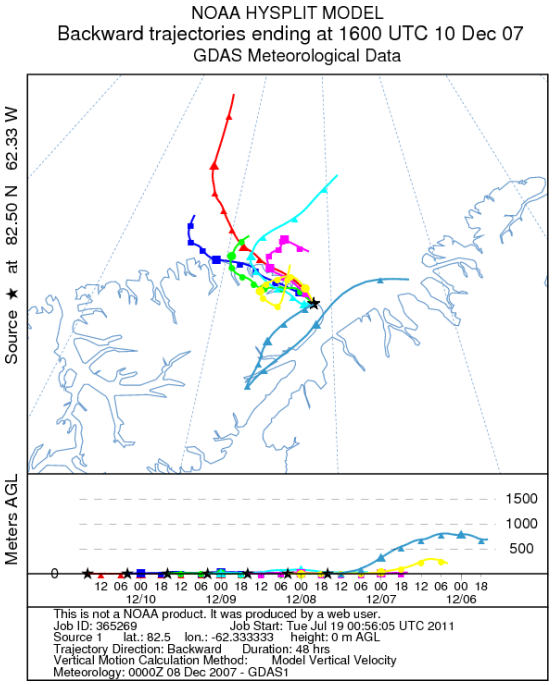
NOAA HYSPLIT MODEL
Backward trajectories ending at 1600 UTC 10 Dec 07
GDAS Meteorological Data
Source ★ at 82.50 N 62.33 W
Meters AGL
1500
1000
500
0
12 06 00 18 12 06 00 18 12 06 00 18 12 06 00 18 12 06 00 18 12 06 00 18
12/10 12/09 12/08 12/07 12/06
This is not a NOAA product. It was produced by a web user.
Job ID: 365269 Job Start: Tue Jul 19 00:56:05 UTC 2011
Source 1 lat.: 82.5 lon.: -62.333333 height: 0 m AGL
Trajectory Direction: Backward Duration: 48 hrs
Vertical Motion Calculation Method: Model Vertical Velocity
Meteorology: 0000Z 08 Dec 2007 - GDAS1

A.2. Fall 2008: Alert mass back trajectories modeled with HYSPLIT for each size segregated sampling time period.

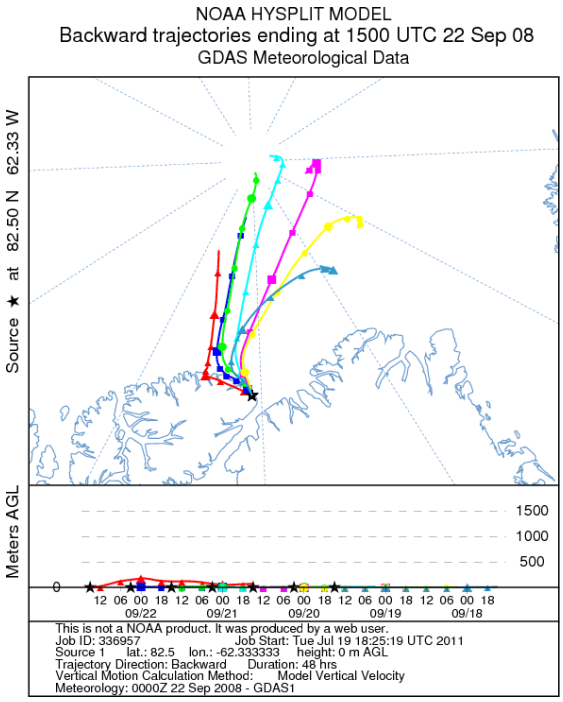

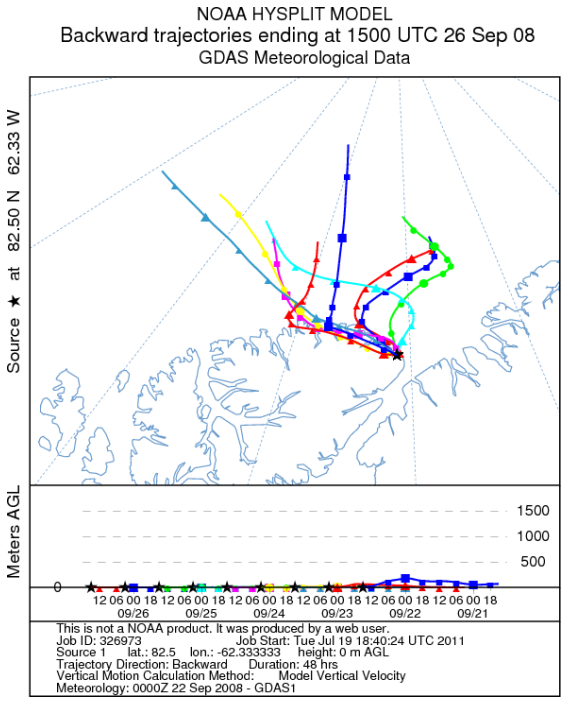

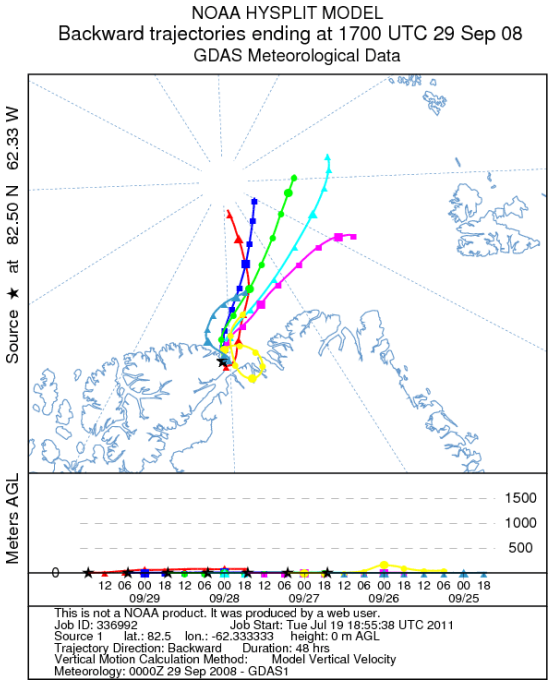

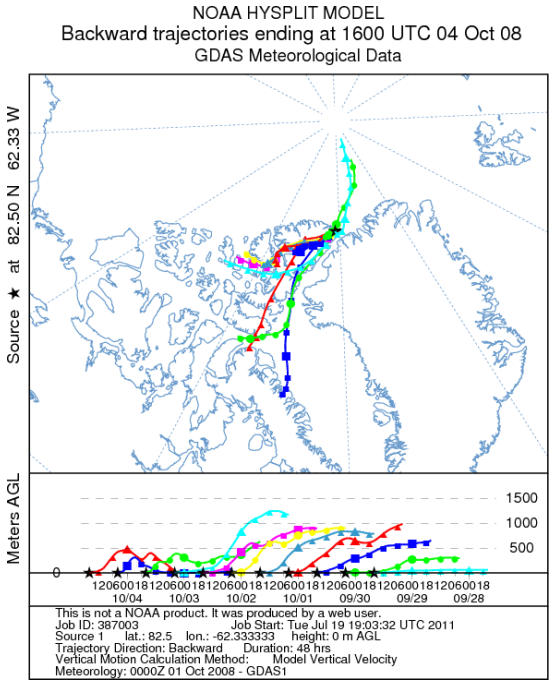

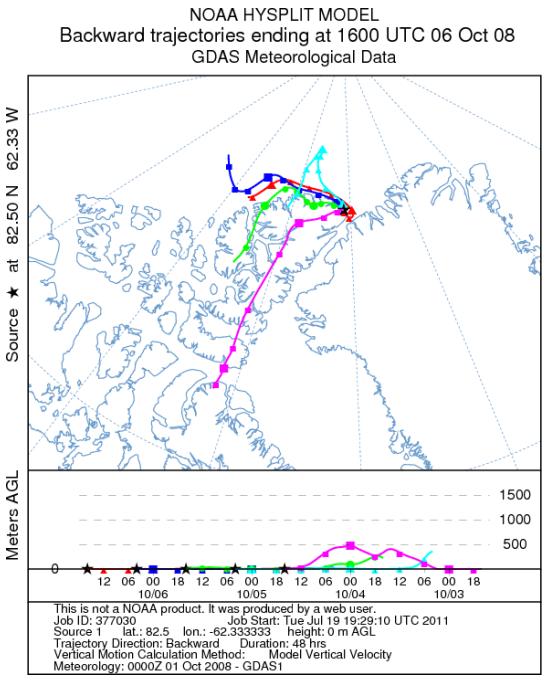
NOAA HYSPLIT MODEL
Backward trajectories ending at 1600 UTC 06 Oct 08
GDAS Meteorological Data
Source ★ at 82.50 N 62.33 W
Meters AGL
1500
1000
500
0
12 06 00 18 12 06 00 18 12 06 00 18 12 06 00 18
10/06 10/05 10/04 10/03
This is not a NOAA product. It was produced by a web user.
Job ID: 377030 Job Start: Tue Jul 19 19:29:10 UTC 2011
Source 1 lat.: 82.5 lon.: -62.333333 height: 0 m AGL
Trajectory Direction: Backward Duration: 48 hrs
Vertical Motion Calculation Method: Model Vertical Velocity
Meteorology: 0000Z 01 Oct 2008 - GDAS1

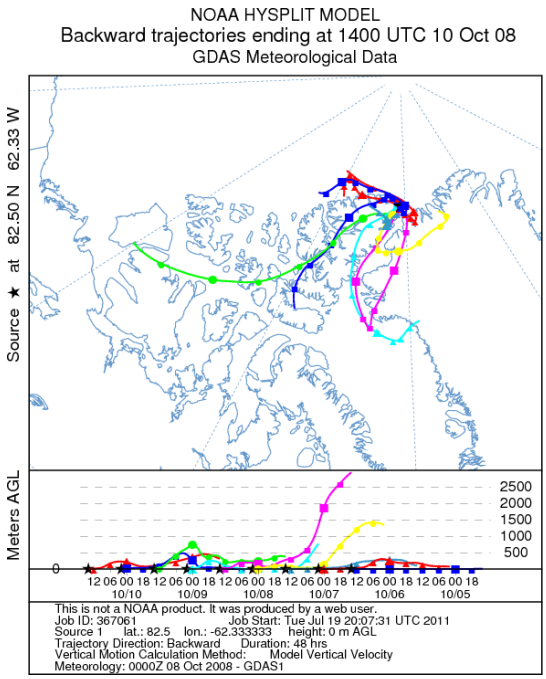
NOAA HYSPLIT MODEL
Backward trajectories ending at 1400 UTC 10 Oct 08
GDAS Meteorological Data
Source ★ at 82.50 N 62.33 W
Meters AGL
2500
2000
1500
1000
500
0
12 06 00 18 12 06 00 18 12 06 00 18 12 06 00 18 12 06 00 18
10/10 10/09 10/08 10/07 10/06 10/05
This is not a NOAA product. It was produced by a web user.
Job ID: 367061 Job Start: Tue Jul 19 20:07:31 UTC 2011
Source 1 lat.: 82.5 lon.: -62.333333 height: 0 m AGL
Trajectory Direction: Backward Duration: 48 hrs
Vertical Motion Calculation Method: Model Vertical Velocity
Meteorology: 0000Z 08 Oct 2008 - GDAS1

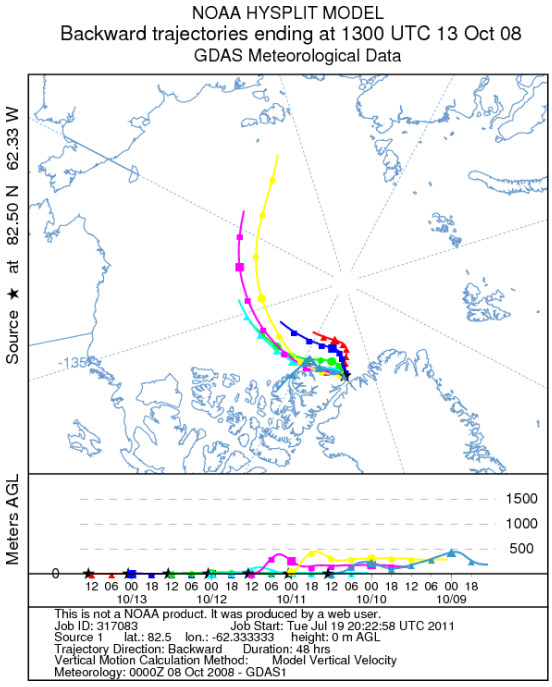
NOAA HYSPLIT MODEL
Backward trajectories ending at 1300 UTC 13 Oct 08
GDAS Meteorological Data
Source ★ at 82.50 N 62.33 W
Meters AGL
1500
1000
500
0
12 06 00 18 12 06 00 18 12 06 00 18 12 06 00 18 12 06 00 18
10/13 10/12 10/11 10/10 10/09
This is not a NOAA product. It was produced by a web user.
Job ID: 317083 Job Start: Tue Jul 19 20:22:58 UTC 2011
Source 1 lat.: 82.5 lon.: -62.333333 height: 0 m AGL
Trajectory Direction: Backward Duration: 48 hrs
Vertical Motion Calculation Method: Model Vertical Velocity
Meteorology: 0000Z 08 Oct 2008 - GDAS1

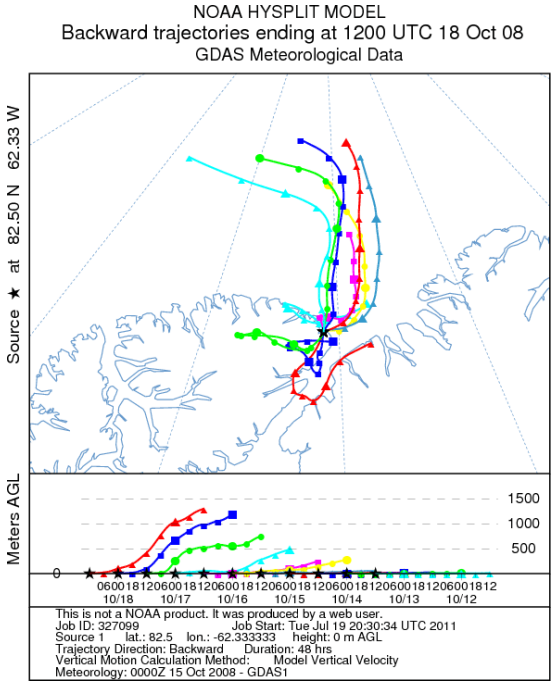
NOAA HYSPLIT MODEL
Backward trajectories ending at 1200 UTC 18 Oct 08
GDAS Meteorological Data
Source ★ at 82.50 N 62.33 W
Meters AGL
1500
1000
500
0
10/18 10/17 10/16 10/15 10/14 10/13 10/12
This is not a NOAA product. It was produced by a web user.
Job ID: 327099 Job Start: Tue Jul 19 20:30:34 UTC 2011
Source 1 lat.: 82.5 lon.: -62.333333 height: 0 m AGL
Trajectory Direction: Backward Duration: 48 hrs
Vertical Motion Calculation Method: Model Vertical Velocity
Meteorology: 0000Z 15 Oct 2008 - GDAS1

APPENDIX B: $\delta^{34}S$ VALUES

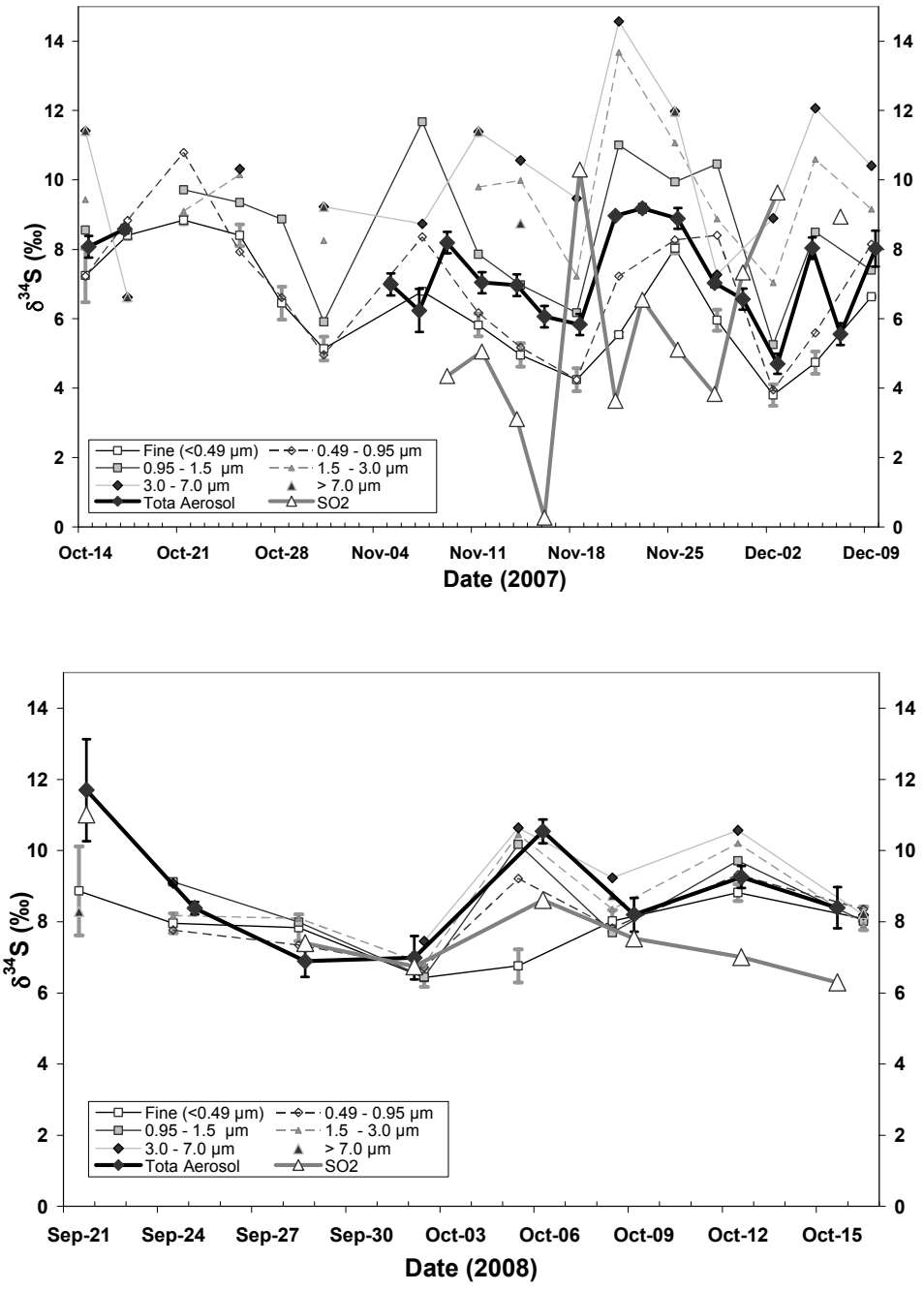

Figure B.1 $\delta^{34}S$ values of sulfate in aerosols and SO_2 collected at Alert for 2007 (top) and 2008 (bottom). Error is displayed for total and fine (< 0.49 µm aerosols).

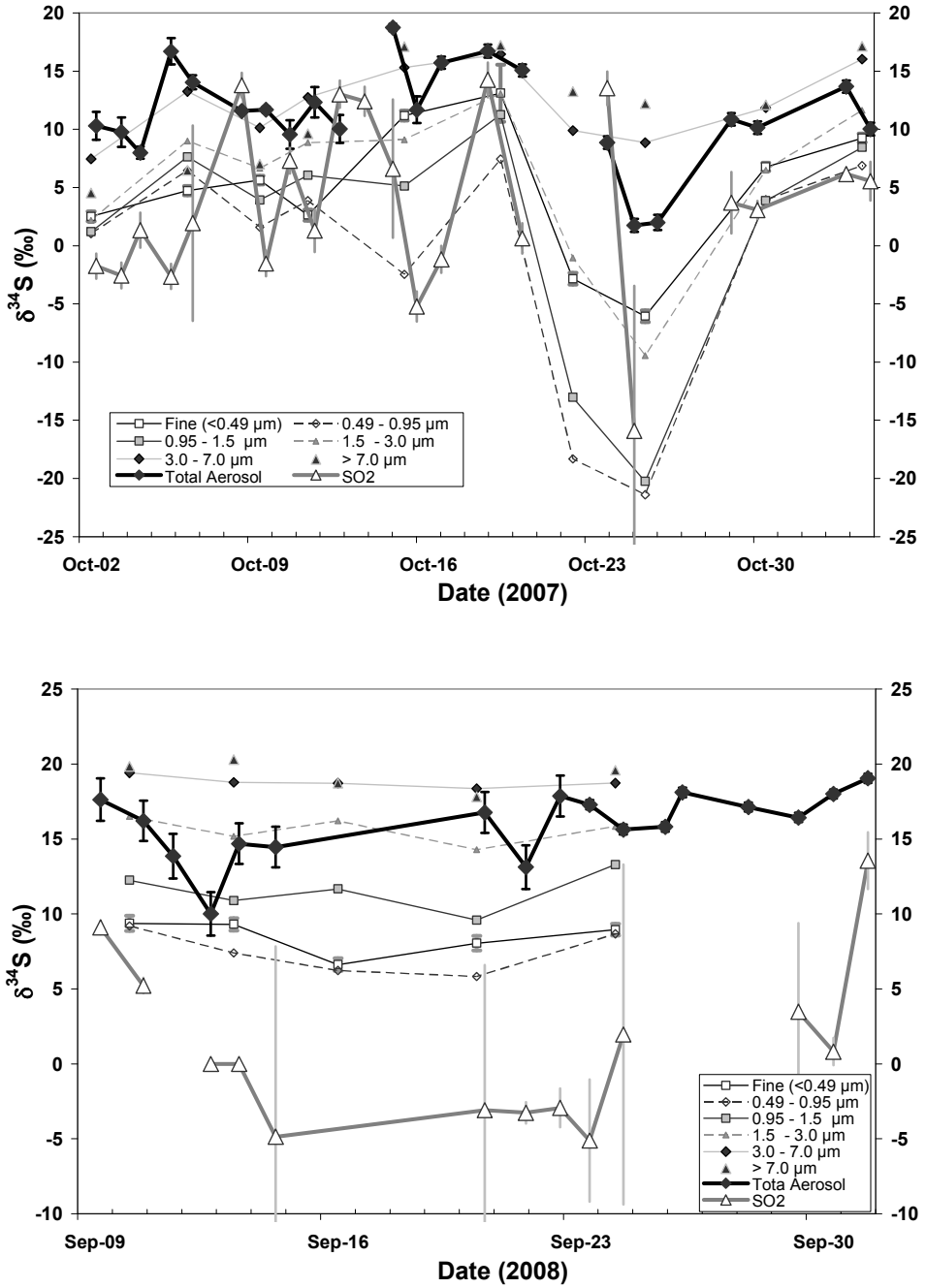

Figure B.2 $\delta^{34}S$ values for aerosol sulfate and SO_2 collected on board the *Amundsen* for 2007 (top) and 2008 (bottom). Error is displayed for total and fine (< 0.49 µm) aerosols and SO_2. Data from Rempillo (2011). SO_2 $\delta^{34}S$ values were not corrected for possible sea salt contamination (Appendix F).

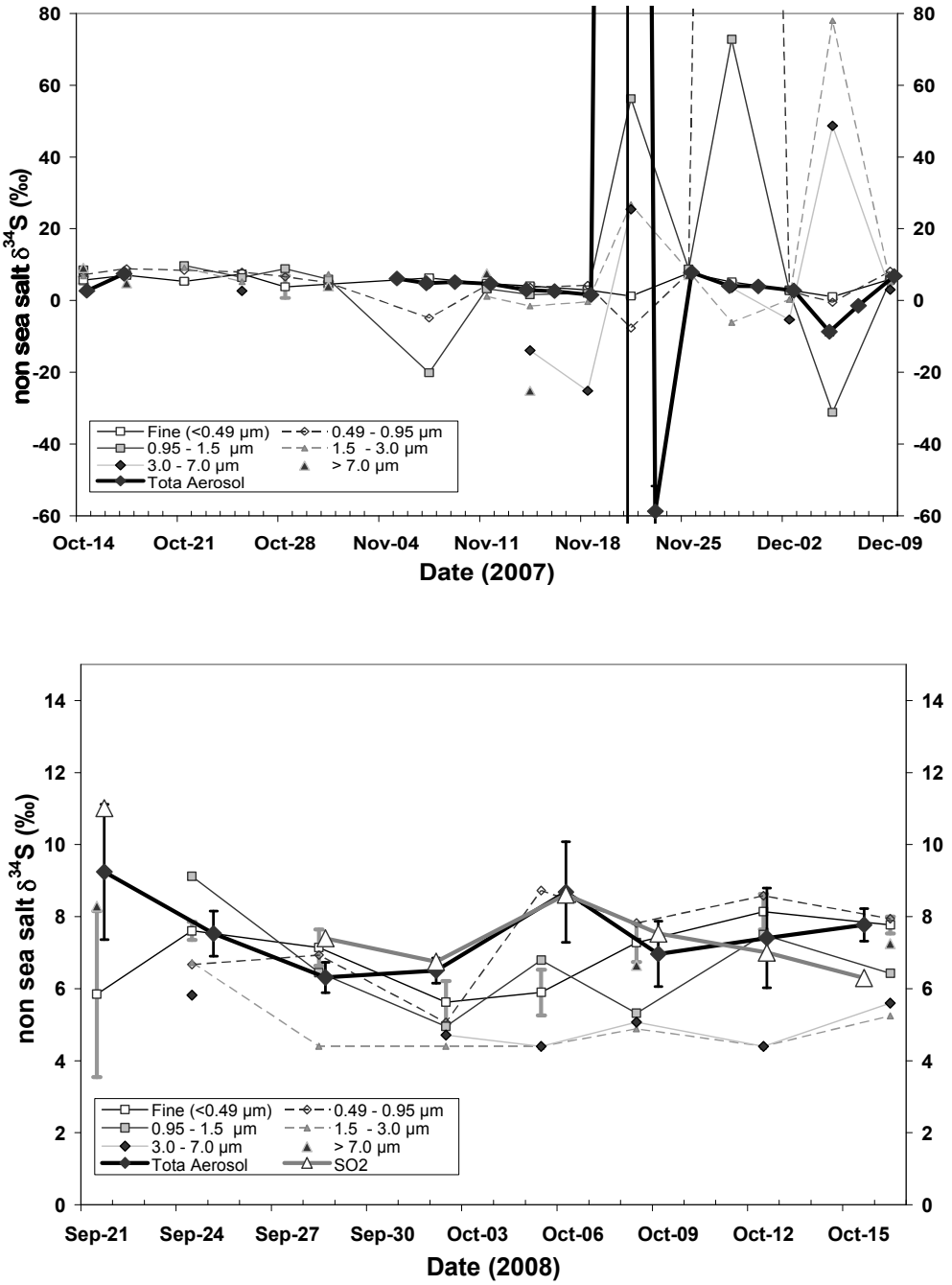

Figure B.3 Calculated non sea salt $\delta^{34}S$ values for aerosol sulfate computed based on equation 3.1 at Alert. Frost flowers are not taken into account. Error is displayed for total and fine (< 0.49 µm aerosols). Note the difference in the displayed vertical axis between the two years.

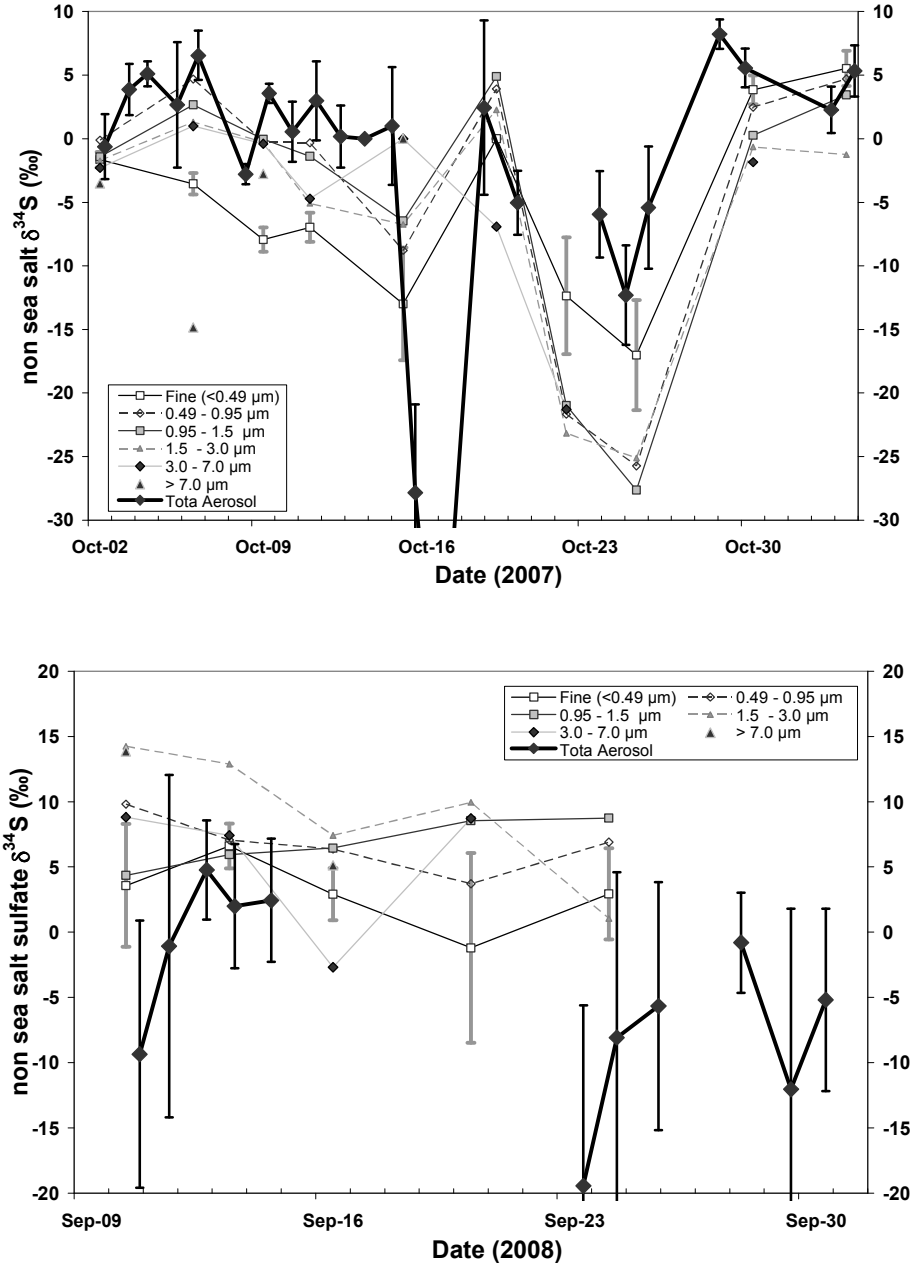

Figure B.4 Calculated non sea salt $\delta^{34}S$ values of aerosol sulfate computed based on equation 3.1 for the *Amundsen* data. Error is displayed for total and fine (< 0.49 µm aerosols). Note the difference in the displayed vertical axis between the two years.

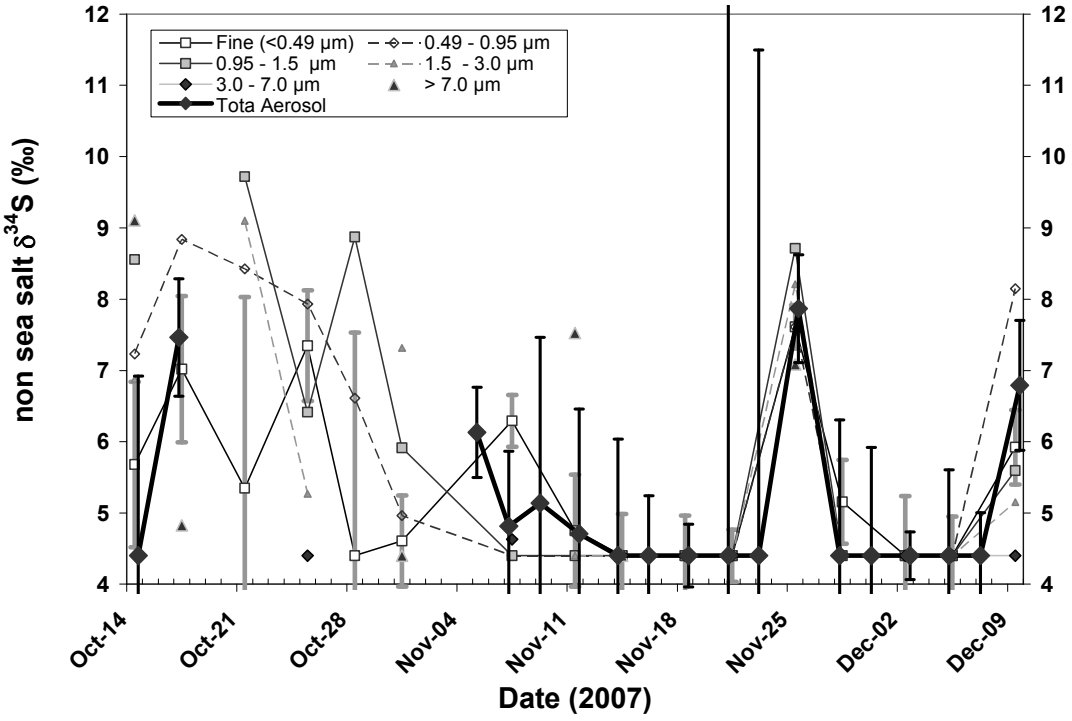

Figure B.5 Non sea salt $\delta^{34}S$ values for aerosol sulfate collected at Alert assuming the minimum frost flower contribution (when FF_{ratio}=0.017) for 2007. $\delta^{34}S$ values assuming maximum frost flower contribution are within error. Error is displayed for total and fine (< 0.49 µm aerosols). Values for 2008 are the same as those that are not corrected for frost flower contribution.

APPENDIX C: APPORTIONMENT

Sulfate and SO_2 concentrations were determined by ion chromatography as explained in Chapters 2.5 and 2.6 for each sample and are displayed in the following Appendix. The figures in the Appendix display total sulfate (i.e., sulfate in each individual sample) in the aerosol and the apportionment of the sulfate. Total sulfate (displayed by a line) is equivalent to the sum of the individual source contributions of sulfate in the sample unless apportionment could not be completely carried out on the sample. Note that the scale of sulfate concentrations differs for each display. Sea salt sulfate was determined by equation 3.7, for Alert, and equation 1.1 for samples from the *Amundsen* (since no frost flowers were present) and is discussed in Chapter 3.4. Contribution from frost flowers is determined for Alert samples by equation 3.6. Since frost flowers are expected to minimal for the majority of sampling period (Chapter 3.3) frost flower contribution is set to be the minimum value found for frost flower concentrations when FF_{ratio} is restricted to 0.017 and $\delta^{34}S_{nss}$ is varied between +4.4 ‰ and +18 ‰ (Chapter 3.3.3.2). Biogenic and anthropogenic sulfate is determined by equations 3.8 and 3.9 in Chapter 3.6.

Biogenic and anthropogenic sulfate apportionment cannot be carried out if in the vicinity of The Smoking Hills (Chapter 3.5.3), and therefore is not displayed during the time the Amundsen is in the vicinity of The Smoking Hills. Also, apportionment of anthropogenic and biogenic cannot be conducted when samples are small (See Chapter 2.7 on isotope measurements). The two largest size fractions at Alert in 2007 (Figure C.1

a/b) are combined for enough samples to run analysis on some of the samples. The figure has been labelled a/b so that each data set (i.e., *Amundsen* and Alert data sets) have similar naming conventions.

Error on anthropogenic apportionment is displayed throughout this appendix. Error on biogenic concentrations are similar to those of anthropogenic concentrations of the same sample (absolute error for biogenic is approximately 84% of the anthropogenic error for the Amundsen data set and 73% for the Alert data. Sea salt error is also displayed. Error is calculated by propagation of error (equation 2.7) and also includes the consideration of frost flowers discussed in Chapter 3.6.2.

Inserts in the figures presented in this Appendix illustrate percent contribution for the different sources of sulfate in aerosols and SO_2. If apportionment for all components was not carried out for a specific sample, that time period is left blank in the insert. If over half of the samples did not have complete apportionment carried out the percent contribution insert is not displayed

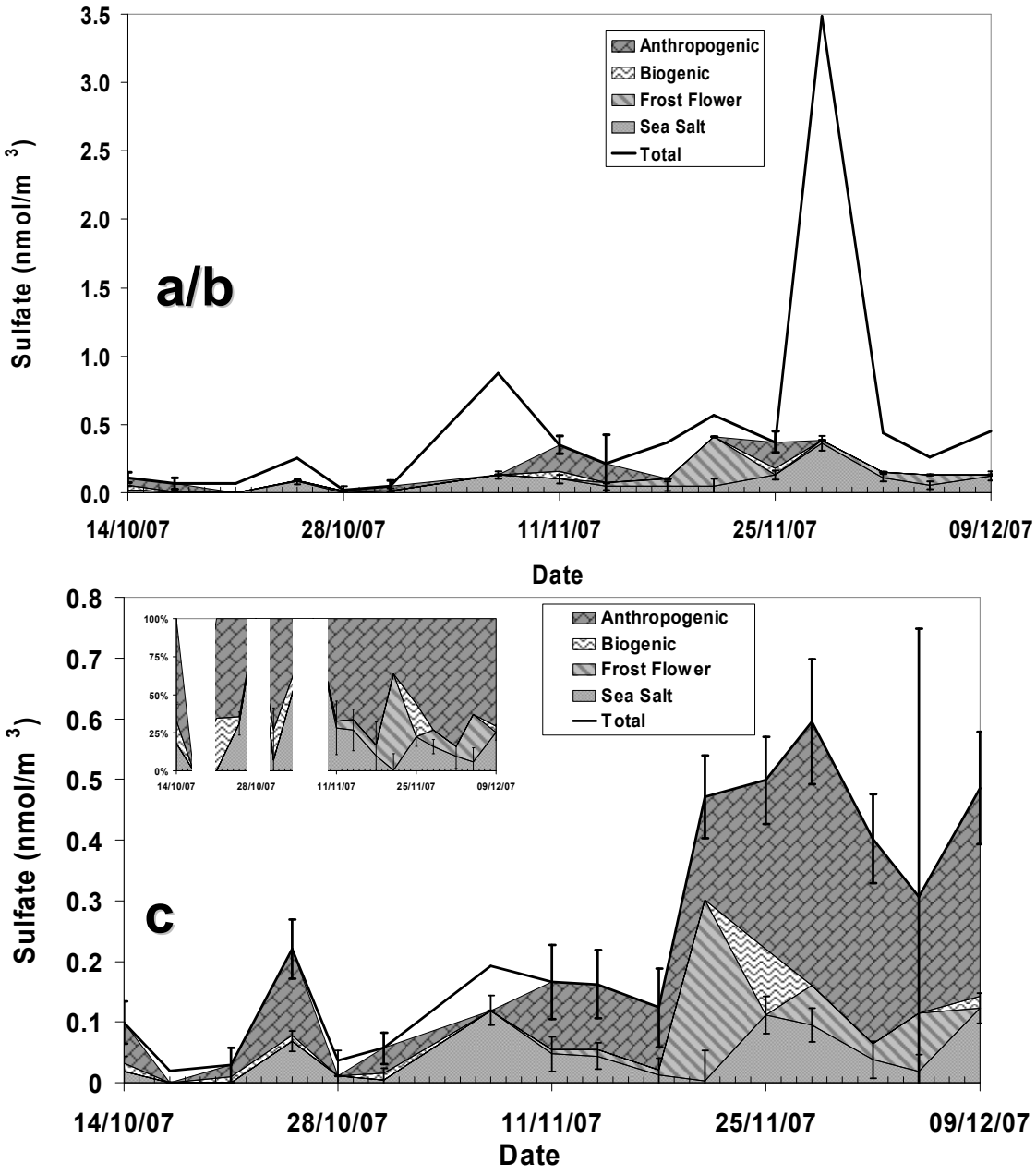

C.1. Concentrations and apportionment for aerosol sulfate at Alert in 2007 for size fractions a/b) > 7.2 µm and 3.0 – 7.2 µm (combined) and c) 1.5 – 3.0 µm.

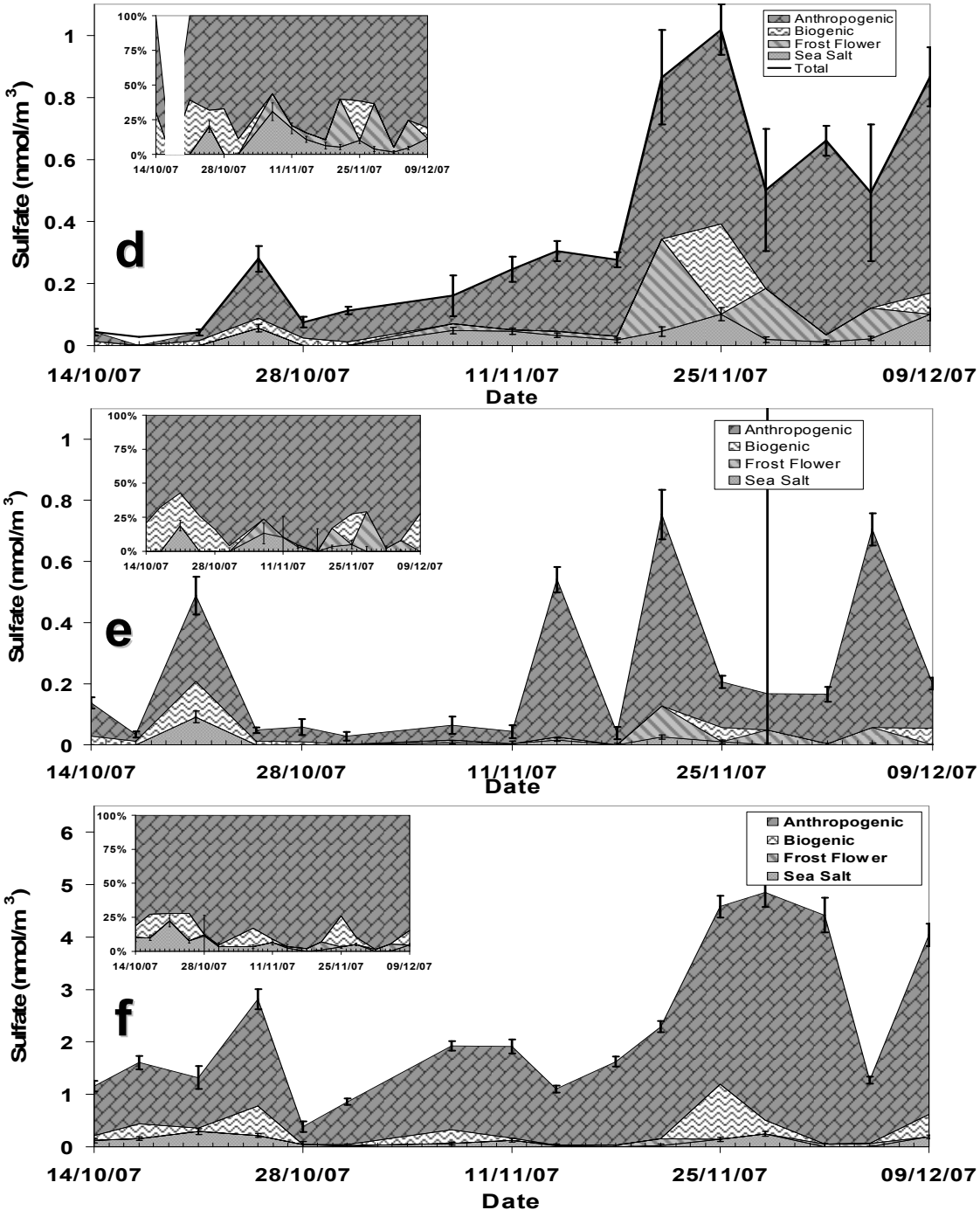

C.2. Concentrations and apportionment for aerosol sulfate at Alert in 2007 for size fractions d) 0.95 -1.5 µm e) 0.49 – 0.95 µm and f) > 0.49 µm.

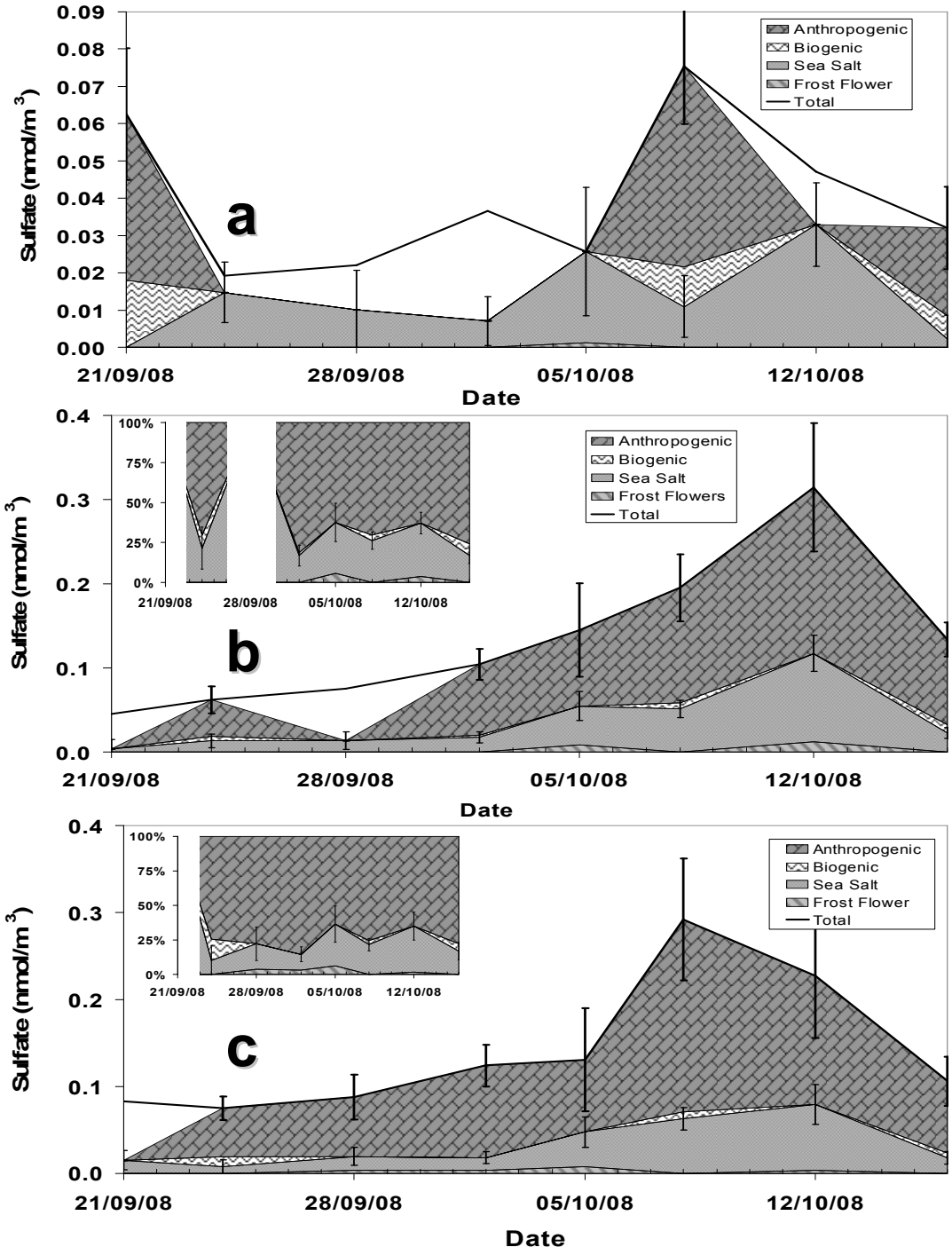

C.3. Concentrations and apportionment for aerosol sulfate at Alert in 2008 for size fractions a) > 7.2 µm b) 3.0 – 7.2 µm and c) 1.5 – 3.0 µm.

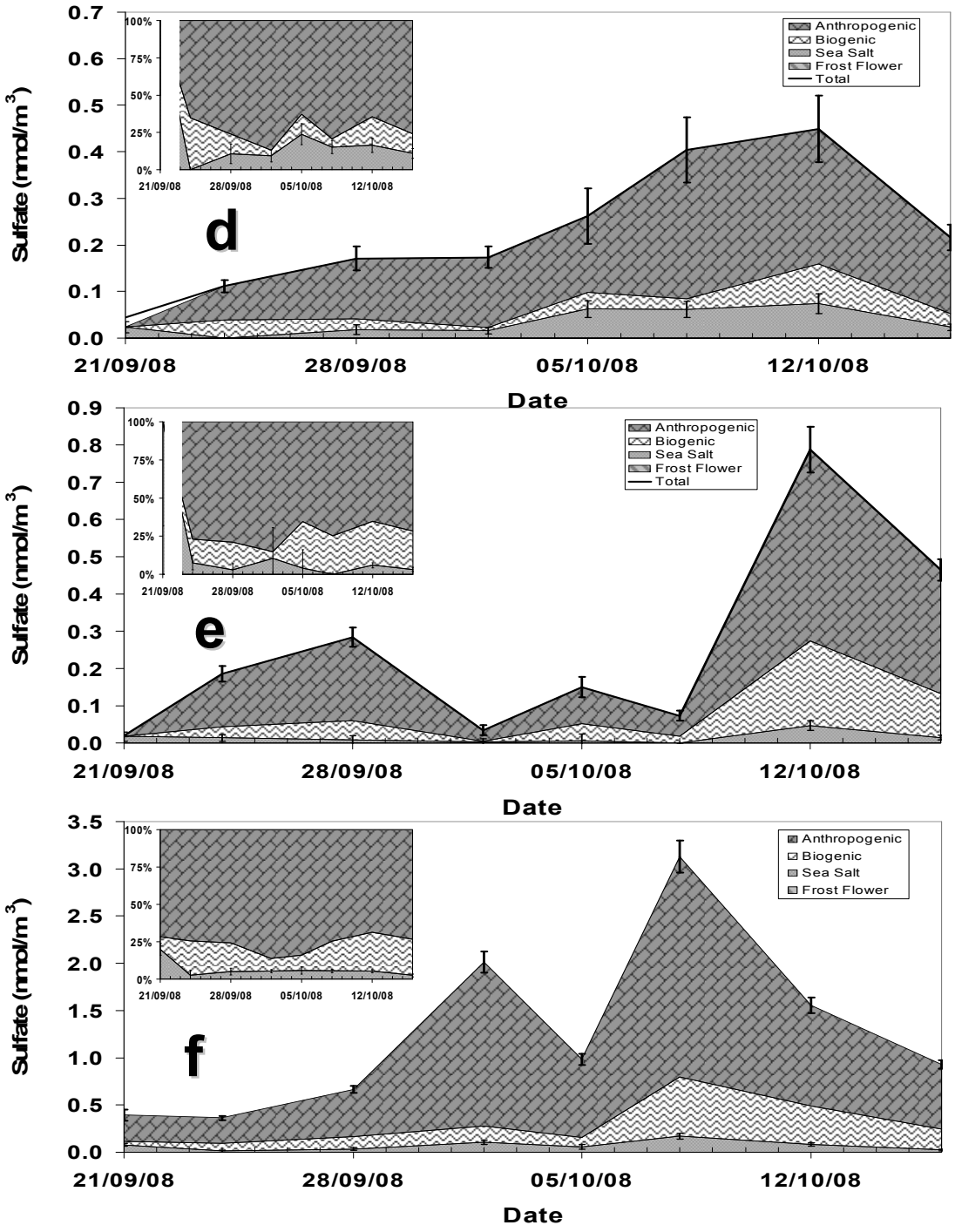

C.4. Concentrations and apportionment for aerosol sulfate at Alert in 2008 for size fractions d) 0.95 -1.5 µm e) 0.49 – 0.95 µm and f) > 0.49 µm.

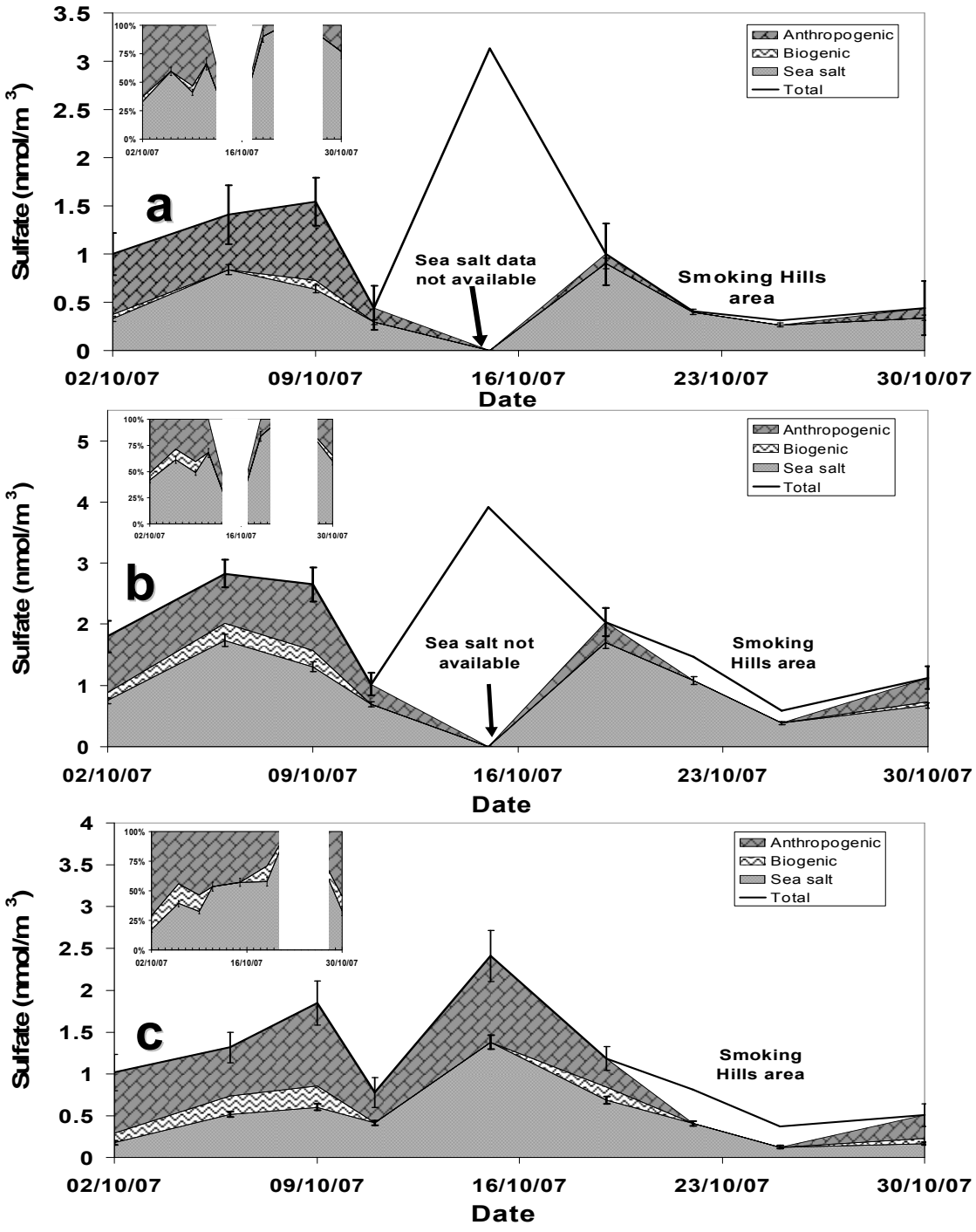

C.5. Concentrations and apportionment for aerosol sulfate for the *Amundsen* data set in 2007 for size fractions a) > 7.2 µm b) 3.0 – 7.2 µm and c) 1.5 – 3.0 µm.

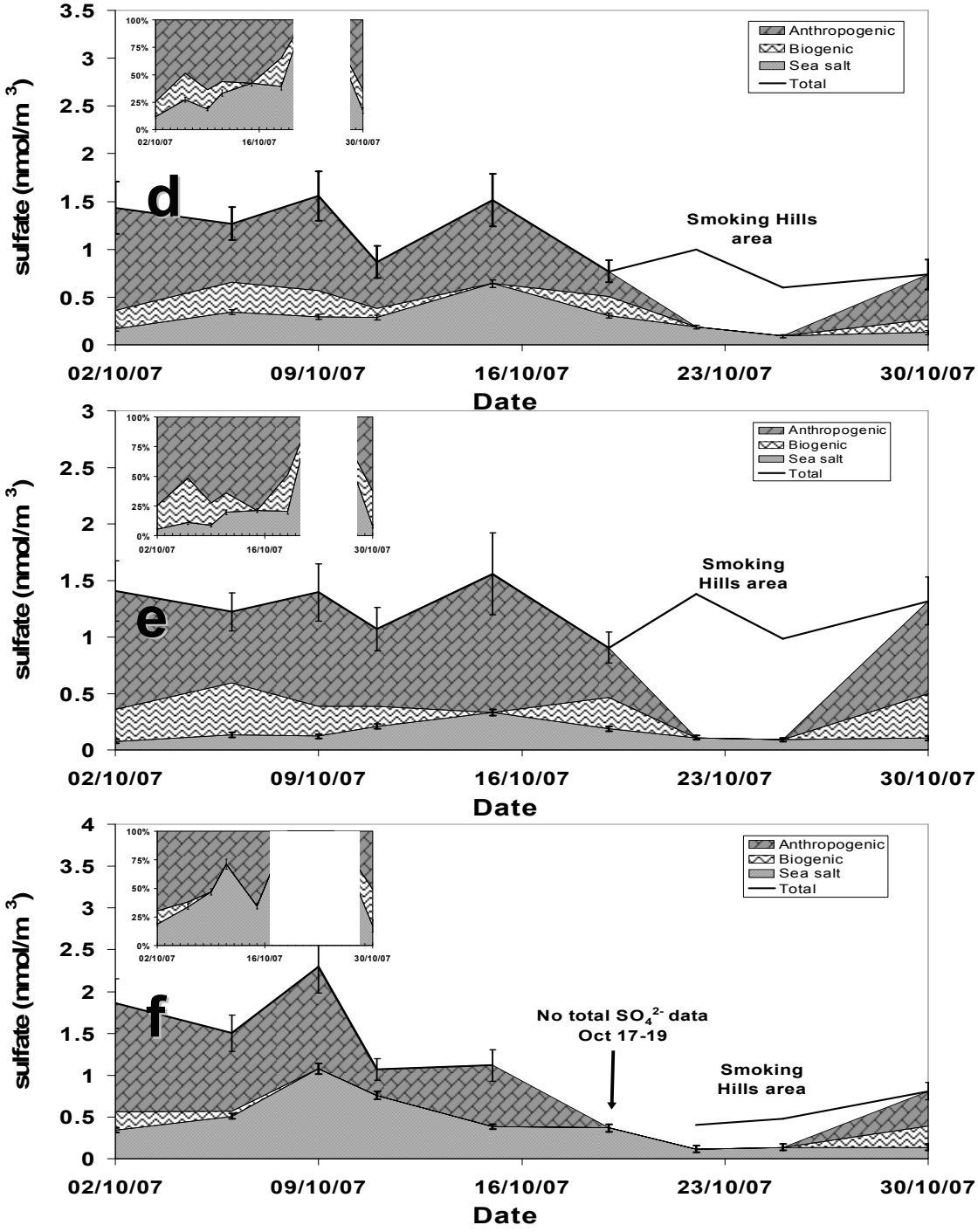

C.6. Concentrations and apportionment for aerosol sulfate for the *Amundsen* data set in 2007 for size fractions d) 0.95 -1.5 µm e) 0.49 – 0.95 µm and f) > 0.49 µm.

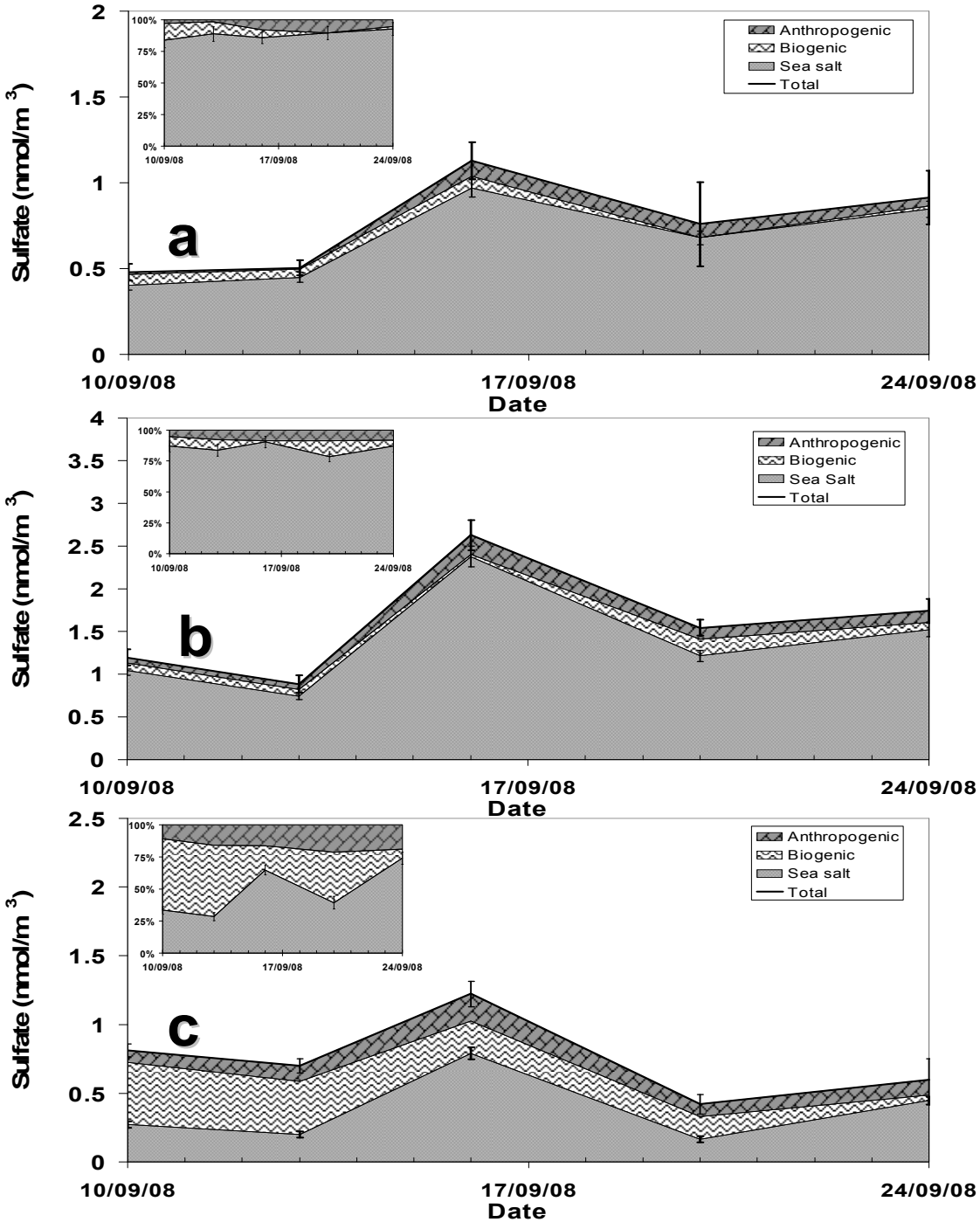

C.7. Concentrations and apportionment for aerosol sulfate for the *Amundsen* data set in 2008 for size fractions a) > 7.2 µm b) 3.0 – 7.2 µm and c) 1.5 – 3.0 µm.

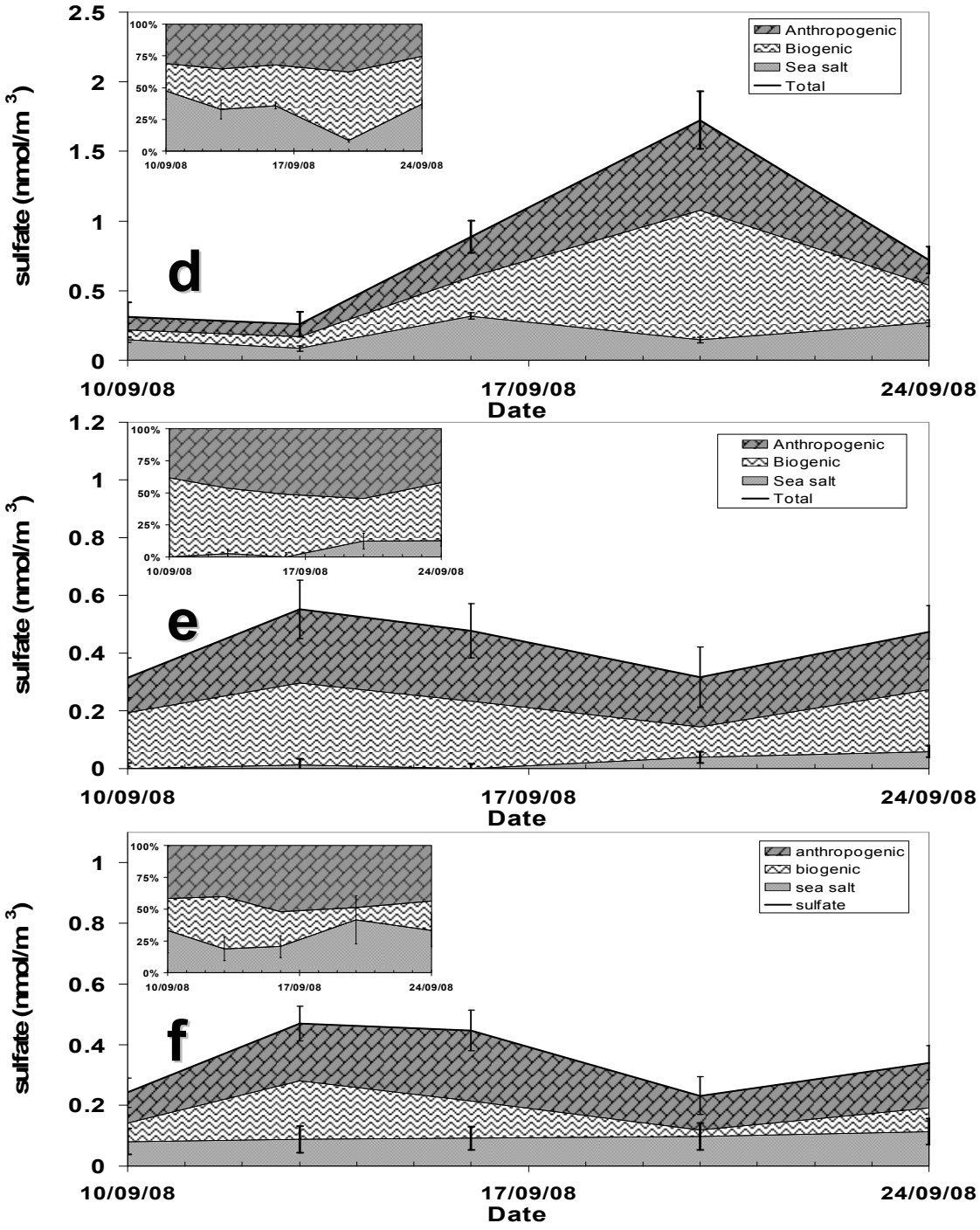

C.8. Concentrations and apportionment for aerosol sulfate for the *Amundsen* data set in 2008 for size fractions d) 0.95 -1.5 µm e) 0.49 – 0.95 µm and f) > 0.49 µm.

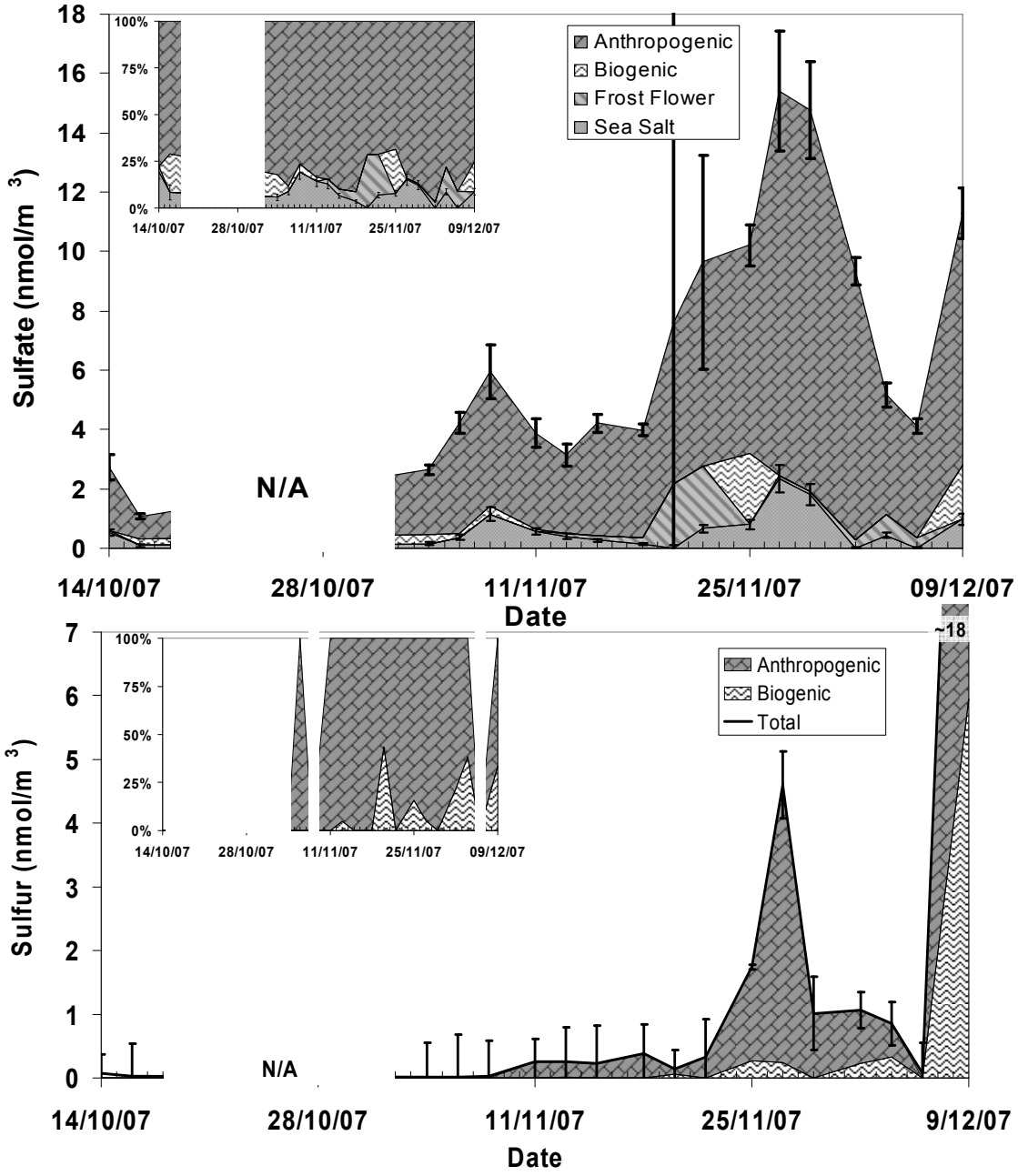

C.9. Concentrations and apportionment for total aerosol sulfate (top) and for SO_2 (bottom) at Alert in 2007.

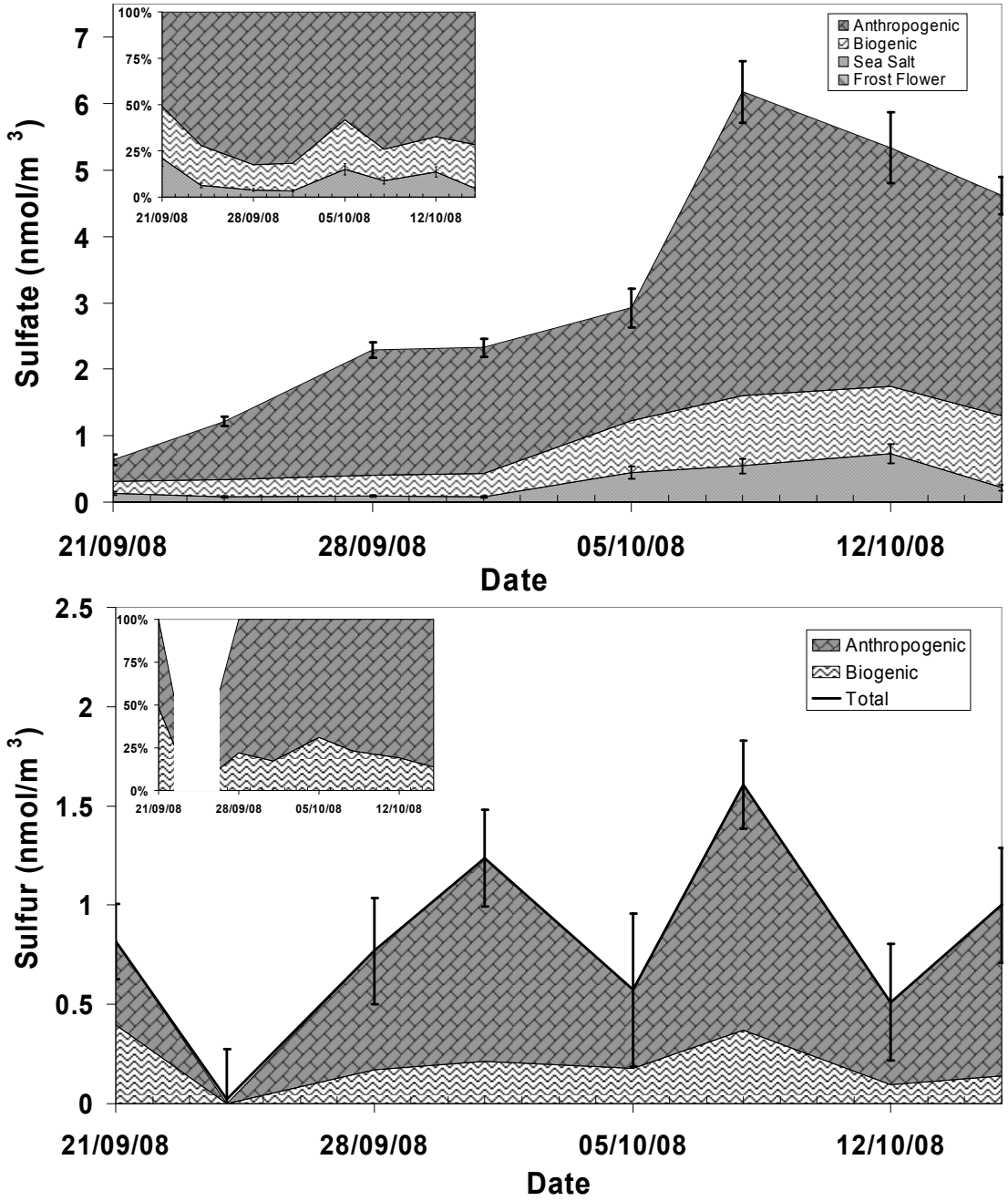

C.10. Concentrations and apportionment for total aerosol sulfate (top) and for SO_2 (bottom) at Alert in 2008.

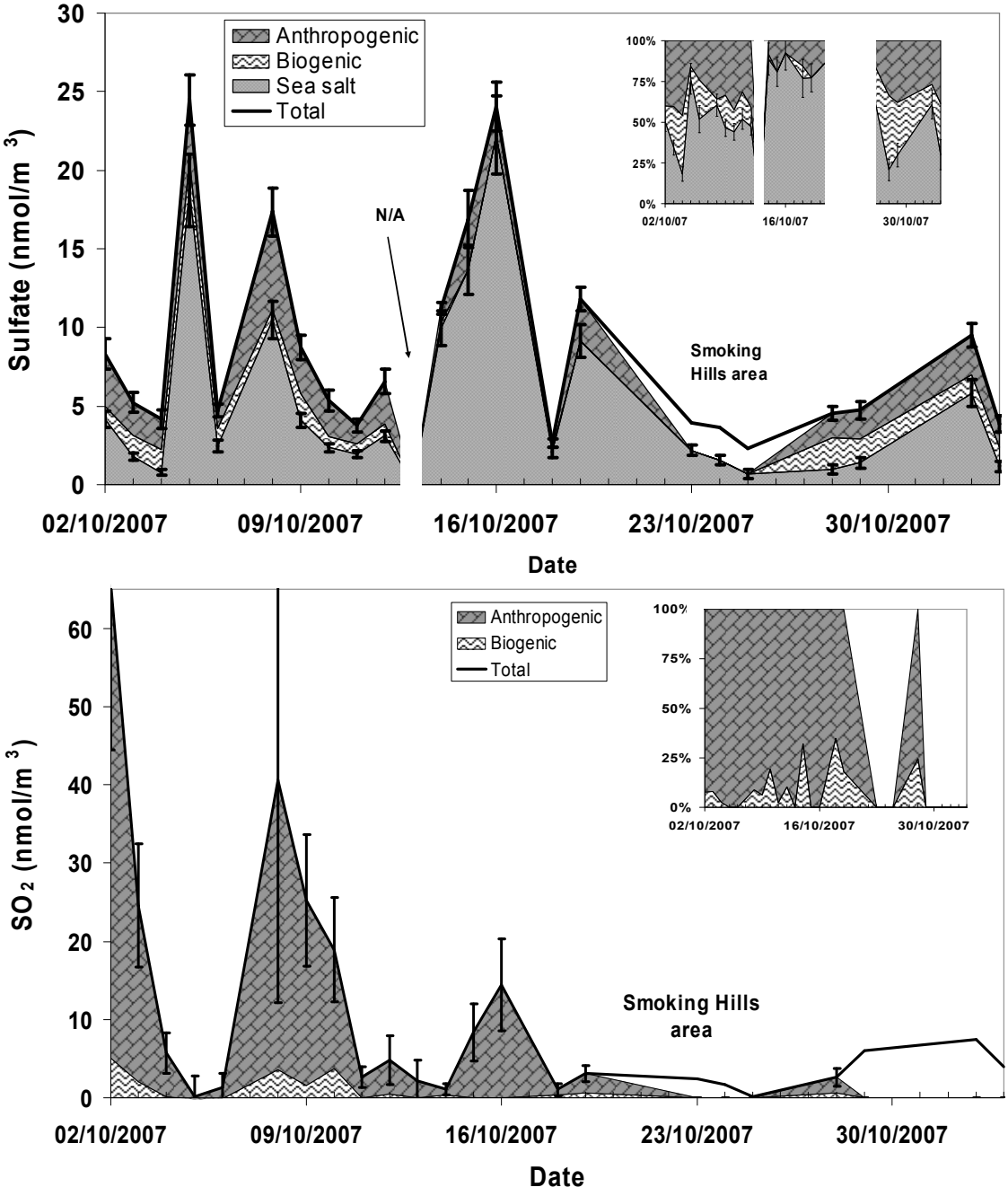

C.11. Concentrations and apportionment for total aerosol sulfate (top) and for SO_2 (bottom) in 2007 from the *Amundsen* data set. SO_2 data corrected for possible sea salt contamination (Appendix F)

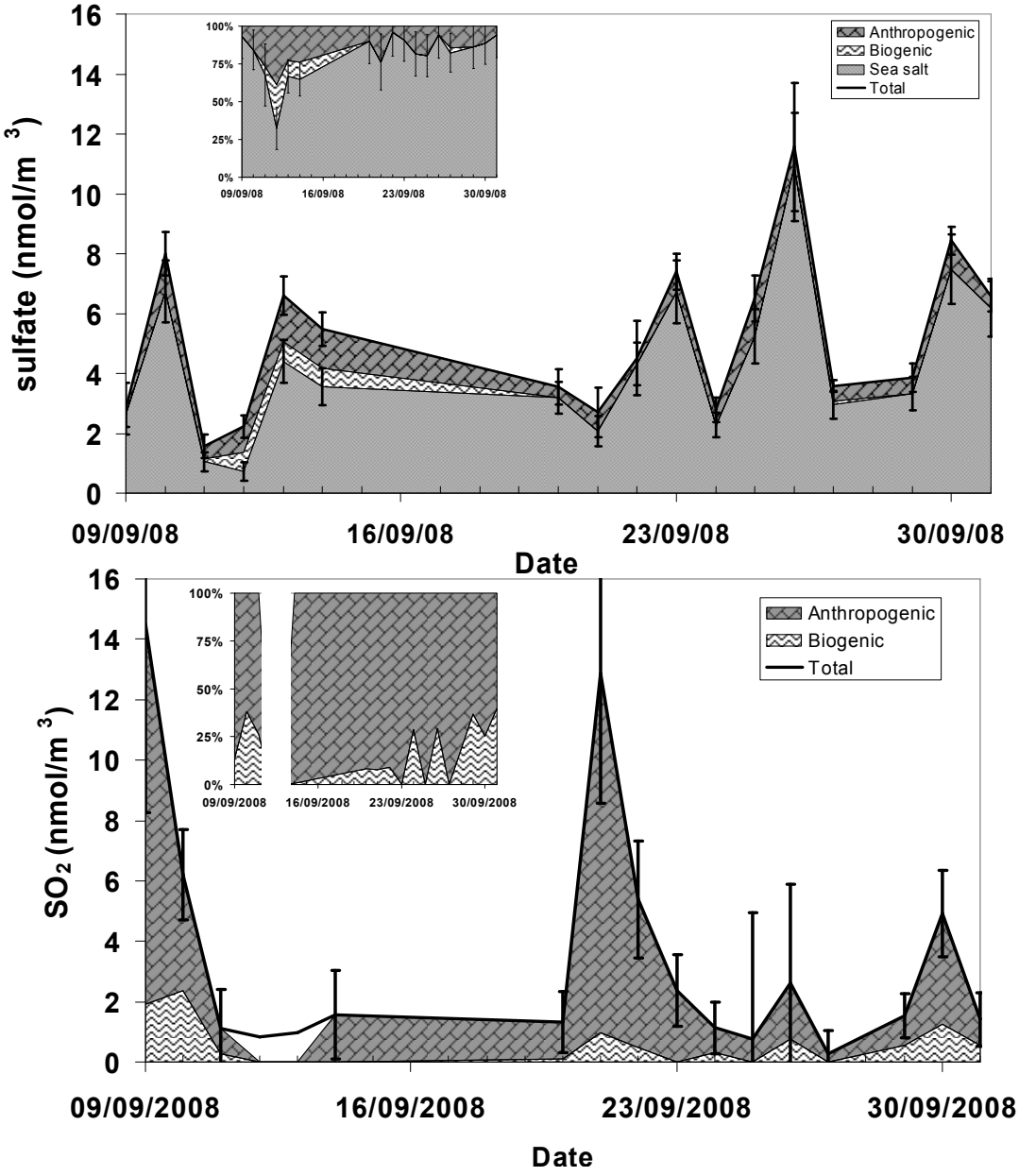

C.12. Concentrations and apportionment for total aerosol sulfate (top) and for SO_2 (bottom) in 2008 from the *Amundsen* data set. SO_2 data corrected for possible sea salt contamination (Appendix F)

APPENDIX D: DETAILS OF THE CALCULATED $\delta^{34}S$ AND NA^{+}/SO_4^{2-} RELATIONSHIP

It was discovered that when plotting calculated $\delta^{34}S_{nss}$ ($\delta^{34}S_{nss\text{-}c}$), based on equation 3.1, versus k^{-1} (Na^{+}/SO_4^{2-} molar ratio), in Figure 3.5, that the shape of the graph followed a similar pattern of a rectangular hyperbola with asymptotes parallel to the coordinate axes. This is different than the linear line observed by Norman et al. (1999), but the higher k^{-1} observed in this study for some samples allows for the observation of the curve.

If frost flower contribution is ignored, equation 3.1 is used to calculate concentrations and $\delta^{34}S$ values; i.e.,

$$\delta^{34}S_T \cdot SO_{4T} = \delta^{34}S_{ss} \cdot SO_{4ss-c} - \delta^{34}S_{nss\text{-}c} \cdot (SO_{4T} - SO_{4ss-c}) \qquad \textbf{3.1}$$

The values will be referred to as calculated values and will be identified with subscript c. Rearranging equation 3.1 yields

$$\delta^{34}S_{nss-c} = \frac{\delta^{34}S_T \cdot SO_{4T} - \delta^{34}S_{ss} \cdot SO_{4ss-c}}{SO_{4T} - SO_{4ss-c}} \qquad \textbf{C.1}$$

When calculating sea salt sulfate (when frost flowers are not present), the sea salt ratio is

$[SO_{4ss\text{-}c}]=Na_T \cdot SS_{ratio}$ **C.2**

where $SS_{ratio}=SO_4^{2-}/Na^+$ of sea water. Equation C.2 can be substituted in equation C.1 and rearrange to give

$$\delta^{34}S_{nss-c} = \frac{(\delta^{34}S_{ss} - \delta^{34}S_T)(SS_{ratio})^{-1}}{\frac{Na_T}{SO_{4T}} - (SS_{ratio})^{-1}} + \delta^{34}S_{ss} \quad \textbf{C.3}$$

The calculated values for $\delta^{34}S_{nss\text{-}c}$, would not represent the true $\delta^{34}S_{nss}$ value if frost flowers are present in the sample. If frost flowers are present, the frost flower terms must be included and thus equation 3.5,

$$\delta^{34}S_T \cdot SO_{4T} = \delta^{34}S_{ff} \cdot SO_{4\,ff} + \delta^{34}S_{ss} \cdot SO_{4\,ss} + \delta^{34}S_{nss} \cdot SO_{4\,nss} \quad \textbf{3.5}$$

must be considered. This equation is rearranged and substituted for the $\delta^{34}S_T$ term in equation C.3. $\delta^{34}S_{ff}$ is equivalent to $\delta^{34}S_{ss}$ (+ 21‰) and is replaced. Rearranging the equation further yields

$$\delta^{34}S_{nss-c} = \frac{(SO_{4T} - SO_{4\,ff} - SO_{4ss})(\delta^{34}S_{ss} - \delta^{34}S_{nss} \cdot SO_{4nss})(SO_{4T} \cdot SS_{ratio})^{-1}}{\frac{Na_T}{SO_{4T}} - (SS_{ratio})^{-1}} + \delta^{34}S_{ss} \quad \textbf{C.4}$$

It is also noted that

$$SO_{4T} = SO_{4\,ff} + SO_{4ss} + SO_{4nss} \qquad \textbf{3.3}$$

SO_{4nss} can be substituted into equation C.4, before rearranging the equation to obtain

$$\delta^{34}S_{nss-c} = \frac{\frac{(\delta^{34}S_{ss} - \delta^{34}S_{nss})}{SS_{ratio}} \cdot \frac{SO_{4nss}}{SO_{4T}}}{\frac{Na_T}{SO_{4T}} - (SS_{ratio})^{-1}} + \delta^{34}S_{ss} \qquad \textbf{C.5}$$

A rectangular hyperbola with asymptotes parallel to the coordinate axes follows the form

$$y = \frac{c}{x - x^0} + y^0 \qquad \textbf{C.6}$$

where the center of the hyperbola is located at (x^0, y^0), and c is a constant. Equation C.5 is in a form similar to equation C.6. When plotting $\delta^{34}S_{nss\text{-}c}$ against k^{-1} (i.e., Na_T/SO_{4T}), a vertical asymptote at $k^{-1} = 16.7 = (SS_{ratio})^{-1}$ is observed in Figure 3.5. Comparing equation C.5 with that of equation C.6, this would corresponds to the x^0 value. The y^0 term would be the y value of the horizontal asymptote. Based on equation C.5, the horizontal asymptote is $\delta^{34}S_{ss}$ (i.e., +21‰).

Although equation has C.5 similar format as a rectangular hyperbola, the numerator in the first term is not constant. The numerator gives information about the curvature of the hyperbola. It is noted that the curvature is dependent on the difference between the

$\delta^{34}S_{nss}$ value and the $\delta^{34}S_{ss}$ value. The curvature is also dependent on the percent contribution of non sea salt sulfate (SO_{4nss}/SO_{4T}). The dependence of these two items allow for spread in the data in Figure 3.5, but still maintains the trend of a rectangular hyperbola with asymptotes at $\delta^{34}S_{nss\text{-}c} = +21‰$ and $k^{-1} = 16.7$.

APPENDIX E: PROOF OF MINIMUM FROST FLOWER CONTRIBUTION

E.1. Proof of equation 3.4

From equation 3.2

$$Na_T = Na_{ff} + Na_{ss}$$

Substitute sea salt and frost flower ratios

i.e., $\mathbf{Na_{ss} = SO_{4ss}/SS_{ratio}}$ and $\mathbf{Na_{ff} = SO_{4ff}/FF_{ratio}}$

$$Na_T = \frac{SO_{4ss}}{SS_{ratio}} + \frac{SO_{4\,ff}}{FF_{ratio}}$$

Use equation 3.3 ($SO_{4T} = SO_{4\,ff} + SO_{4ss} + SO_{4nss}$) to replace SO_{4ss} into the equation

$$Na_T = \frac{SO_{4T} - SO_{4\,ff} - SO_{4nss}}{SS_{ratio}} + \frac{SO_{4\,ff}}{FF_{ratio}}$$

Isolate SO_{4ff}

$$SO_{4\,ff} = \frac{SS_{Ratio}Na_T - SO_{4T} + SO_{4nss}}{\frac{SS_{ratio}}{FF_{ratio}} - 1}$$

To obtain the minimum frost flower contribution, the right side of the above equation must also be at a minimum. The denominator is positive (since $SS_{ratio} > FF_{ratio}$), therefore to obtain a minimum value the numerator must be at a minimum. SS_{ratio} and FF_{ratio} are both positive and are constrained. Na_T and SO_{4T} are measured for each sample. Therefore for SO_{4ff} to be minimum SO_{4nss} is at a minimum. The minimum concentration is 0. Therefore, SO_{4nss}=0 when calculating the minimum contribution of SO_{4ff} and

$$SO_{4\,ff_{min}} = \frac{SS_{Ratio}Na_T - SO_{4T}}{\frac{SS_{ratio}}{FF_{ratio}} - 1} \quad \text{or} \quad SO_{4\,ff_{min}} = \frac{SO_{4T} - SS_{Ratio}Na_T}{1 - \frac{SS_{ratio}}{FF_{ratio}}} \text{ (equation 3.4)}$$

APPENDIX F: SEA SALT INTERFERENCE WITH SULPHUR DIOXIDE COLLECTION

F.1. Previously Reported Concentrations of SO_2

Rempillo (2011) reported concentrations of SO_2 measured on board the *Amundsen* between 2.7 – 135 nmol/m^3 in 2007 and between 0.28 – 27 nmol/m^3 in 2008. The lower limit fell within measurements carried out previously in the Arctic, but the upper limit was larger (e.g., Leck and Persson, 1996; 0.04 - 1.7 nmol/m^3; Hara et al. 1997; below detection limit to ~ 50 nmol/m^3)

Rempillo et al. (2011) determined biogenic SO_2 ranged between 0 and 97 nmol/m^3 in 2007 and 0 to 11 nmol/m^3 in 2008. The highest marine biogenic SO_2 concentration reported previously was 82 nmol/m^3 over the Atlantic Ocean (Seguin et al., 2010) when anthropogenic influence affected the fate of DMS end products. Measurements as high as this in the Arctic were unexpected. Possible contamination issues such as incineration of wastes were studied as a potential source of sulfur with ^{34}S values similar to marine biogenic but it was concluded that incineration was an unlikely source of SO_2 (Rempillo, 2011). Migration of particulate matter from the total aerosol filter to the acetate (SO_2) filter is possible. Carryover over was suspected under rain or fog conditions in some samples from the Atlantic as clear decreases in total aerosol sulfate relative to the sum of sulfate in aerosol fractions were accompanied by elevated sulfur found on the cellulose acetate filters (Eaton, 2006). Additionally, equivalent $\delta^{34}S$ values for sulfur found on both

the cellulose acetate filters and the total particulate filters occur during carryover (Eaton, 2006). However conditions with equivalent high humidity were not present in the Arctic and no evidence of elevated SO_2 with sulfate depletion was observed for the *Amundsen* samples (Rempillo, O., personal communications 2012).

F.2. Gaseous Tracers of Anthropogenic Influence

Gaseous components on the SO_2 filters have been examined in previous works (e.g., Hara et al., 1999; Seguin et al., 2010). The exact components on the filter are not known because of the oxidation by H_2O_2 during the laboratory procedure (Chapter 2.6; Seguin, 2007). Oxidation converts SO_2 collected on the filter to SO_4^{2-}; measureable by ion chromatography. Similarly, gaseous nitrogen, chlorine and bromine containing compounds absorbed on the filter have the potential to be oxidized in the procedure. These compounds would be measured as nitrate, chloride and bromide with ion chromatography. Samples containing nitrate and chloride (night samples only) were found to correlate with SO_2 concentrations over the Atlantic (Seguin, 2007) at much warmer temperatures (between 5 and 25°C) than this study. Hara et al. (1999) found for the majority of the samples collected at Ny-Ålesund, Norway, measured nitrate mostly ranged below the field blank of their study.

F.3. Sea Salt Contamination

Although the exact composition of these gaseous components is not known, chloride and bromide were found in the SO_2 filters extracts for the *Amundsen* samples. Correlation between total SO_2 and the chloride was present for the *Amundsen* data set ($R^2 \sim 0.3$). Bromide was detected on 9 out of 38 samples from the *Amundsen.* A strong relationship (Figure F.1; $R^2 > 0.89$,) between biogenic sulfur and chloride was found. This relationship followed that of the sulfate/chloride sea salt ratio (displayed in Figure F.1). This is consistent with sea salt contamination on the SO_2 filter since the $\delta^{34}S$ value (+18 ‰) for marine biogenic sulfur is similar to the $\delta^{34}S$ value of sea salt sulfate (+ 21 ‰). Sea salt corrections are usually not carried out on the cellulose acetate (SO_2) filters because sea salt sulfate is not in the gas phase but rather in aerosols and would therefore be trapped on the aerosol filter stationed above the cellulose acetate filter on the high volume sampler. Chloride and bromide on the cellulose acetate filter were plotted against each other (Figure F.2) to confirm whether they were consistent with sea salt contamination. A strong relationship was found for between bromide and chloride ($R^2 > 0.85$) and is similar to the sea salt ratio (displayed in Figure F.2).

Possible migration of particulate matter from the total aerosol filter to the SO_2 filter had already been studied for the *Amundsen* data set (Rempillo, O., personal communications 2012) and could not explain the possible source of sea salt contamination. The amount of sea salt contamination is not correlated with the amount of sea salt found on the total aerosol filter collected at the same time ($R^2 = 0.01$). Cellulose acetate filters and similar

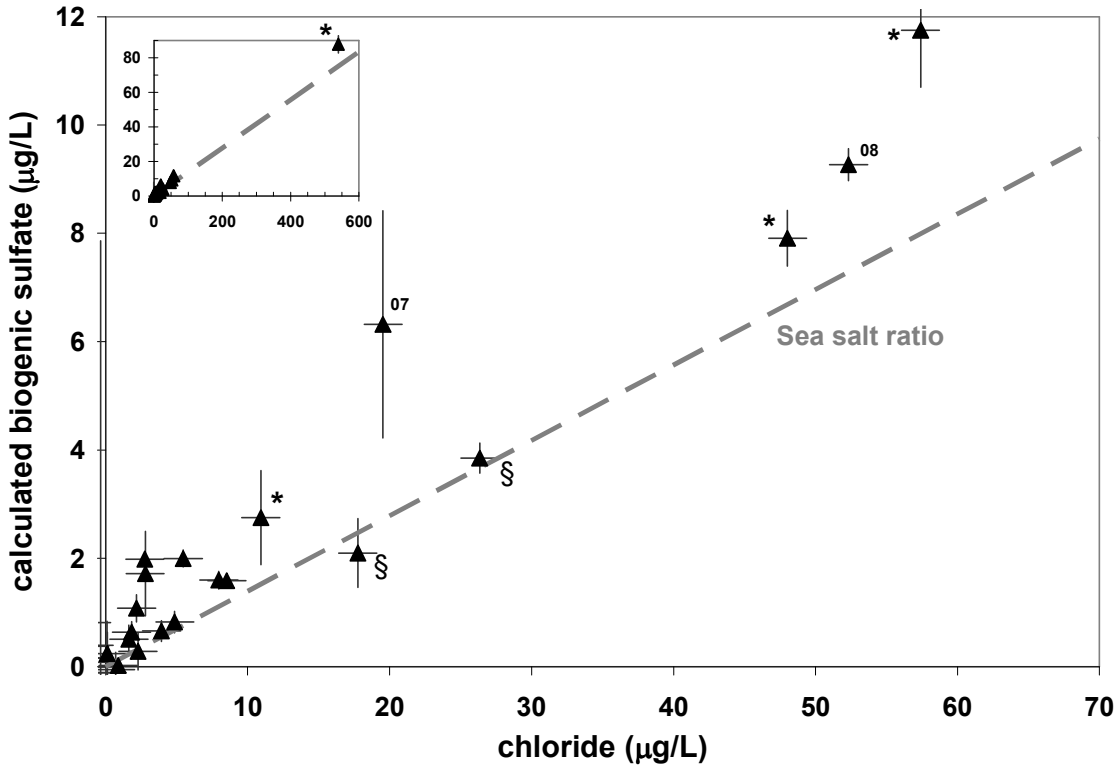

Figure F.1 Chloride and calculated biogenic sulfate found in the eluent from the analysis of the cellulose acetate filters after blank corrections. Note that concentrations are in µg/L of water and are not corrected to atmospheric concentrations. Insert shows total range. Sea salt ratio is displayed for comparison. The eight samples associated with the highest chloride, are associated with snow present during the changing of filters (*), samples that had an average wind speed greater than 13 m/s (§) or the first sample collected during the year (^{07}, ^{08})

techniques were used in numerous campaigns and reports of possible sources of sea salt contamination have not been reported (e.g., Saltzman et al., 1983; Hara et al., 1999; Eaton, 2006; Seguin 2007; Burridge, 2009). Although Seguin (2007) reported chloride

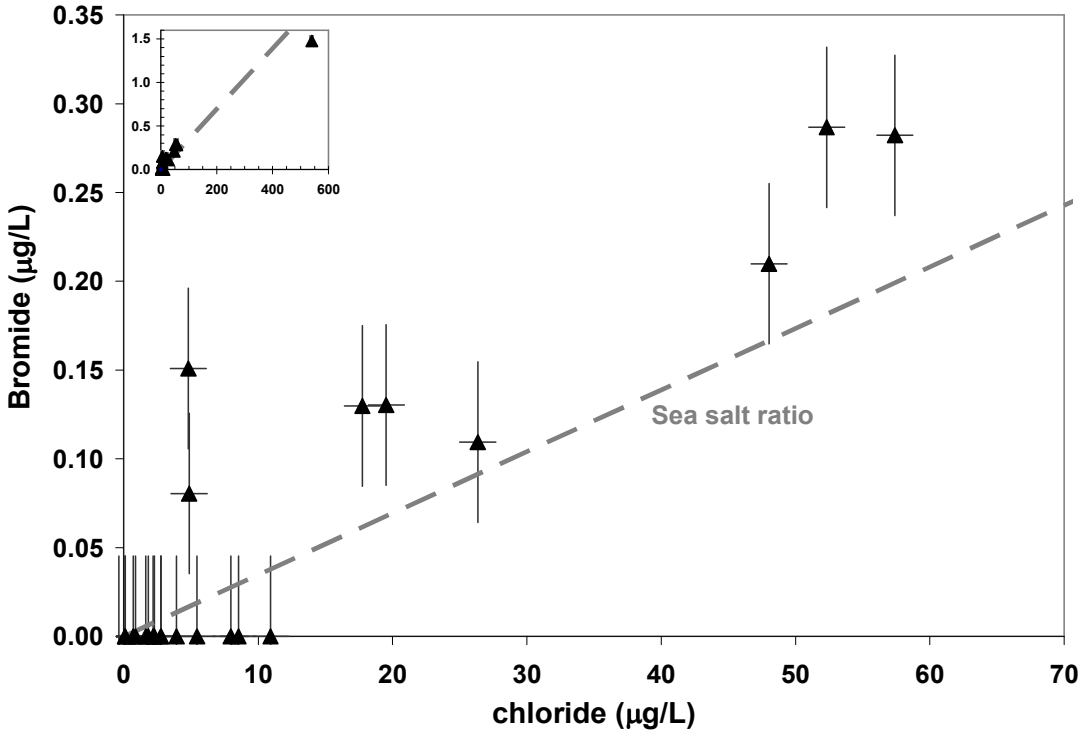

Figure F.2 Chloride and bromide found in the eluent from the analysis of the cellulose acetate filters after blank corrections. Note that concentrations are in µg/L of water and are not corrected to atmospheric concentrations. Insert shows total range. Sea salt ratio is displayed for comparison.

on nighttime filters, the relationship between biogenic sulfur and chloride found from the cellulose acetate filters did not follow that of sea salt.

During the *Amundsen* campaign, sea salt in aerosols and on surfaces was high (Chapter 3.4.1). It was also observed that sea spray was occasionally present as high as the ship's bridge during rough sea conditions which would lead to sea salt on exposed surfaces. Between each sampling period, the SO_2 sample holder on the high volume sampler was

wiped down with 18 MΩ deionized water; a standard procedure for cleaning between samples. It is possible that at such low temperatures, as found during the SOLAS campaign, the deionized water froze to the cold surface of the high volume sampler. Instead of removing the contaminants, sea salt (possibly in snow) may have been added with the frozen water. Snow was observed when changing the filters during four out of the eight highest contaminated filters (Figure F.1). Varying amounts of sea salt contamination from this process leads to a possible explanation of the elevated sulfate and chloride found on the cellulose acetate filters while the total aerosol filters remained uncontaminated as the holders of the total aerosol filters were cleaned and prepared inside the ship. Removable cassettes were not used for SO_2 filters and therefore were subject to contamination from sea spray and/or snow. It would also explain why other campaigns have not reported issues with sea salt contamination on SO_2 filters. Of the remaining four samples that were elevated in chloride, two occurred during stormy conditions when winds average greater than 13 m/s (see Figure 2.2; Figure F.1). The last two points were samples collected at the start of each of the yearly campaigns (Figure F.1), and may be the result of human activity liberating sea salt from exposed surfaces around the *Amundsen* at the start of the campaign after months of these surfaces being in contact with the ocean atmosphere.

It may be argued that the chloride on the cellulose acetate filter may be a form of a gas that contains chlorine. The chloride found on the cellulose acetate filter collected on board the *Amundsen* converts to a median concentration of gaseous chlorine compounds of 4.4 nmol/m^3. If this gaseous component originated from aerosols, depletion in

chloride compared to sodium should be observed in the fine aerosol fraction. Chloride deficit was observed in the fine aerosols in both locations (approximately 1 nmol/m^3). A relationship between chloride depletion and anthropogenic sulfate in total aerosols was studied in Chapter 4.3.2 at Alert and the chloride deficit was found to be on the order of 1 nmol/m^3 with a maximum depletion of 7.5 nmol/m^3. The median for chloride depletion in total aerosols collected at Alert before mid November was 1.5 nmol/m^3. Total aerosol chloride deficit was not observed on the *Amundsen* because of the large source of fresh sea salt that could mask a potential chloride deficit. If a depletion of the same order of magnitude found at Alert was present on board the *Amundsen* and chlorine containing compounds were effectively trapped on the cellulose acetate filter, it would not explain the large amounts of chloride in the eluent that was found (median value would be equivalent to approximately 4.4 nmol/m^3 of gaseous chlorine compounds in the atmosphere). An additional test to measure sodium collected on the acetate filters would be needed to confirm or rule out sea salt contamination. For the purposes of this thesis, chloride found in the cellulose acetate filter extract is assumed to be sea salt contamination and corrections were applied (see Appendix F.4).

It must be noted that chloride (or chlorine containing compounds in the form of chloride) are not usually reported for cellulose acetate filters. Without the chloride information and the $\delta^{34}S$ values, this possible contamination issue may not have been discovered. Future studies using cellulose acetate filters may find it useful to always include chloride and sodium analysis with each sample for quality control on possible sea salt contamination issues.

F.4. Sea Salt Correction

A sea salt correction can be carried out on the cellulose acetate filters using a similar rational to that for equation 1.1. Cations were not measured for the cellulose acetate filters, therefore chloride is used and sea salt contamination is based on the sea salt chloride/sulfate ratio. $\delta^{34}S$ values for SO_2 can also be corrected based on equation 3.1. It is assumed that all chloride found on the cellulose acetate filters was from sea salt contamination.

The majority of biogenic SO_2 concentrations for the *Amundsen* data set are not significantly different than 0 nmol/m^3 once sea salt correction is carried out on the cellulose acetate filters (Chapter 5.2). The large concentrations of biogenic SO_2 reported by Rempillo et al. (2011) are most likely due to sea salt contamination. The conclusions reported by Rempillo et al. (2011) about sufficient biogenic SO_2 for binary nucleation to occur in the Arctic will need to be revisited.

F.5. SO_2 at Alert

Chloride on the cellulose acetate filters collected at Alert was masked due to a large interfering acetate peak from the filter blank (Chapter 2.6). Bromide was found on the Alert samples. Unlike the *Amundsen* data the bromide found on the cellulose acetate filter did not correlate with biogenic sulfate ($R^2 < 0.04$). Contamination would be expected to be much smaller relative to the *Amundsen* since sea salt was a much smaller

contributor of the overall sulfur load in aerosols at Alert relative to the *Amundsen.* If sea salt contamination was present, it was small relative to SO_2 measurements. Therefore no sea salt correction was carried out for Alert samples.

F.6. Gaseous Compounds Trapped on Cellulose Acetate Filters

Previous works studying $HNO_{3(g)}$ used similar techniques for the cellulose acetate filters as were used in this study (Hara et al., 1999), although it is noted that interferences from PAN and other nitrogen containing species may interfere with the analysis (Barrie et al., 1994). Nitrogen containing compounds were found on the cellulose acetate filters collected at Alert (median = 0.46 ± 0.39 (1σ) nmol/m^3); comparable to similar measurements in the Arctic by Hara et al. (1999) whom found that concentrations usually were below their detection limit of 0.6 nmol/m^3.

No correlation with anthropogenic SO_2 or total SO_2 were found with these compounds ($R^2 < 0.15$) at Alert. Bromide was also measured in the eluent from the cellulose acetate filter at Alert, and is not expected to be from sea salt. Relationships with the gaseous components (containing nitrogen and bromine) with aerosol chloride deficit and non sea salt sulfate on the total aerosol were also not observed. Therefore, gaseous species that are librated from the collection of aerosols are either no longer present in the air mass or are not measurable at Alert for the analysis suggested in Seguin et al. (2010).

APPENDIX G: OH· MODELED PARAMETERS

G.1. Steady State Model For HO_x

OH and HO_2 are assumed to be in steady state. Therefore

$$\mathbf{P_{HO_x} = L_{HO_x}} \qquad \textbf{G.1}$$

where P_{HOx} is the production rate and L_{HOx} is the loss rate of the molecule.

G.1.1. HO_2 Concentrations

For HO_2 concentrations, from Table 6.1,

$$\mathbf{P_{HO_2}} = k_{5*}[CO][OH] + 2j_{HCHO}[HCHO] \qquad \textbf{G.2}$$

and

$$\mathbf{L_{HO_2}} = k_2[O_3][HO_2] + k_3[NO][HO_2] \qquad \textbf{G.3}$$

Since HO_2 is in steady state, equations G.2 and G.3 can be equated and rearranged and the expression of HO_2 concentration is as follows

$$[HO_2] = \frac{k_{5*}[CO][OH] + 2j_{HCHO}[HCHO]}{k_2[O_3] + k_3[NO]} \quad \textbf{G.4}$$

G.1.2. OH· Concentrations

For OH·, from Table 6.1,

$$\mathbf{P_{OH}} = 2k_1[O^1D][H_2O] + (k_2[O_3] + k_3[NO])[HO_2] \quad \textbf{G.5}$$

and

$$\mathbf{L_{OH}} = k_4[CH_4][OH] + k_{5*}[CO][OH] + k_{6*}[HCHO][OH] \quad \textbf{G.6}$$

Equation G.4 can be subbed into equation G.5

$$\mathbf{P_{OH}} = 2k_1[O^1D][H_2O] + \left(k_2[O_3] + k_3[NO]\right)\left(\frac{k_{5*}[CO][OH] + 2j_{HCHO}[HCHO]}{k_2[O_3] + k_3[NO]}\right)$$

and simplified to

$$\mathbf{P_{OH}} = 2k_1[O^1D][H_2O] + k_{5*}[CO][OH] + 2j_{HCHO}[HCHO] \quad \textbf{G.7}$$

Equation G.6 and G.7 can be equated and simplified since the k_{5*}[CO][OH] term appears in both the loss and production terms of OH· to give the following expression;

$$2k_1[O^1D][H_2O] + 2j_{HCHO}[HCHO] = k_4[CH_4][OH] + k_{6*}[HCHO][OH] \quad \textbf{G.8}$$

and rearranged to yield OH· concentrations

$$[OH] = \frac{2k_1[O^1D][H_2O] + 2j_{HCHO}[HCHO]}{k_4[CH_4] + k_{6*}[HCHO]} \quad \textbf{G.9}$$

where

$$[O^1D] = \frac{j_{O_3 \rightarrow O^1D}[O_3]}{k_{O^1D:N_2}[N_2] + k_{O^1D:O_2}[O_2]} \quad \textbf{G.10}$$

and j_{HCHO} and $j_{O_3 \rightarrow O^1D}$ are calculated using the TUV model. See Chapter 6.3.1.1 for assumptions of HCHO, CH_4 and O_3 concentrations and Appendix G.2 for *j* values. OH· concentrations are displayed in Figure 6.2 for 2007 and Figure 6.3 for 2008.

G.2. Photolysis Rate Coefficients Used for OH· Model

The OH· concentration model requires the photolysis rates (*j*) for the reactions of $O_3 + h\nu \rightarrow O(^1D) + O_2$ and HCHO + $h\nu$ → H· + HCO·. Photolysis rates were

determined by the Tropospheric Ultraviolet and Visible (TUV) Radiation Model (Version 4.1) and were run for each point that corresponded to an atmospheric DMS measurement. Inputs to the TUV models are discussed in Chapter 6.3.1.1. The photolysis rate coefficients are displayed below.

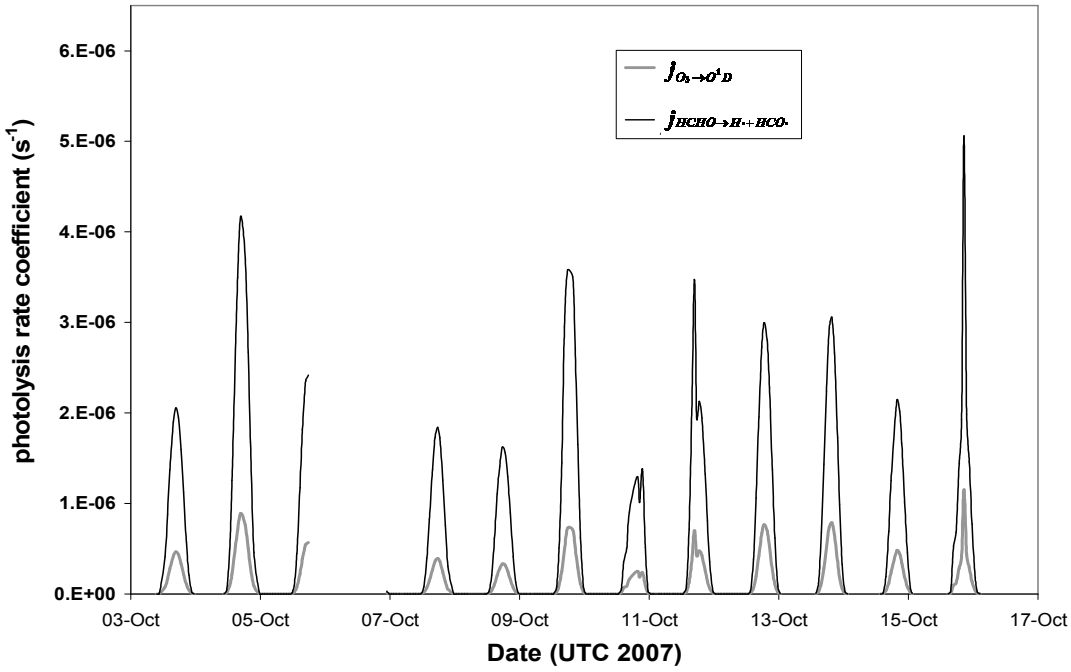

Figure G.1 Photolysis rate coefficients between October 3 and October 17, 2007 for $O_3 + h\nu \rightarrow O(^1D) + O_2$ and HCHO + hv → H· + HCO·.

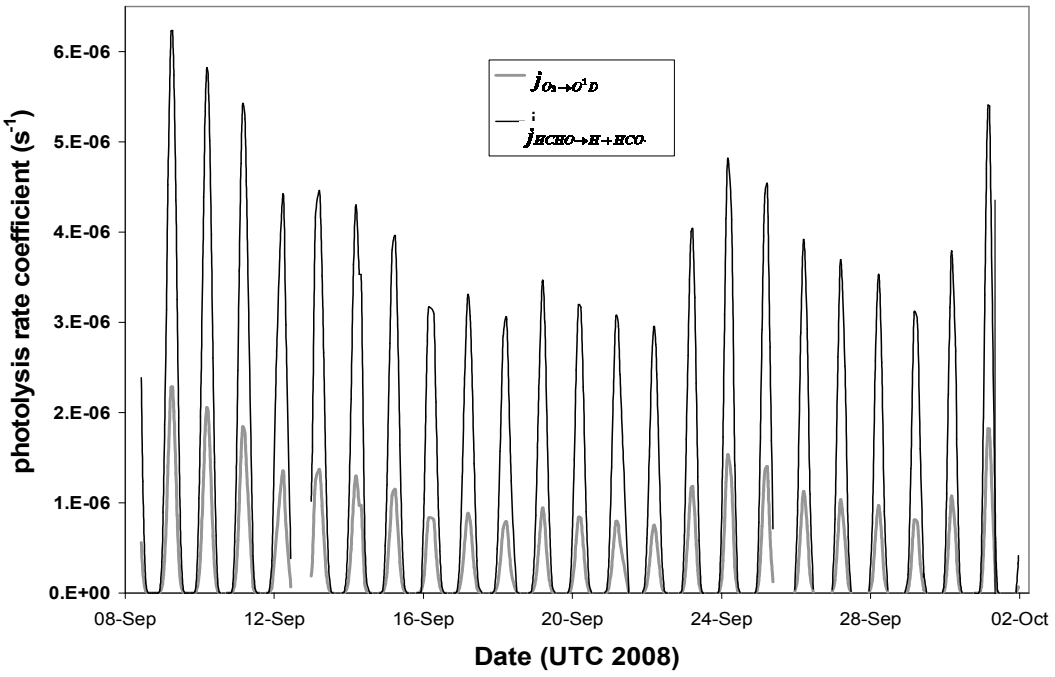

Figure G.2 Photolysis rate coefficients between September 8 and October 2, 2008 for $O_3 + h\nu \rightarrow O^1D + O_2$ and $HCHO + h\nu \rightarrow H\cdot + HCO\cdot$.

APPENDIX H: NO_3 MODELING PARAMETERS

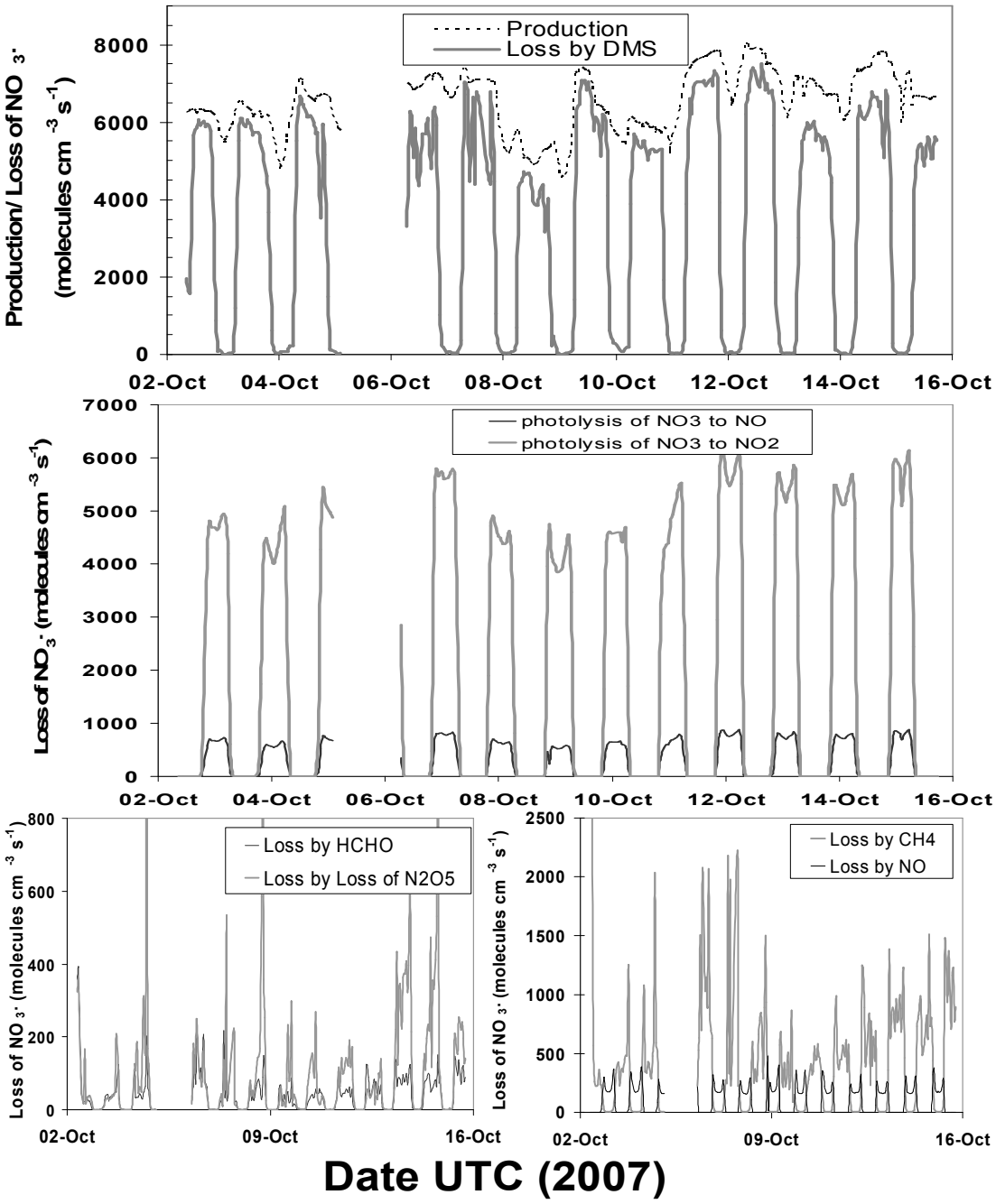

Figure H.1 Modeled NO_3· production and loss rates October 3-17, 2007 on board the *Amundsen*. NO_x ($NO + NO_2$) concentrations are set to 0.88 nmol/m^3.

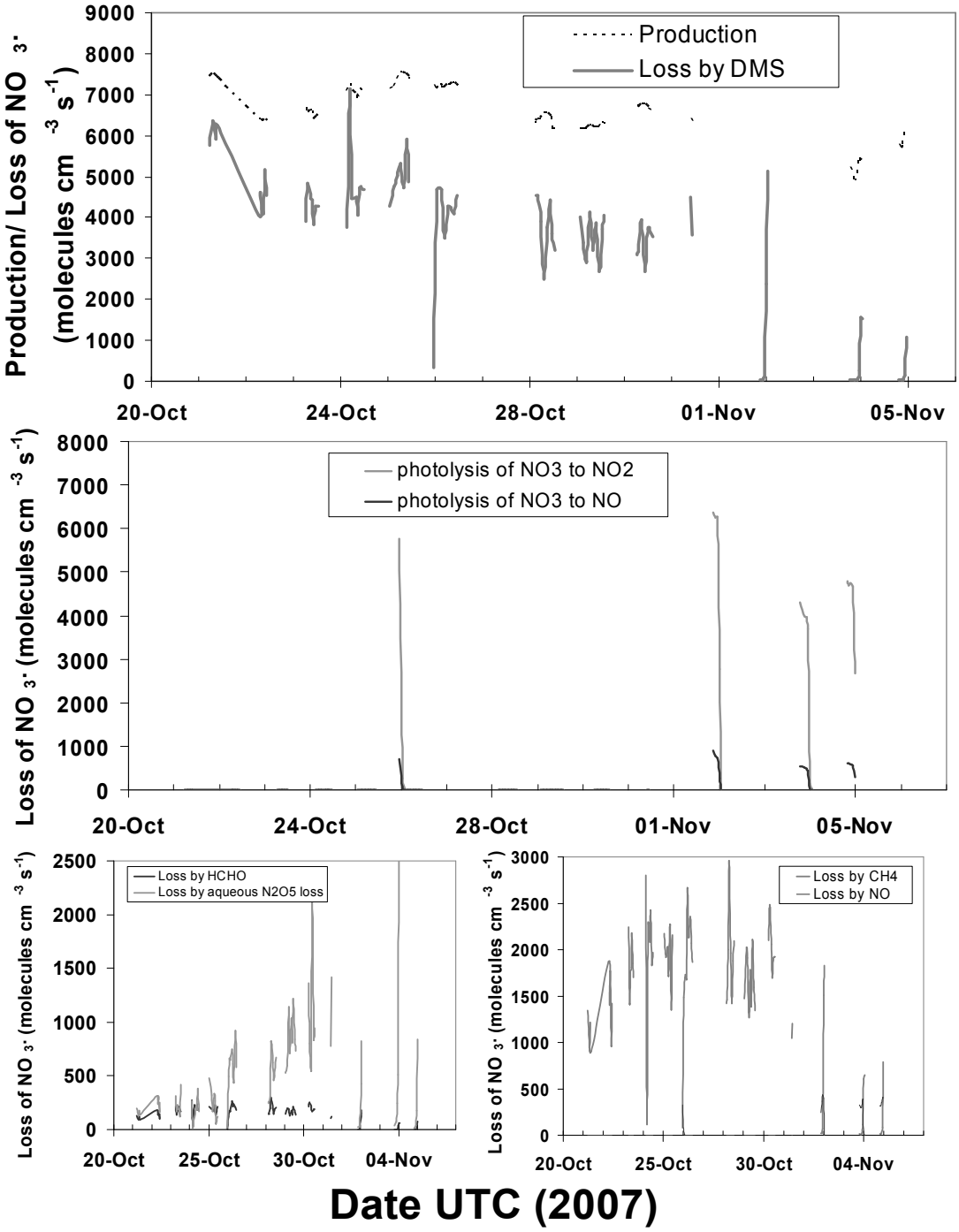

Figure H.2 Modeled NO_3· production and loss rates October 20 – November 6, 2007 on board the *Amundsen*. NO_x ($NO + NO_2$) concentrations are set to 0.88 nmol/m^3. Model was conducted only during times when DMS concentrations were available.

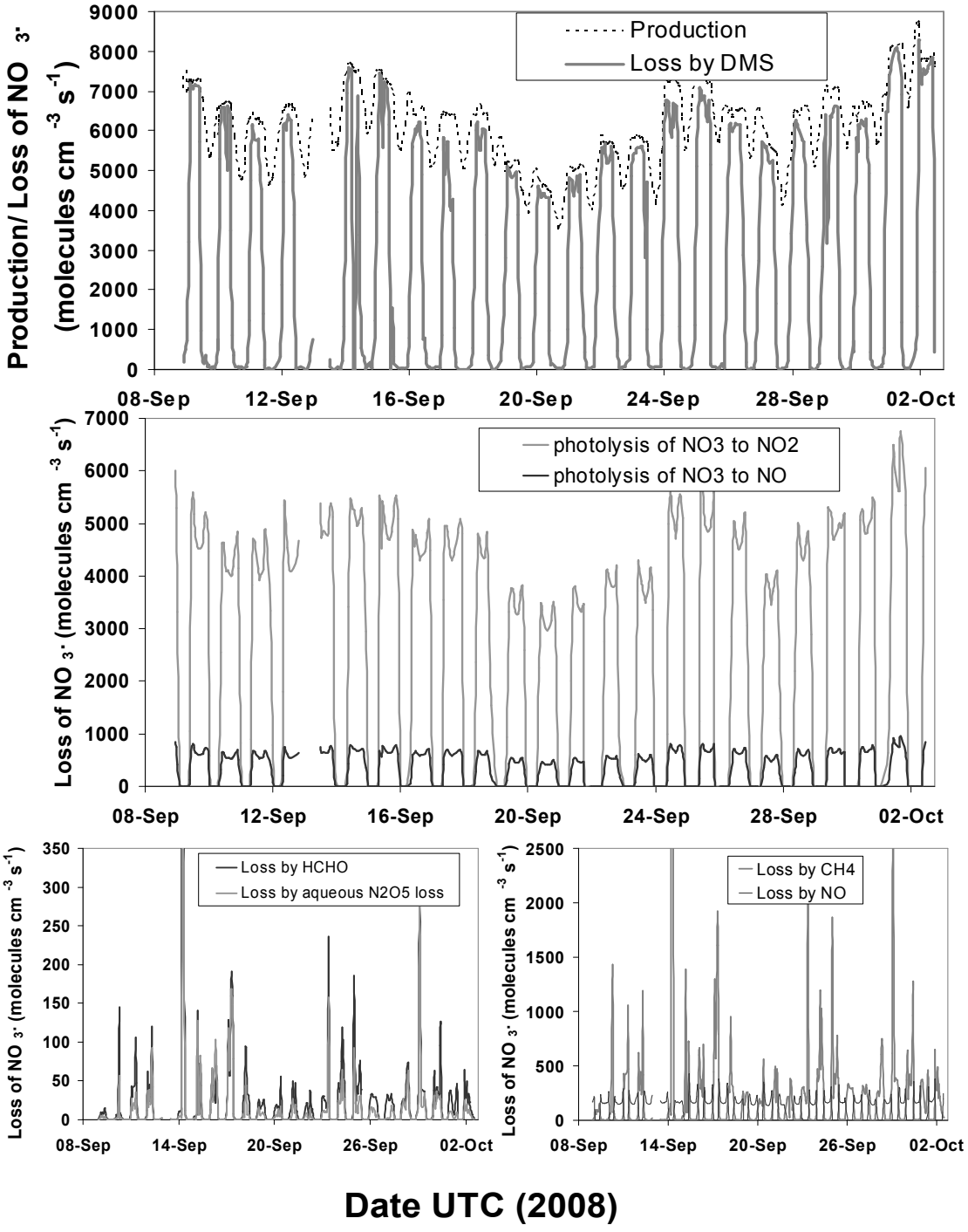

Figure H.3 Modeled NO_3· production and loss rates for 2008 (September 8 – October 2) on board the *Amundsen*. NO_x ($NO + NO_2$) concentrations are set to 0.88 nmol/m^3.

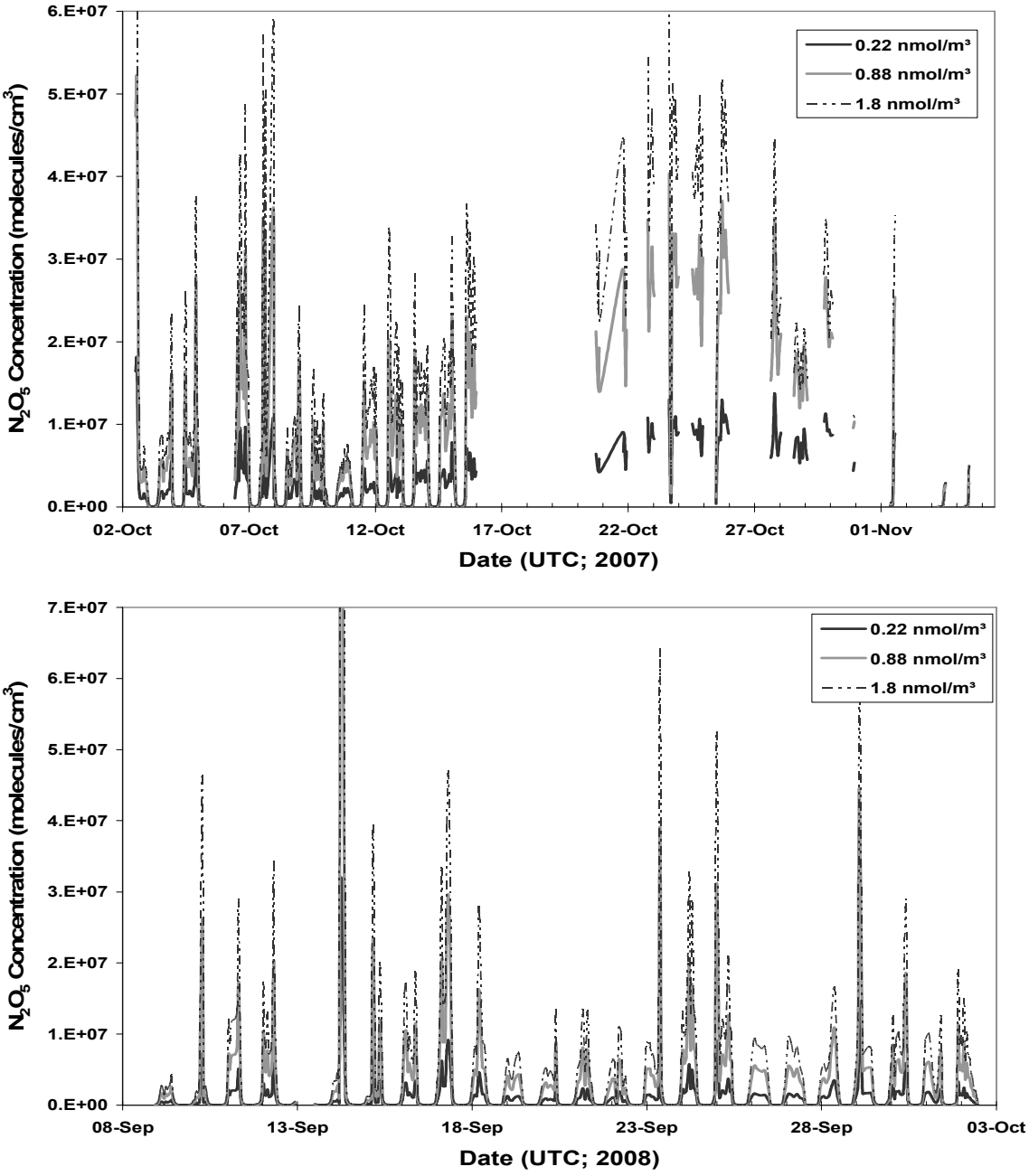

Figure H.4 Modeled N_2O_5 concentrations for 2007 (top) and 2008 (bottom) for the *Amundsen* data set using the range of NO_x concentrations specified in the label.